Numerical Analysis of Multiphase Curvature-driven Interface Evolution with Volume Constraint

博　士　論　文

Numerical Analysis of Multiphase Curvature-driven Interface Evolution with Volume Constraint

(体積保存条件を満たす複数の界面の曲率による運動の数理解析)

金沢大学大学院自然科学研究科

数物科学専攻

計算科学講座

学　籍　番　号　1123102013

名　　前　RHUDAINA Z. MOHAMMAD (ルダイナ・モハマド)

主任指導教員名　KAREL ŠVADLENKA (カレル・シュワドレンカ)

"Long Live the Junction!"

– K. Švadlenka

金沢大学
KANAZAWA UNIVERSITY

Abstract

Numerical Analysis of Multiphase Curvature-driven Interface Evolution with Volume Constraint

Rhudaina Z. Mohammad

The dissertation focuses on two main points. First, we develop a signed distance vector approach for approximating volume-preserving mean curvature motions of interfaces separating multiple phase regions – a variant of the MBO (Merriman-Bence-Osher) threshold dynamics. We construct a vector-valued analogue of the signed distance function, which provides the needed subgrid accuracy on uniform grids without adaptive refinement; thereby, alleviating the well-known MBO time and grid restrictions. We adopt a variational method employing the idea of a vector-type discrete Morse flow, which allows us to easily treat volume constraint via penalization, and even, extend our method to include space-dependent bulk energies and anisotropic energies. We present several numerical tests and computational examples of curvature-driven interface evolutions.

Second, we analyze a penalization method related to the above volume-constrained variational problem – an approximation method that penalizes only the increase in volume. We present existence and regularity results of the sequence of minimizers of the corresponding penalized functional. Without relying on the smoothness of the free boundary, we investigate the behavior of these minimizers for sufficiently large penalty values. Lastly, we prove the existence of a minimizing movement corresponding to our penalized functional and some of its properties.

Dissertation Advisor. **Karel Švadlenka, Ph.D.**
2010 Mathematics Subject Classification. 53C44, 76T30, 49J40, 35R35

Acknowledgements

Foremost, my deepest appreciation and sincerest gratitude is due to my research supervisor, Dr. Karel Švadlenka for the support, guidance, and mentorship he has provided me during my years of study at Kanazawa University. His positive outlook, stimulating suggestions, encouragement and the always insightful discussions I have had with him contributed immensely in the completion of this dissertation. I am truly fortunate to have had the opportunity to work with him.

The author also extends her gratitude to the Division of Mathematical and Physical Sciences, particularly to the dissertation defense committee: Dr. Seiro Omata, Dr. Masato Kimura, Dr. Hiroshi Ohtsuka, and Dr. Katsuyoshi Ohara for their input, suggestions, and valuable comments which definitely helped improve this paper.

This work would not have been possible without the support of the Ministry of Education, Culture, Sports, Science and Technology (MEXT), Japan. Through its Japanese Government (Monbukagakusho) Scholarship Grant, I have had the opportunity to pursue a doctoral degree in Mathematics and learn the culture of mathematical research in Japan. I am equally grateful to my employer, Western Mindanao State University, Philippines for granting me a study leave to fulfill a life's dream.

I wish to thank my fellow graduate students in the Keisan Floor (2F), NST Hall 5 – those who have moved on and those who are still in the quagmire for sharing their research woes and a glimmer of hope for post-graduation normalcy. Special thanks to our lab's daisempai, Dr. Elliott Ginder for the coding tips and discussions on the MBO Method, and most especially for his 2-month lockdown advice which eventually helped me iron out and debug my SDV program.

My special thanks are extended to the faculty members of the Mathematics and Statistics Department, Western Mindanao State University for their continued moral support and encouragement – un pasion por las matematicas.

I am particularly grateful for the support and the camarederie given by my friends, for being such cheerleaders and accepting nothing less than completion from me. I may not be able to mention all of you here, but know that, I am truly grateful for your existence in my life and I hold you all dear in my heart.

I would also like to thank the Mitsuhashi family in Yokohama, for accepting me with open arms into their home and treating me as one of their own – of course, in particular, to my bestfriend, Rika for the never-ending support. A big thanks is equally due to my Filipino family in Kanazawa, especially to our daisempai, Kuya Edwin and Dr. Rizalita Edpalina for all the cozy and homey time spent on laughters and music. It would be remiss of me not to offer my gratitude to my good friend, Dr. Betchaida Payot for being a wonderful big sister and an inspiration. Your infectious love for rocks and for the country is growing on me.

To my beloved mother and my three little brothers who grew up to be such lovely gentlemen, thank you for the life-long support, love, and understanding. Last but not the least, I want to acknowledge the efforts of all those who have been my teachers in the past, which in one or another have influenced this work. Above all, I thank God Almighty for the strength and courage He has bestowed upon me to finish this work.

Contents

List of Figures

List of Tables

List of Algorithms

Dedicado con todos mio maestros y maestras
desde ya aprende yo hasta ya principia
yo gusta con el matematica . . .

Chapter 1

Introduction

The bulk of the present thesis is geared towards developing a scheme for multiphase curvature-driven interface evolutions with volume constraint. By "curvature-driven", we mean that each point of the interface (separating multiple phase regions) moves with a normal velocity equal to a function of its mean curvature. This type of evolutionary problems often appear in differential geometry and analysis (e.g., study of minimal surfaces), and in a variety of applied problems (e.g., crystal or grain growth, phase transitions, flame propagation, image processing).

The most fundamental problem is the *pure mean curvature flow*, where the normal velocity is given by mean curvature. Under such motion, interfaces contract smoothly to enclose zero volume in finite time. To preserve these phase volumes, the average curvature over all interfaces is added to the normal velocity, which regularizes the flow. Such *volume-preserving mean curvature flow* often appears in applications where physical systems (e.g. soap bubbles, droplets, cell structures) evolve to minimize its surface energy while preserving mass. This is also of interest in image processing where smoothing without shrinkage is desired to preserve significant image features.

Due to its theoretical and practical interest, a variety of computational techniques for mean curvature flow have been proposed. Of particular interest is the MBO threshold dynamics [68] where the characteristic function of each phase region is diffused and sharpened separately (taking the $\frac{1}{2}$-level set as the interface). Such level set approach allows the method to naturally handle complicated topological changes and does not require explicit calculation of mean curvature. Its major drawback, however, is its time and grid restrictions on nonadaptive meshes. To address this issue, Esedoglu et al.[36] suggested using the signed distance function, in place of the characteristic function. This provides the needed subgrid accuracies on a uniform mesh to accurately locate the interface and proceed the evolution without stagnation.

Volume-preserving motions can also be produced by thresholding at the level set which preserves the prescribed volume [85]. Unfortunately, this cannot be easily extended to the multiphase case, since average mean curvature of each interface varies, causing interfaces to overlap or create vacuums. To resolve this issue, Švadlenka et al.[94] proposed a vector analogue of the original MBO scheme using a variational approach to solve the vector-valued heat equation and treat the volume constraint via penalization. However, due to the inherent MBO time and grid restrictions, a temporary and localized refinement is introduced in the algorithm.

In this thesis, we are interested in two main points. First, we introduce a signed distance vector modification to the MBO threshold dynamics – a scheme that benefits the main features of its predecessors whilst resolving their key issues. To be precise, we develop a method for realizing volume-preserving multiphase mean curvature flow that (1) naturally handles changes in topology, (2) incorporates interfacial distances in order to alleviate the well-known MBO time and grid restrictions, and (3) set up in a vector-valued fashion to cater any multiphase configuration and easily treat volume constraints using a variational approach via penalization. Using such vector variational scheme, we extend our method to include space-dependent bulk energies and anisotropic energies. The vector analogue of the scalar signed distance function is mathematically appealing since it may provide hint on characterizing multiphase mean curvature flow by interfacial distances as in [8, 41]. It also implicitly contains geometric information of the interface, which defeats the purpose of localized refinement in [94].

Second, we analyze a penalization method related to the above volume-constrained variational problem. In particular, we consider the problem of successively minimizing the functional $\int_\Omega h^{-1}|u-u_{n-1}|^2+|\nabla u|^2$ over all nonnegative functions $u\in H^1(\Omega)$ whose set of positive values have Lebesgue measure equal to $|\{u_0>0\}|$ for a given nonnegative Lipschitz function $u_0\in H^1(\Omega)\cap L^\infty(\Omega)$ and time step size $h>0$. We use an approximation method that penalizes only the increase in measure of the set $\{u>0\}$. We prove the existence and regularity of the sequence of minimizers and investigate their behaviors for sufficiently large penalty value λ. Without relying on the smoothness of the free boundary, we show that the measure of the set $\{u>0\}$ adjusts to its prescribed value provided λ is large enough; hence, the solution to the original problem is attained without having to take λ to infinity. To end, we construct a minimizing movement and show some of its properties.

The thesis is organized as follows. We start with an overview of the pure multiphase mean curvature flow in Chapter 2. In Chapter 3, we construct a vector analogue of the signed distance function (Definition 3.1) and show that this vector distance-based scheme moves the interface according to its mean curvature (Theorem 3.3) and stably imposes symmetric junction angles (Theorem 3.7). The succeeding three chapters extend our method to include volume constraints (Chapter 4), space-dependent bulk energies (Chapter 5), and anisotropic energies (Chapter 6). We present several numerical tests and computational examples of these curvature-driven interface evolutions. Lastly, Chapter 7 presents theoretical results on a penalization method for an evolutionary free boundary problem with volume constraint.

Chapter 2

Overview of Multiphase Mean Curvature Flow

The present chapter provides an introduction to pure multiphase mean curvature flow. In addition, we present previous works on numerical approximation of mean curvature flow highlighting their essential features and key issues in relation to volume preservation and the multiphase case, from which, we build the motivation for this study.

2.1 Multiphase Motion by Pure Mean Curvature

Consider a partition of $\mathbb{R}^N = P_1 \cup P_2 \cup \cdots \cup P_k$ into k phase regions $P_i \subset \mathbb{R}^N$ of positive Lebesgue measure. Define a collection $\Gamma := \bigcup \{\gamma_{ij} : i, j = 1, 2, \ldots, k\}$ of hypersurfaces in $\mathbb{R}^N$ where $\gamma_{ij} = \gamma_{ji}$ denotes the interface separating phases P_i and P_j, that is, $\gamma_{ij} = P_i \cap P_j = \partial P_i \cap \partial P_j (i \neq j)$.

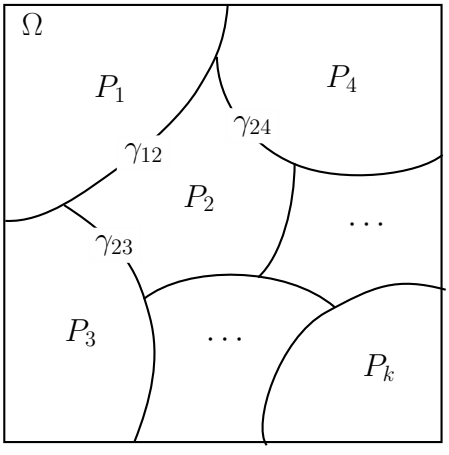

FIGURE 2.1: An illustration of a k-phase configuration of domain Ω.

The objective is to find a family $\{\Gamma(t) := \bigcup \gamma_{ij}(t)\}$ depending on time t such that every point $x \in \gamma_{ij}(t)$ moves with a velocity

$$\mathbf{V}(x) = -\kappa \boldsymbol{\eta}_{ij} \quad \text{on } \gamma_{ij}(t), \tag{2.1}$$

where, κ and $\boldsymbol{\eta}_{ij}$ denotes the mean curvature and unit outer normal from phase P_i to P_j at x, respectively.

Such curvature-driven interface motions often appear in differential geometry and analysis. A number of these literature include local regularity [31, 32]; behaviour of singularities [57–59, 95]; uniqueness and existence of generalized solutions in the two-phase setting – using varifolds of geometric measure theory [14], parametric approach [55], and level-set techniques based on the idea of viscosity solutions [24, 40–43]; as well as, existence, uniqueness, and global regularity of interfacial motion with triple junctions [15, 66]. These problems are not only mathematically appealing, but also of practical interest as it often arises in applications in the physical sciences and engineering. To mention a few, grain boundary motion in annealing pure metals [34, 76], phase changes and moving interfaces [39], fluid dynamics [79, 97], evolution of nanoporosity in dealloying [33], and even, in the field of image processing, e.g. image selective smoothing and edge detection [6, 19, 20, 23, 86].

More often than not, this type of interfacial motion is referred to as *pure multiphase mean curvature flow* since equation (2.1) (as shown in [65, 81]) is derived as the gradient flow for the surface energy functional

$$E(\Gamma) = \sum_{i<j} \int_{\gamma_{ij}} d\mathcal{H}^{N-1} \tag{2.2}$$

where $\mathcal{H}^{N-1}$ denotes the $N-1$-dimensional Hausdorff measure. In this sense, interfaces evolve in order to decrease their surface energies, thereby, playing an important role in the theory of minimal surfaces. In the case when there are three or more phases ($k > 2$), a natural boundary condition arises from the gradient descent for (2.2), known as the symmetric Herring boundary condition which imposes a 120°–120°–120° angle measures at the triple junction [54].

In the two-phase ($k = 2$) setting, on the other hand, it was proven that an interface under mean curvature motion contracts smoothly, becoming more and more spherical, as it shrinks to a point and eventually vanishes in finite time [44, 55]. As an example, consider an N-dimensional sphere of initial radius r_0, then its mean curvature flow is given by

$$\frac{dr}{dt} = -\frac{N-1}{r}, \qquad r(0) = r_0.$$

Hence, the radius of the sphere $r(t)$ at time t is

$$r(t) = \sqrt{r_0^2 - 2(N-1)t},$$

which implies that the sphere shrinks without changing its shape and disappears at time $t = r_0^2/2(N-1)$.

It is also well-known that two-phase mean curvature motion can be characterized in terms of the distance to the interface [8, 41]. More precisely, let $P \in \mathbb{R}^N$ be the phase region whose boundary ∂P coincides with interface Γ. Define the scalar signed distance $\widehat{d} : \mathbb{R}^N \to \mathbb{R}$ by

$$\widehat{d}(x,t) = \operatorname{dist}(x, P(t)) - \operatorname{dist}\big(x, \mathbb{R}^N \backslash P(t)\big)\,.$$

Then, $\nabla\widehat{d}$ and $\Delta\widehat{d}$ gives the outer normal and mean curvature, respectively. Moreover, the normal velocity of a point on the boundary at each time is given by $-\partial\widehat{d}/\partial t$; hence, the evolution is characterized by

$$\frac{\partial\widehat{d}}{\partial t}(x,t) = \Delta\widehat{d}(x,t), \tag{2.3}$$

for any $x \in \partial P(t) = \{\widehat{d}(x,t) = 0\}$, the zero-level set. However, as far as the author's knowledge, such a characterization for the multiphase mean curvature flow has yet to be established and remains an open problem.

2.2 Volume-constrained Interface Evolution

Let us consider the case when interfaces evolve by mean curvature while simultaneously preserving the volume of each phase region, that is, $|P_i(0)| = |P_i(t)|, \quad \forall t \geq 0$ $(i = 1, 2, \ldots, k)$, where $|\cdot| = \mathcal{L}^N(\cdot)$ denotes the N-dimensional Lebesgue measure. This type of motions come in handy in the problem of shape recovery where one achieves smoothing without shrinkage, thereby, preserving important features of the image [29, 87].

This evolutionary problem known as the *volume-preserving multiphase mean curvature motion* is characterized by the velocity of interface that depends on the lengths and curvatures of all other interfaces. In the two-phase case [17, 90], the velocity of interface Γ is simply given by

$$\mathbf{V}(x) = (-\kappa + \kappa_a)\boldsymbol{\eta}(x), \quad x \in \Gamma,$$

where $\kappa_a = \fint_{\Gamma(t)} \kappa(x,t)\, d\mathcal{H}^{N-1}$ denotes the average mean curvature along interface Γ. Adding this extra term κ_a balances the contraction resulting from the pure mean curvature flow and keeps the enclosed volume of the hypersurface constant; thereby regularizing the flow. Under a volume-preserving two-phase flow, a convex hypersurface (interface) remains convex and approaches a constant curvature sphere [9, 45, 56]. Other literature on this problem include existence of global solution starting from non-convex initial hypersurfaces [35] and studies related to constant mean curvature surfaces between parallel places, in particular, stability of cylinders [11] and spherical caps [1] under volume-preserving mean curvature flow.

Moreover, it was shown that volume-preserving mean curvature flow arises as a singular limit of a nonlocal Ginzburg-Landau equation, in other words, a nonlocal mean curvature motion of interfaces which preserves mass [16, 83]. For this reason, such curvature-driven interface evolution problems often arises in physical systems where the mass of the phase regions remains constant as in capillarity [92], biological cell structure [13], soap films, soap bubbles, and droplets [98].

2.3 Numerical Methods on MCF Approximation

Due to its wide array of applications, an interesting selection of numerical methods for realizing mean curvature flow (MCF) were proposed. This section introduces a number of these algorithms and presents their pros and cons with emphasis on volume preservation and multiphase case.

2.3.1 Front Tracking Method

Front tracking method [17, 63, 67, 69] takes a fundamentally straightforward approach to approximating mean curvature interface evolutions. It involves direct discretization of a parametrization of interface and approximate its motion by explicit computation of the mean curvature and normal direction at each interfacial discrete point, including the average curvature over all interfaces for the volume-constrained case. In the multiphase case, triple junctions are treated separately in order to satisfy the required Herring angle conditions. Moreover, note that all calculations solely are concentrated on the interface. For this reason, the front tracking method is said to be computationally efficient.

One major drawback of this method is its inability to handle interfaces that cross or have complicated topology. To overcome this problem, one should explicitly detect and treat changes in topology by some selection of rules (e.g. [17] for mean curvature motion of a network of curves). This requires one to enumerate or make assumptions on all possible topological changes that may typically occur. For example, in the two-dimensional case, it is expected (though not proven) that interfaces interact only through junction-junction collisions [66], which translates the problem to detecting junction collisions and perform some form of "numerical surgery" to generate the next interface evolution. For general interface networks, however, this method can be quite impractical to implement, particularly in higher dimensions.

2.3.2 Threshold Dynamics

The threshold dynamics introduced by Merriman, Bence, and Osher (MBO) takes a level set approach for realizing interfacial motions by mean curvature [68]. This scheme is very easy to implement and avoids the complications of the front tracking method – in the sense that it naturally handles topological changes and does not require explicit calculation of the mean curvature and the normal direction.

In the two-phase case, the interface is defined as a boundary of some compact set which evolves through time by alternating two steps: diffusion and thresholding. At each time interval, the $\frac{1}{2}$-level set of the solution of the heat equation (taking the characteristic function of the compact set as the initial condition) approximates the mean curvature evolution of the interface. In fact, this has been extensively shown to converge to the unique viscosity solution of the mean curvature evolution equation [12, 37, 60]

$$\begin{cases} u_t - tr\left\{\left(I - \dfrac{Du \otimes Du}{|Du|^2}\right) D^2 u\right\} = 0 \\ u(0,x) = \chi_\Gamma(x). \end{cases}$$

Unfortunately, this algorithm is also known to suffer from a time and grid restriction on nonadaptive meshes [68]. This means that in order to accurately resolve the interfacial motions via an MBO process, one must appropriately choose time step size Δt so that diffusion proceeds for a long enough time that the half-level set moves at least one grid point. Otherwise, the thresholding step would keep the interface stationary. (For an illustration of MBO stagnation in the one-dimensional case, see Figure 2.2).

In the general multiphase case, the characteristic function of each phase region is diffused and sharpened separately [68, 84], as shown in Algorithm 2.1. Here, the interfaces are

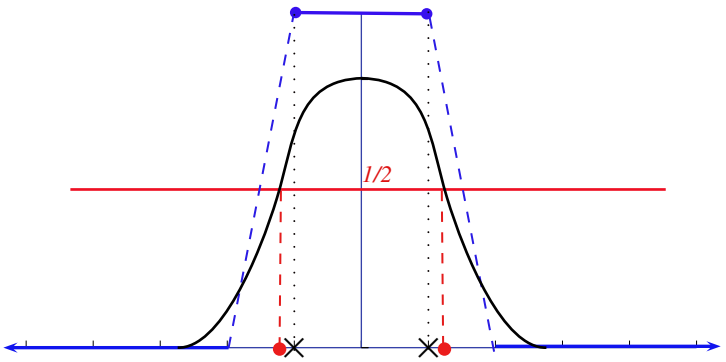

FIGURE 2.2: Thresholding the diffused solution (black) of the characteristic function (blue) reverts to the same characteristic function causing MBO to get "stuck".

taken as the $\frac{1}{2}$-level sets of all k solutions, that is, $\bigcup_{i=1}^{k}\{u_i = \frac{1}{2}\}$. Moreover, the update in the thresholding step maintains the stability of the triple junction imposing symmetric angles [68].

Algorithm 2.1 Multiphase MBO Algorithm

1. INITIALIZATION. Set $u_0^i := \chi_i$, characteristic function of phase P_i $(i = 1, 2, \ldots, k)$.
2. DIFFUSION STEP. For each $i = 1, 2, \ldots, k$, solve scalar heat equation until time Δt:

$$\begin{cases} \dfrac{\partial u^i}{\partial t}(t,x) = \Delta u^i(t,x) & \text{in } (0,\infty)\times\mathbb{R}^N, \\ u^i(0,x) = u_0^i(x) & \text{on } \{t{=}0\}\times\mathbb{R}^N. \end{cases}$$

3. THRESHOLDING STEP. For each $i = 1, 2, \ldots, k$, sharpen the diffused regions by setting u_0^i as the characteristic function of $\{u_i(x) \geq u_j,\ j = 1, 2, \ldots, k\}$.
4. Go back to the diffusion step.

For two-phase volume-preserving motions, Ruuth and Wetton [85] suggested changing the threshold value to $\frac{1}{2} - \frac{1}{2}\kappa_a(t)\sqrt{\pi^{-1}\Delta t}$ where κ_a denotes the average mean curvature along the interface. They showed that at this threshold value, the level set preserves the prescribed phase volume. However, this scheme lacks theoretical justification and cannot be easily extended to the multiphase case. This is because each interface yields different average mean curvature, causing interfaces to possibly overlap or create vacuums.

2.3.3 Distance Function-Based Algorithm

To address the time and grid restriction on the MBO threshold dynamics, Esedoglu, Ruuth, and Tsai proposed replacing the thresholding step by a redistancing scheme [36] where scalar signed distance function is instead, taken as the initial condition in solving the heat equation. Here, the interface is described by the zero-level set of the solution.

Note that the key issue why MBO interface evolutions gets "stuck" lies in the representation of phase regions by the characteristic function. Since the mesh nodal values are

set to either 0 or 1 at the beginning of each time step, the true location of the interface is lost and its discrete representation is pushed to the center of the grid. Unlike characteristic functions, signed distance functions implicitly keep geometric information regarding the interface; thereby, providing subgrid accuracies on a uniform mesh and allows one to accurately locate the interface. Hence, this method usually coined as the "Distance Function-based Diffusion Generated Motion (DFDGM) Algorithm" [34] resolves the mean curvature motion of the interface without the need for adaptive mesh refinement schemes.

As much as DFDGM method alleviates the time and grid restriction, it also inherits both good and bad points of the threshold dynamics. In particular, it can naturally handle complicated topological changes and does not require explicit computations of the mean curvature. However, as in the MBO method, its approximation to volume-preserving mean curvature flow in the multiphase case still remains in question.

2.3.4 Vector-type Threshold Dynamics

Švadlenka, Ginder, and Omata introduced an interesting spin on the threshold dynamics using vectors, while aimed at realizing multiphase mean curvature flow with volume constraint [94]. Since Ruuth's approach [84] can not be easily extended to the volume-presering multiphase case, a need to reformat the multiphase MBO algorithm 2.1 arises. In particular, the authors reformulated the original multiphase MBO scheme in a vector-valued fashion in such a way that volume constraints can be obtained by a constrained gradient flow.

In the two-phase setting ($k = 2$), observe that representing phase regions by the characteristic function is analogous to assigning scalars of equal weights to each phase region, say 1 and -1, the endpoints of a 2-simplex centered at the origin. With this in mind, the authors represented each region in a k-phase configuration, by unit vectors of dimension $k-1$ pointing from the centroid of a standard k-simplex to its vertices called *reference vectors* $\mathbf{p}_i$ $(i = 1, 2, \ldots, k)$. Figure 2.3 shows an example of a 3-phase representation by reference vectors.

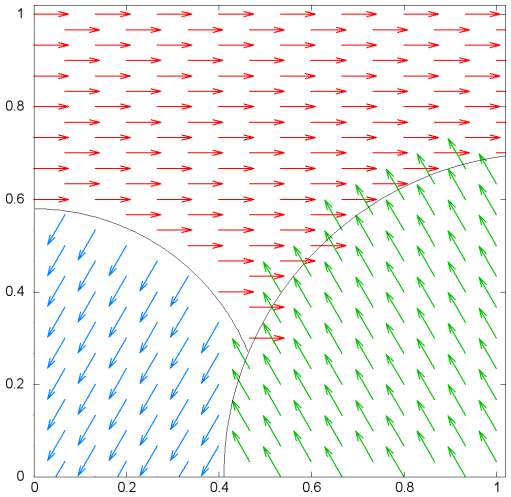

FIGURE 2.3: Assigning corresponding reference vectors to each phase region.

Taking the reference vector field as an initial condition, the vector-valued heat equation is solved followed by a thresholding step that involves finding the closest reference vector to the solution vector at each nodal point (see Algorithm 2.2).

Algorithm 2.2 Vector-type Threshold Dynamics

1. Initialization. Set $\mathbf{u}_0(x) = \mathbf{p}_i$ if $x \in P_i$.
2. Diffusion Step. Solve the vector-valued heat equation until time Δt.
3. Projection Step. Update $\mathbf{u}_0$ by identifying the reference vector closest to solution $\mathbf{u}(\Delta t, x)$, that is,
$$\mathbf{p}_i \cdot \mathbf{u}(\Delta t, x) = \max_{j=1,2,\ldots,k} \mathbf{p}_j \cdot \mathbf{u}(\Delta t, x).$$
This redistribution of reference vectors determines the approximate new phase regions after time Δt, which in turn, defines the new interface network.
4. Go back to the diffusion step.

This method can be thought of as a vector analogue of the original two-phase MBO scheme. In fact, their equivalence can be shown by considering the functions

$$w_i(t, x) = \frac{k-1}{k}\left(\mathbf{u}(t, x) \cdot \mathbf{p}_i + \frac{1}{k-1}\right), \qquad i = 1, 2, \ldots, k.$$

This vector setting allowed the authors to easily treat volume-constrained motions by using a variational approach based on the idea of the discrete Morse flow to solve the vector-valued heat equation and a penalization technique to handle volume constraints.

To overcome the MBO time and grid restriction on nonadaptive meshes, a temporary and localized refinement technique is introduced in the algorithm as follows. Just before the projection step, a record of the interfacial geometry is kept and recalled at the next minimization step. If the interface crosses an element, the geometric information of the interface is used to retriangulate the element and extend the reference vector field, which provides enough subgrid accuracy to proceed to the next evolution.

2.4 Concluding Remarks

We summarize the key features and issues of the above-mentioned numerical methods in Table 2.1. Weighing in both their pros and cons, we think about an MBO-based scheme that takes advantage of the essential features of the above-mentioned modifications whilst resolving their key issues. In particular, our goal is to develop a method for realizing volume-preserving multiphase mean curvature flow that satisfies all six key features listed in Table 2.1. To do this, we adopt the vector approach in [94] in order to cater any multiphase configuration and easily treat volume constraints using a variational approach via penalization. To inherently resolve the MBO time and grid restrictions, we incorporate interfacial distances as in [36] which provides subgrid accuracies without the need for mesh refinement. This requires us to construct a vector analogue of the scalar signed distance function, which in itself, is of mathematical interest, as it suggests a good starting point to characterize multiphase pure mean curvature flow as in [8, 41] using distances to the interface and derive a partial differential equation analogous to

TABLE 2.1: A Summary of Numerical Methods for Mean Curvature Flow

Features of the Numerical Method	Front Tracking	MBO	Ruuth's Method	DFDGM	Vector MBO
1. does not require direct calculation of mean curvature and normal direction	×	✓	✓	✓	✓
2. handles complicated topological changes	×	✓	✓	✓	✓
3. proceeds the evolution without stagnation	✓	×	—	✓	—
4. can be extended to multiphase case	—	✓	✓	✓	✓
5. preserves volume in two-phase case	✓	×	✓	×	✓
6. preserves volume in multiphase case	—	×	×	×	✓

(Here, "—" means an auxilliary scheme is introduced in the algorithm to resolve the issue.)

the heat equation (2.3). This then, serves as our motivation for designing a signed distance vector approach to approximating volume-preserving mean curvature motions of interfaces separating multiple phase regions, as will be discussed in the succeeding chapters.

Chapter 3

A Vector Distance Approach to Multiphase Mean Curvature Flow

In this chapter, we present an MBO-based scheme [68] for treating multiphase mean curvature motions which combines the vector-valued variational approach in [94] with the idea of using interfacial distances [36] to alleviate the well-known MBO time and grid restriction without the need for an adaptive remeshing technique (e.g. [84, 94]). In section 3.1, we construct such signed distance function in a vector setting, which allows us to handle any number of phases. We then modify the MBO Algorithm in section 3.2. In sections 3.3 and 3.4, we formally show that under this scheme, interfaces evolve according to mean curvature flow and that the symmetric Herring angle condition at the triple junction is preserved, respectively. Finally, in section 3.5, we present how we execute our modified MBO algorithm and some numerical tests and examples.

3.1 Construction of the Signed Distance Vector Field

Consider a partition of $\mathbb{R}^N = P_1 \cup P_2 \cup \cdots \cup P_k$ into k phase regions $P_i \subset \mathbb{R}^N$ of positive Lebesgue measure. Define a collection $\Gamma := \bigcup \{\gamma_{ij} : i, j = 1, 2, \ldots, k\}$ of hypersurfaces in $\mathbb{R}^N$ where $\gamma_{ij} = \gamma_{ji}$ denotes the interface separating phases P_i and P_j, that is,

$$\gamma_{ij} = P_i \cap P_j = \partial P_i \cap \partial P_j.$$

Set up reference vectors $\mathbf{p}_i$ corresponding to each phase region P_i as unit vectors of dimension $k-1$ pointing from the centroid of a standard k-simplex to its vertices. (See Appendix A for details on how these reference vectors are constructed.)

We incorporate distances to each phase region P_i, as follows.

Definition 3.1. For $\varepsilon > 0$, we define the **signed distance vector** $\boldsymbol{\delta_\varepsilon} : \mathbb{R}^N \to \mathbb{R}^{k-1}$ by:

$$\boldsymbol{\delta_\varepsilon}(x) := \sum_{i=1}^{k} \left[1 - \min\left(1, \frac{d_i(x)}{\varepsilon}\right)\right] \mathbf{p}_i,$$

where $d_i(\cdot) := dist\,(\cdot, P_i)$ denotes the usual (Euclidean) distance to phase region P_i.

Remark. For any point $x \in \mathbb{R}^N$, the following is true for any pair of reference vectors $\mathbf{p}_i$ and $\mathbf{p}_j$ $(i \neq j)$:

1. If $B(x,\varepsilon) \cap (P_i \cup P_j) = \emptyset$, then $\boldsymbol{\delta}_{\boldsymbol{\varepsilon}}(x) \cdot (\mathbf{p}_i - \mathbf{p}_j) = 0$.
2. If $B(x,\varepsilon) \cap (P_i \cup P_j) \neq \emptyset$, then

$$\boldsymbol{\delta}_{\boldsymbol{\varepsilon}}(x) \cdot (\mathbf{p}_i - \mathbf{p}_j) = \frac{k}{\varepsilon(k-1)} \begin{cases} \varepsilon - d_i(x), & B(x,\varepsilon) \cap P_j = \emptyset \\ d_j(x) - \varepsilon, & B(x,\varepsilon) \cap P_i = \emptyset \\ d_j(x) - d_i(x), & \text{otherwise.} \end{cases}$$

where $B(x,\varepsilon)$ denotes ε-neighborhood of x. Hence,

$$|\boldsymbol{\delta}_{\boldsymbol{\varepsilon}}(x) \cdot (\mathbf{p}_i - \mathbf{p}_j)| \leq \frac{k}{k-1}.$$

Moreover, we note that on interface γ_{ij}, the signed distance vector $\boldsymbol{\delta}_{\boldsymbol{\varepsilon}}$ is defined as the sum of reference vectors $\mathbf{p}_i$ and $\mathbf{p}_j$; while on regions away from the ε-tubular neighborhood of interface Γ, $\boldsymbol{\delta}_{\boldsymbol{\varepsilon}}$ reduces to the reference vector $\mathbf{p}_i$ corresponding to its phase location i.

Example 3.1. *In the two-phase case, $\varepsilon = 1.0$ yields the scalar signed distance function (cf. [36]). In this sense, we see that the vector-valued function $\boldsymbol{\delta}_{\boldsymbol{\varepsilon}}$ is a multiphase extension of the scalar signed distance function.*

Example 3.2. *For any k-phase configuration, the signed distance vector $\boldsymbol{\delta}_{\boldsymbol{\varepsilon}}$ approaches the multiphase vector form of MBO (cf. [94]), as $\varepsilon \to 0$.*

Example 3.3. *A more concrete example of the signed distance vector $\boldsymbol{\delta}_{\boldsymbol{\varepsilon}}$ with $\varepsilon = \frac{1}{6}$ for a four-phase configuration is shown in Figure 3.10.*

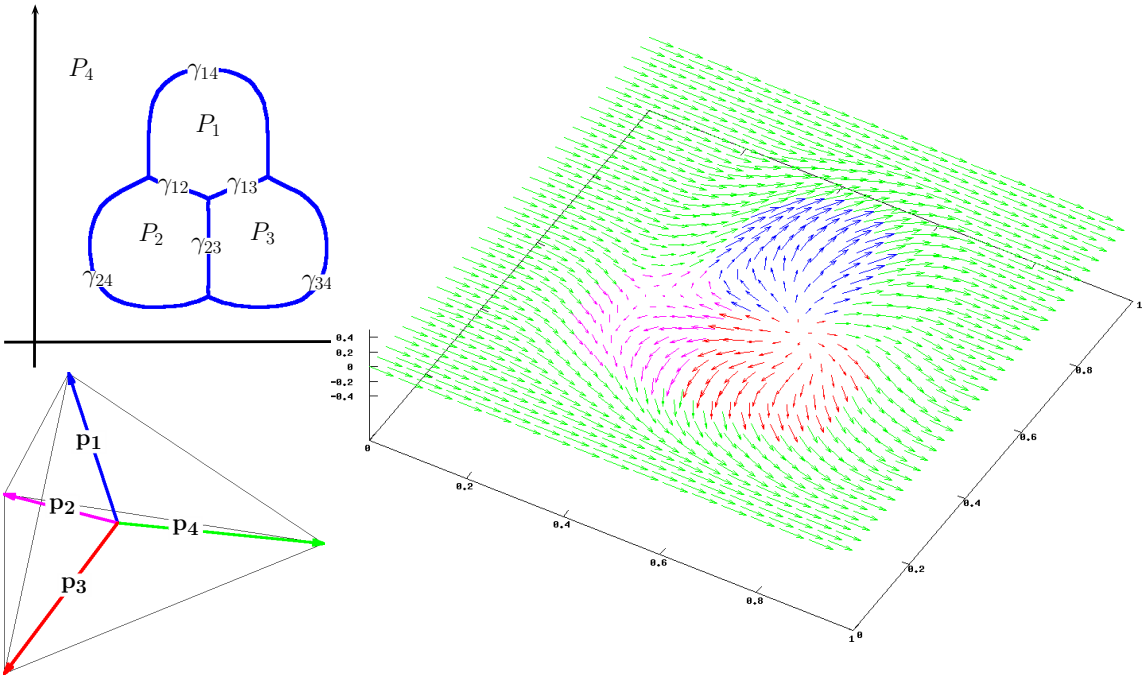

FIGURE 3.1: A 4-phase configuration (top left); the reference vectors $\mathbf{p}_i \in \mathbb{R}^3$ (bottom left); and its corresponding signed distance vector field with $\varepsilon = \frac{1}{6}$ (right).

Note that this construction is continuous, as exhibited in the next theorem.

Theorem 3.2. *For $\varepsilon > 0$, signed distance vector $\boldsymbol{\delta}_{\boldsymbol{\varepsilon}}$ is Lipschitz continuous.*

Proof. For any $x, y \in \mathbb{R}^N$, we see that

$$\begin{aligned} |\boldsymbol{\delta}_{\boldsymbol{\varepsilon}}(x) - \boldsymbol{\delta}_{\boldsymbol{\varepsilon}}(y)| &\leq \frac{1}{\varepsilon}\sum_{i=1}^{k} |\min\{\varepsilon, d_i(y)\} - \min(\varepsilon, d_i(x))|\,|\mathbf{p}_i| \\ &= \frac{1}{\varepsilon}\sum_{i=1}^{k} \begin{cases} |\varepsilon - d_i(x)|, & d_i(x) < \varepsilon \leq d_i(y) \\ |d_i(y) - \varepsilon|, & d_i(y) < \varepsilon \leq d_i(x) \\ |d_i(y) - d_i(x)|, & d_i(x), d_i(y) < \varepsilon \\ 0, & \text{otherwise} \end{cases} \\ &\leq \frac{k}{\varepsilon}|x - y|, \end{aligned}$$

since phase distance d_i is 1-Lipschitz continuous. □

3.2 The Algorithm

In view of the inherent time-grid restriction of the vector-type MBO method [94] on uniform meshes, we claim that taking $\varepsilon \geq \Delta x$ will provide the subgrid accuracy needed to prevent unwanted stagnation of interfaces. In this line, we adopt a similar algorithm as in [94], as follows:

Algorithm 3.1 Signed Distance Vector (SDV) Method for Pure Multiphase MCF

Given an initial interface network $\Gamma_0 := \bigcup\{\gamma_{ij} : i, j = 1, 2, \ldots, k\}$ and a time step size $\Delta t > 0$, we obtain its *mean curvature flow (MCF)* approximation by generating a sequence of time discrete interface networks $\{\Gamma_m\}_{m=1}^{M}$ at times $t = m\Delta t$ $(m = 1, \ldots M)$, as follows:

1. Initialization. Construct $\boldsymbol{\delta}_{\boldsymbol{\varepsilon}}$ with respect to Γ_{m-1}.
2. Diffusion Step. Solve the vector-valued heat equation until time Δt:

$$\begin{cases} \mathbf{u}_t(t, x) = \Delta \mathbf{u}(t, x) & \text{in } (0, \infty) \times \mathbb{R}^N, \\ \mathbf{u}(0, x) = \boldsymbol{\delta}_{\boldsymbol{\varepsilon}}(x) & \text{on } \{t{=}0\} \times \mathbb{R}^N. \end{cases} \tag{3.1}$$

3. Projection Step. For each x, identify the reference vector $\mathbf{p}_i$ closest to the solution $\mathbf{u}(\Delta t, x)$, that is,

$$\mathbf{p}_i \cdot \mathbf{u}(\Delta t, x) = \max_{j=1,2,\ldots,k} \mathbf{p}_j \cdot \mathbf{u}(\Delta t, x). \tag{3.2}$$

This redistribution of reference vectors determines the approximate new phase regions after time Δt, which in turn, defines the new interface network Γ_m.

Our earlier construction of the signed distance vector field [70] is presented in Appendix C. Here, the distance vector is obtained by rotating the sum reference vectors corresponding to the two closest phase regions. The angle of rotation is determined by the distance to the closest interface and the distance to the closest junction point, which in turn, provide the needed subgrid accuracy. In fact, employing this definition of the signed distance vector field as an initial condition in Algorithm 3.1 moves the interface with a normal velocity of minus mean curvature. However, such construction has discontinuities along regions where the point is equidistant to its two closest phase regions. In this sense, Definition 3.1 provides a more stable construction independent of the triple junctions.

3.3 Velocity of Interface

In this section, we estimate the normal velocity of an interface subjected to Algorithm 3.1 and formally show that indeed, it evolves according to mean curvature flow. Here, the interfacial velocity is taken (in the discrete sense) as displacement in the normal direction over time.

Theorem 3.3. *Let $x \in \Gamma := \bigcup\{\gamma_{ij} : i, j = 1, 2, ..., k\}$ such that there exists a unique pair (i, j) for which $x \in \gamma_{ij}$. Then, the normal velocity v of interface Γ at x evolving via SDV method is*

$$v(x) = -\kappa + O(\Delta t), \quad \text{as } \Delta t \to 0,$$

where κ is $(N-1)$-times the mean curvature of Γ at x.

Proof. For simplicity, consider $N = 2$. Fix $\varepsilon > 0$ and select an arbitrary point $x \in \mathbb{R}^2$ on the interface. Without loss of generality, assume $x \in \gamma_{ij}$. Now, rotate and translate the coordinate system so that $x = 0$ in the new coordinate system and the normal $\boldsymbol{\eta}$ to γ_{ij} pointing into P_j lies in the positive x_2 direction.

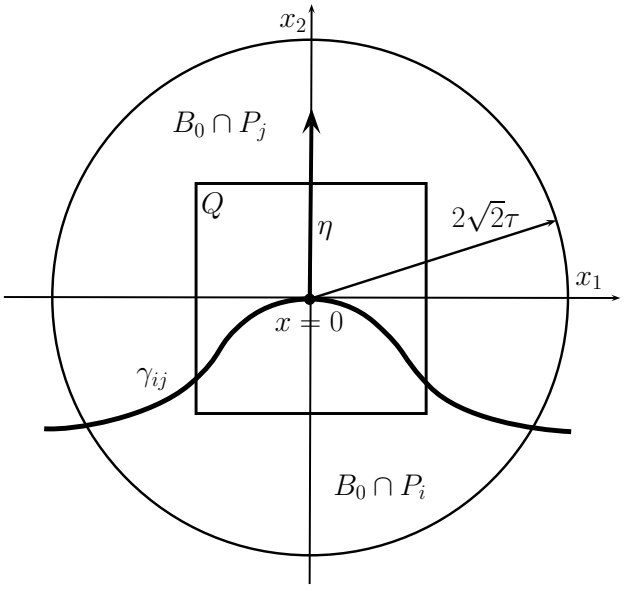

FIGURE 3.2: Setting up interface γ_{ij} in the new coordinate system.

Choose $\tau > 0$, small enough so that $B_0 := B(0, 2\sqrt{2}\tau)$ contains only phases P_i and P_j, that is, for $n \neq i, j$, we have $B_0 \cap P_n = \emptyset$. Assume that there exists a smooth function $\gamma : \mathbb{R} \to \mathbb{R}$ whose graph $(x_1, \gamma(x_1))$ describes the interface γ_{ij} inside the ball B_0. Hence, if κ defines the curvature of the interface γ_{ij} at point $x = (0, 0)$, then $\gamma(0) = 0$, $\gamma'(0) = 0$, and $\gamma''(0) = -\kappa$.

Consider $Q := [-\tau, \tau] \times [-\tau, \tau]$ and assume $\tau < \frac{\varepsilon}{\sqrt{2}}$, which guarantees that every ε-ball centered in Q contains a portion of interface γ_{ij}. Assume further that τ is so small that the following holds:

$$\begin{aligned} d_i(x) &= \operatorname{dist}(x, \gamma_{ij} \cap Q), \qquad \text{if } \ x \in Q \cap P_j, \\ d_j(x) &= \operatorname{dist}(x, \gamma_{ij} \cap Q), \qquad \text{if } \ x \in Q \cap P_i. \end{aligned} \tag{3.3}$$

Let $\mathbf{u}$ be the solution of the vector-type heat equation (3.1). For convenience, we will write t instead of Δt. Then, the normal velocity v of interface γ_{ij} at point $x = 0$ obtained from SDV method can be found from the relation

$$\begin{aligned} 0 &= \mathbf{u}(t, 0, vt) \cdot (\mathbf{p}_i - \mathbf{p}_j) \\ &= \int_Q + \int_{\mathbb{R}^2 \setminus Q} \boldsymbol{\delta_\varepsilon}(x) \cdot (\mathbf{p}_i - \mathbf{p}_j) \Phi_t(x - z) dx =: I + II. \end{aligned}$$

where $z := (0, vt)$. Here, we write the heat kernel as: $\Phi_t(x_1, x_2) := \varphi_t(x_1)\varphi_t(x_2)$ where $\varphi_t(\xi) = \frac{1}{2\sqrt{\pi t}} e^{-\frac{\xi^2}{4t}}$.

Using Remark 3.1, we show that the second integral II is exponentially small:

$$\begin{aligned} |II| &\leq \frac{k}{k-1} \int_{\mathbb{R}} \int_{\mathbb{R} \setminus (-\tau, \tau)} + \int_{\mathbb{R} \setminus (-\tau, \tau)} \int_{\mathbb{R}} \varphi_t(x_1)\varphi_t(x_2 - vt) dx_2 dx_1 \\ &\leq C \left[\int_{\frac{\tau - vt}{2\sqrt{t}}}^{\infty} + \int_{\frac{\tau + vt}{2\sqrt{t}}}^{\infty} e^{-x_2^2} dx_2 + 2 \int_{\frac{\tau}{2\sqrt{t}}}^{\infty} e^{-x_1^2} dx_1 \right] \\ &\leq C \int_{\frac{\tau}{2\sqrt{t}}}^{\infty} e^{-x_1^2} dx_1 \leq C e^{-\frac{\tau^2}{4t}}. \end{aligned} \tag{3.4}$$

(Refer to Lemma D.1 for details on how we arrived at the last inequality (3.4) and Lemmas D.2 and D.3 for succeeding estimates used in this proof.) On the other hand, it follows from Remark 3.1.2 and equation (3.3) that

$$\begin{aligned} I &= \frac{k}{\varepsilon(k-1)} \int_{Q \cap P_i} - \int_{Q \cap P_j} \operatorname{dist}(x, \gamma_{ij} \cap Q) \Phi_t(x - z) dx \\ &= \frac{k}{\varepsilon(k-1)} \int_Q \widehat{d}_{\gamma_{ij} \cap Q}(x) \Phi_t(x - z) dx, \end{aligned} \tag{3.5}$$

where $\widehat{d} : \mathbb{R}^2 \to \mathbb{R}$ denotes the scalar signed distance. Using the Taylor expansion of the scalar signed distance (Proposition B.1) at $x = 0$, equation (3.5) becomes

$$\begin{aligned} I &= \frac{k}{\varepsilon(k-1)} \int_Q \left[\left(x_2 + \tfrac{1}{2}\kappa x_1^2\right) + \left(\tfrac{1}{6}\kappa_{x_1} x_1^3 - \tfrac{1}{2}\kappa^2 x_1^2 x_2\right) + O\Big(|x|^4\Big) \right] \Phi_t(x - z) dx \\ &=: \frac{k}{\varepsilon(k-1)} \left[I_1 + I_2 + I_3 \right]. \end{aligned}$$

We estimate the first integral I in the following claims:

Claim 1. $I_1 = (v+\kappa)\,t + O\Big((1+\tau+\sqrt{t})\sqrt{t}e^{-\frac{\tau^2}{4t}}\Big)$, as $t \to 0$.

Indeed,

$$\begin{aligned}\int_{\mathbb{R}^2} \left(x_2 + \tfrac{1}{2}\kappa x_1^2\right) \Phi_t(x-z)dx &= \int_{\mathbb{R}} x_2\varphi_t(x_2-vt)dx_2 + \kappa\int_0^\infty x_1^2\varphi_t(x_1)dx_1\\ &= \int_{\mathbb{R}} (x_2+vt)\,\varphi_t(x_2)dx_2 + \kappa t\\ &= (v+\kappa)\,t.\end{aligned}$$

Moreover,

$$\begin{aligned}\left|\int_{\mathbb{R}^2\setminus Q} x_2\Phi_t(x-z)dx\right| &\le \int_{\mathbb{R}}\int_{\mathbb{R}\setminus(-\tau,\tau)} + \int_{\mathbb{R}\setminus(-\tau,\tau)}\int_{\mathbb{R}} |x_2|\Phi_t(x_1,x_2-vt)dx_1dx_2\\ &\le \left(\int_{-\infty}^{-\tau-vt} + \int_{\tau-vt}^{\infty} + e^{-\frac{\tau^2}{4t}}\int_{\mathbb{R}}\right)|x_2+vt|\varphi_t(x_2)dx_2\\ &\le C\left(\int_\tau^\infty + e^{-\frac{\tau^2}{4t}}\int_0^\infty\right)(x_2+|v|t)\varphi_t(x_2)dx_2\\ &\le C\left(\sqrt{t}+|v|t\right)e^{-\frac{\tau^2}{4t}},\end{aligned}$$

and

$$\begin{aligned}\left|\int_{\mathbb{R}^2\setminus Q} \tfrac{1}{2}\kappa x_1^2\Phi_t(x-z)dx\right| &\le \int_0^\infty\int_{\mathbb{R}\setminus(-\tau,\tau)} + \int_\tau^\infty\int_{\mathbb{R}} |\kappa|x_1^2\Phi_t(x_1,x_2-vt)dx_1dx_2\\ &\le C|\kappa|\left(t\int_\tau^\infty \varphi_t(x_2)dx_2 + \int_\tau^\infty x_1^2\varphi_t(x_1)dx_1\right)\\ &\le C|\kappa|\left(t+\sqrt{t}(\tau+\sqrt{t})\right)e^{-\frac{\tau^2}{4t}},\end{aligned}$$

which proves the first claim.

Claim 2. $I_2 = -v\kappa^2t^2 + O\Big(\sqrt{t}(\tau+\sqrt{t})e^{-\frac{\tau^2}{4t}}\Big)$, as $t \to 0$.

Indeed,

$$\begin{aligned}\int_{\mathbb{R}^2} \left(\tfrac{1}{6}\kappa_{x_1}x_1^3 - \tfrac{1}{2}\kappa^2x_1^2x_2\right)\Phi_t(x-z)dx &= -\kappa^2\int_0^\infty x_1^2\varphi_t(x_1)\int_{\mathbb{R}} x_2\varphi_t(x_2-vt)dx_1dx_2\\ &= -\kappa^2 t\int_{\mathbb{R}}(x_2+vt)\,\varphi_t(x_2)dx_2 = -v\kappa^2t^2.\end{aligned}$$

Moreover,

$$\begin{aligned}\left|\int_{\mathbb{R}^2\setminus Q} \tfrac{1}{6}\kappa_{x_1}x_1^3\Phi_t(x-z)dx\right| &\le C\left|\int_{\mathbb{R}}\int_{\mathbb{R}\setminus(-\tau,\tau)} + \int_{\mathbb{R}\setminus(-\tau,\tau)}\int_{\mathbb{R}} x_1^3\Phi_t(x_1,x_2-vt)dx_1dx_2\right|\\ &\le C\int_\tau^\infty x_1^3\varphi_t(x_1)dx_1\int_0^\infty \varphi_t(x_2-vt)dx_2\\ &\le C\sqrt{t}\left(\tau+\sqrt{t}\right)^2e^{-\frac{\tau^2}{4t}},\end{aligned}$$

and

$$\begin{aligned}\left|\int_{\mathbb{R}^2\setminus Q} -\tfrac{1}{2}\kappa^2 x_1^2 x_2 \Phi_t(x-z)dx\right| &\leq C\left|\int_{\mathbb{R}}\int_{\mathbb{R}\setminus(-\tau,\tau)} + \int_{\mathbb{R}\setminus(-\tau,\tau)}\int_{\mathbb{R}} x_1^2 x_2 \Phi_t(x_1, x_2 - vt)dx_1 dx_2\right| \\ &\leq C\left(t\int_{\tau}^{\infty} + \sqrt{t}(\tau+\sqrt{t})e^{-\frac{\tau^2}{4t}}\int_0^{\infty}\right)(x_2+|v|t)\varphi_t(x_2)dx_2 \\ &\leq C\left[t\cdot\sqrt{t}e^{-\frac{\tau^2}{4t}} + \sqrt{t}\left(\tau+\sqrt{t}\right)e^{-\frac{\tau^2}{4t}}\cdot|v|t\right] \\ &\leq Ct\sqrt{t}\left(\tau+\sqrt{t}\right)e^{-\frac{\tau^2}{4t}},\end{aligned}$$

proving the second claim.
Claim 3. $I_3 = O(t^2)$, as $t \to 0$.
Indeed,

$$\begin{aligned}|I_3| &\leq C\int_Q \left|x_1^2 + x_2^2\right|^2 \Phi_t(x_1, x_2 - vt)dx_1 dx_2 \\ &\leq C\left(\int_0^{\infty} x_1^4\varphi_t(x_1)\int_{\mathbb{R}}\varphi_t(x_2) + \int_{\mathbb{R}}\varphi_t(x_1)\int_0^{\infty}(x_2+|v|t)^4\varphi_t(x_2)\right)dx_2 dx_1 \\ &\leq Ct^2\left(1+(1+|v|\sqrt{t})^4\right),\end{aligned}$$

which proves the claim.

Finally, it follows from all three claims and equation (3.4) that

$$0 = I + II = \tfrac{k}{\varepsilon(k-1)}\left[(v+\kappa)\,t + O\left((1+\tau+\sqrt{t})\sqrt{t}e^{-\frac{\tau^2}{4t}}\right) + O(t^2)\right] + O(e^{-\frac{\tau^2}{4t}}).$$

This gives $v = -\kappa + O\left(t + (\frac{\varepsilon}{t} + \frac{\tau+1}{\sqrt{t}} + 1)e^{-\frac{\tau^2}{4t}}\right)$, as $t \to 0$. □

3.4 Triple Junction Analysis

In this section, we formally show that SDV scheme (Algorithm 3.1) preserves the symmetric (120°) Herring angle conditions at the triple junction. We utilize a similar argument as in [36], as follows: assume a triple junction at the origin and evolve the configuration via SDV method for one time step $t := \Delta t$; locate the triple junction after time t and denote this by z; and lastly, determine the junction angles at the new junction location point z. We proceed throughout the whole section in this manner.

3.4.1 Heat Kernel Convolution of Phase Distance

To establish the stability of the triple junction, we first need to write down the Taylor expansion of the convolution

$$\zeta^S(z) := \int_{B(0,\tau)} d_S(x)\Phi_t(z-x)dx$$

of distance d_S to the phase region S with the heat kernel $\Phi_t(x)$, when restricted to a τ-neighborhood of the origin (triple junction). In particular, we let S be bounded by two smooth curves intersecting at the origin with an interior angle of $2\theta < \pi$. Without loss of generality, rotate the configuration so that the tangents at the origin form a wedge Σ symmetric with respect to the negative x_2-axis. Choose $\tau > 0$, small enough so that $S \cap B(0,\tau) \subset \mathbb{R} \times (-\infty, 0]$.

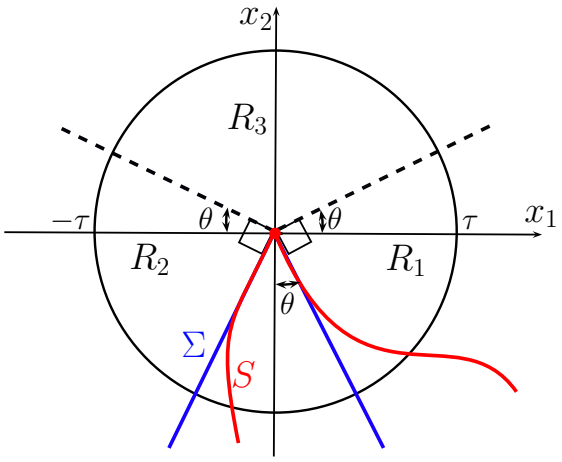

FIGURE 3.3: Approximating phase region S by its corresponding tangent wedge Σ.

We estimate d_S by the distance d_Σ to the approximating wedge Σ and compute its Gaussuan convolution as follows.

Lemma 3.4. *The convolution of distance d_Σ to the tangent wedge Σ with the heat kernel Φ_t, restricted to some open ball $B(0,\tau)$ has the following Taylor expansion at the origin:*

$$\zeta^\Sigma(z) = \frac{\sqrt{t}}{\sqrt{\pi}}\left(\frac{\pi}{2}+1-\theta\right) + \frac{1}{\pi}\left(\frac{\pi}{2}\sin\theta+\cos\theta\right)z_2 + (1+z_2)\,\psi_1(t) + (z_1^2+z_2^2)\psi_2(t)$$
$$+ \frac{4\cos^2\theta+\sin 2\theta+\pi-2\theta}{16\sqrt{\pi t}}z_1^2 + \frac{4\sin^2\theta-\sin 2\theta+\pi-2\theta}{16\sqrt{\pi t}}z_2^2 + O\left(\frac{|z|^3}{t}\right),$$

where $\psi_1(t) = O((1+t+\tau)e^{-\frac{\tau^2}{4t}})$ and $\psi_2(t) = O(t^{-2}(\tau+\sqrt{t})^3 e^{-\frac{\tau^2}{4t}})$, as $t \to 0$.

Proof. Note that

$$d_\Sigma(x) = \begin{cases} x_1\cos\theta + x_2\sin\theta, & \text{in } R_1 := \{x : -x_1\cot\theta \le x_2 \le x_1\tan\theta\} \\ -x_1\cos\theta + x_2\sin\theta, & \text{in } R_2 := \{x : x_1\cot\theta \le x_2 \le -x_1\tan\theta\} \\ |x|, & \text{in } R_3 := \{x : x_2 \ge |x_1|\tan\theta\} \\ 0, & \text{otherwise.} \end{cases}$$

Then, using the integrals in Lemma D.4, we have

$$\int_{R_1\cup R_2} d_\Sigma(x)\Phi_t(x)dx = 2\cos\theta\int_{R_1} x_1\Phi_t(x)dx + 2\sin\theta\int_{R_1} x_2\Phi_t(x)dx$$
$$= \frac{\sqrt{t}}{\sqrt{\pi}}\left[\cos\theta\,(\sin\theta+\cos\theta) + \sin\theta\,(\sin\theta-\cos\theta)\right] = \frac{\sqrt{t}}{\sqrt{\pi}},$$

and

$$\int_{R_3} d_\Sigma(x)\Phi_t(x)dx = \frac{1}{4\pi t}\int_\theta^{\pi-\theta}\int_0^\infty r^2 e^{-\frac{r^2}{4t}}\,dr d\rho = \frac{t}{\sqrt{4\pi t}}\int_\theta^{\pi-\theta} d\rho = \frac{\sqrt{t}}{2\sqrt{\pi}}(\pi-2\theta).$$

Moreover, since $d_\Sigma(x) \le |x|$, then we have

$$\left|\int_{\mathbb{R}^2\setminus B(0,\tau)} d_\Sigma(x)\Phi_t(x)dx\right| \le \frac{1}{4\pi t}\int_0^{2\pi}\int_\tau^\infty r^2 e^{-\frac{r^2}{4t}}\,dr d\phi \le C\left(\tau+\sqrt{t}\right)e^{-\frac{\tau^2}{4t}}.$$

Thus, $\zeta^\Sigma(0) = \frac{\sqrt{t}}{\sqrt{\pi}}\left(\frac{\pi}{2}+1-\theta\right) + O\left((\tau+\sqrt{t})e^{-\frac{\tau^2}{4t}}\right)$, as $t\to 0$.

Next, we evaluate the first partial derivatives of ζ^Σ. Note that d_Σ and Φ_t are symmetric with respect to $x_1 = 0$, then

$$\int_{B(0,\tau)} d_\Sigma(x)\,\frac{\partial}{\partial z_1}\Phi_t(z-x)\Big]_{z=0} dx = \frac{1}{2t}\int_{B(0,\tau)} x_1 d_\Sigma(x)\Phi_t(x)dx = 0,$$

Hence, the partial derivative with respect to z_1: $\zeta^\Sigma_{z_1}(0) = 0$. On the other hand, we see that

$$\int_{R_1\cup R_2} d_\Sigma(x)\,\frac{\partial}{\partial z_2}\Phi_t(z-x)\Big]_{z=0} dx = \int_{R_1}\frac{x_2}{t}\left(x_1\cos\theta + x_2\sin\theta\right)\Phi_t(x)dx = \frac{\sin\theta}{2} - \frac{\cos\theta}{\pi}$$

$$\int_{R_3} d_\Sigma(x)\,\frac{\partial}{\partial z_2}\Phi_t(z-x)\Big]_{z=0} dx = \frac{1}{2t}\int_\theta^{\pi-\theta}\int_0^\infty r^3\sin\rho\,\frac{e^{-\frac{r^2}{4t}}}{4\pi t}\,dr d\rho = \frac{2\cos\theta}{\pi}.$$

Similarly,

$$\left|\int_{\mathbb{R}^2\setminus B(0,\tau)} d_\Sigma(x)\,\frac{\partial}{\partial z_2}\Phi_t(z-x)\Big]_{z=0} dx\right| \le \frac{1}{2t}\int_0^{2\pi}\int_\tau^\infty r^3|\sin\rho|\frac{e^{-\frac{r^2}{4t}}}{4\pi t}\,dr d\rho = O(e^{-\frac{\tau^2}{4t}}).$$

Thus, we get $\zeta^\Sigma_{z_2}(0) = \frac{1}{2}\sin\theta + \frac{1}{\pi}\cos\theta + O(e^{-\frac{\tau^2}{4t}})$, as $t\to 0$.

Continuing with the quadratic terms, we have

$$\begin{aligned}
\int_{R_1\cup R_2} d_\Sigma(x)\,\frac{\partial^2}{\partial z_1^2}\Phi_t(z-x)\Big]_{z=0} dx &= \frac{1}{t}\int_{R_1} d_\Sigma(x)\left(\frac{x_1^2}{2t}-1\right)\Phi_t(x)dx \\
&= \frac{1}{2t^2}\int_{R_1}\left(x_1^3\cos\theta + x_1^2 x_2\sin\theta - 2t d_\Sigma(x)\right)\Phi_t(x)dx \\
&= \frac{1}{2\sqrt{\pi t}}\left(\sin 2\theta + \cos^2\theta\right),
\end{aligned}$$

and

$$\begin{aligned}
\int_{R_3} d_\Sigma(x)\,\frac{\partial^2}{\partial z_1^2}\Phi_t(z-x)\Big]_{z=0} dx &= \frac{1}{4t^2}\int_{R_3}|x|\left(x_1^2-2t\right)\Phi_t(x)dx \\
&= \frac{1}{8t^2\sqrt{\pi t}}\int_0^\infty\int_\theta^{\pi-\theta} r^2\left(r^2\cos^2\rho - 2t\right)\varphi_t(r)d\rho dr \\
&= \frac{1}{8\sqrt{\pi t}}\left(\pi - 2\theta - 3\sin 2\theta\right).
\end{aligned}$$

Moreover,

$$\begin{aligned}\left|\int_{\mathbb{R}^2\setminus B(0,\tau)} d_\Sigma(x)\,\frac{\partial^2}{\partial z_1^2}\Phi_t(z-x)\Big|_{z=0}dx\right| &\le \int_{\mathbb{R}^2\setminus B(0,\tau)}|x|\left|\frac{x_1^2-2t}{4t^2}\right|\Phi_t(x)dx\\ &\le C\int_\tau^\infty r^2\frac{r^2+t}{t^3}e^{-\frac{r^2}{4t}}dr\\ &\le \quad C\frac{(\tau+\sqrt{t})^3}{\tau^2}e^{-\frac{\tau^2}{4t}}\end{aligned}$$

Hence, we get

$$\zeta^\Sigma_{z_1z_1}(0)=\frac{1}{8\sqrt{\pi t}}\left(4\cos^2\theta+\sin 2\theta+\pi-2\theta\right)+O(\tau^{-2}(\tau+\sqrt{t})^3e^{-\frac{\tau^2}{4t}}),\quad t\to 0.$$

Similarly,

$$\zeta^\Sigma_{z_2z_2}(0)=\frac{1}{8\sqrt{\pi t}}\left(4\sin^2\theta-\sin 2\theta+\pi-2\theta\right)+O(\tau^{-2}(\tau+\sqrt{t})^3e^{-\frac{\tau^2}{4t}}),\quad t\to 0.$$

In addition, since

$$\frac{\partial}{\partial z_2\partial z_1}\Phi_t(z-x)\Big|_{z=0}=\frac{x_1x_2}{4t^2}\Phi_t(x),$$

then by a symmetry argument, we have $\zeta^\Sigma_{z_1z_2}(0)=0$. Finally, since d_Σ is 1-Lipschitz, then for $k\ge 3$, we have

$$\left|\zeta^\Sigma_{z_{i_1}z_{i_2}\cdots z_{i_k}}(0)\right|\le\int_{\mathbb{R}^2}\left|\frac{\partial}{\partial x_{i_k}}d_\Sigma(x)\right|\left|\frac{\partial^{k-1}}{\partial x_{i_1}\cdots\partial x_{i_{k-1}}}\Phi_t(x)\right|dx\le Ct^{\frac{1-k}{2}}.$$

□

Using the above approximation, we can now set up the heat kernel convolution of the distance d_S to phase region S.

Lemma 3.5. *The Gaussian convolution of phase distance d_S, restricted to some open ball $B(0,\tau)$ satisfies the following Taylor expansion at the origin:*

$$\begin{aligned}\zeta^S(z) \;=\; &\frac{\sqrt{t}}{\sqrt{\pi}}\Big(\frac{\pi}{2}+1-\theta+\psi(t)\Big)+\psi(t)z_1+\frac{1}{\pi}\Big(\frac{\pi}{2}\sin\theta+\cos\theta+\psi(t)\Big)z_2\\ &+\frac{1}{16\sqrt{\pi t}}(4\cos^2\theta+\sin 2\theta+\pi-2\theta+\psi(t))z_1^2+\frac{1}{\sqrt{t}}\psi(t)z_1z_2\\ &+\frac{1}{16\sqrt{\pi t}}(4\sin^2\theta-\sin 2\theta+\pi-2\theta+\psi(t))z_2^2+O\left(t^{-1}|z|^3\right),\end{aligned}$$

where $\psi(t)=O\left(\sqrt{t}\right)$, as $t\to 0$.

Proof. For any $x\in\partial B_r:=\partial B(0,r)$ where $0<r\le\tau\ll 1$, we note that

$$|d_S(x)-d_\Sigma(x)|\le\mathcal{H}\left(\partial S\cap B_r,\partial\Sigma\cap B_r\right)\le Cr^2,$$

where $\mathcal{H}(\cdot,\cdot)$ denotes the Hausdorff distance.

Hence, for $k \geq 0$, we have

$$\begin{aligned}\left|\zeta^S_{i_1 i_2 \cdots i_k}(0) - \zeta^\Sigma_{i_1 i_2 \cdots i_k}(0)\right| &\leq \int_{B(0,\tau)} |d_S(x) - d_\Sigma(x)| \left| \frac{\partial^k}{\partial x_{i_1} \cdots \partial x_{i_k}} \Phi_t(x) \right| dx \\ &\leq C \int_{\mathbb{R}^2} |x|^2 \left| \frac{\partial^k}{\partial x_{i_1} \cdots \partial x_{i_k}} \Phi_t(x) \right| dx \\ &\leq \frac{C}{t^{k+1}} \int_0^\infty r^{k+3} e^{-\frac{r^2}{4t}} dr \leq C t^{\frac{2-k}{2}}.\end{aligned}$$

Finally, adjusting Lemma 3.4 to the above estimates yields the desired result. □

3.4.2 Stability of the Triple Junction

For simplicity, take $N = 2$. Consider a triple junction of a k-phase network where three interfaces meet, say γ_{12}, γ_{13} and γ_{23}. Let $2\theta_i$ be the interior angle of phase region $P_i (i = 1, 2, 3)$ at the triple junction. Without loss of generality, translate and rotate the whole plane $\mathbb{R}^2$ so that the junction is at the origin and P_1-boundary interfaces γ_{12} and γ_{13} make an angle of $\theta_1 \in (0, \frac{\pi}{2})$ with the negative x_2 axis, as shown in Figure 3.4.

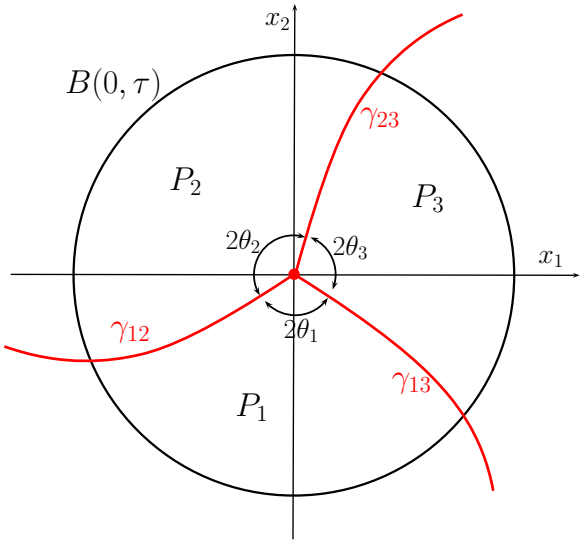

FIGURE 3.4: Setting up the triple junction in the new coordinate system.

Choose $\tau > 0$, small enough so that $P_1 \cap B(0,\tau)$ is in the lower half plane with

$$B(0,\tau) \subset \{x \in P_1 \cup P_2 \cup P_3 : B(x,\varepsilon) \cap P_i \neq \emptyset \ (i = 1, 2, 3)\}$$

and such that for any $x \in P_i \cap B(0,\tau)(i = 1, 2, 3)$, the distance to phase region $P_j (j \neq i)$ satisfies $d_j(x) = \text{dist}(x, \gamma_{ij} \cap B(0,\tau))$. We then perform one step of the SDV method with time step t.

At time t, we determine the location z of the triple junction by solving

$$\begin{cases} \mathbf{u}(t,z) \cdot (\mathbf{p}_1 - \mathbf{p}_2) = 0 \\ \mathbf{u}(t,z) \cdot (\mathbf{p}_1 - \mathbf{p}_3) = 0 \end{cases} \tag{3.6}$$

where $\mathbf{u}$ solves the vector-type heat equation (3.1), that is,

$$\mathbf{u}(t,z) = \int_{B(0,\tau)} + \int_{\mathbb{R}^2\setminus B(0,\tau)} \boldsymbol{\delta_\varepsilon}(x)\Phi_t(x-z)dx =: I + II.$$

For any distinct $i,j \in \{1,2,3\}$, we have by Remark 3.1.2,

$$\begin{aligned} |II\cdot(\mathbf{p}_i-\mathbf{p}_j)| &\le \frac{k}{k-1}\frac{1}{4\pi t}\int_\tau^\infty\int_0^{2\pi} re^{-\frac{r^2-2rs\cos(\theta-\omega)+s^2}{4t}}d\theta dr \\ &\le \frac{C}{t}\int_{\tau-s}^\infty (r+s)e^{-\frac{r^2}{4t}}dr \le C\tfrac{1}{\sqrt{t}}e^{-\frac{\tau^2}{4t}}. \end{aligned} \tag{3.7}$$

where z is written as (s,ω) in polar coordinates. Moreover,

$$I\cdot(\mathbf{p}_i-\mathbf{p}_j) = \frac{k}{\varepsilon(k-1)}\int_{B(0,\tau)}[d_j(x)-d_i(x)]\,\Phi_t(x-z)dx \tag{3.8}$$

$$= \frac{k}{\varepsilon(k-1)}\big[\zeta^j(z)-\zeta^i(z)\big]. \tag{3.9}$$

Here, we write $\zeta^i := \zeta^{P_i}$, the Gaussian convolution of the distance to phase region P_i.

By Lemma 3.5, we have

$$\begin{aligned} \zeta^1(z) &= A(\theta_1)\sqrt{t} + B(\theta_1)z_2 + \tfrac{1}{\sqrt{t}}D(\theta_1)z_1^2 + \tfrac{1}{\sqrt{t}}E(\theta_1)z_2^2 \\ &\quad + \psi(t)(\sqrt{t}+z_1+z_2+\tfrac{1}{\sqrt{t}}z_1z_2) + O(t^{-1}|z|^3) =: \beta(\theta_1,z_1,z_2) \\ \zeta^2(z) &= \beta(\theta_2, -\cos\theta_3 z_1 - \sin\theta_3 z_2, \sin\theta_3 z_1 - \cos\theta_3 z_2) \\ \zeta^3(z) &= \beta(\theta_3, \cos\theta_2 z_1 - \sin\theta_2 z_2, -\sin\theta_2 z_1 - \cos\theta_2 z_2), \end{aligned} \tag{3.10}$$

where

$$\begin{aligned} A(\theta) &= \tfrac{1}{\sqrt{\pi}}\left(\tfrac{\pi}{2}+1-\theta\right) & D(\theta) &= \tfrac{1}{16\sqrt{\pi}}\left(4\cos^2\theta+\sin 2\theta+\pi-2\theta\right) \\ B(\theta) &= \tfrac{1}{\pi}\left(\tfrac{\pi}{2}\sin\theta+\cos\theta\right) & E(\theta) &= \tfrac{1}{16\sqrt{\pi}}\left(4\sin^2\theta-\sin 2\theta+\pi-2\theta\right) \end{aligned}$$

and $\psi(t) = O(\sqrt{t})$, as $t \to 0$. The expansions for ζ^2 and ζ^3 are obtained from ζ^1 by $(\theta_1+\theta_2)$-counterclockwise and $(\theta_1+\theta_3)$-clockwise rotations, respectively.

Remark. From (3.6), (3.7), (3.9) and (3.10), we deduce the following:

1. If $\theta_i = \frac{\pi}{3}$ $(i=1,2,3)$, then z moves with a speed of at most $O(1)$.
2. If $\theta_i = \frac{\pi}{3} + O(1)$ $(i=1,2,3)$, then z moves with a speed of at least $O(\frac{1}{\sqrt{t}})$.

We now locate the triple junction after one SDV time step as follows.

Lemma 3.6. *After time t, the triple junction moves via SDV method from the origin to the point $z=(z_1,z_2)$:*

$$\begin{aligned} z_1 &= \frac{4\sqrt{\pi t}}{3\pi+2\sqrt{3}}(2\theta_2+\theta_1-\pi) + O(\delta\sqrt{t}+t) \\ z_2 &= \frac{4\sqrt{\pi t}}{2+\pi\sqrt{3}}\left(\theta_1-\frac{\pi}{3}\right) + O(\delta\sqrt{t}+t), \end{aligned}$$

where $\delta = \max(\theta_1-\frac{\pi}{3}, \theta_2-\frac{\pi}{3})$.

Proof. Using expansions (3.10) and relations (3.7) and (3.9), we rewrite equation (3.6) in terms of $\xi_i := \frac{1}{\sqrt{t}} z_i$, as follows:

$$\begin{aligned} 0 &= a_0 + b_0\xi_1 - c_0\xi_2 + O(\sqrt{t} + |\xi|^2) \\ 0 &= a_1 - b_1\xi_1 - c_1\xi_2 + O(\sqrt{t} + |\xi|^2) \end{aligned}$$

where the coefficients are given by

$$\begin{aligned} a_0 &= \tfrac{1}{\sqrt{\pi}}(\theta_1 - \theta_2) & a_1 &= \tfrac{1}{\sqrt{\pi}}(\theta_1 - \theta_3) \\ b_0 &= B(\theta_2)\sin\theta_3 & b_1 &= B(\theta_3)\sin\theta_2 \\ c_0 &= B(\theta_2)\cos\theta_3 + B(\theta_1) & c_1 &= B(\theta_3)\cos\theta_2 + B(\theta_1). \end{aligned}$$

Note that

$$\begin{aligned} b_0c_1 + b_1c_0 &= B(\theta_1)B(\theta_2)\sin\theta_3 + B(\theta_2)B(\theta_3)\sin\theta_1 + B(\theta_1)B(\theta_3)\sin\theta_2 \\ &= \tfrac{3\sqrt{3}}{2} B(\tfrac{\pi}{3})B(\tfrac{\pi}{3}) + O(\delta), \\ c_0a_1 - a_0c_1 &= \tfrac{1}{\sqrt{\pi}}[(\theta_1 - \theta_3)(B(\theta_2)\cos\theta_3 + B(\theta_1)) - (\theta_1 - \theta_2)(B(\theta_3)\cos\theta_2 + B(\theta_1))] \\ &= \tfrac{1}{\sqrt{\pi}}\,(\theta_2 - \theta_3)\cdot \tfrac{3}{2} B(\tfrac{\pi}{3}) + O(\delta^2) \\ &= \tfrac{3}{2\sqrt{\pi}} B(\tfrac{\pi}{3})\,(2\theta_2 + \theta_1 - \pi) + O(\delta^2), \\ a_0b_1 + a_1b_0 &= \tfrac{1}{\sqrt{\pi}}\,[(\theta_1 - \theta_2)B(\theta_3)\sin\theta_2 + (\theta_1 - \theta_3)B(\theta_2)\sin\theta_3] \\ &= \tfrac{1}{\sqrt{\pi}}\,(2\theta_1 - \theta_2 - \theta_3)\cdot \tfrac{\sqrt{3}}{2} B(\tfrac{\pi}{3}) + O(\delta^2) \\ &= \tfrac{3\sqrt{3}}{2\sqrt{\pi}} B(\tfrac{\pi}{3})\,\big(\theta_1 - \tfrac{\pi}{3}\big) + O(\delta^2), \end{aligned}$$

where $\delta = \max(\theta_1 - \frac{\pi}{3}, \theta_2 - \frac{\pi}{3})$. Thus, we get

$$\begin{aligned} \xi_1 &= \frac{c_0a_1 - a_0c_1}{b_0c_1 + b_1c_0} + O(\sqrt{t}) = \frac{2\theta_2 + \theta_1 - \pi}{\sqrt{3\pi}B(\frac{\pi}{3})} + O(\delta + \sqrt{t}), \quad \text{as } t \to 0 \\ \xi_2 &= \frac{a_0b_1 + a_1b_0}{b_0c_1 + b_1c_0} + O(\sqrt{t}) = \frac{\theta_1 - \frac{\pi}{3}}{\sqrt{\pi}B(\frac{\pi}{3})} + O(\delta + \sqrt{t}), \quad \text{as } t \to 0. \end{aligned}$$

□

Next, we look at the effect of the SDV interface evolution after time t on the phase interior angles of the triple junction located at point $z := z\,(\theta_1, \theta_2)$ given by Lemma 3.6. Consider the map $\Theta : \mathbb{R}^2 \to \mathbb{R}^2$ which defines the junction angles at time t as follows:

$$\Theta(\theta_1, \theta_2) = \frac{1}{2}\left(\cos^{-1}\!\left(\frac{N_{31}\cdot N_{12}}{\|N_{31}\|\|N_{12}\|}\right),\ \cos^{-1}\!\left(\frac{N_{12}\cdot N_{23}}{\|N_{12}\|\|N_{23}\|}\right)\right),$$

where the normal N^{ij} to interface $\gamma_{ij} (i, j = 1, 2, 3)$ is defined by

$$\begin{aligned} N^{ij}(z) &:= \nabla\left(\mathbf{u}(t, z)\cdot(\mathbf{p}_i - \mathbf{p}_j)\right) \\ &= \tfrac{k}{\varepsilon(k-1)}\left(\zeta^j_{z_1}(z) - \zeta^i_{z_1}(z),\ \zeta^j_{z_2}(z) - \zeta^i_{z_2}(z)\right) + O(e^{-\frac{\tau^2}{4t}}),\ \ t \to 0. \end{aligned}$$

Here, the partial derivatives of ζ^i are computed from expansions (3.10). We now establish the stability of triple junction in the following theorem:

Theorem 3.7. *Let $(\widehat{\theta}_1, \widehat{\theta}_2) := \Theta(\theta_1, \theta_2)$, be the junction angles after time step Δt. Then, there exists a 2×2 matrix M whose largest singular value $\sigma < 1$ such that*

$$\begin{bmatrix} \widehat{\theta}_1 - \frac{\pi}{3} \\ \widehat{\theta}_2 - \frac{\pi}{3} \end{bmatrix} = M \begin{bmatrix} \theta_1 - \frac{\pi}{3} \\ \theta_2 - \frac{\pi}{3} \end{bmatrix} + O(\delta^2 + \sqrt{\Delta t}), \tag{3.11}$$

as $\Delta t \to 0$. Here, $\delta = \max(\theta_1 - \frac{\pi}{3}, \theta_2 - \frac{\pi}{3})$.

Proof. For convenience, we write t instead of Δt. Using the Taylor expansions (3.10), we see that at point $z := z(\frac{\pi}{3}, \frac{\pi}{3})$, we have

$$\|N^{12}\| = \|N^{23}\| = \|N^{31}\| = \tfrac{k\sqrt{3}}{\varepsilon(k-1)} B(\tfrac{\pi}{3}) + O(\sqrt{t}))$$

and

$$N^{31} \cdot N^{12} = N^{12} \cdot N^{23} = -\tfrac{1}{2} \left(\tfrac{k\sqrt{3}}{\varepsilon(k-1)} B(\tfrac{\pi}{3}) \right)^2 + O(\sqrt{t}),$$

as $t \to 0$. Hence,

$$\Theta(\tfrac{\pi}{3}, \tfrac{\pi}{3}) = (\tfrac{\pi}{3}, \tfrac{\pi}{3}) + O(\sqrt{t}), \quad t \to 0.$$

On the other hand, write $\Theta := (\frac{1}{2}\cos^{-1}\Psi^1, \frac{1}{2}\cos^{-1}\Psi^2)$. Hence, $\Psi^i(\frac{\pi}{3}, \frac{\pi}{3}) = -\frac{1}{2}$, for $i = 1, 2$. Now, using expansions (3.10) and Lemma 3.6, we arrive at the following partial derivatives:

$$\begin{aligned} \Psi^1_{\theta_1}(\tfrac{\pi}{3}, \tfrac{\pi}{3}) &= \|N^{12}\|^{-2} \big[\big(N^{31} - \Psi^1 N^{12}\big) \cdot N^{12}_{\theta_1}(\tfrac{\pi}{3}, \tfrac{\pi}{3}) + \big(N^{12} - \Psi^1 N^{31}\big) \cdot N^{31}_{\theta_1}(\tfrac{\pi}{3}, \tfrac{\pi}{3}) \big] \\ &= -\frac{\sqrt{3}}{4} \left[1 + \sqrt{3} \frac{B'(\frac{\pi}{3})}{B(\frac{\pi}{3})} + \frac{2\sqrt{3}}{\sqrt{\pi}} \frac{E(\frac{\pi}{3}) - D(\frac{\pi}{3})}{B(\frac{\pi}{3})^2} \right] + O(\sqrt{t}) \\ &=: \quad \alpha + O(\sqrt{t}), \qquad t \to 0. \end{aligned}$$

In a similar fashion, we get

$$\begin{aligned} \Psi^1_{\theta_2}(\tfrac{\pi}{3}, \tfrac{\pi}{3}) &= O(\sqrt{t}), \quad t \to 0, \\ \Psi^2_{\theta_1}(\tfrac{\pi}{3}, \tfrac{\pi}{3}) &= O(\sqrt{t}), \quad t \to 0 \\ \Psi^2_{\theta_2}(\tfrac{\pi}{3}, \tfrac{\pi}{3}) &= \alpha + O(\sqrt{t}), \quad t \to 0. \end{aligned}$$

(See Appendix E for details on how the above calculations were carried out.) It follows that

$$D\Theta(\tfrac{\pi}{3}, \tfrac{\pi}{3}) = -\tfrac{\sqrt{3}}{3} \begin{bmatrix} \alpha & 0 \\ 0 & \alpha \end{bmatrix} + O(\sqrt{t}),$$

as $t \to 0$. Take $M := -\frac{\sqrt{3}}{3}\alpha \mathbf{I_2}$ whose singular value $\sigma = \frac{\sqrt{3}}{3}\alpha \approx 0.2451 < 1$. Finally, equation (3.11) follows from the Taylor expansion of Θ near $(\frac{\pi}{3}, \frac{\pi}{3})$. □

The above theorem guarantees that at every time step of SDV algorithm 3.1, the phase interior angles at the triple junction that are initially close to the symmetric configuration will always tend to get closer to $\frac{2\pi}{3}$ with an error of order $\sqrt{\Delta t}$. In fact, it follows from Theorem 3.11 that over a period of time $T \geq 0$ (assuming no topological changes occured on the interface evolving via SDV method with time step size Δt), the junction angles

stably imposes the symmetric Herring condition [54] at the triple junction, as exhibited in the following corollary.

Corollary 3.8. *At time step $n = \lfloor T/\Delta t \rfloor$, let $\theta_i^n\,(i = 1, 2)$ be the angle measure at triple junction $x = 0$ of an interface network evolving via SDV method. Then, for some constant $C > 0$,*

$$\left|\theta_i^n - \frac{\pi}{3}\right| \;\leq\; C\left(\sqrt{\Delta t} + \sigma^{\lfloor T/\Delta t \rfloor}\right).$$

Proof. Fix $n = \lfloor T/\Delta t \rfloor$ for a given time $T > 0$. Denote $x_n = |\theta_1^n - \frac{\pi}{3}|$, $y_n = |\theta_2^n - \frac{\pi}{3}|$, and $\delta_n = \max(x_n, y_n)$. Applying Theorem 3.7 iteratively gives

$$\begin{aligned}
x_n &\leq \sigma x_{n-1} + C\left(\delta_{n-1}^2 + \sqrt{\Delta t}\right)\\
&\leq \sigma\left(\sigma x_{n-2} + C\left(\delta_{n-2}^2 + \sqrt{\Delta t}\right)\right) + C\left(\delta_{n-1}^2 + \sqrt{\Delta t}\right)\\
&= \sigma^2 x_{n-2} + C\,(1+\sigma)\sqrt{\Delta t} + C\left(\delta_{n-1}^2 + \sigma\delta_{n-2}^2\right)\\
&\leq \sigma^2\left(\sigma x_{n-3} + C\left(\delta_{n-3}^2 + \sqrt{\Delta t}\right)\right) + C\,(1+\sigma)\sqrt{\Delta t} + C\left(\delta_{n-1}^2 + \sigma\delta_{n-2}^2\right)\\
&= \sigma^3 x_{n-3} + C\left(1+\sigma+\sigma^2\right)\sqrt{\Delta t} + C\left(\delta_{n-1}^2 + \sigma\delta_{n-2}^2 + \sigma^2\delta_{n-3}^2\right)\\
&\;\;\vdots\\
&\leq \sigma^n x_0 + C\left(1+\sigma+\cdots+\sigma^{n-1}\right)\sqrt{\Delta t} + C\left(\delta_{n-1}^2 + \sigma\delta_{n-2}^2 + \cdots + \sigma^{n-1}\delta_0^2\right)\\
&= \frac{C\sigma}{1-\sigma}\sqrt{\Delta t} + \sigma^n\left(x_0 - \frac{C\sqrt{\Delta t}}{1-\sigma}\right) + C\sum_{j=1}^{n}\sigma^{j-1}\delta_{n-j}^2
\end{aligned}$$

Note that $\delta_j = O(\sigma\delta_{j-1} + \sqrt{\Delta t})$ where $j = 1, 2, \ldots, n$. Then at any jth time step, we have

$$\delta_j^2 \leq C\left(\sigma\delta_{j-1} + \sqrt{\Delta t}\right)^2 \leq C\left(\sigma^2\delta_{j-1}^2 + \Delta t\right)$$

Hence,

$$\begin{aligned}
\sum_{j=1}^{n}\sigma^{j-1}\delta_{n-i}^2 &= \delta_{n-1}^2 + \sigma\delta_{n-2}^2 + \sigma^2\delta_{n-3}^2 + \cdots + \sigma^{n-1}\delta_0^2\\
&\leq C\left(\sigma^2\delta_{n-2}^2 + \Delta t\right) + \sigma\delta_{n-2}^2 + \sigma^2\delta_{n-3}^2 + \cdots + \sigma^{n-1}\delta_0^2\\
&\leq C\left(\sigma+\sigma^2\right)\delta_{n-2}^2 + C\Delta t + \sigma^2\delta_{n-3}^2 + \cdots + \sigma^{n-1}\delta_0^2\\
&= C\sigma\,(1+\sigma)\,\delta_{n-2}^2 + C\Delta t + \sigma^2\delta_{n-3}^2 + \cdots + \sigma^{n-1}\delta_0^2\\
&\;\;\vdots\\
&\leq C\sigma^{n-1}\left(1+\sigma+\cdots+\sigma^{n-1}\right)\delta_0^2 + C\left(1+\sigma+\cdots+\sigma^{2(n-2)}\right)\Delta t\\
&= C\sigma^n\frac{1-\sigma^{n-1}}{1-\sigma}\delta_0^2 + C\frac{\sigma(1-\sigma^{2(n-2)})}{1-\sigma}\Delta t\\
&= \sigma^n\frac{C\delta_0^2}{1-\sigma} - C\sigma^{2n-1}\frac{\delta_0^2}{1-\sigma} + \frac{C\sigma}{1-\sigma}\Delta t - C\sigma^{2n-3}\frac{\Delta t}{1-\sigma}\\
&= \sigma^n\frac{C\delta_0^2}{1-\sigma} + \frac{C\sigma}{1-\sigma}\Delta t - C\sigma^{2n}\frac{\delta_0^2\sigma^2 + \Delta t}{\sigma^3(1-\sigma)},
\end{aligned}$$

which gives the desired result. The same holds for y_n. □

3.5 Numerical Results

In this section, we present several numerical tests and experiments, starting with our treatment of the numerical computations involved in our algorithm. In addition, we look at how well our method compares to the original MBO method [68] and present some computational examples.

3.5.1 Numerical Computations

We adopt a variational method centered on the idea of a vector-type discrete Morse flow (DMF), which solves the heat equation by discretizing time and defining a sequence of minimization problems approximating the original problem [61, 82] (see Appendix F). For a k-phase configuration of domain $\Omega \subset \mathbb{R}^N$, we impose Neumann boundary conditions and rewrite the multiphase SDV algorithm 3.1 for approximating mean curvature flow, as follows:

Algorithm 3.2 SDV Method for Pure Multiphase MCF via Minimization

Given an initial interface network $\Gamma_0 := \bigcup \{\gamma_{ij} : i, j = 1, 2, \ldots, k\}$ and a time step size $\Delta t > 0$, we obtain its MCF approximation by generating a sequence of time discrete interface networks $\{\Gamma_m\}_{m=1}^{M}$ at times $t = m\Delta t$ $(m = 1, \ldots M)$, as follows:

1. Initialization. Set $\mathbf{u}_0 := \boldsymbol{\delta}_{\boldsymbol{\varepsilon}}$ with respect to Γ_{m-1}.
2. Minimization. Discretize $\Delta t = h \times K$ and successively solve the following problem for $n = 1, 2, \ldots, K$:

$$\mathcal{J}_n^h(\mathbf{u}) = \int_\Omega \left(\frac{|\mathbf{u} - \mathbf{u}_{n-1}|^2}{2h} + \frac{|\nabla \mathbf{u}|^2}{2} \right) dx. \tag{3.12}$$

3. Projection. Define the new interface $\Gamma_m = \bigcup_{i \neq j} (\partial P_i(\mathbf{u}_K) \cap \partial P_j(\mathbf{u}_K)) \cap \Omega$ where

$$P_i(\mathbf{u}) := \left\{ x \in \Omega : \mathbf{p}_i \cdot \mathbf{u}(\Delta t, x) = \max_{j=1,2,\ldots,k} \mathbf{p}_j \cdot \mathbf{u}(\Delta t, x) \right\},$$

the set corresponding to phase P_i with respect to $\mathbf{u}$.

In constructing the signed distance vector $\boldsymbol{\delta}_{\boldsymbol{\varepsilon}}$, we compute the distance d_i of each node to phase region P_i using the exact Euclidean distance to its piecewise linear interface. We then improve the value accurate to second order by fitting a circle into the three discrete interface points closest to the point projection of the node onto the piecewise linear interface, and computing the distance to the fitted circle.

We approximate functional by utilizing the finite element method (FEM). The domain Ω is triangulated into a finite number of elements, over which the function is assumed to be piecewise linear and continuous. Throughout the whole paper, we use a nearly uniform mesh where interior elements are isosceles triangles whose base and altitude are both equal to the mesh size Δx. An example of a mesh triangulation of a square domain Ω into 32 elements is illustrated in Figure 3.5.

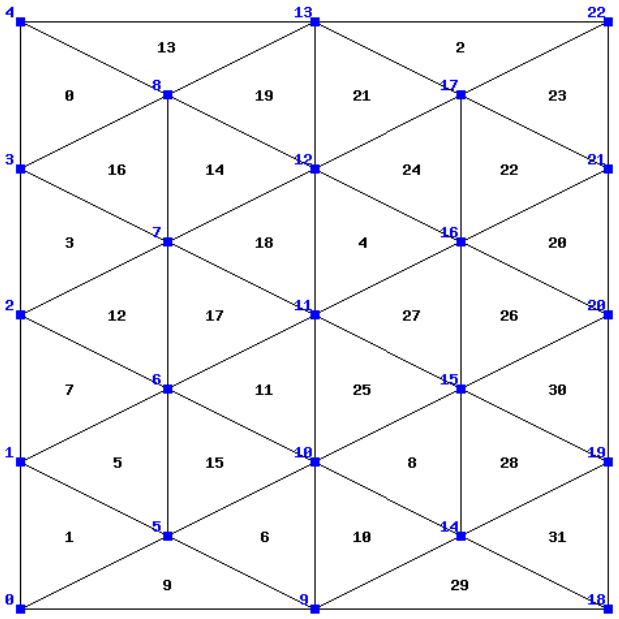

FIGURE 3.5: Triangulating domain $\Omega = [0,1] \times [0,1]$ into 32 nearly uniform elements (black) with 22 nodes (blue).

Moreover, the minimizers are then found via gradient descent method, as follows:

Algorithm 3.3 Steepest Descent Method

To approximate a solution $\mathbf{u}$ to the minimization problem (4.1), we perform:

1. Given an initial approximation $\mathbf{v}$, set $\mathbf{u} := \mathbf{v}$.
2. Set $\mathbf{z} = \nabla \mathcal{J}_n^h(\mathbf{u})$. If $\|\mathbf{z}\|_2 = 0$, then stop.
3. Solve $\min_{\tau>0} \mathcal{J}_n^h(\mathbf{u} - \tau\mathbf{z})$ for step length τ by a bisection line-search method.
4. Set $\mathbf{u} := \mathbf{u} - \tau\mathbf{z}$. Go to step 2.

3.5.2 Error Analysis: Shrinking Circle Test

In this subsection, we consider the classic two-phase problem for testing algorithms realizing mean curvature flow and look at the errors of SDV method in comparison to the original MBO method.

Take a circle of radius $r_0 = 0.35$ on a $[0,1] \times [0,1]$ domain as our initial condition. Note that its mean curvature evolution remains a circle of radius $r(t)$ satisfying

$$\frac{dr}{dt} = -\frac{1}{r} \iff r(t) = \sqrt{r_0^2 - 2t}.$$

For various mesh size and time step configurations, we run the original MBO and SDV method with this initial setup for $\varepsilon = \Delta x, 2\Delta x, 5\Delta x, 1.0$ until the exact extinction time $T = m\Delta t = 0.06125$. We note that SDV method with $\varepsilon = 1.0$ corresponds to the two-phase signed distance (DFDGM) scheme in [34, 36].

At each time step, we use a Least-Squares fitting method to fit the resulting interface points $\{x_i\}$ in a circle and record its radius r_{fit}. In particular, we minimize $\sum_i \left(|x_i - C|^2 - r^2\right)^2$ with respect to the center C and radii r. The error on the radius of the shrinking circle is taken as the average over time $[0, T/2]$. Results are summarized in Table 3.1 for the original MBO method, and Tables 3.3, 3.2, 3.4, and 3.5 for the SDV method with varying ε values.

TABLE 3.1: MBO Method: Errors for varying mesh-time configurations

mesh\time	2	4	8	16	32	64	128	256
10×10	0.01508	0.00604	–	–	–	–	–	–
20×20	0.01229	0.01154	0.00660	0.00294	–	–	–	–
40×40	0.00151	0.00174	0.00072	0.00167	0.00377	–	–	–
80×80	0.00223	0.00171	0.00096	0.00071	0.00069	0.00266	–	–
160×160	0.00088	0.00192	0.00104	0.00047	0.00066	0.00029	0.00053	–
320×320	0.00129	0.00210	0.00120	0.00070	0.00011	0.00010	0.00038	0.00082

TABLE 3.2: SDV Method ($\varepsilon = \Delta x$): Errors for varying mesh-time configurations

mesh\time	2	4	8	16	32	64	128	256
10×10	0.00478	0.00416	0.00684	0.00981	0.01424	0.01912	0.02764	0.04201
20×20	0.00201	0.00257	0.00270	0.00382	0.00505	0.00749	0.01075	0.01540
40×40	0.00224	0.00174	0.00093	0.00097	0.00124	0.00211	0.00351	0.00524
80×80	0.00136	0.00202	0.00083	0.00014	0.00003	0.00024	0.00075	0.00158
160×160	0.00140	0.00202	0.00109	0.00056	0.00015	0.00044	0.00031	0.00006
320×320	0.00147	0.00201	0.00106	0.00053	0.00011	0.00008	0.00040	0.00054

TABLE 3.3: SDV Method ($\varepsilon = 2\Delta x$): Errors for varying mesh-time configurations

mesh\time	2	4	8	16	32	64	128	256
10×10	0.01226	0.00471	0.00523	0.00995	0.01213	0.01189	0.01301	0.02007
20×20	0.00499	0.00258	0.00277	0.00412	0.00506	0.00642	0.00792	0.01015
40×40	0.00290	0.00185	0.00105	0.00120	0.00149	0.00239	0.00375	0.00543
80×80	0.00154	0.00204	0.00084	0.00020	0.00011	0.00037	0.00099	0.00202
160×160	0.00142	0.00202	0.00110	0.00059	0.00010	0.00035	0.00021	0.00014
320×320	0.00147	0.00200	0.00107	0.00054	0.00012	0.00006	0.00037	0.00049

TABLE 3.4: SDV Method ($\varepsilon = 5\Delta x$): Errors for varying mesh-time configurations

mesh\time	2	4	8	16	32	64	128	256
10×10	0.01492	0.00787	0.00428	0.00828	0.01055	0.01100	0.01302	0.02136
20×20	0.02259	0.01325	0.00382	0.00222	0.00371	0.00426	0.00627	0.01031
40×40	0.00834	0.00396	0.00126	0.00173	0.00182	0.00182	0.00227	0.00362
80×80	0.00262	0.00209	0.00098	0.00059	0.00046	0.00063	0.00096	0.00131
160×160	0.00170	0.00204	0.00114	0.00067	0.00004	0.00021	0.00002	0.00033
320×320	0.00153	0.00201	0.00108	0.00056	0.00015	0.00002	0.00031	0.00038

TABLE 3.5: DFDGM ($\varepsilon = 1.0$): Errors for varying mesh-time configurations

mesh\time	2	4	8	16	32	64	128	256
10×10	0.01492	0.00787	0.00428	0.00828	0.01055	0.01100	0.01302	0.02136
20×20	0.02410	0.01402	0.00430	0.00214	0.00372	0.00426	0.00627	0.01032
40×40	0.02570	0.01556	0.00583	0.00105	0.00165	0.00175	0.00229	0.00361
80×80	0.02533	0.01548	0.00611	0.00103	0.00105	0.00089	0.00087	0.00122
160×160	0.02544	0.01557	0.00605	0.00100	0.00091	0.00065	0.00044	0.00045
320×320	0.02555	0.01561	0.00610	0.00100	0.00089	0.00058	0.00032	0.00022

From Table 3.1, we see that as time step Δt decreases relative to the mesh size, the original MBO method ceases to evolve the interface until extinction time as indicated by the symbol "–". This confirms the time-grid restriction of the MBO method on uniform mesh configurations.

On the other hand, SDV evolutions of the interface does not show any tendency of stagnation, which indicates that the distance to the phase regions provides the needed subgrid accuracy to help relax the inherent time-grid restrictions. Note that one can achieve a fairly good MCF approximation using phase distances even on small (at least one mesh size Δx) tubular neighborhood of the interface; thereby, saving computational costs. In particular, smaller ε values behave well on coarse mesh/time configurations. On finer mesh/time configurations, we see that SDV scheme with large ε values gives a better MCF approximation since they hold more geometric information regarding the interface.

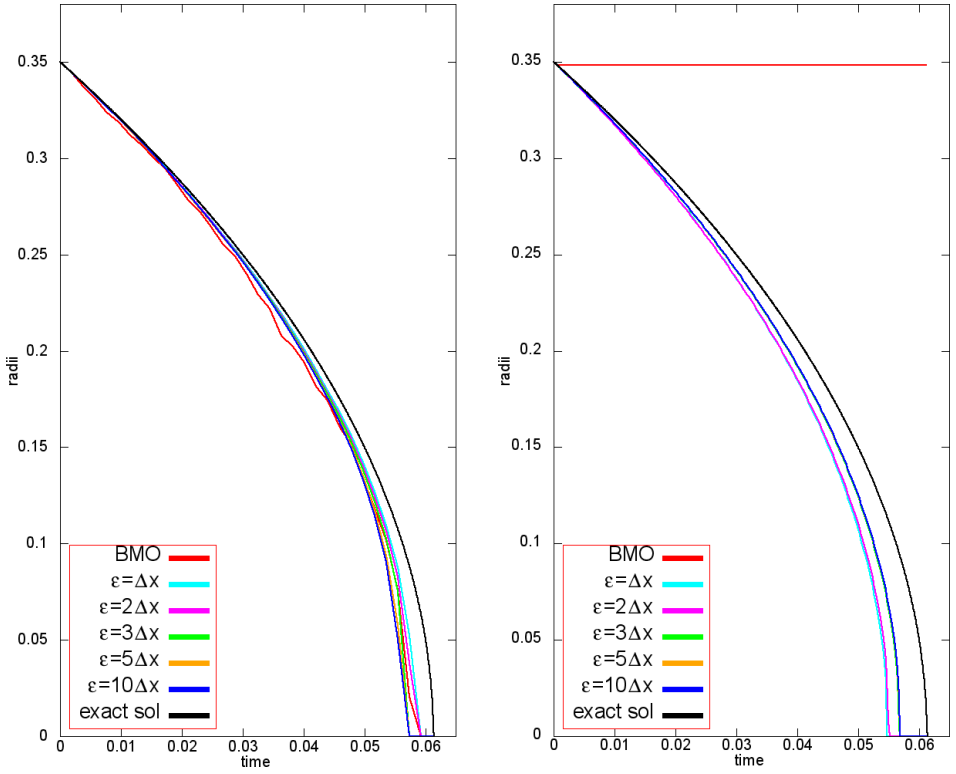

FIGURE 3.6: Evolution of the radius of a circle generated via MBO (red) and SDV method (non-red) on a 40×40 mesh with $\Delta t = T/32$ (left) and $\Delta t = T/256$ (right) versus the exact solution (black).

Take for example, a configuration with 40×40 mesh resolution and time step size $\Delta t = T/32$. In this setup, Table 3.1 seem to indicate that MBO method does not stagnate interface evolution, however, Figure 3.6 reveals that this interface evolution is quite unstable and shows tendency of stagnation. In contrast, SDV method behaves fairly well under this configuration even with a distance tubular range ε as small as the mesh size Δx. Moreover, we observe that SDV method works well even on a smaller time step size $\Delta t = T/256$ after the onset of MBO interface stagnation. Under this configuration, it is noticeable how phase distances help alleviate the MBO time-grid restriction. As is evident from Figure 3.6, SDV mean curvature evolutions with larger $\varepsilon = 5\Delta x, 1.0$ are closer to the exact solution since their signed distance vector $\boldsymbol{\delta_\varepsilon}$ implicitly carries more geometric information regarding the interface.

Note that at certain unevenly distributed configurations, the error unexpectedly jumps to irregular values. We expect that this is caused by numerical hanging of the interface on the nodes in some special cases. Moreover, the error is highly sensitive to the way of its calculation, especially around the initial state and before the extinction. However, it can be said on the whole that the error converges to zero approximately linearly in both space and time, as expected from the MBO approximation and as seen from the error tables.

3.5.3 Triple Junction: Stability Test

In this subsection, we wish to check if our method imposes the symmetric Herring conditions at the triple junction.

Consider a three-phase initial condition where a T-shaped interface is rotated 90° counterclockwise such that the T-junction point is located at point $(0.25, 0.25)$. On a $[0,1] \times [0,1]$ domain, take phase P_3 as the region to the left of line $x = 0.25$, and the remaining top and bottom regions as phases P_1 and P_2, respectively (Figure 3.7).

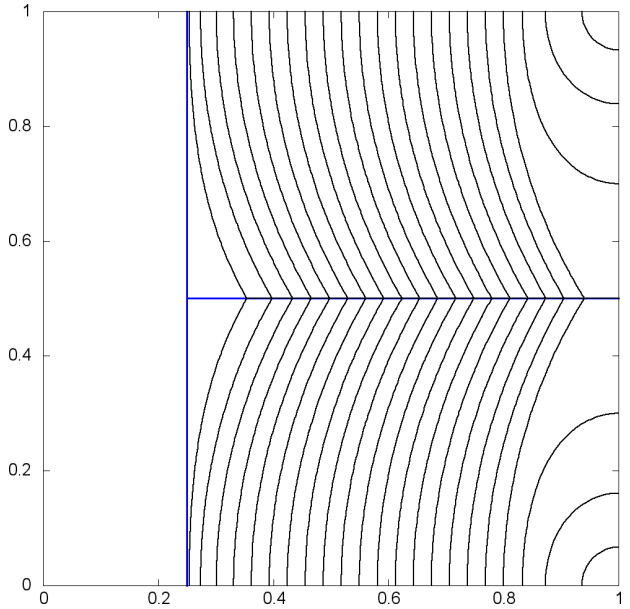

FIGURE 3.7: Evolution of the initial T-junction (blue) via SDV method and its underlying interface network at different times (black).

We triangulate the domain into $12,800$ elements ($\Delta x = 0.0125$) and evolve the interface via SDV method with time step $\Delta t = 1.5 \times 10^{-3}$ and DMF partition $K = 30$. We wish to investigate the evolution of the initial T-junction and its underlying interface network, in particular, we look at the stability of the triple junction.

Let us consider the stable configuration of the problem (cf. [46]). Note that interface γ_{12} lies on the line $y = \frac{1}{2}$ for any $t \geq 0$. Moreover, we can define interface γ_{23} by

$$\gamma_{23}(t, y) := u(y) + vt, \quad y \in (0, \tfrac{1}{2}),$$

where u describes the shape of interface and v denotes its transport velocity. Hence, interface $\gamma_{13}(t, y) = \gamma_{23}(t, \frac{1}{2} - y)$. If the graph $\gamma := \gamma_{23}$ evolves by mean curvature, then it satisfies the equation

$$\frac{\partial \gamma}{\partial t} = \frac{\gamma_{yy}}{1 + \gamma_y^2} \quad \Longleftrightarrow \quad v = \frac{u''}{1 + (u')^2} = \left(\tan^{-1} u'\right)'.$$

By the Neumann boundary condition, we have $u'(0) = 0$, and thus,

$$vy \quad = \quad \tan^{-1} u'(y). \tag{3.13}$$

The Herring condition [54] at the triple junction, on the other hand, gives

$$u'(\tfrac{1}{2}) = \cot(\tfrac{\pi}{3}) = \tfrac{1}{\sqrt{3}}.$$

Hence, the transport velocity $v = 2\tan^{-1}(\frac{1}{\sqrt{3}}) = \frac{\pi}{3}$.

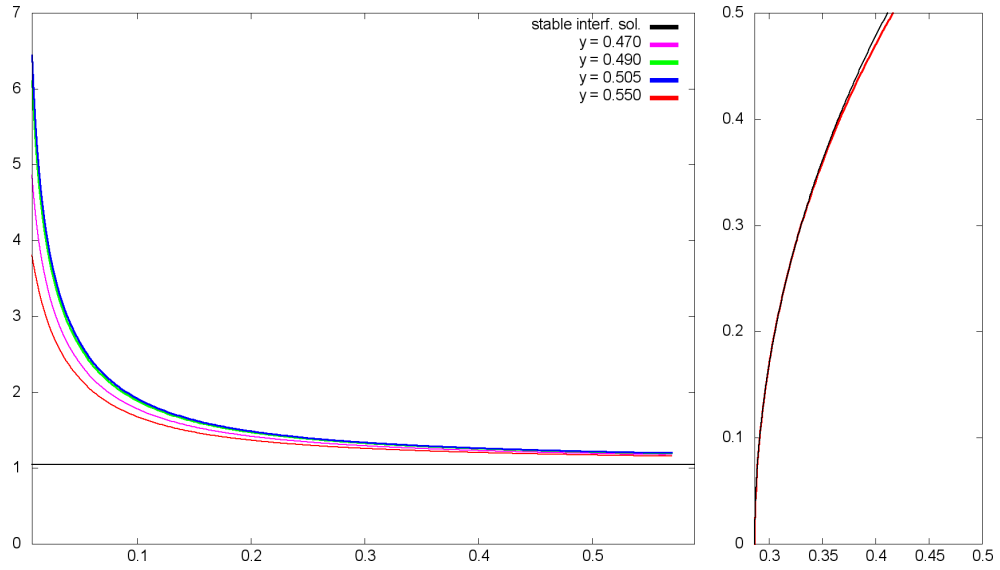

FIGURE 3.8: Transport velocities at $y = 0.47, 0.49, 0.505, 0.55$ (left) and interface profile at time $t = 50\Delta t$ (right) of the SDV numerical solution (colored) versus the constantly transported stable solution (black).

In Figure 3.8, we see that the transport velocity of the numerical interface solution approaches $v = \frac{\pi}{3}$. In fact, for the first few time steps, the interface rapidly approaches the $120°$–$120°$–$120°$ junction angle conditions, and then gradually adjusts itself to reach its stable configuration.

From (3.13), we determine the shape of the constantly transported stable solution by

$$u(y) \quad = \quad -\tfrac{3}{\pi}\ln\left|\cos(\tfrac{\pi}{3}y)\right| + c, \quad y \in (0, \tfrac{1}{2})$$

where the constant c of horizontal shift may be chosen appropriately. Comparing this with the numerical interface solution obtained via SDV method, we see that it is in good agreement with the exact shape of interface in the stable state, as shown in Figure 3.8 for time $t = 50\Delta t$.

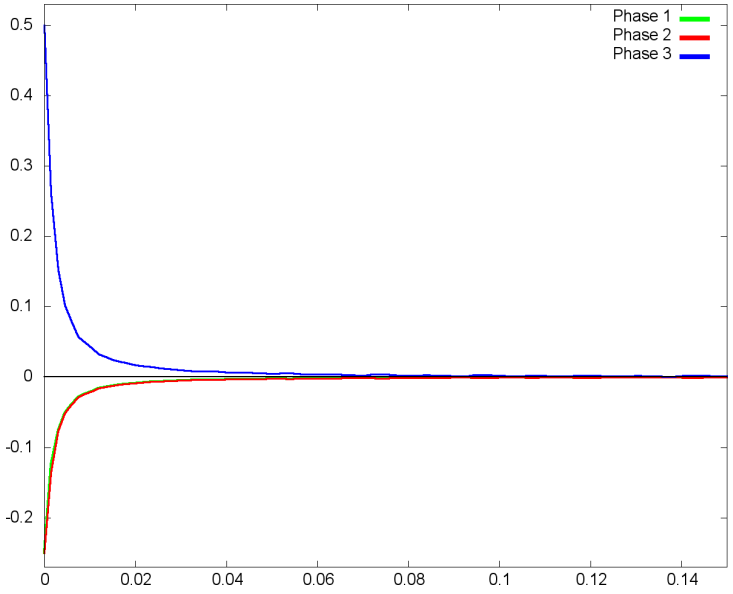

FIGURE 3.9: Relative error plot of the phase interior angle measures at the triple junction for the first 100 time steps.

To end, we measure the junction angles at each time step using the tangents to the quadratic interpolation of the piecewise linear interface near the triple junction. It is evident from the relative error plot (Figure 3.9) that the triple junction first rapidly approximates the angle conditions, which is consistent with the previous result. Thereafter, the numerical interface solution gradually reaches a stable state with junction angles of measure $120^\circ \pm 0.16$ yielding a relative error of at most 0.14%; thereby confirming that our method stably imposes the Herring angle conditions at the triple junction.

3.5.4 Numerical Examples

We present numerical examples of mean curvature evolution using the SDV method. In Figure 3.10, we take a smooth closed curve as an initial condition whose mean curvature evolution shrinks inward to a circle until concentrically collapsing to a single point. We also consider a four-phase initial condition that evolves into a shrinking triple bubble and eventually vanishes. Note that the $120^\circ - 120^\circ - 120^\circ$ angle conditions at the triple junctions are satisfied.

Here, the domain $\Omega := [0,1]\times[0,1]$ is triangulated into $12,800$ elements and the evolution time step $\Delta t = 5.0 \times 10^{-5}$ is discretized into 30 DMF iterations. Note that under this configuration, the original MBO algorithm [68] fails to generate such mean curvature flow approximation as it stagnates after approximately $t = 5\Delta t$. However, our method

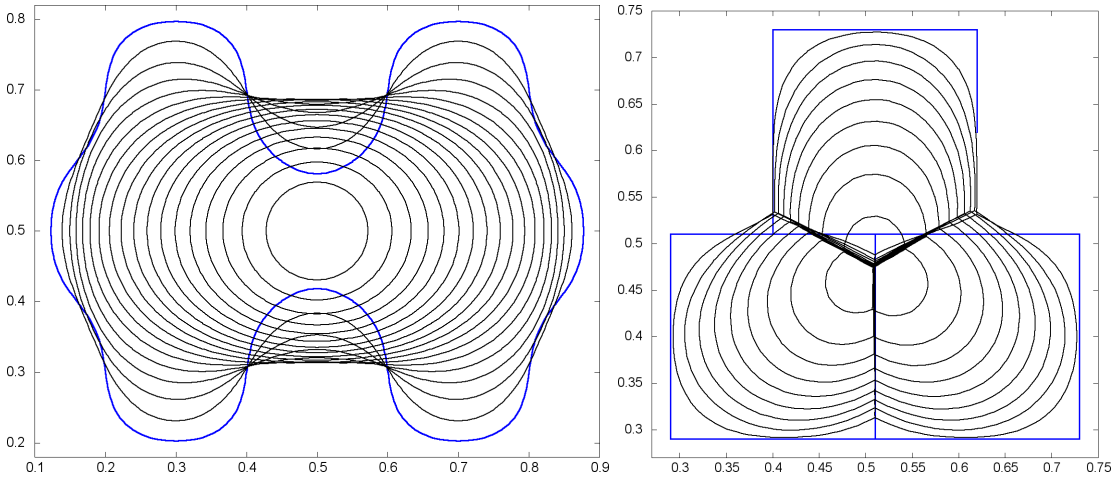

FIGURE 3.10: An example of a two-phase (left) and four-phase (right) mean curvature evolution generated via SDV method.

naturally alleviates this MBO time and grid restriction without having to retriangulate elements based on its interfacial geometry (cf. [94]).

3.6 Concluding Remarks

We designed a method for approximating multiphase mean curvature motion of interfaces using vector-valued signed distance function. Our method is based on the vector reformulation of the alternating diffusion and thresholding scheme of the MBO algorithm. This vector setting allowed us to handle any number of phases. Moreover, using signed distance vector field as the initial condition, we showed that interface evolution via our method does not stagnate on nonadaptive meshes – alleviating the well-known MBO restriction without the need for retriangulization. We also formally established that SDV method evolves interfaces with a normal velocity equal to its minus mean curvature up to a linear order of time and naturally imposes the Herring angle conditions at the triple junction points.

It would also be interesting to know how well this method handles nonsymmetric junction angles. The MBO-based scheme for nonsymmetric junction angles in [88] forces one to either use a finer mesh or a larger time step to prevent stagnation in the generated interfacial motions; hence, its SDV counterpart should be able to alleviate this problem. Lastly, we state an open problem: "Can pure k-phase mean curvature flow be characterized by our construction of signed distance vector, in particular,

$$\boldsymbol{\delta}(x) := \sum_{i=1}^{k} dist\,(x, P_i)\,\mathbf{p}_i,$$

the distance linear combination of the reference vectors $\mathbf{p}_i$? Can the theory in [8, 41] be used and/or extended to the multiphase case?"

Chapter 4

On Volume-preserving Multiphase Mean Curvature Flow

This chapter tackles the problem of incorporating volume constraint in the SDV method, so that a volume-preserving mean curvature motion of the interface is realized. In particular, we look into altering either the diffusion or projection step in Algorithm 3.1, in such a way that the normal velocity of the interface is then given by minus mean curvaure plus a term constant along the interface, which depends on the lengths and average curvatures of all other interfaces. We first look at the problem in the two-phase case and present a method of treating the volume constraint in section 4.1. We then, extend this to the multiphase case in section 4.2. Finally, in section 4.3, we present several numerical tests and examples.

4.1 Two-phase Flow under Volume Constraint

Consider a two-phase mean curvature flow where volumes of both phase regions are preserved. In this case, the velocity of the interface γ is simply given by

$$\mathbf{V}(x) = (-\kappa(x) + \kappa_a)\boldsymbol{\eta}(x), \quad \text{a.e. in } \gamma,$$

where κ is the mean curvature, κ_a is the average mean curvature along the interface and $\boldsymbol{\eta}$ denotes the outer normal to the interface [56]. Ruuth and Wetton [85] introduced a two-phase volume-preserving MBO scheme, which retains solving heat equation with the characteristic function as its initial condition, and treats volume constraint in the thresholding step. Instead of taking the usual $\frac{1}{2}$-level set, the solution is truncated at value $\frac{1}{2} - \frac{1}{2}\kappa_a(t)\sqrt{\pi^{-1}\Delta t}$, that is, the level set which preserves the prescribed volume. This approach automatically evolves the interface with a normal velocity of $-\kappa + \kappa_a$ without having to directly compute the mean curvature or the average mean curvature.

Let us look at the same scheme in the light of the two-phase SDV method. Following the same argument as in the proof of Theorem 3.3, it is easy to show that the prescribed volume will be preserved if we change the threshold value from 0 to $\varepsilon^{-1}\kappa_a\Delta t$. Unfortunately, this cannot be easily extended to the multiphase case, since different interfaces give different average mean curvature values. Phase regions may either overlap, or not

even touch at all, creating vacuums; thus, the global interaction of the phase regions are ignored. Moreover, this scheme lacks theoretical justifications.

In this line, we take a different approach and incorporate the volume constraint into the diffusion process while retaining the same projection step. Let us continue in the two-phase setting and discretize time $\Delta t = h \times K$. We solve the heat equation by successively minimizing the functionals

$$\mathcal{J}_n^h(u) = \int_\Omega \left(\frac{|u - u_{n-1}|^2}{h} + |\nabla u|^2 \right) dx, \quad n = 1, 2, \ldots, K, \tag{4.1}$$

taking u_0 as the scalar ε-signed distance function δ_ε with respect to the interface. Note that the first variation of the above functional yields

$$\begin{aligned} 0 &= \frac{d}{d\tau} \mathcal{J}_n^h(u + \tau\phi)\Big|_{\tau=0} \\ &= 2\int_\Omega \frac{u - u_{n-1}}{h}\phi + \nabla u \cdot \nabla \phi. \\ &= 2\int_\Omega \left(\frac{u - u_{n-1}}{h} - \Delta u \right) \phi + 2\int_{\partial\Omega} \phi \frac{\partial u}{\partial \boldsymbol{\eta}}, \end{aligned}$$

for any $\phi \in C_0^\infty(\Omega)$. Hence, in the weak sense, the minimizer u satisfies

$$\frac{u - u_{n-1}}{h} - \Delta u = 0. \tag{4.2}$$

Moreover, we see that interpolating the corresponding minimizers with respect to time and then taking $h \to 0$ yields the solution of heat equation [82].

We incorporate a volume constraint under Dirichlet boundary conditions into the minimization problem 4.1. In the following theorem, we look at the behaviour of the minimizer on the phase boundary and derive its the free boundary condition.

Theorem 4.1 (cf. [94])**.** *Let u be the minimizer of functional*

$$\mathcal{J}(u) = \int_\Omega \left(\frac{|u - u_*|^2}{h} + |\nabla u|^2 \right) dx, \tag{4.3}$$

over set $A := \{u \in H_0^1(\Omega) : |\{u > 0\}| = V\}$ where $u_* \in H^1(\Omega)$, h denotes the length of the discrete time step, and $V \in (0, |\Omega|)$ is the prescribed volume. Then,

$$\left[(\partial_{\boldsymbol{\eta}} u)^2 \right]_\gamma = \lambda \quad \text{on } \partial\{u > 0\} \cap \Omega,$$

for some constant $\lambda > 0$. Here, $[\,\cdot\,]_\gamma$ denotes the jump of the function across interface γ, the zero-level set of u.

Proof. Let $\zeta \in C_0^\infty(\Omega, \mathbb{R}^2)$ and $\rho > 0$ small. Define $u_\rho \in A$ by $u_\rho(\tau_\rho(x)) = u(x)$ where $\tau_\rho(x) = x + \rho\zeta(x)$. To preserve the volume of $\{u_\rho > 0\}$, we must have

$$\begin{aligned} V &= \int_\Omega \chi_{\{u_\rho > 0\}} = \int_{\tau_\rho^{-1}\Omega} \chi_{\{u>0\}} \det(D\tau_\rho) \\ &= \int_\Omega \chi_{\{u>0\}} \left(1 + \rho\nabla \cdot \zeta + O(\rho^2)\right), \end{aligned}$$

which implies that

$$0 \;=\; \int_{\{u>0\}} \nabla\cdot\zeta + O(\rho).$$

Taking $\rho \to 0$ and using the divergence theorem, we get the following condition on ζ,

$$\int_{\partial\{u>0\}} \zeta\cdot\boldsymbol{\eta}. \tag{4.4}$$

Then, for any ζ satisfying (4.4), we must have

$$\lim_{\rho\downarrow 0} \frac{\mathcal{J}(u_\rho)-\mathcal{J}(u)}{\rho} = 0. \tag{4.5}$$

First, we note that

$$\begin{aligned}
\mathcal{J}(u_\rho) &= \mathcal{J}(u\circ\tau_\rho^{-1}) \\
&= \int_\Omega \frac{1}{h}|u\circ\tau_\rho^{-1}-u_*|^2 + |\nabla u(\tau_\rho^{-1})\cdot D\tau_\rho^{-1}|^2 \\
&= \int_{\tau_\rho^{-1}\Omega} \frac{1}{h}|u-u_*\circ\tau_\rho|^2\det(D\tau_\rho) + |\nabla u\cdot(D\tau_\rho)^{-1}|^2\det(D\tau_\rho).
\end{aligned}$$

Meanwhile,

$$u_*\circ\tau_\rho(x) = u_*(x+\rho\zeta(x)) = u_*(x)+\rho\nabla u_*(x)\cdot\zeta(x)+O(\rho^2),\quad \rho\to 0,$$

and by the divergence theorem,

$$\int_\Omega \nabla\cdot(u_*^2\zeta) = \int_{\partial\Omega} u_*^2\zeta\cdot\boldsymbol{\eta} = 0.$$

Hence, we get

$$\begin{aligned}
\int_\Omega |u_\rho-u_*|^2-|u-u_*|^2 &= \int_\Omega |(u-u_*)-\rho(\nabla u_*\cdot\zeta)+O(\rho^2)|^2\det(D\tau_\rho)-|u-u_*|^2 \\
&= \int_\Omega -2\rho(u-u_*)(\nabla u_*\cdot\zeta)+\rho|u-u_*|^2\nabla\cdot\zeta+O(\rho^2) \\
&= \rho\int_\Omega (u^2-2uu_*)\nabla\cdot\zeta-2u(\nabla u_*\cdot\zeta)+\nabla\cdot(u_*^2\zeta)+O(\rho) \\
&= \rho\int_\Omega (u^2-2uu_*)\nabla\cdot\zeta-2u(\nabla u_*\cdot\zeta)+O(\rho),\quad \rho\to 0.
\end{aligned}$$

On the other hand, note that

$$(D\tau_\rho)^{-1} = (I+\rho D\zeta)^{-1} = I-\rho D\zeta+O(\rho^2),\quad \rho\to 0.$$

Then, we have

$$\begin{aligned}
\int_\Omega |\nabla u_\rho|^2-|\nabla u|^2 &= \int_\Omega \left|\nabla u-\rho\nabla u\cdot D\zeta+O(\rho^2)\right|^2\left(1+\rho\nabla\cdot\zeta+O(\rho^2)\right)-|\nabla u|^2 \\
&= \rho\int_\Omega |\nabla u|^2\nabla\cdot\zeta-2\nabla u D\zeta\nabla u+O(\rho),\quad \rho\to 0.
\end{aligned}$$

Hence, (4.5) becomes

$$0 = \int_\Omega \frac{(u^2 - 2uu_*)\nabla\cdot\zeta - 2u(\nabla u_*\cdot\zeta)}{h} + \int_\Omega |\nabla u|^2\nabla\cdot\zeta - 2\nabla u D\zeta\nabla u =: I + II. \quad (4.6)$$

Write

$$\zeta(x) := \phi\frac{\nabla u}{|\nabla u|},$$

where ϕ is a compactly supported scalar function such that

$$\int_{\partial\{u>0\}} \phi = 0, \quad (4.7)$$

which follows from (4.4) and noting that $\boldsymbol{\eta} = -\nabla u/|\nabla u|$.

Let $P := \{u > 0\}$. Then, by Green's theorem, we have

$$\begin{aligned} I &= \frac{1}{h}\int_\Omega (u^2-2uu_*)\nabla\cdot\left(\phi\frac{\nabla u}{|\nabla u|}\right) - 2u\phi\frac{\nabla u_*\cdot\nabla u}{|\nabla u|} \\ &= \frac{1}{h}\int_{P\cup\Omega\setminus\hat{P}} -\phi\left(2u\nabla u - 2u\nabla u_* - 2u_*\nabla u\right)\cdot\frac{\nabla u}{|\nabla u|} - 2u\phi\frac{\nabla u_*\cdot\nabla u}{|\nabla u|} \\ &\qquad + \frac{1}{h}\int_{\partial\{u>0\}}\left[\phi\left(u^2-2uu_*\right)\frac{\nabla u}{|\nabla u|}\cdot\boldsymbol{\eta}\right]_\gamma \\ &= \int_{P\cup\Omega\setminus\hat{P}} -2\phi|\nabla u|\frac{u-u_*}{h} + \int_{\partial\{u>0\}}\left[\frac{2uu_*-u^2}{h}\phi\right]_\gamma \\ &= \int_{P\cup\Omega\setminus\hat{P}} -2\phi|\nabla u|\frac{u-u_*}{h}. \end{aligned}$$

Meanwhile, we see that

$$\begin{aligned} \nabla u^T D\zeta\nabla u &= \phi\nabla u^T D\left(\frac{\nabla u}{|\nabla u|}\right)\nabla u + \frac{1}{|\nabla u|}\nabla u^T\left(\nabla u\otimes\nabla\phi\right)\nabla u \\ &= \frac{1}{|\nabla u|}\nabla u^T\left(\nabla u\nabla\phi^T\right)\nabla u = |\nabla u|\nabla u\cdot\nabla\phi. \end{aligned}$$

Plugging this in the second integral II and using Green's theorem, we get

$$\begin{aligned} II &= \int_\Omega |\nabla u|^2\nabla\cdot\left(\phi\frac{\nabla u}{|\nabla u|}\right) - 2|\nabla u|\nabla u\cdot\nabla\phi \\ &= \int_{P\cup\Omega\setminus\hat{P}} -\phi\nabla\left(|\nabla u|^2\right)\cdot\frac{\nabla u}{|\nabla u|} + \int_{\partial\{u>0\}}\left[\phi|\nabla u|^2\frac{\nabla u}{|\nabla u|}\cdot\boldsymbol{\eta}\right]_\gamma \\ &\qquad + \int_{P\cup\Omega\setminus\hat{P}} 2\nabla\cdot(|\nabla u|\nabla u)\phi - 2\int_{\partial\{u>0\}}\left[\phi|\nabla u|\nabla u\cdot\boldsymbol{\eta}\right]_\gamma \\ &= 2\int_{P\cup\Omega\setminus\hat{P}} -\phi|\nabla u|\nabla(|\nabla u|)\cdot\frac{\nabla u}{|\nabla u|} + \phi\left(\nabla u\cdot\nabla(|\nabla u|) + |\nabla u|\Delta u\right) \\ &\qquad + \int_{\partial\{u>0\}}\left[-\phi|\nabla u|^2 + 2|\nabla u|\nabla u\cdot\frac{\nabla u}{|\nabla u|}\right]_\gamma \\ &= \int_{P\cup\Omega\setminus\hat{P}} 2\phi|\nabla u|\Delta u + \int_{\partial\{u>0\}}\phi\left[|\nabla u|^2\right]_\gamma \end{aligned}$$

Thus, (4.6) becomes

$$0 \;=\; \int_{P\cup\Omega\setminus\hat{P}} 2\phi|\nabla u|\left(-\frac{u-u_*}{h}+\Delta u\right)+\int_{\partial\{u>0\}}\phi\left[|\nabla u|^2\right]_\gamma .$$

Using (4.2), we have for any ϕ satisfying (4.7),

$$\int_{\partial\{u>0\}}\phi\left[|\nabla u|^2\right]_\gamma = 0,$$

that is,

$$\left[|\nabla u|^2\right]_\gamma = \left[\left(\frac{\partial u}{\partial \boldsymbol{\eta}}\right)^2\right]_\gamma = \lambda, \quad \text{on } \partial\{u>0\}\cap\Omega,$$

for some constant $\lambda > 0$. □

In view of the results in [5] and the above free boundary condition, we can rewrite the minimization problem (4.3) as follows

$$\min_{H_0^1(\Omega)}\int_\Omega\left(\frac{|u-u_*|^2}{h}+|\nabla u|^2+\lambda\chi_{\{u>0\}}\right)dx. \tag{4.8}$$

Moreover, one can expect that this minimization is "in the continuous setting" equivalent to solving the parabolic free boundary problem

$$u_t = \Delta u + \lambda(t)\mathcal{H}^1\lfloor_{\{u>0\}}, \tag{4.9}$$

where $\mathcal{H}^1$ denotes the one-dimensional Hausdorff measure.

Hence, if we wish to preserve the volumes of phase regions, then we must solve (4.9), instead of the heat equation in the diffusion step of Algorithm 3.1. To be precise, we write out the two-phase volume-preserving SDV scheme below:

Algorithm 4.1 Two-phase Volume-preserving SDV Method

Given an initial interface $\Gamma_0 := \partial D_0$ for some region $D_0 \subset \mathbb{R}^2$ and a time step size $\Delta t > 0$, we generate a sequence of time-discrete approximations $\{\Gamma_n\}$ to its *volume-preserving mean curvature motion* at time $t = n\Delta t$, by obtaining Γ_n from Γ_{n-1} as follows:

1. Construct the scalar ε-signed distance function

$$\delta_\varepsilon(x) = \frac{1}{\varepsilon}\begin{cases} \min\left(\varepsilon, \operatorname{dist}(x,\Gamma_0)\right), & x\in D_0 \\ -\min\left(\varepsilon, \operatorname{dist}(x,\Gamma_0)\right), & x\in\mathbb{R}^2\setminus D_0. \end{cases} \tag{4.10}$$

2. For a suitable λ, solve parabolic equation (4.9) with δ_ε as the initial condition.

3. Set $\Gamma_n := \partial D_n$, where $D_n := \{x : u(\Delta t, x) > 0\} \subset \mathbb{R}^2$.

Next, we estimate the normal velocity of the interface evolved via Algorithm 4.1 in the following theorem.

Theorem 4.2. *For the choice* $\lambda(t) = -\frac{4}{\varepsilon\sqrt{\pi}}\kappa_a\sqrt{t}$*, Algorithm 4.1 evolves interface* Γ_0 *according to volume-preserving mean curvature motion with normal velocity*

$$v = -\kappa + \kappa_a + O(\Delta t), \quad \text{as } \Delta t \to 0.$$

Proof. We proceed in the same manner as in the proof of Theorem 3.3. Thus, we have a situation of Figure 3.2, where we identify phase P_i with D_0, phase P_j with $\mathbb{R}^2\backslash D_0$, and γ_{ij} with Γ_0. For simplicity, we denote $t := \Delta t$. Then, the normal velocity v of interface Γ_0 at point $x = 0$ follows from

$$\begin{aligned} 0 &= u(t,0,vt) \\ &= \int_{\mathbb{R}^2} \delta_\varepsilon(x)\Phi_t(x-z)dx + \int_0^t\int_{\mathbb{R}^2} \mu(s,x)\Phi_{t-s}(x-z)dxds =: A + B, \end{aligned}$$

where $z = (0, vt)$ and $\mu(s,x) = \lambda(s)\mathcal{H}^1\lfloor_{\{u>0\}}$.

The proof of Theorem 3.3 shows that

$$A = \frac{1}{\varepsilon}\left[(v+\kappa)\,t + O(t^2)\right], \text{ as } t \to 0. \tag{4.11}$$

Denote $P(s) := \{x : u(x,s) > 0\}$. Then, for B, we have

$$\begin{aligned} B &= \int_0^t\int_{\partial P(s)} \lambda(s,x)\Phi_{t-s}(x-z)dS(x)ds \\ &= -\frac{1}{\varepsilon}\int_0^t\left(\int_{\partial P(s)\cap Q} + \int_{\partial P(s)\backslash Q}\right)\frac{\kappa_a\sqrt{s}}{\pi^{3/2}(t-s)}e^{-\frac{|x-(0,vt)|^2}{4(t-s)}}dS(x)ds \\ &=: -\frac{\kappa_a}{\varepsilon\pi^{3/2}}(I + II), \end{aligned} \tag{4.12}$$

where $Q := [-\tau,\tau]\times[-\tau,\tau]$. Note that integral II is exponentially small:

$$\begin{aligned} |II| &\le \int_0^t\int_{\partial P(s)\backslash Q}\frac{\sqrt{s}}{t-s}e^{-\frac{\tau^2}{4(t-s)}}dS(x)ds \\ &\le \max_{s\in[0,t]}|\partial P(s)|\int_0^t\frac{\sqrt{s}}{t-s}e^{-\frac{\tau^2}{4(t-s)}}ds \\ &\le C\max_{s\in[0,t]}\sqrt{s}\int_{\frac{\tau^2}{4t}}^\infty\frac{1}{s}e^{-s}ds \\ &\le Ct\sqrt{t}\int_{\frac{\tau^2}{4t}}^\infty e^{-s}ds = Ct\sqrt{t}e^{-\frac{\tau^2}{4t}}. \end{aligned} \tag{4.13}$$

Here, we assume that $\partial P(s)$ has finite length for $s \in [0,t]$. For integral I, we have

$$\begin{aligned} I &= \int_0^t\int_{\partial P(s)\cap Q}\frac{\sqrt{s}}{t-s}e^{-\frac{|x-(0,vt)|^2}{4(t-s)}}dS(x)ds \\ &= \int_0^t\int_{-\tau}^{\tau}\int_{-\infty}^{\gamma(s,x_1)}\frac{\partial}{\partial x_2}\left(\frac{\sqrt{s}}{t-s}e^{-\frac{x_1^2+(x_2-vt)^2}{4(t-s)}}\right)\sqrt{1+\gamma'(s,x_1)^2}dx_2dx_1ds \\ &= \int_0^t\int_{\frac{-\tau}{\rho}}^{\frac{\tau}{\rho}}\left(\int_{-\infty}^0 + \int_0^\omega\right) - \frac{\sqrt{s}}{2\rho}y_2e^{-\frac{|y|^2}{4}}\sqrt{1+\gamma'(s,\rho y_1)^2}dy_2dy_1ds =: I_1 + I_2, \end{aligned} \tag{4.14}$$

where $\omega = \rho^{-1}\left(\gamma(s,\rho y_1) - vt\right)$ and $\rho = \sqrt{t-s}$. Using the following expansions at $\mathbf{0} = (0,0)$

$$\begin{aligned}\sqrt{1+\gamma'(s,\rho y_1)^2} &= \sqrt{1+\gamma'(\mathbf{0})^2} + \frac{\gamma'(\mathbf{0})}{\sqrt{1+\gamma'(\mathbf{0})}}\left(\gamma_t'(\mathbf{0})s + \rho\gamma''(\mathbf{0})x_1\right) + O(s^2+\rho^2x_1^2)\\ &= 1 + O\left(s^2+(\rho y_1)^2\right),\end{aligned}$$

and

$$\gamma(s,\rho y_1) = vs + O\left(s^2+(\rho y_1)^2\right),$$

we can estimate integral I_2 as follows:

$$\begin{aligned}|I_2| &\le C\sqrt{t}\int_0^t\int_{\frac{-\tau}{\rho}}^{\frac{\tau}{\rho}}\int_0^{\omega}\frac{|y_2|}{\sqrt{t-s}}e^{-\frac{|y|^2}{4}}\left(1+s^2+(t-s)y_1^2\right)dy_2dy_1ds\\ &\le C\sqrt{t}\int_0^t\int_{-\infty}^{\infty}\frac{1}{\sqrt{t-s}}e^{-\frac{y_1^2}{4}}\left(1+s^2+(t-s)y_1^2\right)\int_0^{\omega}|y_2|dy_2dy_1ds.\end{aligned}$$

Noting that

$$\int_0^{\omega}|y_2|dy_2 = \frac{\omega^2}{2} \le (t-s)(v^2+y_1^4) + \frac{s^4}{t-s},$$

and

$$\int_{\mathbb{R}} y_1^n e^{-\frac{y_1^2}{4}}dy_1 = O(1),\quad n=0,2,4,6.$$

yields the following estimate

$$|I_2| \le C\sqrt{t}\int_0^t \frac{1}{(t-s)^{3/2}}\left((t-s)^2+s^4\right)\left(1+s^2+(t-s)\right)ds = O(t^2),\quad t\to 0. \tag{4.15}$$

Next, we expand integral I_1 as follows

$$\begin{aligned}I_1 &= \int_0^t\int_{\frac{-\tau}{\rho}}^{\frac{\tau}{\rho}}\frac{\sqrt{s}}{\sqrt{t-s}}e^{-\frac{y_1^2}{4}}\sqrt{1+\gamma'(s,\rho y_1)^2}\int_{-\infty}^0 -\tfrac{1}{2}y_2e^{-\frac{y_2^2}{4}}dy_2dy_1ds\\ &= \int_0^t\frac{\sqrt{s}}{\sqrt{t-s}}\left[\int_{\mathbb{R}} - \int_{\mathbb{R}\setminus[-\frac{\tau}{\rho},\frac{\tau}{\rho}]}e^{-\frac{y_1^2}{4}}dy_1 + \int_{-\frac{\tau}{\rho}}^{\frac{\tau}{\rho}}O(s^2+\rho^2y_1^2)e^{-\frac{y_1^2}{4}}dy_1\right]ds\\ &=: I_{11}+I_{12}+I_{13}.\end{aligned} \tag{4.16}$$

Substituting $s = t\sin^2\theta$, we have

$$I_{11} = 2\sqrt{\pi}\int_0^t\frac{\sqrt{s}}{\sqrt{t-s}}ds = 4t\sqrt{\pi}\int_0^{\frac{\pi}{2}}\sin^2\theta d\theta = \pi^{3/2}t. \tag{4.17}$$

Moreover,

$$\begin{aligned}|I_{12}| &\le 2\int_0^t\frac{\sqrt{s}}{\sqrt{t-s}}\int_{\frac{\tau}{\rho}}^{\infty}e^{-\frac{y_1^2}{4}}dy_1ds\\ &\le 2\int_0^t\sqrt{s}\int_{\frac{\tau}{\rho}}^{\infty}\frac{y_1}{\tau}e^{-\frac{y_1^2}{4}}dy_1ds\\ &\le C\sqrt{t}\int_0^t e^{-\frac{\tau^2}{4(t-s)}}ds \le Ct\sqrt{t}e^{-\frac{\tau^2}{4t}},\end{aligned} \tag{4.18}$$

and

$$\begin{aligned} |I_{13}| &\leq C\sqrt{t}\int_0^t \frac{1}{\sqrt{t-s}}\left[s^2\int_{\mathbb{R}} e^{-\frac{y_1^2}{4}}dy_1 + (t-s)\int_{\mathbb{R}} y_1^2 e^{-\frac{y_1^2}{4}}dy_1\right]ds \\ &\leq C\sqrt{t}\left(\int_0^t \frac{(t-s)^2}{\sqrt{s}}ds + \int_0^t \sqrt{t-s}ds\right) = O(t^2), \end{aligned} \tag{4.19}$$

as $t \to 0$. Finally, combining the resulting integrals from (4.11) to (4.19), we get

$$0 = A + B = \frac{1}{\varepsilon}\left[(v+\kappa)\,t - \kappa_a t + O\left(t^2 + t\sqrt{t}e^{-\frac{\tau^2}{4t}}\right)\right], \text{ as } t \to 0,$$

which gives the desired result. □

This tells us that with a suitable choice of $\lambda(t)$, we are assured that a two-phase volume-preserving mean curvature motion of interfaces is realized via Algorithm 4.1. Extending this to the multiphase case, however, would require calculation of λ at each time step – not an easy task. Hence, we turn to the minimization problem (4.8), which is numerically easier to implement as compared to solving parabolic equation (4.9). To solve this minimization problem, we use a penalization technique [2] which allows us to perform nonvolume-preserving variations without having to compute λ. For a small positive number ϱ, we consider the minimization problem:

$$\min_{H^1(\Omega)} \int_\Omega \left(\frac{|u-u_*|^2}{h} + |\nabla u|^2\right) + \rho^{\operatorname{sgn}(V-|\{u>0\}|)}(V - |\{u>0\}|), \tag{4.20}$$

where V is the prescribed volume. It was shown that as $\rho \to 0$, the penalized solution converges to a solution of the constrained minimization problem (4.3). What's more is that it was shown that the exact minimizer can be achieved for some sufficiently small penalty $\varrho \ll 1$ without having to take the limit to zero [2]. This fact provides a great advantage in numerical computations.

Similar results were obtained by Tilli [93] for the problem of minimizing the Dirichlet integral where two or more level sets have prescribed measure, using a technique that penalizes only the decrease in measure. Translating this to our problem results in the following minimization problem

$$\min_{H^1(\Omega)} \int_\Omega \left(\frac{|u-u_*|^2}{h} + |\nabla u|^2\right)dx + \frac{1}{\varrho}\left(|\{u>0\}| - V\right)_+. \tag{4.21}$$

We draw inspiration from this penalized minimization and extend it to the multiphase case, as will be shown in the succeeding section. We further look into this volume-contrained variational problem in Chapter 7 and study the behaviour of its minimizer for small penalty values.

4.2 Multiphase Flow under Volume Constraint

In the previous section, we streamlined our SDV scheme in such a way that it easily translates into the multiphase case. Our numerical scheme is based on a simplification of the theory in [2] given by Tilli [93], which penalizes only the decrease in volume;

thereby, keeping the penalization term always nonnegative. However, since the tendency of volume change in each phase region is not a priori known, we instead, opt to penalize both increase and decrease in volume of the phase regions.

Note that such minimization problem can be easily extended to the multiphase case by adding penalties for each phase region. We summarize this volume-preserving scheme in the following algorithm.

Algorithm 4.2 Multiphase Volume-preserving SDV Method

Given an initial interface network $\Gamma_0 := \bigcup \{\gamma_{ij} : i, j = 1, 2, \ldots, k\}$ and a time step size $\Delta t > 0$, we obtain its approximation of the *volume-preserving mean curvature flow* by generating a sequence of time discrete interface networks $\{\Gamma_m\}_{m=1}^{M}$ at times $t = m\Delta t$ $(m = 1, \ldots M)$, as follows:

1. Initialization. Set $\mathbf{u}_0 := \boldsymbol{\delta}_{\boldsymbol{\varepsilon}}$ with respect to Γ_{m-1}.

2. Minimization. Discretize $\Delta t = h \times K$. For a small positive number ϱ, successively minimize $(n = 1, 2, \ldots, K)$:

$$\mathcal{F}_n^h(\mathbf{u}) = \mathcal{J}_n^h(\mathbf{u}) + \frac{1}{\varrho} \sum_{i=1}^{k} \left| \omega_i - \mathcal{L}^N(P_i(\mathbf{u})) \right|^2, \tag{4.22}$$

   where V_i denotes the prescribed volume of phase P_i, $\mathcal{L}^N$ denotes the N-dimensional Lebesgue measure, and

$$P_i(\mathbf{u}) := \left\{ x \in \Omega : \mathbf{p}_i \cdot \mathbf{u}(\Delta t, x) = \max_{j=1,2,\ldots,k} \mathbf{p}_j \cdot \mathbf{u}(\Delta t, x) \right\},$$

   the set corresponding to phase P_i with respect to solution $\mathbf{u}$.

3. Projection. Define the new interface $\Gamma_m = \bigcup_{i \neq j} (\partial P_i(\mathbf{u}_K) \cap \partial P_j(\mathbf{u}_K)) \cap \Omega$.

4.3 Numerical Results

In this section, we present a numerical analysis of the penalty parameter in our volume-preserving SDV scheme. We also present numerical test on the stability of the triple junction under volume constraint and some numerical examples of volume-preserving mean curvature flow in the multiphase case.

4.3.1 Analysis of the Penalty Parameter

Consider a volume-preserving two-phase case where two disjoint circles of radii $r_1 = 0.1996$ and $r_2 = 0.1384$ make up one phase.Since volume is preserved, the larger circle will grow as the smaller circle shrinks and eventually vanishes, hence satisfying the

following differential equation

$$\begin{cases} \dfrac{dr_1}{dt} = -\dfrac{1}{r_1} + \dfrac{2}{r_1 + r_2}, \\ \dfrac{dr_2}{dt} = -\dfrac{1}{r_2} + \dfrac{2}{r_1 + r_2}. \end{cases} \tag{4.23}$$

We run the volume-preserving SDV method with $\varepsilon = \Delta x$ for penalty parameters $\varrho = 10^{-i}$ where $i = 0, 1, \ldots, 10$. Here, the domain $\Omega = [0,1] \times [0,1]$ is triangulated into $12,800$ elements ($\Delta x = 0.0125$) and time step $\Delta t = 2.5 \times 10^{-4}$ is discretized into DMF $K = 30$ partitions. We then, compare these results with the precise approximation of the exact solution to the ordinary differential equation (4.23) using Runge-Kutta (RK4) method of order 4.

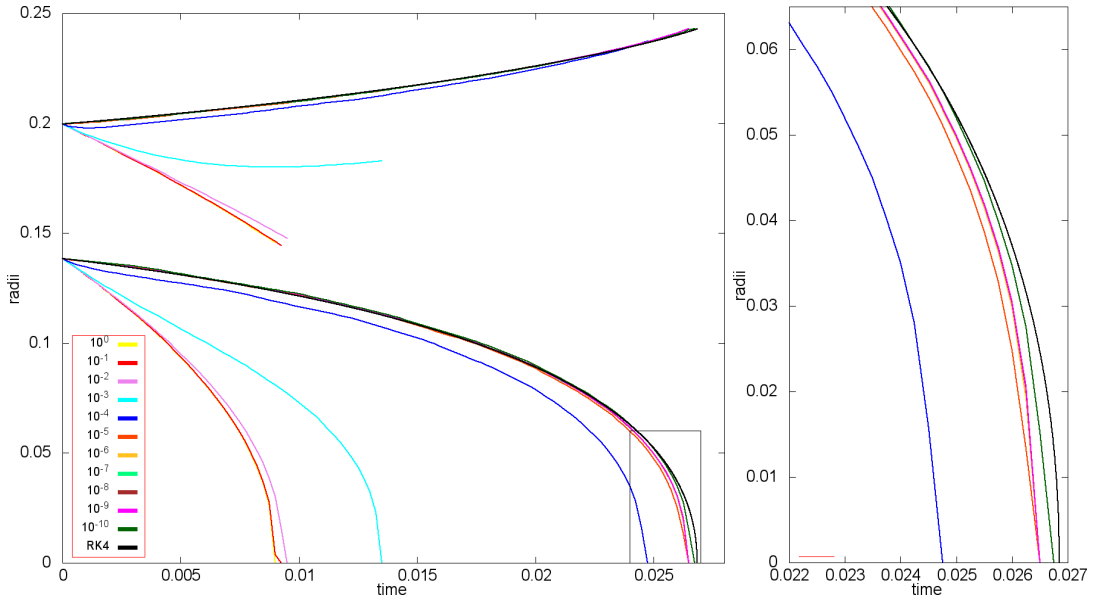

FIGURE 4.1: Evolution of radii (left) for varying penalties ϱ (colored lines) and exact solution (black line). A closer look at the evolution of smaller circle (right) for time $t \geq 0.022$ where penalties $\varrho = 10^{-6}, \ldots, 10^{-9}$ overlap.

For large penalty parameters $\varrho = 10^{0}, 10^{-1}, \ldots, 10^{-3}$, Figure 4.1 shows that weak penalization on the phase volumes allows the bigger circle to shrink when in fact, it should grow. For stronger penalty parameters $\varrho = 10^{-4}, 10^{-5}, \ldots, 10^{-10}$, on the other hand, the result behaves, as expected, similar to the exact solution where the bigger circle grows as the smaller circle shrinks. We note that as $\varrho \to 0$, result approaches the exact solution. This is indeed, consistent with the fact that exact solution can be achieved with a sufficiently small penalty without taking $\varrho \to 0$ [2, 93]. Moreover, the fact that the solution almost does not change when $\varrho \to 0$, justifies the use of penalty method on our algorithm.

4.3.2 Junction Stability: Double Bubble Test

Consider a three-phase volume-preserving case where two phases are identical squares sharing one common side of length 0.28. Denote P_1 as the left initial square phase, P_2 as the right initial square phase, and P_3 as the remaining phase. The stationary solution

of such configuration is known as a double bubble [53] which consists of three circular arcs meeting at two points at equal 120° angles. Since the initial square phases P_1 and P_2 have equal volume, the common circular arc would have zero curvature, hence, a line separating the two identical circular arcs.

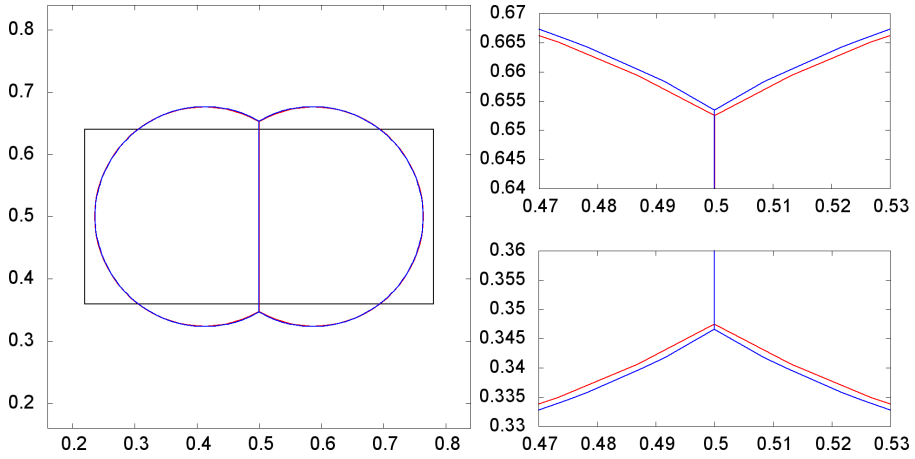

FIGURE 4.2: Three-phase initial configuration (left in black); its numerical (blue) and exact (red) stationary solution. A closer look at the interface network near the triple junctions (right).

We run SDV method with $\varepsilon = 3\Delta x$ under penalty parameter $\varrho = 10^{-6}$. Here, $\Omega = [0,1] \times [0,1]$ is triangulated into 12800 elements with mesh size $\Delta x = 1.25 \times 10^{-2}$ and time step $\Delta t = 5 \times 10^{-4}$ with DMF partition $K = 30$. We test if the stationary solution of the volume-preserving flow via SDV method satisfies the *double bubble theorem* by measuring phase volumes and contact angles θ_i (interior angle of phase $P_i (i = 1, 2, 3)$) at both triple junction points J_1 and J_2 located above and below line $y = 0.5$, respectively. Here, the junction angles are computed using the tangents to the quadratic interpolation of the piecewise linear interface near the triple junction.

TABLE 4.1: Double Bubble: Phase Volumes under penalty parameter $\varrho = 10^{-6}$.

phase region	prescribed volume	stationary state volume	absolute error
P_1	0.0784	0.078385	1.5×10^{-5}
P_2	0.0784	0.078385	1.5×10^{-5}
P_3	0.8432	0.843229	2.9×10^{-5}

TABLE 4.2: Double Bubble: Contact Angle Measures at the Triple Junctions

angle	triple junction J_1	relative error	triple junction J_2	relative error
θ_1	120.012°	1.0×10^{-4}	120.013°	1.0×10^{-4}
θ_2	119.846°	1.3×10^{-3}	119.845°	1.3×10^{-3}
θ_3	120.023°	1.9×10^{-4}	120.023°	1.9×10^{-4}

The phase volumes and contact angle measures at both triple junctions of the numerical stationary solution are shown in Tables 4.1 and 4.2. We see that the volume of each phase region is preserved under penalty parameter $\varrho = 10^{-6}$ with a loss of at most 0.0001%. This volume loss may be credited to the approximation error arising in the numerical computation of phase volumes inside individual finite elements.

At both triple junctions, the interior angles of the initial phase squares rapidly increase from 90° to 120° ± 0.64 after 10 time steps, then gradually adjusts to its stationary state of measure 120° ± 0.15 at time $t = 500\Delta t$. On the other hand, the junction angle of the outside phase decreases from 180° to 120° ± 0.85 after 10 time steps, then gradually stabilizes to a measure of 120° ± 0.02 at time $t = 500\Delta t$.

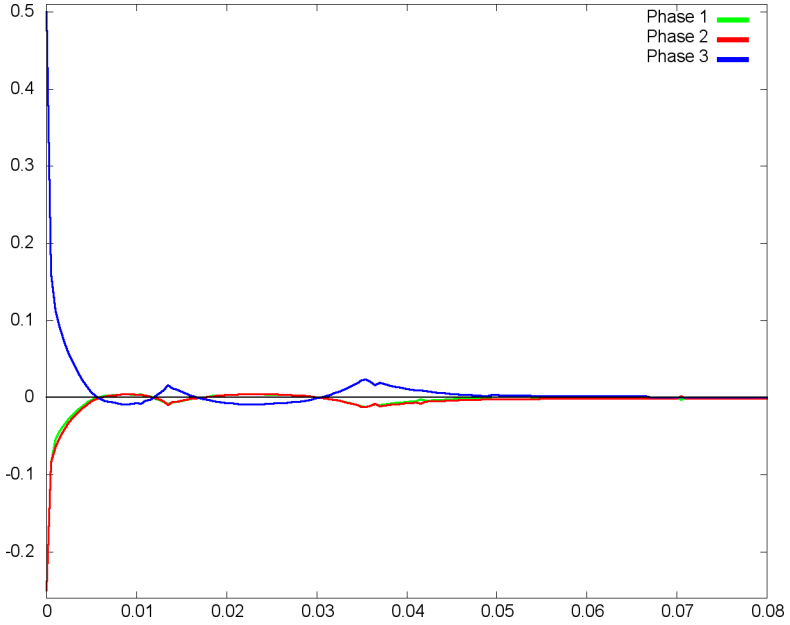

FIGURE 4.3: Relative error plot of the phase interior angle measures at junction J_1 for the first 160 time steps.

This is in fact, depicted in the relative error plot (Figure 4.3) of phase interior angle measures at junction J_1. In particular, we see that after time $t = 10\Delta t$, the junction angles whilst preserving phase volume, tries to achieve a stable state until approximately $t = 120\Delta t$. This confirms that SDV method stably preserves the Herring (120°) angle conditions, and hence, the stationary volume-preserving solution evolved via SDV method indeed, approximates a double bubble.

4.3.3 Example: Ten-phase Volume-preserving Flow

Consider a ten-phase configuration where the initial interfaces are circular arcs. The domain $\Omega = [0,1] \times [0,1]$ is triangulated into 12,800 elements and time step $\Delta t = 2.5 \times 10^{-4}$ with DMF partition $K = 30$. We preserve the phase volumes using SDV method with $\varepsilon = \Delta x$ under a penalty parameter $\varrho = 10^{-6}$.

Figure 4.4 depicts the mean curvature evolution of the initial circular arcs with volume constaint. Under this motion, we see that the top leftmost bubble slides to the right forming a quadruple junction point at time $t = 133\Delta t$, which immediately splits after one time step into two triple junctions and stably cradles itself between two bubbles. Hence, SDV method is able to naturally handle topological changes. Observe also that the symmetric Herring angle conditions are satisfied. In fact, the contact angles at the triple junctions behave in a similar manner as in the double bubble case, where the angle measure rapidly tends to the symmetric condition and then, gradually adjusts to its stationary angle measure 120° ± 0.24°.

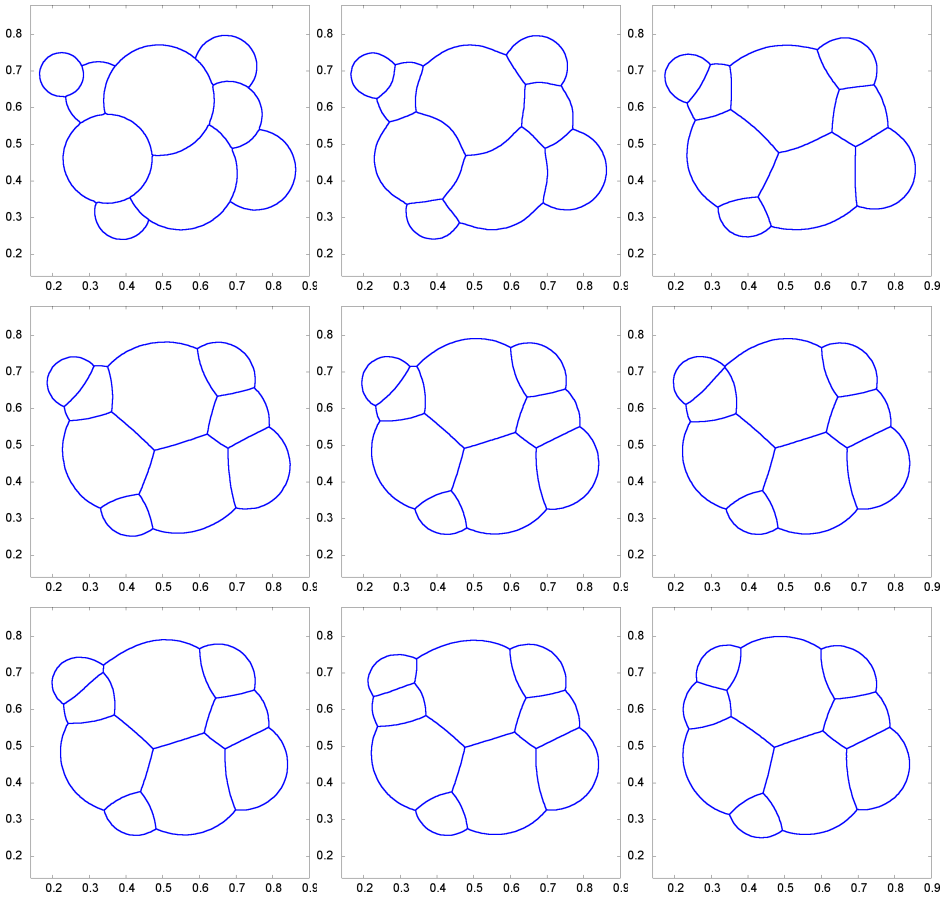

FIGURE 4.4: Initial 10-phase configuration (top left); its evolution after $\Delta t = 2.5\times10^{-4}$ (top center) and at different times; and its stationary solution (bottom right).

TABLE 4.3: 10-phase Flow: Phase Volumes under penalty parameter $\varrho = 10^{-6}$.

phase region	prescribed volume	stationary state volume	absolute error
P_1	0.011185	0.011208	2.3×10^{-5}
P_2	0.011592	0.011585	7.0×10^{-6}
P_3	0.012702	0.012687	1.5×10^{-5}
P_4	0.016988	0.016985	3.0×10^{-6}
P_5	0.019179	0.019178	1.0×10^{-6}
P_6	0.028773	0.028767	6.0×10^{-6}
P_7	0.046392	0.046393	1.0×10^{-6}
P_8	0.052734	0.052734	1.0×10^{-7}
P_9	0.064719	0.064722	3.0×10^{-6}
P_{10}	0.735737	0.735741	4.0×10^{-6}

Note also that the volume of each phase region is well preserved relative to the penalty parameter $\varrho = 10^{-6}$, as shown in Table 4.3. Under this configuration, we were able to achieve a fairly good approximation of multiphase volume-preserving MCF without the need for any auxilliary mesh refinement technique – an advantage of the vector-type MBO method [94].

4.4 Concluding Remarks

Up to this point, we were able to develop a signed distance vector approach for realizing volume-preserving mean curvature flow in the multiphase case. We have shown that our SDV method benefits the key features of its predecessors and at the same time resolves their underlying issues (see Table 4.4).

TABLE 4.4: SDV Method in comparison to other MBO-variant Algorithms

Features of the Numerical Method	Original MBO	Ruuth's Method	DFDGM	Vector MBO	SDV Method
1. does not require direct calculation of mean curvature and normal direction	✓	✓	✓	✓	✓
2. handles complicated topological changes	✓	✓	✓	✓	✓
3. proceeds the evolution without stagnation	×	—	✓	—	✓
4. can be extended to multiphase case	✓	✓	✓	✓	✓
5. preserves volume in two-phase case	×	✓	×	✓	✓
6. preserves volume in multiphase case	×	×	×	✓	✓

(Here, "—" means a refinement technique is needed to alleviate MBO time and grid restrictions.)

The key in approximating volume-constrained multiphase flow lies in the variational approach to solving the vector-valued heat equation. The volume of the phase regions are easily preserved using a penalization technique. In fact, we showed that the numerical SDV solution does not change for small penalty values, which confirms the theory [2, 93] that the exact solution can be achieved with a sufficiently small penalty without passing the limit in the penalty parameter. In the succeeding chapters, we experiment with this vector variational approach to incorporate space-dependent bulk energies (Chapter 5) and generalize to anisotropic mean curvature flow (Chapter 6).

Chapter 5

Multiphase Mean Curvature Flow considering Bulk Energies

The present chapter deals with volume-preserving multiphase mean curvature evolution of interfaces considering space-dependent bulk energy density. We start with an introduction to the problem and some related works in section 5.1. In section 5.2, we present an extension of our method to realize volume-preserving multiphase mean curvature flow considering phase energies. We also show our method evolves the interface according to its mean curvature plus the difference in bulk energies at the interface. Lastly, in section 5.3, we present numerical experiments and computational examples.

5.1 Introduction

Consider a k-phase configuration where each phase region P_i $(i = 1, \dots, k)$ have prescribed bulk energy density $e_i = \operatorname{div} \mathbf{f}$ for some vector-valued function $\mathbf{f} : \mathbb{R}^N \to \mathbb{R}^N$. We wish to find a family $\{\Gamma(t) := \bigcup \gamma_{ij}(t)\}$ of hypersurfaces depending on time t such that every point $x \in \Gamma(t)$ moves with a velocity

$$\mathbf{V}(x) \quad = \quad -(\kappa + e_i - e_j)\boldsymbol{\eta}_{ij}, \quad x \in \gamma_{ij}, \tag{5.1}$$

where κ and $\boldsymbol{\eta}_{ij}$ denotes the mean curvature and unit normal vector from phase P_i to P_j at x, respectively. This interfacial motion is derived as the gradient flow for the energy functional

$$E(\Gamma) = \sum_{i<j} \int_{\gamma_{ij}} d\mathcal{H}^{N-1} + \sum_{i=1}^{k} \int_{P_k} e_i(x) d\mathcal{L}^N \tag{5.2}$$

where $\mathcal{H}^{N-1}$ is the $(N-1)$-dimensional Hausdorff measure and $\mathcal{L}^N$ is the N-dimensional Lebesgue measure.

Let us verify this derivation for the two-phase problem in $\mathbb{R}^2$. Consider a smooth Jordan curve $\gamma := \gamma_{12}$ parametrized as follows:

$$\gamma(s) = (\gamma_1(s), \gamma_2(s)), \qquad s \in [a, b], \qquad \gamma(a) = \gamma(b).$$

Then, the mean curvature and outer normal is given by

$$\kappa = \frac{\gamma_1'\gamma_2'' - \gamma_2'\gamma_1''}{|\gamma'|^3}, \qquad \boldsymbol{\eta} = \frac{1}{|\gamma'|}\left(\gamma_2', -\gamma_1'\right).$$

Thus, for some vector $\mathbf{u}(x) = (u_1(x), u_2(x))$ and $\mathbf{v} = (v_1(x), v_2(x))$, the energy functional (5.2) becomes

$$\begin{aligned} E(\gamma) &= \int_\gamma d\mathcal{H}^1 + \int_\gamma \mathbf{u}\cdot\boldsymbol{\eta}\, d\mathcal{H}^1 - \int_\gamma \mathbf{v}\cdot\boldsymbol{\eta}\, d\mathcal{H}^1 \\ &= \int_a^b |\gamma'(s)|ds + \int_a^b (u_1(\gamma_1,\gamma_2)\gamma_2' - u_2(\gamma_1,\gamma_2)\gamma_1')ds \\ &\qquad + \int_a^b (v_1(\gamma_1,\gamma_2)\gamma_2' - v_2(\gamma_1,\gamma_2)\gamma_1')ds. \end{aligned}$$

The gradient flow of this energy can be found from its first variation. For any smooth curve $\zeta(s),\ s\in[a,b]$ where $\zeta(a) = \zeta(b)$, we have

$$\begin{aligned} \frac{d}{d\epsilon}\int_a^b |\gamma'(s) + \epsilon\zeta'(s)|ds\Big|_{\epsilon=0} &= \int_a^b \frac{\gamma_1'(s)\zeta_1'(s) + \gamma_2'(s)\zeta_2'(s)}{|\gamma'(s)|}ds \\ &= -\int_a^b \frac{d}{ds}\left(\frac{\gamma_1'(s)}{|\gamma'(s)|}, \frac{\gamma_2'(s)}{|\gamma'(s)|}\right)\cdot\zeta ds \\ &= \int_a^b \frac{\left(\gamma_1\gamma_2\gamma_2'' - (\gamma_2')^2\gamma_1'',\ \gamma_1\gamma_2\gamma_1'' - (\gamma_1')^2\gamma_2''\right)}{|\gamma'(s)|^3}\cdot\zeta ds \\ &= \int_\gamma \kappa\boldsymbol{\eta}\cdot\zeta, \end{aligned}$$

and

$$\begin{aligned} &\frac{d}{d\epsilon}\int_a^b (u_1(\gamma_1+\epsilon\zeta_1,\gamma_2+\epsilon\zeta_2)(\gamma_2'+\epsilon\zeta_2') - u_2(\gamma_1+\epsilon\zeta_1,\gamma_2+\epsilon\zeta_2)(\gamma_1'+\epsilon\zeta_1'))ds\Big|_{\epsilon=0} \\ &= \int_a^b u_1(\gamma_1,\gamma_2)\zeta_2' + \left(\frac{\partial u_1}{\partial\gamma_1}\zeta_1 + \frac{\partial u_1}{\partial\gamma_2}\zeta_2\right)\gamma_2' - u_2(\gamma_1,\gamma_2)\zeta_1' - \left(\frac{\partial u_2}{\partial\gamma_1}\zeta_1 + \frac{\partial u_2}{\partial\gamma_2}\zeta_2\right)\gamma_1' \\ &= \int_a^b -\frac{\partial u_1}{\partial\gamma_1}\gamma_1'\zeta_2 + \frac{\partial u_1}{\partial\gamma_1}\gamma_2'\zeta_1 + \frac{\partial u_2}{\partial\gamma_2}\gamma_2'\zeta_1 - \frac{\partial u_2}{\partial\gamma_2}\gamma_1'\zeta_2 \\ &= \int_a^b \left(\frac{\partial u_1}{\partial\gamma_1} + \frac{\partial u_2}{\partial\gamma_2}\right)(\gamma_2', -\gamma_1)\cdot\zeta = \int_\gamma e_1\boldsymbol{\eta}\cdot\zeta. \end{aligned}$$

Similarly, we get

$$\frac{d}{d\epsilon}\int_a^b (v_1(\gamma_{1,\epsilon},\gamma_{2,\epsilon})\gamma_{2,\epsilon}' - v_2(\gamma_{1,\epsilon},\gamma_{2,\epsilon})\gamma_{1,\epsilon}'ds\Big|_{\epsilon=0} = \int_\gamma e_2\boldsymbol{\eta}\cdot\zeta,$$

where $\gamma_\epsilon = \gamma + \epsilon\zeta$. Thus, we have

$$\frac{d}{d\epsilon}E(\gamma+\epsilon\zeta)\Big|_{\epsilon=0} = \int_\gamma (\kappa + e_1 - e_2)\boldsymbol{\eta}\cdot\zeta,$$

which confirms the normal velocity (5.1) on interface γ.

A related two-phase problem under volume constraint was considered in [50, 94]. It was shown that two-phase interfacial motions with normal velocity

$$v = -\kappa - f + \widetilde{\lambda}(t),$$

for some function $\widetilde{\lambda}$ of time (with a magnitude that precisely guarantees volume preservation) can be realized by applying the original MBO process to the following partial differential equation in an N-dimensional space under Neumann boundary conditions:

$$u_t \quad = \quad \Delta u + \frac{f}{\sqrt{4\pi t}} + \lambda \mathcal{H}^1 \lfloor_{\partial\{u>\frac{1}{2}\}},$$

where λ is a non-local term depending only on time. This term is a Lagrange multiplier, chosen so that the region enclosed by the $\frac{1}{2}$-level set of the solution preserves the phase volume for all times. Moreover, f is a term related to a given outer force and $\mathcal{H}^1 \lfloor_{\partial\{u>\frac{1}{2}\}}$ is the $(N-1)$-dimensional Hausdroff measure supported in the boundary of the set $\{x : u(t,x) > \frac{1}{2}\}$. This modification to the original MBO scheme was applied to carry out a two-dimensional simulation of gas bubbles rising from the bottom of a container filled with a viscous field, taking $f = \beta y$ where y is the coordinate direction of gravity and β is a constant expressing buoyancy determined by the physical configuration.

One can think of the above two-phase configuration as a system where the gas phase enclosed by the interface has zero bulk energy, while the outer liquid phase has bulk energy density f. We wish to extend this the multiphase setting using our SDV method to incorporate the influence of pressure force in the parabolic framework, where the bulk energy can be interpreted as an energy potential.

5.2 Incorporating Bulk Energies in SDV Method

In this section, we extend the results in [50, 94] to realize multiphase mean curvature motions considering space-dependent bulk energies.

Consider the vector-valued nonhomogenous heat equation

$$\begin{cases} \mathbf{u}_t(t,x) = \Delta \mathbf{u}(t,x) + \mathbf{w}(x) & \text{in } (0,\infty) \times \mathbb{R}^N, \\ \mathbf{u}(0,x) = \boldsymbol{\delta}_{\boldsymbol{\varepsilon}}(x) & \text{on } \{t=0\} \times \mathbb{R}^N. \end{cases} \tag{5.3}$$

where $\mathbf{w}$ is a term related to the prescribed phase energies. The question is how to construct the $(k-1)$-dimensional vector $\mathbf{w}$ so that a normal velocity $v = -\kappa - e_i + e_j$ is realized at interface γ_{ij} using our method.

We apply our SDV process to (5.3) and estimate the normal velocity of interfaces. We wish to determine the conditions for $\mathbf{w}$, so that interfacial velocity (5.1) is achieved. For simplicity, take $N = 2$. Fix $\varepsilon > 0$ and $x \in \gamma_{ij}$. We proceed in a similar fashion as in the proof of Theorem 3.3 where we set up a neighborhood of x in a new coordinate system as shown in Figure 3.2.

Let $\mathbf{u}$ be the solution of equation (5.3). For convenience, we write t instead of Δt. Then, the normal velocity v of interface γ_{ij} at point $x = 0$ evolved by applying our SDV process

to (5.3) can be found from the relation

$$\begin{aligned} 0 &= \mathbf{u}(t,0,vt)\cdot(\mathbf{p}_i-\mathbf{p}_j) \\ &= \int_{\mathbb{R}^2} \boldsymbol{\delta}_{\boldsymbol{\varepsilon}}(x)\cdot(\mathbf{p}_i-\mathbf{p}_j)\Phi_t(x-z)dx \\ &\quad + \int_0^t \left(\int_Q + \int_{\mathbb{R}^2\setminus Q}\right) \mathbf{w}(x)\cdot(\mathbf{p}_i-\mathbf{p}_j)\Phi_{t-s}(x-z)dxds \\ &=: I + II + III \end{aligned} \tag{5.4}$$

where $z := (0, vt)$. By Theorem 3.3, we have

$$I = \frac{k}{\varepsilon(k-1)}\left[(v+\kappa)\,t + O\left((1+\tau+\sqrt{t})\sqrt{t}e^{-\frac{\tau^2}{4t}}\right) + O(t^2)\right] + O(e^{-\frac{\tau^2}{4t}}).$$

Moreover, if $\mathbf{w}\cdot(\mathbf{p}_i-\mathbf{p}_j)$ is bounded in $\mathbb{R}^2$, then we can show that integral *III* is exponentially small as follows:

$$\begin{aligned} |III| &\le \max_{\mathbb{R}^2\setminus Q}\mathbf{w}(x)\cdot(\mathbf{p}_i-\mathbf{p}_j)\int_0^t\int_{\mathbb{R}^2\setminus Q}\Phi_{t-s}(x-z)dxds \\ &= C\int_0^t\left(\int_{\mathbb{R}}\int_{\mathbb{R}\setminus(-\tau,\tau)} + \int_{\mathbb{R}\setminus(-\tau,\tau)}\int_{\mathbb{R}}\right)\varphi_{t-s}(x_1)\varphi_{t-s}(x_2-vt)dx_2dx_1ds \\ &\le C\int_0^t e^{-\frac{\tau^2}{4(t-s)}}ds \\ &= C\int_{\frac{\tau^2}{4t}}^{\infty} s^{-2}e^{-s}ds \\ &\le C\max_{s\ge\frac{\tau^2}{4t}}\frac{1}{s^2}\int_{\frac{\tau^2}{4t}}^{\infty}e^{-s}ds \\ &= O(t^2e^{-\frac{\tau^2}{4t}}). \end{aligned}$$

Now, using the expansion of $\mathbf{w}$ around 0, we have

$$\begin{aligned} II &= \int_0^t\int_{-\tau}^{\tau}\int_{-\tau}^{\tau}\mathbf{w}(x)\cdot(\mathbf{p}_i-\mathbf{p}_j)\Phi_{t-s}(x-z)dxds \\ &= \int_0^t\int_{-\infty}^{\infty}\int_{-\infty}^{\infty}(\mathbf{w}(0)+O(x))\cdot(\mathbf{p}_i-\mathbf{p}_j)\Phi_{t-s}(x-z)dxds + O(t^2e^{-\frac{\tau^2}{4t}}) \\ &=: II_1 + II_2 + O(t^2e^{-\frac{\tau^2}{4t}}). \end{aligned}$$

Note that

$$\begin{aligned} II_1 &= \mathbf{w}(0)\cdot(\mathbf{p}_i-\mathbf{p}_j)\int_0^t\int_{-\infty}^{\infty}\varphi_{t-s}(x_1)\int_{-\infty}^{\infty}\varphi_{t-s}(x_2)dx_2dx_1ds \\ &= \mathbf{w}(0)\cdot(\mathbf{p}_i-\mathbf{p}_j)\int_0^t ds = \mathbf{w}(0)\cdot(\mathbf{p}_i-\mathbf{p}_j)t. \end{aligned}$$

Moreover, since $2k > k-1$ for $k > 1$, then

$$|\mathbf{p}_i-\mathbf{p}_j| = \sqrt{\frac{2k}{k-1}} \le \frac{2k}{k-1}.$$

(See Appendix A for the properties of symmetric reference vectors.)

Thus, we see that

$$\begin{aligned}
|II_2| &\leq C\int_0^t\int_{-\infty}^{\infty}\int_{-\infty}^{\infty}|x\cdot(\mathbf{p}_i-\mathbf{p}_j)|\Phi_{t-s}(x-z)dxds\\
&\leq C|\mathbf{p}_i-\mathbf{p}_j|\int_0^t\int_{-\infty}^{\infty}\int_{-\infty}^{\infty}|x_1+x_2|\varphi_{t-s}(x_1)\varphi_{t-s}(x_2-vt)dx_2dx_1ds\\
&\leq \frac{Ck}{k-1}\int_0^t\left(\int_0^{\infty}x_1\varphi_{t-s}(x_1)dx_1+\int_{-\infty}^{\infty}|x_2|\varphi_{t-s}(x_2-vt)dx_2\right)ds\\
&\leq \frac{Ck}{k-1}\int_0^t\left(\frac{\sqrt{t-s}}{\sqrt{\pi}}+\int_0^{\infty}(x_2+|v|t)\varphi_{t-s}(x_2)dx_2\right)ds\\
&= \frac{Ck}{k-1}\int_0^t\left(\frac{2\sqrt{t-s}}{\sqrt{\pi}}+|v|t\right)ds=\frac{Ck}{k-1}\left(\sqrt{t}+t\right)t.
\end{aligned}$$

Then, (5.4) gives

$$0 = \left[\frac{k}{\varepsilon(k-1)}(v+\kappa)+\mathbf{w}(0)\cdot(\mathbf{p}_i-\mathbf{p}_j)+O(\sqrt{t})\right]t,\quad t\to 0.$$

This leads to the following theorem.

Theorem 5.1. *Let $x\in\Gamma:=\bigcup\{\gamma_{ij}:i,j=1,2,...,k\}$ such that there exists a unique pair (i,j) for which $x\in\gamma_{ij}$. Suppose $\mathbf{w}\cdot(\mathbf{p}_i-\mathbf{p}_j)$ is bounded in $\mathbb{R}^N$ and*

$$\mathbf{w}(x)\cdot(\mathbf{p}_i-\mathbf{p}_j)=\frac{k}{\varepsilon(k-1)}(e_i-e_j)(x),$$

where e_i denotes the energy density function of phase P_i. Then, the normal velocity v of interface Γ at x evolving via an SDV process on (5.3) *is given by*

$$v(x)=-\kappa-e_i+e_j+O(\Delta t),\quad \text{as } \Delta t\to 0,$$

where κ is $(N-1)$-times the mean curvature of γ_{ij} at x.

A simple design for vector-valued function $\mathbf{w}$ would be:

$$\mathbf{w}(x)=\begin{cases}\dfrac{\mathbf{p}_i-\mathbf{p}_j}{2\varepsilon}(e_i-e_j)(x), & x\in D_{\omega_1,\omega_2}\\ 0, & \text{otherwise,}\end{cases}\tag{5.5}$$

where

$$D_{\omega_1,\omega_2}:=\{x\in\Omega:\operatorname{dist}(x,\gamma_{ij})<\omega_1,\ \operatorname{dist}(x,P_r)>\omega_2\,(\forall r\neq i,j)\},$$

for some $\omega_1,\omega_1>0$. Note that

$$\frac{|\mathbf{p}_i-\mathbf{p}_j|^2}{2\varepsilon}(e_i-e_j)=\frac{k}{\varepsilon(k-1)}(e_i-e_j)<+\infty$$

(see Appendix A for properties of symmetric reference vectors).

Similar calculations were carried out in extending the MBO Vector Threshold Scheme [94] to include interfacial motions considering space-dependent bulk energies (see Appendix G). We employed this algorithm in [89] to simulate two-dimensional rising gas bubbles (in a three-phase setting) with prescribed contact angles.

5.3 Numerical Results

In this section, we present some numerical experiments using our algorithm to simulate rising gas bubbles in a liquid-filled container. Here, we incorporate the influence of pressure force in the parabolic framework where the bulk energy density is taken as an energy potential. In particular, we consider an initial condition where the first $k-1$ phase regions are gas bubbles with zero bulk energies, i.e. $e_1 = e_2 = \cdots = e_{k-1} = 0$, while the liquid phase P_k has bulk energy density $e_k = f : \mathbb{R}^N \to \mathbb{R}$. It is expected from Theorem 5.1 that the normal velocity at each interface using our method is given by

$$v(x) = \begin{cases} -\kappa, & x \in \gamma_{ij} \ (i, j \neq k), \\ -\kappa + f, & x \in \gamma_{ik} \ (i \neq k). \end{cases}$$

Since mass is preserved, we add a term that penalizes the phase volumes. More precisely, we write out the algorithm.

Algorithm 5.1 Multiphase SDV Method with Volume Constraints and Bulk Energies

Given time step size $\Delta t > 0$ and initial interface network $\Gamma_0 := \bigcup \{\gamma_{ij} : i, j = 1, 2, \ldots, k\}$ where each phase region P_i have prescribed energy density e_i, we obtain its volume-preserving MCF approximation by generating a sequence of time discrete interface networks $\{\Gamma_m\}_{m=1}^{M}$ at times $t = m\Delta t$ $(m = 1, \ldots M)$, as follows:

1. Initialization. Set $\mathbf{u}_0 := \boldsymbol{\delta_\varepsilon}$ with respect to Γ_{m-1}.
2. Minimization. Discretize $\Delta t = h \times K$. For a small positive number ϱ, successively minimize $(n = 1, 2, \ldots, K)$:

$$\mathcal{F}_n^h(\mathbf{u}) = \mathcal{J}_n^h(\mathbf{u}) + \frac{1}{2}\int_\Omega (\mathbf{w} \cdot \mathbf{u})\, dx + \frac{1}{\varrho}\sum_{i=1}^{k} \left|V_i - \mathcal{L}^N(P_i(\mathbf{u}))\right|^2,$$

   where V_i denotes the prescribed volume of phase region P_i, $\mathcal{L}^N$ denotes the N-dimensional Lebesgue measure, and

$$P_i(\mathbf{u}) := \left\{ x \in \Omega : \mathbf{p}_i \cdot \mathbf{u}(\Delta t, x) = \max_{j=1,2,\ldots,k} \mathbf{p}_j \cdot \mathbf{u}(\Delta t, x) \right\},$$

   the set corresponding to phase P_i with respect to solution $\mathbf{u}$.
3. Projection. Define the new interface $\Gamma_m = \bigcup_{i \neq j} (\partial P_i(\mathbf{u}_K) \cap \partial P_j(\mathbf{u}_K)) \cap \Omega$.

5.3.1 Rising Bubbles with Equal Volumes

Consider a three-phase initial condition where phase regions P_1 and P_2 are circles of equal radius $r = 0.125$ centered at $(0.3, 0.4)$ and $(0.7, 0.4)$, respectively. The region outside the two circles denotes the external phase P_3 with bulk energy density $f = 10y$. As in [50, 94], y denotes the coordinate direction of gravity and $\beta = 10$ is a constant expressing buoyancy.

It is expected that under volume-preserving mean curvature motion, both interfaces will behave in a similar manner and move up at constant speed. However, due to the implicit nature of our algorithm, it may happen that the motion of one interface depends on the other, for example, interfaces may move at different speeds, collide, or pull away from each other. To be sure that this does not happen in our method, we conduct a simple test to check that the resulting motion of interfaces γ_{13} and γ_{23} behave accordingly and are independent of each other.

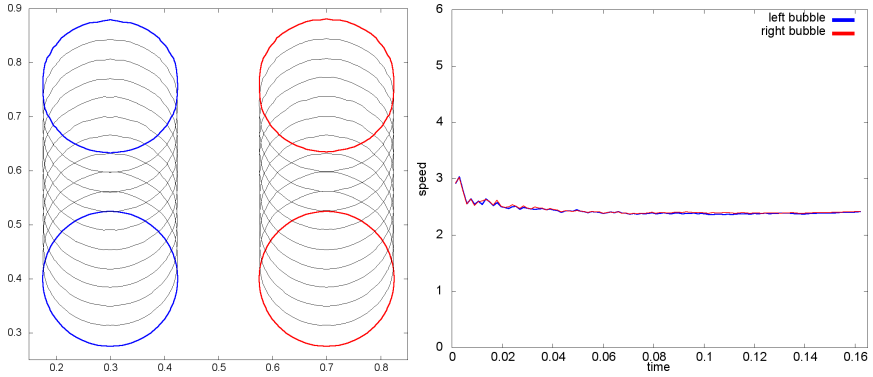

FIGURE 5.1: The motion of two split bubbles of equal volumes (in a three-phase setting) in liquid-filled container with bulk energy density $f = 10y$ ($\omega_1 = \omega_2 = 2\Delta)x$ at different times (left) and the plot of their speed versus time (right).

Under parameters $\varepsilon = \Delta x$, $\varrho = 10^{-6}$, and $\omega_1 = \omega_2 = 2\Delta x$, we run our method and plot the resulting evolution in Figure 5.1. Here, the domain $[0, 1] \times [0, 1]$ is triangulated into $12,800$ elements (with mesh size $\Delta x = 0.0125$) and time step size $\Delta t = 1.5 \times 10^{-3}$ is discretized into 30 DMF partitions. We also compute the speed of the interface by tracking the motion of a representative interface node, in this case, the centroid. It is clear from the results that our method moves both interfaces upward in a similar manner and at a constant speed relative to computation error, which can be improved by the choice of parameters.

5.3.2 Rising Bubbles with Unequal Volumes

It is known that buoyant force on a bubble is proportional to its volume, hence, bigger bubbles rise faster than smaller bubbles. In the following setup, we check whether or not this behavior is captured by our method.

Consider a three-phase initial condition where two circles of unequal area make up phase regions P_1 and P_2 with zero energy density and the remaining region as the external phase P_3 with prescribed bulk energy $f = 10y$. In particular, we take P_1 as a circle of

radius $r_1 = 0.13$ centered at $(0.25, 0.35)$ and P_2 as a circle of radius $r_2 = 0.17$ centered at $(0.7, 0.35)$.

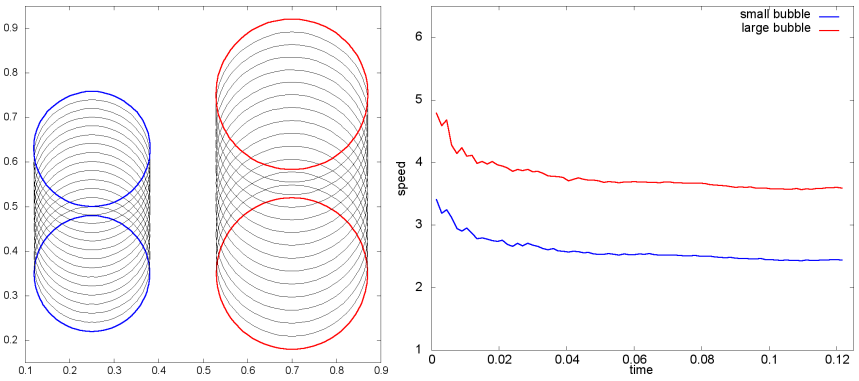

FIGURE 5.2: The motion of two split bubbles of different volumes (in a three-phase setting) in a liquid-filled container with $\omega_1 = \omega_2 = 2\Delta x$ at different times (left) and the plot of their speed versus time (right).

Using the same parameters as in the previous experiment, we see that the interface with a larger enclosed volume rises faster as expected (Figure 5.2). Moreover, the motion of both interfaces approaches a constant speed, relative to computation errors.

5.3.3 General Transport Motions

So far, we have experimented with bulk energy densities resulting in upward motions, that is, bubbles moving in the vertical direction. Let us now take $f = \alpha x + \beta y$. Consider a simple two-phase case where the interface is a circle C of radius r_0 centered at (x_0, y_0). Note that the total force around this interface is given by

$$\begin{aligned}\int_C f\boldsymbol{\eta} &= \int_C (\alpha x + \beta y)\langle x - x_0, y - y_0\rangle \\ &= r_0 \int_0^{2\pi} (\alpha(x_0 + r_0\cos t) + \beta(y_0 + r_0 \sin t))\,\langle \cos t, \sin t\rangle dt \\ &= r_0^2 \int_0^{2\pi} \langle \alpha\cos^2 t, \beta \sin^2 t\rangle dt = \tfrac{1}{2} A_C \langle \alpha, \beta\rangle,\end{aligned}$$

where A_C is the area of circle C. This tells us that the motion of the interface is in the $\langle \alpha, \beta\rangle$-direction and that the influence of the pressure force on the interface varies proportionally to its enclosed volume.

Let us check whether our algorithm is able to move interfaces in any arbitrary direction. Take a circle of radius 0.15 centered at $(0.3, 0.3)$ as our initial condition. We trianglulate the domain $[0, 1]\times[0, 1]$ into 12, 800 elements (with mesh size $\Delta x = 0.0125$) and discretize time step size $\Delta t = 5.0 \times 10^{-4}$ into 30 DMF partitions.

Under parameters $\varepsilon = 5\Delta x$, $\varrho = 10^{-7}$, $\omega_1 = \omega_2 = 2\Delta x$, and $\alpha = \beta = 50$, we run our method and plot the resulting evolution in Figure 5.3. We also compute the speed of the interface by tracking the motion of its centroid. Results indicate that our algorithm can move interface in a $\langle \alpha, \beta\rangle$-direction at a relatively constant speed while preserving the prescribed phase volume.

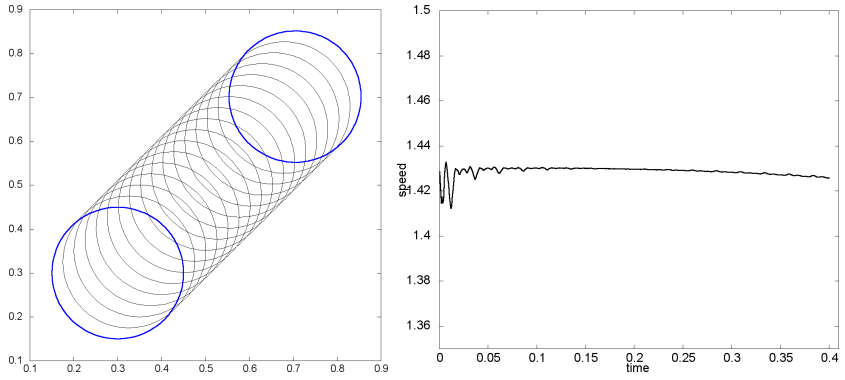

FIGURE 5.3: The volume-constrained motion of a gas-liquid interface with liquid bulk energy $f = 50(x+y)$ in the $\langle 1,1\rangle$-direction (left) and its speed versus time plot (right).

5.3.4 Example: Six-phase Volume-preserving Flow with Buoyancy

Consider a six-phase configuration where phase regions P_1 and P_2 are polygons of different heights and initially attached to the floor boundary, P_3 and P_4 are two overlapping quadrilaterals, P_5 is a circle whose volume is smaller than the volume of phase P_2 below it, and P_6 is the remaining external phase region (see Figure 5.4) with bulk energy density $f = 25y$.

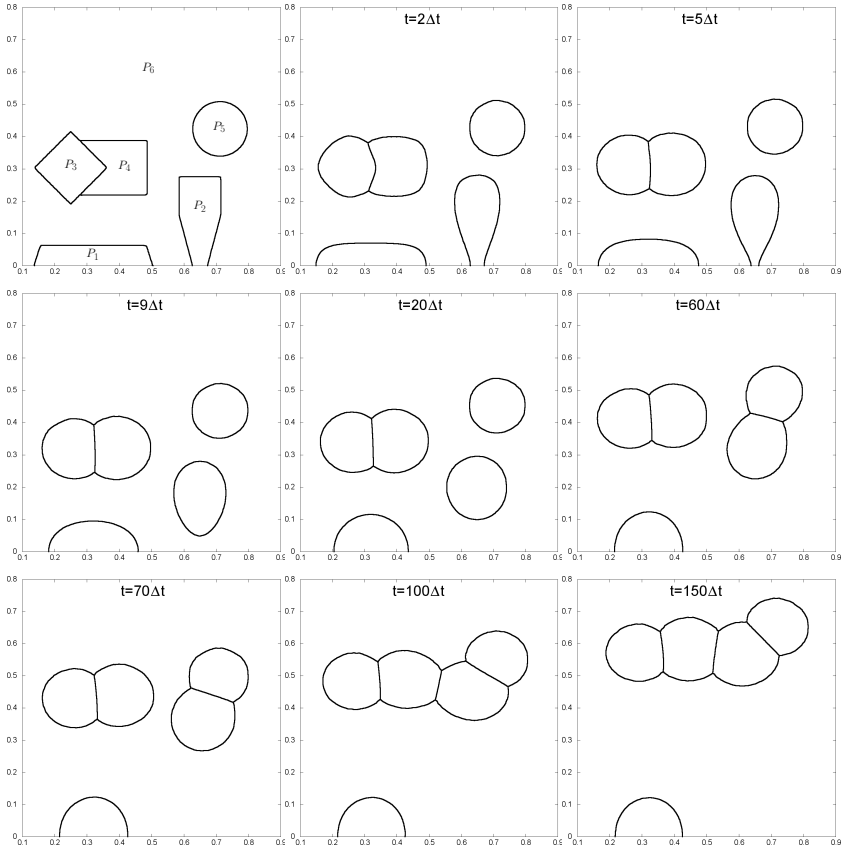

FIGURE 5.4: Initial 6-phase configuration (top left) and its volume-preserving mean curvature evolution with zero gas bulk energies and liquid bulk energy $f = 25y$ under volume penalty $\varrho = 10^{-6}$ with time step size $\Delta t = 10^{-3}$ at different times.

The domain $[0,1]\times[0,1]$ is triangulated into 28,800 elements (with mesh size $\Delta x = 8.33\times 10^{-3}$) and time step size $\Delta t = 0.0010$ (with $K = 20$ DMF partitions). We preserve the phase volumes under a penalty parameter $\varrho = 10^{-6}$ and $\omega_1 = \omega_2 = \Delta x$. Under the above parameters, we evolve the interface using our SDV scheme with $\varepsilon = \Delta x$ and plot the resulting evolution at different times $t = 2\Delta t, 5\Delta t, 9\Delta t, 20\Delta t, 60\Delta t, 70\Delta t, 100\Delta t, 150\Delta t$. One can think of this setup as a simulation of multiple gas bubbles rising in a liquid-filled container.

Observe that our method evolves interfaces by its mean curvature while being pushed upwards by the prescribed buoyant force and trying to preserve all phase volumes. This is especially evident in the motion of phase regions P_3 and P_4 as it evolves into a double bubble (see Figure 5.5). Note that the double bubble slightly tilts counterclockwise due to the difference in phase volumes ($V_3 = 0.025223$, $V_4 = 0.028242$), resulting in phase P_4 to rise a little faster than P_3.

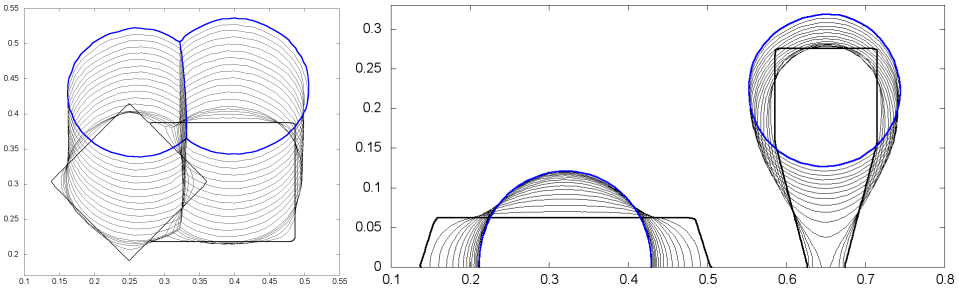

FIGURE 5.5: A closer look at the first evolution of the rising double bubble (left) and the two phase regions initially attached to the boundary floor (right).

The motion of the two phase regions P_1 and P_2 that are initially attached to the boundary floor is a result of the competition between the buoyant force pushing the bubbles upwards and the surface tension force holding the bubbles down (Figure 5.4). In the case of phase region P_1 with a relatively low height and larger contact angle, the adhesive force prevails and the bubble stays attached to the boundary floor until reaching a stable state with a 90° contact angle (due to the Neumann boundary condition). On the other hand, phase region P_2 detaches itself from the boundary floor since a large portion of the region is away from the boundary floor and the initial contact angle is small enough that its curvature evolution and the buoyant force can easily peel it from the bottom.

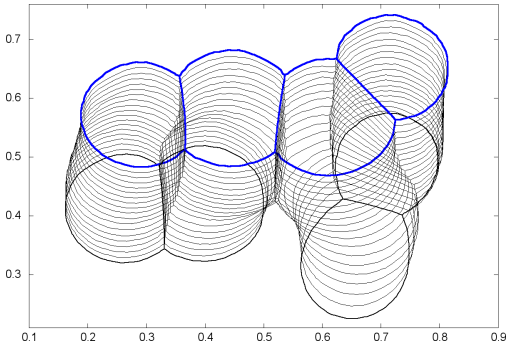

FIGURE 5.6: A closer look at the evolution of the interface forming a four bubble link.

Phase P_2 then, continues to rise up and evolve into a circle. However, since its volume $V_2 = 0.029114$ is relatively larger than that phase region P_5 ($V_5 = 0.022442$), it is able to catch up to this bubble and attaches itself onto it. The two phase regions then, evolves

to form a double bubble while moving up and turning clockwise (since P_2 rises faster than P_5). At this stage, we now have two rising double bubbles $P_3 - P_4$ and $P_2 - P_5$ while phase P_1 remains attached to the boundary floor. Note that the volume difference in the later formed double bubble ($|V_2 - V_5| > |V_3 - V_4|$) is greater than that of double bubble $P_3 - P_4$. This means the double bubble $P_2 - P_5$ turns faster than that of $P_3 - P_4$, causing phase P_2 to attach to P_4 forming a four bubble link (Figure 5.6). This link then continue to evolve according to its mean curvature as it is being pushed upwards by the buoyant force.

TABLE 5.1: 6-phase Flow: Phase Volumes under penalty parameter $\varrho = 10^{-6}$.

phase region	prescribed volume ($t = 0$)	phase volumes at $t = 150\Delta t$	absolute error
P_1	0.021743	0.021512	2.3×10^{-4}
P_2	0.029114	0.029125	1.1×10^{-5}
P_3	0.025223	0.025238	1.5×10^{-5}
P_4	0.028242	0.028259	1.7×10^{-5}
P_5	0.022442	0.022484	4.2×10^{-5}
P_6	0.873236	0.873376	1.4×10^{-4}

Finally, as depicted in Table 5.1, all phase volumes are preserved relative to the prescribed penalty parameter, and at the same time, the symmetric junction angle conditions are satisfied.

5.4 Concluding Remarks

By applying our signed distance vector scheme to a vector-valued non-homogeneous heat equation, we were able to extend our algorithm to approximate mean curvature motions of interfaces separating multiple phases with prescribed bulk energies. This allowed us to simulate multiple rising gas bubbles in a liquid-filled container, as exemplified in our numerical experiments. As a side note, we comment that our construction of the vector function $\mathbf{w}$ is in respect analogous to the characteristic function. This means that there is a possibility that the interfacial motions may stagnate as it is being driven by the external force. One can, of course, construct a continuous vector $\mathbf{w}$ as need be, however, we reiterate that our choice of $\mathbf{w}$ is to reduce computational costs and rely on the signed distance vector to provide subgrid accuracies.

Chapter 6

Volume-preserving Anisotropic Mean Curvature Flow

This chapter deals with anisotropic mean curvature flows. In particular, we generalize our signed distance vector scheme to allow anisotropic energies. Section 6.1 provides a background on anisotropic mean curvature flows and some related numerical scheme, which leads us to our algorithm in section 6.2. In section 6.3, we investigate the accuracy of our method and present numerical results and examples.

6.1 Introduction

Anisotropic mean curvature flow is characterized by the gradient descent of the anisotropic surface energy

$$E_\phi(\Gamma) \quad = \quad \int_\Gamma \phi(\boldsymbol{\eta})\, d\mathcal{H}^{N-1},$$

for a given anisotropy function $\phi : \mathbb{R}^N \to \mathbb{R}$. Note that pure mean curvature flow follows from the Euclidean distance $\phi(\cdot) = |\cdot|$. Here, we assume $\phi \in C^3(\mathbb{R}^{N+1}\backslash\{0\})$ is nonnegative, convex, and positively homogeneous of degree one. A typical example is the discrete l^r-norm given by

$$\phi(x) = \|x\|_{l^r} = \left(\sum_{i=1}^{N} |x_i|^r\right)^{\frac{1}{r}}, \qquad 1 \le r < \infty,$$

where $x = (x_1, \ldots, x_N)$.

For $\zeta \in C_0^\infty(U)$ where U denotes a neighborhood of Γ, define $\psi_\epsilon = x + \epsilon\zeta(x)\boldsymbol{\eta}(x)$ for $x \in U$ and consider $\Gamma_\epsilon = \psi_\epsilon(\Gamma)$. Then, (as shown in [28, Lemma 8.2]) we have

$$\left.\frac{d}{d\epsilon} E_\phi(\Gamma_\epsilon)\right|_{\epsilon=0} \quad = \quad \int_\Gamma \kappa_\phi \zeta\, d\mathcal{H}^{N-1},$$

where the anisotropic mean curvature is defined by

$$\kappa_\phi \quad = \quad \operatorname{div}_\Gamma \boldsymbol{\eta}_\phi(x), \qquad x \in \Gamma.$$

Here, div_Γ denotes the surface divergence on Γ and $\boldsymbol{\eta}_\phi = \nabla\phi(\boldsymbol{\eta})$ is called the Cahn-Hoffman vector. Hence, the velocity of interface Γ under ϕ-curvature flow is given by

$$V = -\mathrm{div}_\Gamma \nabla\phi(\boldsymbol{\eta}),$$

in the direction of the outer normal $\boldsymbol{\eta}$ of Γ. Such evolutionary problems are related to the description of crystal growth [18] and appear in physical systems involving phase boundary motions [10, 51, 52]. Generalized solutions [24] and some regularity properties [47] have also been established.

The corresponding volume-preserving flow is a modification of the anisotropic mean curvature flow, with an extra term that balances the contraction and keeps the enclosed volume of the hypersurface constant, where velocity of the interface is given by

$$V(x) = \left(-\kappa_\phi + \fint_\Gamma \kappa_\phi\right)\boldsymbol{\eta}_\phi(x), \quad x \in \Gamma.$$

Under this motion, convex hypersurfaces in Euclidean space have been proven to remain smooth and convex for all time, and converge to a limit determined by the anisotropy [9]. In the succeeding sections, we are interested in the extent of our SDV method to realize volume-preserving anisotropic mean curvature flow.

6.2 A Numerical Scheme for Anisotropic Evolution

There is an existing number of numerical methods for anisotropic mean curvature flow which includes, e.g., the case of graphs [26, 27], curve shortening flow [30], and curves with triple junctions [13].

The direct approach is to solve the gradient flow of the surface free energy by minimizing

$$E_\phi(\xi(\Gamma)) - E_\phi(\Gamma)\frac{1}{2h}\langle\xi,\xi\rangle,$$

over all where $\xi(\Gamma)$, small deformation of Γ for a given time step size $h > 0$. The minimizer is an approximation to the anisotropic mean curvature evolution of Γ by time h [91]. This variational problem have been studied in a number of literature (e.g., [3, 21, 22]).

The anisotropic generalization of the two-phase MBO threshold dynamics is as follows. Given an anisotropy function ϕ, the anisotropic mean curvature evolution of the interface is approximated by the $\frac{1}{2}$-level set of the solution of

$$\begin{cases} u_t(x,t) \in \mathrm{div}\,\left(\phi(\nabla u)\partial\phi(\nabla u)\right), & t > 0,\, x \in \mathbb{R}^N \\ u(\cdot,0) = \chi_P, \end{cases}$$

where ∂ denotes the subdifferential and P is the region enclosed by the interface. Its variational variant was introduced in [21], which is numerically simpler to solve by considering the minimization problem

$$\min_{u\in H^1(\Omega)} \int_\Omega \phi(\nabla u(x))^2 + \frac{1}{h}\left(u(x) - \chi_P(x)\right)^2 dx$$

In their numerical experiment, the authors experimented with an implicit method based on iterative resolutions of the above variational problem. Here, the solution $u(\cdot, x)$ is approximated with $w_n(x)$ where $h = nh'$ and n is a fixed (small) integer, by successively minimizing for $i = 0, \ldots, n-1$, the functional

$$\int_\Omega \phi(\nabla w(x))^2 + \frac{1}{h'}\left(w(x) - w_i(x)\right)^2 dx,$$

where $w_0 = \chi_P$. This is in fact, the variational scheme for the isotropic mean curvature flow introduced in [94]. As a result, the inherent MBO time and grid restriction still lingers in the algorithm where one either appropriately chooses the time step size to proceed the approximation without stagnation or introduces some form of mesh refinement.

In this light, we invoke the signed distance vector scheme to provide subgrid accuracies to prevent the resulting evolution from getting stuck. More precisely, for a given time step size $\Delta t = h \times K$, we successively minimize ($n = 1, 2, \ldots, K$):

$$\mathcal{J}_n^{h,\phi}(u) = \int_\Omega \left(\frac{|u - u_{n-1}|^2}{2h} + \frac{|\phi(\nabla u)|^2}{2} \right) dx$$

where

$$u_0(x) \quad = \quad \delta_\varepsilon(x) := \frac{1}{\varepsilon} \begin{cases} \min\left(\varepsilon, \mathrm{dist}(x, \Gamma)\right), & x \in P \\ -\min\left(\varepsilon, \mathrm{dist}(x, \Gamma)\right), & x \in \mathbb{R}^N \backslash P. \end{cases}$$

To realize volume-preserving anisotropic mean curvature flow, we add the penalization term to our functional as follows.

Algorithm 6.1 Two-phase SDV Method for Volume-preserving Anisotropic Flow

Given an initial interface network $\Gamma_0 := \partial P$ and a time step size $\Delta t > 0$, we obtain an approximation of the *volume-preserving anisotropic mean curvature flow* at time $t = m\Delta t$, by obtaining Γ_m from Γ_{m-1} as follows:

1. Initialization. For all $x \in \Omega$, set $u_0 := \delta_\varepsilon(x)$ with respect to Γ_{m-1}.
2. Minimization. Discretize $\Delta t = h \times K$. For a small positive number ϱ, successively minimize ($n = 1, 2, \ldots, K$):

$$\mathcal{F}_n^{h,\phi}(u) = \mathcal{J}_n^{h,\phi}(u) + \frac{1}{\varrho} \sum_{i=1}^{k} \left| \mathcal{L}^N(P) - \mathcal{L}^N(\{u > 0\}) \right|^2.$$

3. Projection. Set $\Gamma_m := \partial\{u > 0\}$, the zero-level set of the solution.

6.3 Numerical Results

In this section, we conduct numerical test to determine the accuracy of our method in comparison with the ϕ-MBO algorithm [21], including some computational examples.

6.3.1 Shrinking Anisotropic Circle Test

Let us start with a simple two-phase problem. Consider an anisotropic circle of initial radius r given by the set $\Gamma(0) = \{x : \phi^*(x) = r\}$ where ϕ^* is the dual of ϕ defined by

$$\phi^*(x) \quad = \quad \sup_{p \in \mathbb{R}^N \setminus \{0\}} \frac{x \cdot p}{\phi(p)}.$$

Note that the anisotropic distance between $x, y \in \mathbb{R}^N$ is given by $\phi^*(x - y)$. Then, the anisotropic mean curvature evolution of ϕ-circle (as shown in [48, Theorem 1.7.3]) is given by

$$\Gamma(t) = \{x : \phi^*(x) = \sqrt{r^2 - 2t}\}, \quad 0 \le t \le r^2/2,$$

which generalizes the isotropic mean curvature flow of a circle. For this test, we consider a square-type anisotropy function defined by

$$\phi(x) = \sum_{i=1}^{2} \sqrt{\sigma |x|^2 + x_1^2}, \tag{6.1}$$

the regularized l^1-anisotropy. With a smoothing parameter $\sigma = 10^{-6}$, we take its corresponding circle with radius $r = 0.25$ on a $[0, 1] \times [0, 1]$ domain as our initial condition.

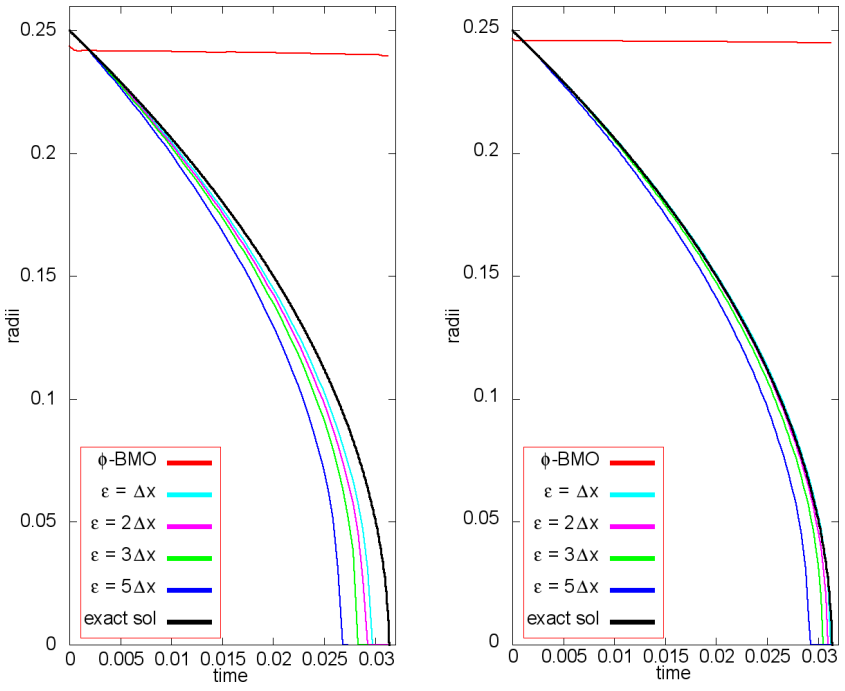

FIGURE 6.1: Evolution of the radius of an anisotropic circle evolved using ϕ-MBO scheme (red) and SDV method (non-red) on an 80×80 (left) and 160×160 (right) mesh resolution with time step size $\Delta t = T/64$ and $\Delta t = T/128$, respectively.

On varying mesh size and time step configurations, we run the SDV method for $\varepsilon = \Delta x, 2\Delta x, 3\Delta x, 5\Delta x$ until the exact extinction time $T = 0.03125$. We then, compare this resulting motion with the approximation via anisotropic MBO scheme [21], as well as, the exact solution (Figure 6.1). We see that for mesh-time configurations where ϕ-MBO scheme stagnates, our algorithm is able to alleviate the time and grid restrictions

and provides a fine approximation to the exact evolution of the anisotropic circle. In particular, on a 160×160 mesh resolution with time step size $\Delta t = T/128$, the resulting motion of SDV scheme with smaller ε values can hardly be distinguished from the exact solution; thereby, saving computational costs.

As in the isotropic case, the order of convergence is basically linear, but it is noticeable that results are more accurate on smaller SDV ε values. However, we should also mention that for even smaller time intervals (far from the onset of stagnation), larger SDV ε values would come into play since they provide more geometric information on the interfaces as is needed to overcome the time and grid restrictions, as was observed in our SDV approximation for isotropic mean curvature.

6.3.2 Example: Two-phase Anisotropic Mean Curvature Flow

Examples of anisotropic mean curvature flow generated via SDV method are given in this subsection. Consider a circle of radius 0.35 on a $[0,1] \times [0,1]$ domain as our initial condition. The domain is triangulated into $12,800$ elements and the time step size $\Delta t = 2.5 \times 10^{-4}$ is discretized into 30 DMF partitions. We run SDV method with $\varepsilon = 3\Delta x$ until its extinction and plot the resulting evolution of the circle under different anisotropic energies. Note that under this configuration, ϕ-MBO numerical scheme [21] stagnates due to time and grid restrictions as in the MBO threshold dynamics [68]. We show that using our algorithm, we are able to realize anisotropic mean curvature flow without stagnation.

First, we consider some examples of anisotropy found in the text [28].

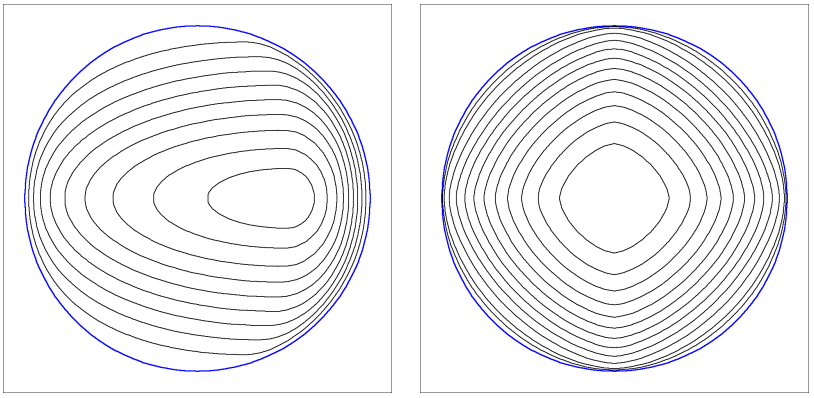

FIGURE 6.2: Anisotropic mean curvature evolution of a circle via SDV method under anisotropic energies ϕ_1 ($a = 5.5$, $b = 4.5$) and ϕ_2 ($a = 0.20$).

The first evolution of the initial circle in Figure 6.2 is generated under anisotropy function

$$\phi_1(x) = \sqrt{(a + b\,\mathrm{sgn}\,(x_1))\,x_1^2 + x_2^2},$$

for some constant $a, b > 0$. The second example, on the other hand, follows an anisotropy function often used in a physical context defined as

$$\phi_2(x) = \left(1 - a\left(1 - \frac{\|x\|_{l^4}^4}{\|x\|_{l^2}^4}\right)\right)\|x\|_{l^2},$$

for some $a > 0$. We see that our algorithm is able to handle anisotropic mean curvature motion resulting in smooth interfaces.

Next, we consider anisotropy functions with sharp corners (e.g., regular polygons) as shown in Figure 6.3. The first example evolves under a six-fold anisotropy

$$\phi_3(x) = \left(|\mu_1|^m + \left|\tfrac{1}{2}\mu_1 + \tfrac{\sqrt{3}}{2}\mu_2\right|^m + \left|-\tfrac{1}{2}\mu_1 + \tfrac{\sqrt{3}}{2}\mu_2\right|^m\right)^{1/m}$$

where $m \in \mathbb{N}$ and $\mu_i = \sqrt{\sigma|x|^2 + x_i^2}$ $(i = 1, 2)$ for a given smoothing parameter σ.

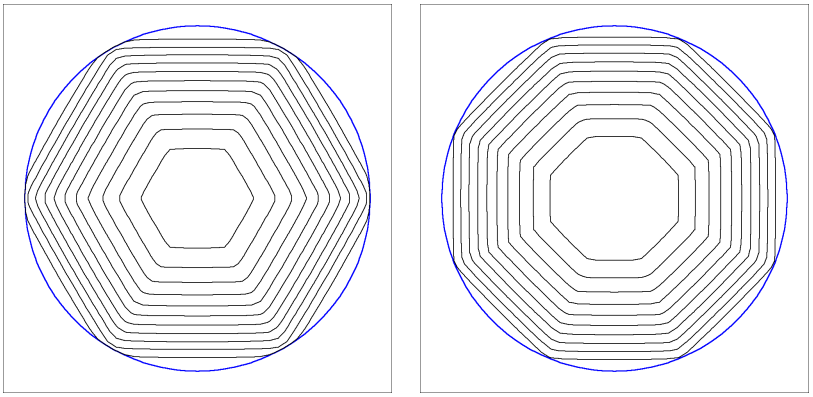

FIGURE 6.3: Anisotropic mean curvature evolution of a circle via SDV method under anisotropic energies ϕ_3 ($\sigma = 10^{-12}$, $m = 101$) and ϕ_4.

This can be generalized to any regular n-fold anisotropy as follows

$$\phi(x) = \left(\sum_{i=0}^{n-1} |\mathbf{e}_i \cdot \boldsymbol{\mu}|^m\right)^{1/m} \tag{6.2}$$

where $\boldsymbol{\mu} = (\mu_1, \mu_2)$ and vectors $\mathbf{e}_i$ $(i = 1, \ldots, n-1)$ are given by

$$\mathbf{e}_i = \begin{bmatrix} \cos\frac{i\pi}{n} & -\sin\frac{i\pi}{n} \\ \sin\frac{i\pi}{n} & \cos\frac{i\pi}{n} \end{bmatrix} \mathbf{e}_0$$

for any given vector $\mathbf{e}_0$. In other words, the vector $\mathbf{e}_i$'s are generated by successively rotating $\mathbf{e}_0$ by an angle of π/n. The second example in Figure 6.3 (top right) is the resulting motion of an eight-fold anisotropy ϕ_4 with parameters $n = 8$, $m = 101$, $\sigma = 10^{-12}$, and $\mathbf{e}_0 = \langle \cos\frac{\pi}{8}, \sin\frac{\pi}{8} \rangle$. We see that with small enough smoothing parameter, we are able to achieve a fairly good approximation of a regular n-fold anisotropic evolution without stagnation.

6.3.3 Example: Two-phase Volume-preserving Anisotropic Flow

Consider the same setup as in the previous subsection. We generate its anisotropic evolution while preserving the enclosed phase volume using our algorithm with $\varepsilon = 3\Delta x$ and penalty parameter $\varrho = 10^{-6}$.

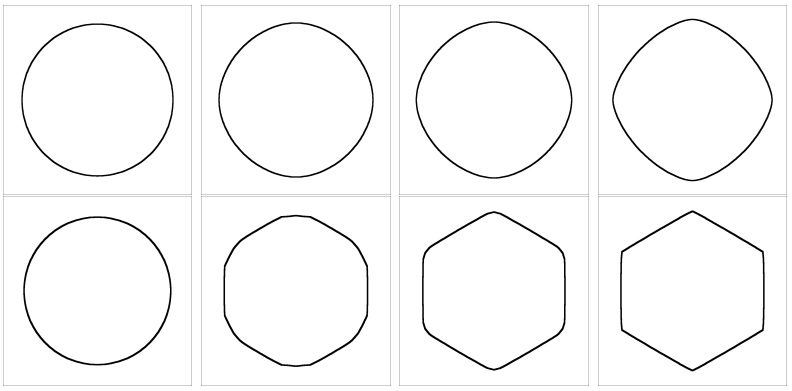

FIGURE 6.4: Volume-preserving SDV evolution driven by anisotropy ϕ_2 with $a = 0.20$ (top) and ϕ_4 with parameters $n = 8$, $m = 101$, $\sigma = 10^{-12}$, $\mathbf{e}_0 = \langle 0, 1\rangle$ (bottom).

Figure 6.4 shows the volume-preserving mean curvature evolution of a circle under anisotropy functions yielding centroid-symmetric interfaces. On both simulations, the difference of phase volumes in their initial and stationary state is at most 5.17×10^{-4}. Hence, the enclosed phase volumes are well-preserved, relative to the choice of penalty parameter.

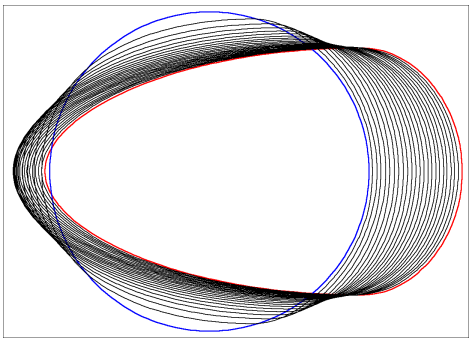

FIGURE 6.5: Volume-constrained evolution of a circle via SDV method driven by anisotropy ϕ_1 ($a = 5.5$, $b = 4.5$) under penalty paramter $\varrho = 10^{-6}$.

Figure 6.5, on the other hand, considers the volume-constrained evolution of a circle driven by anisotropy function ϕ_1 (with parameters $a = 5.5$, $b = 4.5$). In this setup, the enclosed phase volume is also well preserved with a volume difference of 1.16×10^{-4} under penalty parameter $\varrho = 10^{-6}$. However, due to its asymmetric nature, the interface continue to move to the right until reaching the boundary.

6.3.4 An Attempt: 7-phase Volume-preserving Anisotropic Flow

In this subsection, we experiment with a vector analogue of Algorithm 6.1 to realize multiphase volume-preserving anisotropic flow. To be precise, for a small positive number ϱ, we successively minimize ($n = 1, 2, \ldots, K$):

$$\mathcal{F}_n^h(\mathbf{u}) = \int_\Omega \left(\frac{|\mathbf{u} - \mathbf{u}_{n-1}|^2}{2h} + \frac{|\phi(\nabla \mathbf{u})|^2}{2} \right) dx + \frac{1}{\varrho} \sum_{i=1}^{k} \left| \alpha_i - \mathcal{L}^N(P_i(\mathbf{u})) \right|^2,$$

where $\mathbf{u}_0 := \boldsymbol{\delta}_{\boldsymbol{\varepsilon}}(x)$ with respect to $\Gamma := \bigcup \{\gamma_{ij} : i, j = 1, 2, \ldots, k\}$, α_i denotes the prescribed volume of phase P_i, and

$$P_i(\mathbf{u}) := \{x \in \Omega : \mathbf{p}_i \cdot \mathbf{u}(x) \geq \mathbf{p}_j \cdot \mathbf{u}(x),\ \forall j = 1, 2, ..., k\},$$

the set corresponding to phase P_i with respect to solution $\mathbf{u}$.

Consider a 7-phase configuration where the initial interfaces are circular arcs. The domain $\Omega = [0, 1] \times [0, 1]$ is triangulated into 6049 elements and time step size $\Delta t = 5.0 \times 10^{-4}$ with DMF partition $K = 20$. We preserve the phase volumes using SDV method with $\varepsilon = \Delta x$ under a penalty parameter $\varrho = 10^{-5}$ and a square-type anisotropy (6.1) defined as the regularized l^1-anisotropy. Note that this is consistent with our n-fold anisotropy function (6.2) with parameters $m = 1, n = 2, \mathbf{e}_0 = \langle 0, 1 \rangle$.

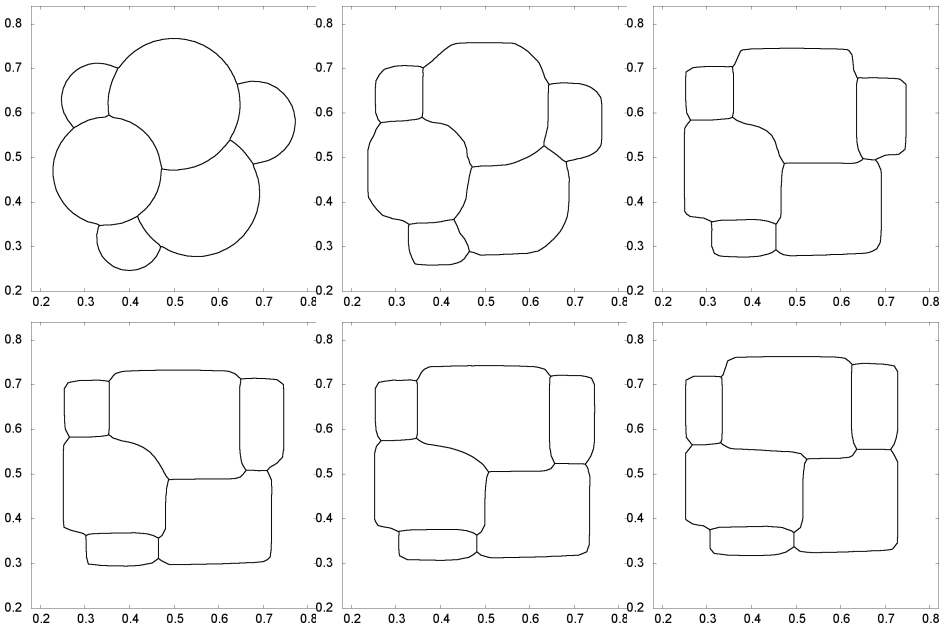

FIGURE 6.6: Initial 7-phase configuration (top left); its volume-preserving anisotropic evolution after one time step $\Delta t = 5.0 \times 10^{-4}$ (top center); at $t = 10\Delta t$ (top right); at $t = 100\Delta t$ (bottom left); at $t = 200\Delta t$ (bottom center); and its stationary solution (bottom right).

Figure 6.6 shows the resulting motion of the initial overlapping circles under the SDV method for volume-preserving flow driven by a square-type anisotropy (Algorithm 5.1). We see that our algorithm evolves the interfaces in an attempt to have an enclosed square region (as set by the anisotropy function (6.1)) while preserving the phase volumes. Unfortunately, since our algorithm only imposes the symmetric Herring angle conditions, we were not able to accurately capture the evolution near the triple junction resulting in nonsquare phase regions in the stationary solution.

For this square-type anisotropy, we conjecture that a $180° - 90° - 90°$ angle condition must be satisfied at the junction. This requires us to modify the projection step in the algorithm, possibly by using a similar projection circle as in [88].

6.4 Concluding Remarks

We have presented a signed distance vector approach for realizing volume-preserving anisotropic mean curvature flows, which alleviates the time and grid restriction in [21]. Although we were only successful in the two-phase case, our vector setting also allowed us to experiment with multiphase anisotropic mean curvature flows. One issue that needs to be resolved is the evolution at the triple junction using our current method. To do this, we first need to know what exactly are the junction angle conditions set by the prescribed anisotropy function. Once this is known, some form of nonsymmetric reference vectors (as in [88]) in conjunction with our signed distance vector may be adopted to get a closer approximation of the evolution of the triple junction under anisotropic mean curvature flow. This is one problem that we would like to work on in the future. Another would be to show that our method evolves interfaces according to its anisotropic mean curvature – a similar analysis as in [36, 37, 94].

Chapter 7

On Evolutionary Free Boundary Problem with Volume Constraint

This chapter focuses on a penalization technique in relation to the volume-constrained variational method employed in our SDV scheme. We prove the existence and regularity of the sequence of minimizers of the penalized functional. We also investigate the behavior of these minimizers for large penalty values, and construct a minimizing movement and show some of its propeties. (For the list of notations and some preliminary results utilized in this chapter, please refer to Appendix H.)

7.1 Introduction

Let $\Omega \subset \mathbb{R}^N$ be an open bounded connected domain with smooth convex Lipschitz boundary. Consider a Lipschitz continuous function $u_0 \in H^1(\Omega) \cap L^\infty(\Omega)$ whose set of positive values has Lebesgue measure $\alpha \in (0, |\Omega|)$. Given time step $h = T/M$ for some fixed time $T \in (0, \infty)$ and $M \in \mathbb{N}$, we search for a sequence of functions $u_n \in H^1(\Omega)$ by successively solving the following problem for $n = 1, 2, \ldots, M$,

$$\begin{cases} u_n = \arg\min\limits_{\mathcal{A}} \displaystyle\int_\Omega \left(\frac{|u - u_{n-1}|^2}{h} + |\nabla u|^2 \right) dx \\ \mathcal{A} := \left\{ u \in H^1(\Omega) : \ |\{u > 0\}| = \alpha \right\}. \end{cases} \tag{7.1}$$

The above problem appears in our numerical approximation of volume-preserving mean curvature flow by MBO algorithm (see Chapter 4). It is known that it is possible to realize this geometrical evolution if one solves the L^2-gradient flow of the Dirichlet functional in the admissible set consisting of H^1-functions having 0-level set with a given volume α. The time-semidiscretization of this gradient flow problem leads to the minimization problem (7.1), which is then solved numerically by a penalization technique. The purpose of the present chapter is to provide a basic analysis for the above problem, which could serve as a starting point for a rigorous proof of convergence and other properties of the volume-preserving MBO algorithm. In particular, by studying a similar penalty form as in Chapter 4, we show that for sufficiently large (but finite) penalty coefficient the volume of level sets adjusts to the exact value, and thus we

justify the usage of this penalization in the numerical scheme. Moreover, the topic is interesting from the pure mathematical point of view since free boundary problems with global constraints have been treated only in the stationary (elliptic) case.

The problem of minimizing only the Dirichlet integral over set $\mathcal{A}$ assuming a given boundary value was considered in [2] using a penalization technique by minimizing for $\varepsilon > 0$, the functional

$$\mathcal{J}_\varepsilon(u) := \int_\Omega |\nabla u|^2 + f_\varepsilon\left(|\{u > 0\}|\right)$$

where

$$f_\varepsilon(x) := \begin{cases} \dfrac{1}{\varepsilon}(x-\alpha), & x \geq \alpha \\ \varepsilon(x-\alpha), & x \leq \alpha. \end{cases}$$

In [2], the authors showed that minimizer u_ε of $\mathcal{J}_\varepsilon$ is a weak solution of the free boundary problem for Laplace equation with free boundary condition $-\partial_\eta u_\varepsilon = \lambda_\varepsilon$ for some constant $\lambda_\varepsilon > 0$ in the sense of [4]; thereby allowing them to use the regularity theory established therein. Hence, smooth inward and outward perturbations of the set $\{u_\varepsilon > 0\}$ were possible. This lead them to establish that for small enough ε, the minimizer u_ε actually solves the original problem of minimizing the Dirichlet functional $\int_\Omega |\nabla u|^2$ under the constraint $|\{u > 0\}| = \alpha$, since the measure of $\{u_\varepsilon > 0\}$ automatically adjusts to the prescribed value.

Similar results were obtained by Tilli [93] for the problem of minimizing the Dirichlet integral over all H^1-functions where each l_i-level set has prescribed Lebesgue measure $\alpha_i\,(i = 1, 2, \ldots, k)$. He used a technique that penalizes only those functions whose level sets are of measure less than the prescribed value, that is, for $\lambda > 0$,

$$\min_{H^1(\Omega)} \int_\Omega |\nabla u|^2 + \lambda \sum_{i=1}^{k} \left(\alpha_i - |\{u = l_i\}|\right)_+ . \tag{7.2}$$

The smooth inward perturbation of the level sets (which require smoothness of the free boundary and normal derivatives) was avoided since for any minimizer of (7.2), the measures of the level sets do not exceed their prescribed values. Moreover, without any information on smoothness, outward perturbations of the level sets were done by simply replacing u in the set $l_i < u < l_{i+1}$ by $w_\delta = l_i + c(u - l_i - \delta)_+$, where $\delta \in (l_i, l_{i+1})$ and c is chosen so that l_i-level set is replaced by a larger set $\{l_i \leq u \leq l_i + \delta\}$ while the other level sets are preserved. Using this technique, the same result as in [2] was obtained without employing the smoothness of the free boundary, namely, there exists a finite value λ_0 such that for any $\lambda \geq \lambda_0$, the minimizer u of (7.2) exactly satisfies the volume constraints $|\{u = l_i\}| = \alpha_i\ (i = 1, 2, \ldots, k)$.

In this chapter, we consider the simpler one-phase case when u_0 is nonnegative, and adopt a similar penalization technique as in [93] to solve the original problem (7.1). In particular, we consider a method that penalizes only the increase in measure of the set $\{u > 0\}$. For a penalty parameter $\lambda > 0$, we define

$$\mathcal{F}(h, u, u_{n-1}) = \mathcal{F}_n^h(u) := \int_\Omega \left(\frac{|u - u_{n-1}|^2}{h} + |\nabla u|^2 \right) dx + \lambda f(|\{u > 0\}|),$$

where the penalization function $f(x) = (x-\alpha)_+$, and we consider the problem of successively minimizing the above functional for $n = 1, 2, \ldots, M$,

$$\min_{u \in H^1(\Omega)} \mathcal{F}(h, u, u_{n-1}). \tag{7.3}$$

We first establish the existence and regularity of minimizer u_n of $\mathcal{F}_n^h$ at each time level in sections 7.2, 7.3, and 7.4. Without relying on the smoothness of the free boundary as in [93], we show then that for sufficiently large penalty parameter λ, depending on h but independent of n, the measure of the set $\{u_n > 0\}$ adjusts to its prescribed value (section 7.5). As a consequence, the solution to the original problem is attained without passing the limit in λ. Moreover, we construct a minimizing movement associated to $\mathcal{F}$ and u_0 exists and show some of its properties (section 7.6).

7.2 Existence of minimizer and its properties

In this section, we show the existence of a sequence of minimizers and some of its properties.

Theorem 7.1. *For $h, \lambda > 0$, there exists a sequence $\{u_n\}_{n=1}^M \subset H^1(\Omega)$ such that u_n minimizes $\mathcal{F}_n^h$.*

Proof. Fix $h, \lambda > 0$. We first show that for any given function $v \in H^1(\Omega)$, there exists $u \in H^1(\Omega)$ which minimizes

$$\mathcal{F}(h, u, v) = \int_\Omega \frac{|u-v|^2}{h} + |\nabla u|^2 + \lambda f(|\{u > 0\}|).$$

Since $\mathcal{F}$ is nonnegative, then there exists a minimizing sequence $\{u^k\} \subset H^1(\Omega)$ such that

$$\mathcal{F}(h, u, v) \longrightarrow \inf_{H^1(\Omega)} \mathcal{F}(h, \cdot, v).$$

We show that a subsequence $\{u^k\}$ converges to a minimizer of $\mathcal{F}$. Note that

$$\int_\Omega |\nabla u^k|^2 \leq \sup_k \mathcal{F}(h, u^k, v) < +\infty,$$

which implies that $\{\nabla u^k\}$ is uniformly bounded in $L^2(\Omega)$. Then, by L^2-weak compactness, we can find a subsequence (still denoted by u^k) such that for some $\phi \in L^2(\Omega)$, we have

$$\nabla u^k \quad \rightharpoonup \quad \phi \ \text{ weakly in } L^2(\Omega). \tag{7.4}$$

Note that

$$\|u^k - v\|^2_{L^2(\Omega)} = h \int_\Omega \frac{|u^k - v|^2}{h} \quad \leq \quad h \sup_k \mathcal{F}(h, u^k, v) < +\infty,$$

and so, we have

$$\|u^k\|_{L^2(\Omega)} \quad \leq \quad \|u^k - v\|_{L^2(\Omega)} + \|v\|_{L^2(\Omega)} < +\infty.$$

It follows that $\{u^k\}$ is uniformly bounded in $H^1(\Omega)$. Thus, by Rellich-Kondrachov theorem, there exists a subsequence (still denoted by u^k) such that for some $u \in L^2(\Omega)$, we have

$$u^k \longrightarrow u \text{ strongly in } L^2(\Omega), \tag{7.5}$$

which also implies a weak L^2-convergence. Hence,

$$\lim_{k\to\infty}\int_\Omega \frac{|u^k - v|^2}{h} = \lim_{k\to\infty}\int_\Omega \frac{\left(u^k\right)^2 - 2u^k v + v^2}{h} = \int_\Omega \frac{|u-v|^2}{h}. \tag{7.6}$$

Moreover, by (7.4) and (7.5), we see that for any $\psi \in C_0^\infty(\Omega)$,

$$\int_\Omega \phi\cdot\psi = \lim_{k\to\infty}\int_\Omega \nabla u^k\cdot\psi = -\lim_{k\to\infty}\int_\Omega u^k \operatorname{div}\psi = -\int_\Omega u\operatorname{div}\psi,$$

implying that $\nabla u = \phi$ in the weak sense. Thus, $\nabla u^k \rightharpoonup \nabla u$ weakly in $L^2(\Omega)$.

Now, $\int_\Omega |\nabla u^k - \nabla u|^2 \geq 0$ implies

$$2\int_\Omega \nabla u^k\cdot\nabla u \leq \int_\Omega |\nabla u^k|^2 + \int_\Omega |\nabla u|^2.$$

Taking the limit inferior and applying the above weak convergence, we get

$$\int_\Omega |\nabla u|^2 \leq \liminf_{k\to\infty}\int_\Omega |\nabla u^k|^2. \tag{7.7}$$

Moreover, there exists a nonnegative function $\gamma \in L^\infty(\Omega;[0,1])$ such that

$$\chi_{\{u^k>0\}} \rightharpoonup \gamma \quad \text{weakly star in } L^\infty(\Omega),$$

which implies that

$$\int_\Omega \gamma = \lim_{k\to\infty}\int_\Omega \chi_{\{u^k>0\}} = \lim_{k\to\infty}|\{u^k>0\}|. \tag{7.8}$$

By (7.5), we can find a subsequence (still denoted by u^k) such that $u^k \to u$ almost everywhere in Ω. Since $\gamma \leq 1$, then

$$\int_\Omega |\gamma - 1|\chi_{\{u>0\}} = \int_{\{u>0\}} 1 - \chi_{\{u^k>0\}} + \int_\Omega \left(\chi_{\{u^k>0\}} - \gamma\right)\chi_{\{u>0\}} \longrightarrow 0,$$

which implies that $\gamma = 1$ almost everywhere in $\{u>0\}$. By (7.8),

$$|\{u>0\}| = \int_\Omega \chi_{\{u>0\}} \leq \int_\Omega \gamma = \lim_{k\to\infty}|\{u^k>0\}|.$$

Since f is continuous and nondecreasing, we get

$$f(|\{u>0\}|) \leq \lim_{k\to\infty} f(|\{u^k>0\}|). \tag{7.9}$$

Thus, combining (7.6), (7.7), and (7.9) yields

$$\mathcal{F}(h,u,v) \leq \liminf_{k\to\infty}\mathcal{F}(h,u^k,v) = \inf_{H^1(\Omega)}\mathcal{F}(h,\cdot,v) \leq \mathcal{F}(h,u,v),$$

and so, $u \in H^1(\Omega)$ is a minimizer.

Finally, since $u_0 \in H^1(\Omega)$, then by the above claim, there exists $u_1 \in H^1(\Omega)$ which minimizes $\mathcal{F}_1^h = \mathcal{F}(h, \cdot, u_0)$. Inductively, we can find $u_n \in H^1(\Omega)$ which minimizes $\mathcal{F}_n^h$ for all $n = 2, \ldots, M$. □

From hereon, we shall denote this sequence of minimizers by $\{u_n\} \subset H^1(\Omega)$. These minimizers are in fact, nonnegative and bounded from above by the L^∞-norm of u_0 as follows.

Theorem 7.2. *If u_n minimizes $\mathcal{F}_n^h$ $(n = 1, \ldots, M)$ for $h, \lambda > 0$, then*

$$0 \leq u_n(x) \leq \|u_0\|_\infty,$$

for almost every $x \in \Omega$.

Proof by Induction. Note that $0 \leq u_0 \leq \|u_0\|_\infty$. Fix n and assume that

$$0 \leq u_{n-1} \leq \|u_0\|_\infty \quad \text{a.e. in } \Omega. \tag{7.10}$$

Suppose $|\{u_n < 0\}| \neq 0$. Consider $\phi := \max(u_n, 0) \in H^1(\Omega)$ where

$$\nabla\phi = \begin{cases} \nabla u_n, & u_n > 0 \\ 0, & \text{otherwise,} \end{cases}$$

in the weak sense. Note that $|\{u_n > 0\}| = |\{\phi > 0\}|$. Hence, $f(|\{u_n > 0\}|) = f(|\{\phi > 0\}|)$. Moreover,

$$\int_\Omega |\nabla\phi|^2 = \int_{\{u_n > 0\}} |\nabla u_n|^2 \leq \int_\Omega |\nabla u_n|^2.$$

and

$$\begin{aligned} \int_\Omega |\phi - u_{n-1}|^2 &= \int_{\{u_n > 0\}} |u_n - u_{n-1}|^2 + \int_{\{u_n < 0\}} u_{n-1}^2 \\ &= \int_\Omega (u_n - u_{n-1})^2 + \int_{\{u_n < 0\}} 2u_n u_{n-1} - u_n^2 \\ &< \int_\Omega |u_n - u_{n-1}|^2, \end{aligned}$$

since by (7.10), $2u_n u_{n-1} \leq 0$ and $u_n \neq 0$ in set $\{u_n < 0\}$. Thus, $\mathcal{F}_n^h(\phi) < \mathcal{F}_n^h(u_n)$, which contradicts the minimality of u_n.

Suppose $|S| := |\{u_n > \|u_0\|_\infty\}| \neq 0$. Take $\phi := \min(u_n, \|u_0\|_\infty) \in H^1(\Omega)$ where

$$\nabla\phi = \begin{cases} \nabla u_n, & u_n < \|u_0\|_\infty \\ 0, & \text{otherwise,} \end{cases}$$

in the weak sense. Note that $\{u_n > 0\} = S \cup \{0 < u_n \leq \|u_0\|_\infty\} = \{\phi > 0\}$. Then, we have $f(|\{u_n > 0\}|) = f(|\{\phi > 0\}|)$. Moreover,

$$\int_\Omega |\nabla\phi|^2 = \int_{\{u < \|u_0\|_\infty\}} |\nabla u_n|^2 \leq \int_\Omega |\nabla u_n|^2.$$

and

$$\begin{aligned}\int_\Omega |\phi - u_{n-1}|^2 &= \int_{\Omega\setminus S} |u_n - u_{n-1}|^2 + \int_S |\|u_0\|_\infty - u_{n-1}|^2 \\ &= \int_\Omega |u_n - u_{n-1}|^2 + \int_S \|u_0\|_\infty^2 - u_n^2 - 2u_{n-1}\left(\|u_0\|_\infty - u_n\right) \\ &= \int_\Omega |u_n - u_{n-1}|^2 + \int_S \left(\|u_0\|_\infty - u_n\right)\left(\|u_0\|_\infty + u_n - 2u_{n-1}\right) \\ &< \int_\Omega |u_n - u_{n-1}|^2,\end{aligned}$$

since in set S, we have $\|u_0\|_\infty - u_n < 0$ and $\|u_0\|_\infty + u_n - 2u_{n-1} > 2(\|u_0\|_\infty - u_{n-1}) \geq 0$ which follows from (7.10). Hence, $\mathcal{F}_n^h(\phi) < \mathcal{F}_n^h(u_n)$. A contradiction! □

We end this section with some estimates regarding the minimizer, which we shall utilize in the succeeding arguments.

Lemma 7.3. *If u_n minimizes $\mathcal{F}_n^h\,(n = 1, \ldots, M)$ for $h, \lambda > 0$, then*

(i.) $\|\nabla u_n\|_{L^2(\Omega)} \leq \|\nabla u_0\|_{L^2(\Omega)}$,

(ii.) $\|u_n - u_{n-1}\|_{L^2(\Omega)} \leq \sqrt{h}\|\nabla u_0\|_{L^2(\Omega)}$,

(iii.) $f(|\{u_n > 0\}|) \leq \lambda^{-1}\|\nabla u_0\|_{L^2(\Omega)}^2$.

Proof. Denote

$$\mathcal{J}(u) := \int_\Omega |\nabla u|^2 + \lambda f(|\{u > 0\}|).$$

Then, $\mathcal{F}_n^h(u_n) \leq \mathcal{F}_n^h(u_{n-1}) = \mathcal{J}(u_{n-1})$ implies

$$\mathcal{J}(u_n) \leq \int_\Omega \frac{|u_n - u_{n-1}|^2}{h} + \mathcal{J}(u_n) \leq \mathcal{J}(u_{n-1}),$$

which implies that $\mathcal{J}(u_n) \leq \mathcal{J}(u_{n-1}) \leq \cdots \leq \mathcal{J}(u_0)$. Since $|\{u_0 > 0\}| = \alpha$, then

$$\mathcal{F}_n^h(u_n) \leq \mathcal{F}_n^h(u_{n-1}) = \mathcal{J}(u_{n-1}) \leq \mathcal{J}(u_0) = \|\nabla u_0\|_{L^2(\Omega)}^2,$$

which yields the desired results. □

7.3 Interior Regularity of Minimizer

In this section, we establish the interior regularity of the sequence of minimizers. By virtue of Theorem H.7, we first show that the minimizer is locally Hölder continuous.

Theorem 7.4. *If u_n minimizes $\mathcal{F}_n^h\,(n = 1, \ldots, M)$ for $h, \lambda > 0$, then u_n is locally Hölder continuous. In particular, the (local) Hölder constant of u_n do not depend on n.*

Proof. Consider an arbitrary ball B_R such that $\overline{B_R} \subset \Omega$. Define function

$$\phi = \eta^2 (u_n - k)_+ ,$$

where $\eta \in C_0^\infty(\Omega; [0,1])$ such that $\eta \equiv 1$ in a smaller concentric ball B_r and $|\nabla \eta| \leq c/(R-r)$ for some constant $c > 1$. Fix $k \in \mathbb{R}$ and denote $A_R^+ := B_R \cap \{u_n > k\}$. By Theorem 7.2, we can assume that $k \leq \|u_0\|_\infty$. Since f is 1-Lipschitz continuous, then

$$\begin{aligned} f\left(|\{u_n - \phi > 0\}|\right) - f\left(|\{u_n > 0\}|\right) &\leq \left||\{u_n - \phi > 0\}| - |\{u_n > 0\}|\right| \\ &\leq \left|\{u_n - \phi > 0\} \cap A_R^+\right| + \left|\{u_n > 0\} \cap A_R^+\right| \\ &\leq 2\left|A_R^+\right|. \end{aligned}$$

Then, $\mathcal{F}_n^h(u_n) \leq \mathcal{F}_n^h(u_n - \phi)$ implies that

$$0 \leq -2\int_{A_R^+} \frac{u_n - u_{n-1}}{h}\phi + \int_{A_R^+} \frac{\phi^2}{h} - 2\int_{A_R^+} \nabla u_n \cdot \nabla \phi + \int_{A_R^+} |\nabla \phi|^2 + 2\lambda |A_R^+|. \quad (7.11)$$

Since u_n is bounded by $\|u_0\|_\infty$ almost everywhere, then

$$\begin{aligned} -\int_{A_R^+} (u_n - u_{n-1})\phi &= \int_{A_R^+} (u_{n-1} - u_n)\eta^2 (u_n - k) \\ &\leq \int_{A_R^+} |u_{n-1} - k - (u_n - k)|(u_n - k) \\ &\leq \int_{A_R^+} |u_{n-1} - k||u_n - k| + \int_{A_R^+} (u_n - k)^2 \\ &\leq \int_{A_R^+} \left(|u_{n-1}| + |k|\right)\left(|u_n| + |k|\right) + \int_{A_R^+} (u_n - k)^2 \\ &\leq 4\|u_0\|_\infty^2 |A_R^+| + \frac{R^2}{(R-r)^2}\int_{A_R^+} (u_n - k)^2, \end{aligned}$$

and

$$\int_{A_R^+} \phi^2 = \int_{A_R^+} \eta^4 (u_n - k)^2 \leq \frac{R^2}{(R-r)^2}\int_{A_R^+} (u_n - k)^2.$$

Using Young's inequality, we have for some $\varepsilon_1 \in (0,1)$,

$$\begin{aligned} -2\int_{A_R^+} \nabla u_n \cdot \nabla \phi &= -2\int_{A_R^+} \nabla u_n \cdot \left[\eta^2 \nabla u_n + 2(u_n - k)\eta \nabla \eta\right] \\ &\leq (-2 + \varepsilon_1)\int_{A_R^+} \eta^2 |\nabla u_n|^2 + \frac{4}{\varepsilon_1}\int_{A_R^+} (u_n - k)^2 |\nabla \eta|^2. \end{aligned}$$

Again, by Young's inequality, we have for some $\varepsilon_2 \in (0, 1 - \varepsilon_1)$,

$$\begin{aligned} \int_{A_R^+} |\nabla \phi|^2 &= \int_{A_R^+} \eta^4 |\nabla u_n|^2 + 4\int_{A_R^+} \eta^3 (u_n - k)\nabla u_n \cdot \nabla \eta + 4\int_{A_R^+} \eta^2 (u_n - k)^2 |\nabla \eta|^2 \\ &\leq (1 + \varepsilon_2)\int_{A_R^+} \eta^4 |\nabla u_n|^2 + 4\Big(1 + \tfrac{1}{\varepsilon_2}\Big)\int_{A_R^+} \eta^2 (u_n - k)^2 |\nabla \eta|^2 \\ &\leq (1 + \varepsilon_2)\int_{A_R^+} \eta^2 |\nabla u_n|^2 + 4\Big(1 + \tfrac{1}{\varepsilon_2}\Big)\int_{A_R^+} (u_n - k)^2 |\nabla \eta|^2. \end{aligned}$$

Thus, (7.11) becomes

$$\begin{aligned}(1-\varepsilon_1-\varepsilon_2)\int_{A_r^+}|\nabla u_n|^2 \le\ & (-1+\varepsilon_1+\varepsilon_2)\int_{A_R^+\setminus A_r^+}\eta^2|\nabla u_n|^2+4\Big(1+\tfrac{1}{\varepsilon_1}+\tfrac{1}{\varepsilon_2}\Big)\int_{A_R^+}(u_n-k)^2|\nabla\eta|^2\\ &+\ \frac{3R^2}{h(R-r)^2}\int_{A_R^+}(u_n-k)^2+2\max\left(\frac{4\|u_0\|_\infty^2}{h},\lambda\right)|A_R^+|.\\ \le\ & \frac{C}{(R-r)^2}\int_{A_R^+}(u_n-k)^2+2\max\left(\frac{4\|u_0\|_\infty^2}{h},\lambda\right)|A_R^+|,\end{aligned}$$

where $C(h,R):=\max\Big(4c(1+\frac{1}{\varepsilon_1}+\frac{1}{\varepsilon_2}),3R^2h^{-1}\Big)$. Hence,

$$\int_{A_r^+}|\nabla u_n|^2 \ \le\ \rho\left[\frac{1}{(R-r)^2}\max_{A_R^+}(u_n-k)^2+1\right]|A_R^+|,$$

where $\rho(1-\varepsilon_1-\varepsilon_2)=\max\Big(4c(1+\frac{1}{\varepsilon_1}+\frac{1}{\varepsilon_2}),\,3R^2h^{-1},\,8\|u_0\|_\infty^2h^{-1},\,2\lambda\Big)$. Analogously, taking $\phi=\eta^2(u_n-k)_-$ yields the above inequality for $A_R^-:=B_R\cap\{u_n<k\}$. Moreover, by Theorem 7.2, u_n is bounded with $\operatorname{ess\,sup}u_n\le\|u_0\|_\infty$. It follows that u_n belongs to Di Giorgi class $B_2(\Omega,\|u_0\|_\infty,\rho,\infty,0)$.

Fix $x_0\in\Omega$ and consider an open ball $B_R:=B(x_0,R)\subset\Omega$ for some $R\le1$. For any $x,y\in B_R$, denote $r=|x-y|<R$. By Theorem H.7 [62, Chapter 2, Theorem 6.1], we can find constants $\gamma<1$ and $C(\gamma,N,R)>0$ such that

$$|u_n(x)-u_n(y)| \ \le\ \sup_{B_r}u_n-\inf_{B_r}u_n\le C|x-y|^\gamma.$$

Then, u_n is Hölder continuous near x_0. □

Next, we show that the minimizer is a subsolution to an elliptic partial differential equation on domain Ω. In fact, on the region where it is strictly positive, the minimizer is a solution and locally a C^2 function.

Theorem 7.5. *If u_n minimizes $\mathcal{F}_n^h$ $(n=1,...,M)$ for $h,\lambda>0$, then (in the weak sense)*

(i.) $\Delta u_n\ge\dfrac{u_n-u_{n-1}}{h}$ *in* Ω,

(ii.) $\Delta u_n=\dfrac{u_n-u_{n-1}}{h}$ *in the open set* $\{u_n>0\}$.

Proof. For $\varepsilon>0$ and nonnegative functions $\phi\in C_0^\infty(\Omega)$, consider $\psi:=u_n-\varepsilon\phi$. Hence, if $\psi(x)>0$ for some $x\in\Omega$, then clearly we have $u_n(x)>\varepsilon\phi(x)>0$. Thus, we get $f(|\{\psi>0\}|)\le f(|\{u_n>0\}|)$, which implies that

$$\begin{aligned}0 \ &\le\ \mathcal{F}_n^h(\psi)-\mathcal{F}_n^h(u_n)\\ &\le\ -2\varepsilon\int_\Omega\left(\frac{u_n-u_{n-1}}{h}\phi+\nabla u_n\cdot\nabla\phi\right)+\varepsilon^2\int_\Omega\left(\frac{|\phi|^2}{h}+|\nabla\phi|^2\right).\end{aligned}$$

Dividing by 2ε and taking $\varepsilon\to0$ yields

$$\int_\Omega\frac{u_n-u_{n-1}}{h}\phi+\nabla u_n\cdot\nabla\phi\le0, \tag{7.12}$$

thereby, proving (***i***).

To prove (***ii***), it suffices to show the reverse inequality of (7.12). Consider $\psi := u_n + \varepsilon\phi$ where $\phi \in C_0^\infty(\{u_n > 0\})$ with

$$|\varepsilon| < \frac{m}{\max \phi} \text{ where } m := \min_{\operatorname{supp}\phi} u_n > 0.$$

It follows that the penalization of ψ is equal to that of u_n, and so, we get

$$\begin{aligned} 0 &\leq \mathcal{F}_n^h(\psi) - \mathcal{F}_n^h(u_n) \\ &\leq 2\varepsilon \int_{\{u_n>0\}} \left(\frac{u_n - u_{n-1}}{h}\phi + \nabla u_n \cdot \nabla\phi \right) + \varepsilon^2 \int_{\{u_n>0\}} \left(\frac{|\phi|^2}{h} + |\nabla\phi|^2 \right). \end{aligned}$$

Dividing by 2ε and taking $\varepsilon \to 0$ gives the desired result. □

Corollary 7.6. *If u_n minimizes $\mathcal{F}_n^h (n=1, ..., M)$ for $h, \lambda > 0$, then $u_n \in C^2_{\text{loc}}(\{u_n > 0\})$.*

Proof. Fix $x_0 \in \{u_n > 0\}$. Consider function $\phi \in C_0^\infty(\{u_n > 0\})$ such that $\phi \equiv 1$ in $B_r := B(x_0, r) \subset \{u_n > 0\}$ for some $r > 0$. Let $w = \psi * g$ where where ψ denotes the fundamental solution of Laplace equation and function g is defined by

$$g := \frac{u_n - u_{n-1}}{h}\phi.$$

By Theorem 7.4 and [49, Lemma 4.2], we see that $w \in C^2(\Omega)$ and $\Delta w = g$ in Ω. Hence, by Theorem 7.5, we get

$$\Delta(u_n - w) = \frac{u_n - u_{n-1}}{h}(1 - \phi) = 0 \quad \text{in } B_r,$$

which implies that $u_n - w$ is harmonic (hence, C^∞) in B_r. Thus, u_n is C^2 near x_0. □

The following remark will be utilized in the succeeding arguments.

Remark. Fix a ball $B_r \subset \Omega$. Define functional

$$\mathcal{I}_{n,B_r}(u) := \int_{B_r} \left(\frac{|u - u_{n-1}|^2}{h} + |\nabla u|^2 \right) dx.$$

Then, there exists a unique minimizer $v \in A := \{v \in H^1(B_r) : v = u_n \text{ on } \partial B_r\}$ such that

$$\mathcal{I}_{n,B_r}(v) = \min_A \mathcal{I}_{n,B_r}(\cdot).$$

Moreover, in the weak sense,

$$\Delta v = \frac{v - u_{n-1}}{h} \quad \text{in } B_r, \tag{7.13}$$

which follows from the proof of Theorem 7.5 by simply dropping the penalty arguments.

Existence. A similar argument as in the proof of Theorem 7.1 shows that we can find a minimizing sequence $\{u^k\} \subset A$ that is uniformly bounded in $H^1(B_r)$ and whose

subsequence converges weakly in $H^1(B_r)$ to some $v \in H^1(B_r)$ and

$$\mathcal{I}_{n,B_r}(v) \leq \liminf_{k\to\infty} \mathcal{I}_{n,B_r}(u^k).$$

Note that there exists a trace operator $T : H^1(B_r) \to L^2(\partial B_r)$. Since T is a compact operator, then we can find a subsequence (still denoted by u^k) such that

$$T(u^k) \to T(v) \text{ strongly in } L^2(\partial B_r).$$

Noting that $T(u^k) = u_n$ on ∂B_r, we see $v = u_n$ on ∂B_r in the sense of trace, and so, $v \in A$.

Uniqueness. Suppose there exist minimizers $u, v \in A$, that is, $\mathcal{I}_{n,B_r}(u) = \mathcal{I}_{n,B_r}(v) = m$. Consider $w := \frac{1}{2}(u+v)$. By the parallelogram law, we have

$$\begin{aligned}
\|w - u_{n-1}\|^2_{L^2(B_r)} &= \left\|\tfrac{1}{2}(u-u_{n-1}) + \tfrac{1}{2}(v-u_{n-1})\right\|^2_{L^2(B_r)} \\
&= \tfrac{1}{2}\|u-u_{n-1}\|^2_{L^2(B_r)} + \tfrac{1}{2}\|v-u_{n-1}\|^2_{L^2(B_r)} - \left\|\frac{u-v}{2}\right\|^2_{L^2(B_r)} \\
\|\nabla w\|^2_{L^2(B_r)} &= \tfrac{1}{2}\|\nabla u\|^2_{L^2(B_r)} + \tfrac{1}{2}\|\nabla v\|^2_{L^2(B_r)} - \left\|\frac{\nabla u - \nabla v}{2}\right\|^2_{L^2(B_r)}
\end{aligned}$$

Hence,

$$\begin{aligned}
m \leq \mathcal{I}_{n,B_r}(w) &= \tfrac{1}{2}\mathcal{I}_{n,B_r}(u) + \tfrac{1}{2}\mathcal{I}_{n,B_r}(v) - \frac{1}{4}\int_{B_r}\frac{|u-v|^2}{h} - \frac{1}{4}\int_{B_r}|\nabla(u-v)|^2 \\
&\leq m - \frac{1}{4h}\|u-v\|^2_{L^2(B_r)},
\end{aligned}$$

which implies that $\|u-v\|_{L^2(B_r)} = 0$, and so, $u = v$ almost everywhere in B_r.

Using the above remark, we now show that as $\lambda \to \infty$, the set of positive values of the minimizer u_n preserves the prescribed measure. Later, we shall establish that for large enough $\lambda > 0$, this prescribed measure can be attained without having to take λ to infinity.

Theorem 7.7. *If u_n minimizes $\mathcal{F}^h_n$ $(n = 1, \ldots, M)$, then we have*

$$\alpha \leq |\{u_n > 0\}| \leq \alpha + \lambda^{-1}\|\nabla u_0\|^2_{L^2(\Omega)}. \tag{7.14}$$

Proof. Assume that $|\{u_n > 0\}| < \alpha$. We will deduce a contradiction by constructing a suitable perturbation v of the minimizer u_n.

Since $u_n \geq 0$, then setting $E := \{u_n = 0\}$, we have $|E| > |\Omega| - \alpha > 0$. Take $x \in \partial E \backslash \partial\Omega$ such that

$$|B(x,r) \cap E| > 0, \tag{7.15}$$

for all $r > 0$. Fix r, sufficiently small such that $B_r := B(x,r) \subset \Omega$ and

$$0 < |B_r| \leq \alpha - |\{u_n > 0\}|. \tag{7.16}$$

Let $v \in H^1(\Omega)$ be the unique minimizer of $\mathcal{I}_{n,B_r}$ in B_r and equal to u_n outside B_r. Then, we must have $\mathcal{I}_{n,B_r}(v) \le \mathcal{I}_{n,B_r}(u_n)$, that is,

$$\int_{B_r} \frac{|v-u_{n-1}|^2}{h} + |\nabla v|^2 \le \int_{B_r} \frac{|u_n-u_{n-1}|^2}{h} + |\nabla u_n|^2. \tag{7.17}$$

Note that $f(|\{u_n > 0\}|) = 0$. Also, by (7.16), we have

$$\begin{aligned} |\{v>0\}| &= |\{u_n>0\}\backslash B_r| + |\{v>0\}\cap B_r| \\ &\le |\{u_n>0\}| + |B_r| \le \alpha, \end{aligned}$$

which implies that $f(|\{v > 0\}|) = 0$.

On the other hand, (7.17) gives $\mathcal{F}_n^h(v) \le \mathcal{F}_n^h(u_n)$. Since u_n minimizes $\mathcal{F}_n^h$, then we get $\mathcal{F}_n^h(v) = \mathcal{F}_n^h(u_n)$. Equivalently, $\mathcal{I}_{n,B_r}(v) = \mathcal{I}_{n,B_r}(u_n)$, which follows from the previous remark that $v = u_n$. By (7.15), we see that v is a nonconstant function. Note that

$$\Delta v - \frac{v}{h} = -\frac{u_{n-1}}{h} \le 0 \quad \text{in } B_r.$$

By [49, Theorem 3.5], v cannot achieve a nonpositive minimum in B_r, that is, $v > 0$ in B_r. However, since $|B(x,r)\cap E| > 0$, then $v \neq u_n$. A contradiction!

Lastly, the second inequality of (7.14) follows from the first inequality and Lemma 7.3, as follows:

$$|\{u_n>0\}| - \alpha = f(|\{u_n>0\}| - \alpha) \le \lambda^{-1}\|\nabla u_0\|^2_{L^2(\Omega)},$$

which gives the desired result. □

Following the arguments in [77], we show that the minimizer u_n is locally Lipschitz continuous. To start, we establish the following lemma that guarantees Lipschitz continuity at the free boundary.

Lemma 7.8. *(cf. [77, Lemma 4.1]) If u_n minimizes $\mathcal{F}_n^h\,(n = 1,\dots,M)$ for $h, \lambda > 0$, then there exists constants $r_0 > 0$ and $C(r_0) > 0$ such that if $x \in \Omega$ satisfies*

$$r(x) := dist(x, \{u_n = 0\}) < \min\left(\frac{dist(x,\partial\Omega)}{2}, r_0\right), \tag{7.18}$$

then $u_n(x) \le Cr\sqrt{\lambda}$. Here, constant C does not depend on N and λ.

Proof. Let $x \in \Omega$ such that (7.18) holds. Assume that $u_n(x) > 0$, that is, $r := r(x) > 0$. (The case when $u_n(x) = 0$ is trivial.) We claim that for some $M > 0$, we have $u_n(x) \le Mr$. Suppose not. Then for any $M > 0$, there exists $x_0 \in \Omega$ satisfying (7.18) such that

$$u_n(x_0) > Mr. \tag{7.19}$$

By Theorem 7.2, we see that for any n,

$$\int_\Omega |u_n|^p \le |\Omega|\|u_0\|^p_\infty < \infty, \quad \forall p \ge 1,$$

and so, $\sup_{n\ge1} \|u_{n-1}\|_{L^p(\Omega)} < +\infty$.

It follows from [49, Theorem 8.17 and 8.18] that

$$u_n(x_0) \;\leq\; C_1\left(\inf_{B(x_0,\frac{3}{4}r)} u_n(x) + k(r),\right) \tag{7.20}$$

where $C_1 = C_1(r,h,q) > 0$ with the property $\lim_{r\downarrow 0} C_1(r,h,q) > 0$, $q > N$, and

$$k(r) = r^{2(1-N/q)} \sup_{n\geq 1} \left\| \frac{u_{n-1}}{h} \right\|_{L^{q/2}(\Omega)} = o(r) \quad \text{as } r \downarrow 0. \tag{7.21}$$

Let $y \in \partial B(x_0,r) \cap \{u_n = 0\}$ and consider a function $v \in H^1(B(y,r))$ such that

$$\mathcal{I}_{n,B(y,r)}(v) = \min_A \mathcal{I}_{n,B(y,r)}(\cdot),$$

where $A := \{v \in H^1(B(y,r)) : v = u_n \text{ on } \partial B(y,r)\}$. By the previous remark, we have for any $\phi \in C_0^\infty(B(y,r))$,

$$\int_{B(y,r)} \frac{v - u_{n-1}}{h}\phi + \nabla v \cdot \nabla \phi = 0. \tag{7.22}$$

By Theorem 7.5, we have (in the weak sense)

$$\Delta(u_n - v) \;\geq\; \frac{u_n - v}{h}, \quad \text{in } B(y,r),$$

and so, [49, Theorem 8.1] gives

$$\sup_{B(y,r)} (u_n - v) \leq \sup_{\partial B(y,r)} (u_n - v) = 0.$$

This implies that

$$0 \leq u_n \leq v \quad \text{in } B(y,r). \tag{7.23}$$

Now, extend function v by u_n outside the ball, and define

$$\widehat{v} := \begin{cases} v, & \text{on } B(y,r) \\ u_n, & \text{on } \overline{\Omega\backslash B(y,r)}. \end{cases}$$

By the minimality of u_n and taking $\phi = v - u_n$ in (7.22), we get

$$\begin{aligned} \int_{B(y,r)} \frac{|v-u_n|^2}{h} + |\nabla(v-u_n)|^2 \;&=\; \mathcal{F}_n(u_n) - \mathcal{F}_n(v) + \lambda\left(f(|\{\widehat{v}>0\}|) - f(|\{u_n>0\}|)\right) \\ &\quad +\; 2\int_{B(y,r)} \frac{(v-u_{n-1})(v-u_n)}{h} + \nabla v \cdot \nabla(v-u_n) \\ &\leq\; \lambda\left(f(|\{\widehat{v}>0\}|) - f(|\{u_n>0\}|)\right) \end{aligned} \tag{7.24}$$

By (7.23), we see that $\{u_n > 0\} \cap B(y,r) \subseteq \{v > 0\} \cap B(y,r)$. It follows from Theorem 7.7 that

$$\begin{aligned} |\{\widehat{v}>0\}| \;&=\; |\{v>0\} \cap B(y,r)| + |\{u_n>0\}\backslash B(y,r)| \\ &\geq\; |\{u_n>0\} \cap B(y,r)| + |\{u_n>0\}\backslash B(y,r)| \\ &=\; |\{u_n>0\}| \geq \alpha. \end{aligned}$$

Thus, (7.24) becomes

$$\begin{aligned}\int_{B(y,r)} |\nabla(v-u_n)|^2 &\leq \lambda\left(|\{\widehat{v}>0\}| - |\{u_n>0\}|\right)\\ &= \lambda|\{\widehat{v}>0\}\cap\{u_n=0\}\cap B(y,r)|. \end{aligned} \tag{7.25}$$

By (7.21), there exists small $\varepsilon_1 \ll 1$ such that for $r<\varepsilon_1$, we have

$$k(r) \leq r \inf_{B(x_0,\frac{3}{4}r)} u_n(x).$$

Also, by (7.23), we get

$$\inf_{B(x_0,\frac{3}{4}r)} u_n(x) \leq \inf_{B(x_0,\frac{3}{4}r)\cap B(y,r)} u_n(x) \leq \inf_{B(x_0,\frac{3}{4}r)\cap B(y,r)} v(x).$$

Hence, (7.19) and (7.20) implies

$$Mr < u_n(x_0) \leq C_1(1+r) \inf_{B(x_0,\frac{3}{4}r)\cap B(y,r)} v(x),$$

that is,

$$v(x) \geq \frac{Mr}{2C_1}, \quad \text{in } B(x_0,\tfrac{3}{4}r)\cap B(y,r).$$

Invoking this inequality in [49, Theorem 8.18] yields the following for $1\leq p<N/(N-2)$,

$$\begin{aligned}\inf_{B(y,\frac{1}{2}r)} v(x)+k(r) &\geq C_2(r,h)r^{-N/p}\|v\|_{L^p(B(y,r))}\\ &\geq C_2 r^{-N/p}\|v\|_{L^p(B(x_0,\frac{3}{4}r)\cap B(y,r))}\\ &\geq C_2 r^{-N/p}|B(x_0,\tfrac{3}{4}r)\cap B(y,r)|^{1/p}\frac{Mr}{2C_1}\\ &=: 2C_3Mr.\end{aligned}$$

where $\lim_{r\downarrow 0} C_3(C_2,C_1^{-1})>0$. Again, by (7.21), we can find sufficiently small $\varepsilon_2 \ll 1$ so that for $r<\varepsilon_2$, we have

$$k(r) \leq r \inf_{B(y,\frac{1}{2}r)} v(x) < \inf_{B(y,\frac{1}{2}r)} v(x),$$

which implies that

$$\inf_{B(y,\frac{1}{2}r)} v(x) \geq C_3 Mr. \tag{7.26}$$

Now, define a function

$$w(x) = C_3Mr\left\{\exp\left(-\frac{\mu\rho^2(x)}{r^2}\right)-\exp(-\mu)\right\},$$

where $\rho(x)=\operatorname{dist}(x,y)$ and

$$\mu \geq N+\sqrt{N^2+\frac{r_0^2}{h}}. \tag{7.27}$$

Here, we take $r_0 = \min(\varepsilon_1, \varepsilon_2) \ll 1$. Then, we have

$$\begin{aligned} \Delta w - \frac{w - u_{n-1}}{h} &\geq \Delta w - \frac{w}{h} \\ &= C_3 M r \exp\left(-\frac{\mu\rho^2}{r^2}\right)\left(\frac{4\mu^2\rho^2}{r^4} - \frac{2\mu N}{r^2} - \frac{1}{h}\right) + \frac{C_3 M r}{h}\exp(-\mu) \\ &\geq 0 \quad \text{in } B(y,r)\backslash B(y,\tfrac{1}{2}r). \end{aligned} \tag{7.28}$$

(Indeed, if $x \in B(y,r)\backslash B(y,\frac{1}{2}r)$, then $\frac{1}{2}r \leq \rho(x) \leq r$. Also from (7.27), we get

$$(\mu - N)^2 \geq N^2 + \frac{r_0^2}{h}.$$

Then, we have

$$\begin{aligned} \frac{4\mu^2\rho^2}{r^4} - \frac{2\mu N}{r^2} - \frac{1}{h} &\geq \frac{\mu^2}{r^2} - \frac{2\mu N}{r^2} - \frac{1}{h} = \frac{(\mu - N)^2}{r^2} - \frac{N^2}{r^2} - \frac{1}{h} \\ &\geq \frac{r^2}{h}\left(r_0^2 - r^2\right) \geq 0.) \end{aligned}$$

Meanwhile, we note that for any $x \in \partial B(y,r)$, we have $v(x) = u_n(x) \geq 0$, and so, $w(x) = 0 \leq v(x)$. Also, (7.26) implies that if $\rho(x) = \frac{1}{2}r$, then

$$\begin{aligned} w(x) &= C_3 M r\left\{\exp\left(-\tfrac{1}{4}\mu\right) - \exp(-\mu)\right\} \leq C_3 M r \\ &\leq \inf_{B(y,\frac{1}{2}r)} v(x) \\ &\leq v(x) \quad \text{in } B(y,\tfrac{1}{2}r). \end{aligned}$$

Hence, we have

$$w(x) \leq v(x) \quad \text{on } \partial(B(y,r)\backslash B(y,\tfrac{1}{2}r)).$$

Note that from (7.28), we get

$$\Delta w - \frac{w}{h} \geq -\frac{u_{n-1}}{h} = \Delta v - \frac{v}{h} \quad \text{in } B(y,r)\backslash B(y,\tfrac{1}{2}r).$$

Then, the maximum principle [49, Theorem 8.1] gives

$$\sup_{B(y,r)\backslash B(y,\frac{1}{2}r)} (w - v) \leq \sup_{\partial\left(B(y,r)\backslash B(y,\frac{1}{2}r)\right)} (w - v) \leq 0,$$

that is,

$$w(x) \leq v(x) \quad \text{in } B(y,r)\backslash B(y,\tfrac{1}{2}r).$$

There exists constant $C_4 > 0$ such that $w(x) \geq C_4(r - \rho)$ in $B(y,r)\backslash B(y,\frac{1}{2}r)$. (Indeed, if $x \in B(y,r)\backslash B(y,\frac{1}{2}r)$, then $\frac{1}{2}r \leq \rho(x) < r$, that is, $r - \rho \leq \frac{1}{2}r$. Moreover, since the exponential function is nonincreasing, then for some $\delta > 0$,

$$w(x) \geq \tfrac{1}{2}\delta C_3 M r \geq \varepsilon C_3 M(r - \rho).$$

Take $C_4 := \delta C_3 M > 0$.) Combining this with (7.26) implies that

$$v(x) \geq C_5 M(r - \rho) \quad \text{in } B(y,r), \tag{7.29}$$

for some constant $C_5 > 0$.

Take two disjoint balls $B(y_i, \frac{1}{8}r) \subset B(y, \frac{1}{2}r)$ for $i = 1, 2$. For $\xi \in \partial B(y, r)$, let $z_i(\xi)$ be the point on the line segment $\overline{\xi y_i}$ such that the length of segment $\ell_i(\xi) := \overline{\xi z_i(\xi)}$ becomes the largest with $z_i(\xi) \notin B(y_i, \delta r)$ and $u(z_i(\xi)) = 0$. In case $u(x) \neq 0$ for all $x \in \overline{\xi y_i}$, we set $z_i(\xi) = \xi$. For $x \in B(y, r) \backslash y_i$, let $\xi_i(x) \in \partial B(y, r)$ be a point such that $x \in \overline{y_i \xi_i}$. Then by (7.29), we have for some $C_6 > 0$

$$v(x) \geq C_5 M(r - \rho) \geq \psi_i(x) := C_6 M r \frac{\operatorname{dist}(y_i, \xi_i) - \operatorname{dist}(y_i, x)}{\operatorname{dist}(y_i, \xi_i)}.$$

Hence,

$$\int_\xi^{z_i} \frac{d}{d\ell_i} \psi_i d\ell_i =: \psi_i(z_i) \quad \leq \quad v(z_i) := \int_\xi^{z_i} \frac{d}{d\ell_i} (v - u_n)\, d\ell_i,$$

that is,

$$\int_\xi^{z_i} \frac{C_5 M r}{\operatorname{dist}(y_i, \xi)} d\ell_i \quad \leq \quad \int_\xi^{z_i} |\nabla (v - u_n)|\, d\ell_i.$$

Integrating with respect to $\xi \in \partial B(y, r)$, summing up with respect to i, noting that $r/\operatorname{dist}(y_i, \xi) = O(1)$ as $r \downarrow 0$, squaring both sides, and finally, invoking Schwarz' inequality yields

$$C_6^2 M^2 |V| \quad \leq \quad \int_V |\nabla (v - u_n)|^2 , \tag{7.30}$$

where

$$V := V_1 \cup V_2, \qquad V_i = \bigcup_{\xi \in \partial B(y,r)} \ell_i(\xi).$$

Combining this with (7.25) gives

$$C_6^2 M^2 |V| \leq \lambda |\{v > 0\} \cap \{u_n = 0\} \cap B(y, r)| \leq \lambda |\{u_n = 0\} \cap B(y, r)|, \tag{7.31}$$

thereby, contradicting the arbitrariness of M.

Finally, we note that $\{u_n = 0\} \cap B(y, r) \subset V$. By (7.31), we get

$$C_6^2 M^2 |\{u_n = 0\} \cap B(y, r)| \leq C_6 M |V| \leq \lambda |\{u_n = 0\} \cap B(y, r)|.$$

Hence, invoking the above claim gives $u_n(x) \leq r C_6^{-1} \sqrt{\lambda}$ for any $x \in \Omega$ satisfying (7.18). □

Using the above lemma, we can show that the minimizer u_n is locally Lipschitz in Ω.

Theorem 7.9. *If u_n minimizes $\mathcal{F}_n^h$ $(n = 1, \ldots, M)$ for $h, \lambda > 0$, then $u_n \in C^{0,1}_{\mathrm{loc}}(\Omega)$. In particular, the (local) Lipschitz coefficients of u_n do not depend on n.*

Proof. A similar argument as in the proof of [77, Proposition 4.1] where $Q_{\max} = \sqrt{\lambda}$. □

7.4 Regularity of Minimizer up to the Boundary

In this section, we establish the regularity of minimizer u_n up to the fixed Neumann boundary. Our argument is based on the extension of the harmonic analysis in [80] and the results in [77] for the time-discrete term. However, instead of the penalization term, both papers involve a singular term of the form $\int_\Omega Q^2(x)\chi_{\{u>0\}}dx$ for some measurable function Q satisfying $0 < Q_{\min} \le Q \le Q_{\max}$. Translating this to our problem requires the use of Theorem 7.7 and the maximum principle where $Q^2_{\max}$ becomes λ.

7.4.1 Hölder Continuity up to the Boundary

We first show that minimizer u_n is Hölder continuous up to the fixed Neumann boundary, although the Hölder exponent now is not arbitrary, but instead is controlled by the Lipschitz constant $L > 0$ of $\partial\Omega$. Our argument is analogous to the proof of [80, Lemma 2] for harmonic functions. The main tool here employs the idea in [74] for the Dirichlet growth estimate by augmenting the Dirichlet norm with $\frac{1}{\sqrt{h}}\|\cdot\|_{L^2}$, which is related to the time-discrete term.

For simplicity, we consider the equation

$$\Delta z - \frac{1}{h}z = 0, \quad \text{in } B_t$$

since the generalization to the case with coefficients a^{ij}, d is easy. Let $H \in H^1(B_t)$ be a harmonic function in B_t with $H = z$ on ∂B_t. Then, the function $U \in H^1_0(B_t)$ defined by $U = z - H$ satisfies

$$\Delta U - \frac{1}{h}U - \frac{1}{h}H = 0, \quad \text{in } B_t.$$

For the above U, define linear operator T by $TU = v \in H^1_0(B_a)$ (where $a \le t$) such that

$$\Delta v - \frac{1}{h}U = 0, \quad \text{in } B_a.$$

Thus, $U = v + w$ where function $w \in H^1_0(B_a)$ fulfills

$$\Delta w - \frac{1}{h}H = 0, \quad \text{in } B_a.$$

As in [74], we define spaces S_γ and $S_{\gamma,0}$ for $0 < \gamma < 1$ as follows: $u \in S_{\gamma,0}(B_a)$ if and only if $u \in H^1(B_a)$ and there exists $E > 0$ such that

$$\|\nabla u\|_{L^2(B_a)} \le E\left(\frac{r}{\delta}\right)^{\frac{N}{2}-1+\gamma}, \quad 0 \le r \le \delta = a - |x_1 - x_0| \tag{7.32}$$

for every $x_1 \in B(x_0, a)$. If $u \in S_\gamma(B_a)$, we define norm $|||u|||_{S_\gamma}$ as the larger of $'\|u\|_{H^1_0}$ and the smallest E satisfying (7.32). Here, The space $S_{\gamma,0}$ is the subspace of S_γ for which $u \in H^1_0(B_a)$ and the norm $|||u|||_{S_{\gamma,0}}$ is the larger of $\|u\|_{H^1_0}$ and the smallest E as above.

Lemma 7.10. *(cf. [74, Theorem 4.5]) There exists $a_1 > 0$ depending only on h and N such that if $0 < a \le a_1$ and $0 < \gamma \le \mu := 1 - \frac{N}{2p}$ for some $p > N/2$, then $|||v|||_{S_{\gamma,0}(B_a)} \le \frac{1}{2}|||U|||_{S_{\gamma,0}(B_a)}$, that is, $\|T\| \le \frac{1}{2}$.*

Proof. Note that $v = TU \in H_0^1(B_a)$ satisfies

$$\int_{B_a} \nabla\phi \cdot \nabla v + \phi\, f = 0, \quad \forall \phi \in H_0^1(B_a),$$

where $f = \frac{1}{h}U$. By [74, Theorem 2.2] and definition of norm $|||\cdot|||_{S_\gamma}$, we have

$$|U(x) - U(x_1)| \;\le\; C(N,\gamma)|||U|||_{S_{\gamma,0}(B_\delta(x_1))}\delta^{1-\frac{N}{2}-\gamma}|x - x_1|^\gamma, \quad 0 \le |x - x_1| \le \delta/2$$

and

$$\int_{B_\delta(x_1)} |U|^2 \;\le\; \delta^2|||U|||^2_{S_\gamma(B_\delta(x_1))} \le C\delta^2|||U|||^2_{S_{\gamma,0}(B_\delta(x_1))},$$

for each $x_1 \in B_a$ where $\delta = a - |x_1 - x_0|$.

Hence,

$$\begin{aligned}
\int_{B_\delta(x_1)} |U(x_1)| &\le \int_{B_\delta(x_1)} |U(x_1) - U(x)| + \int_{B_\delta(x_1)} |U(x)| \\
&\le C(N,\gamma)|||U|||_{S_{\gamma,0}(B_\delta)}\delta^{1-\frac{N}{2}-\gamma}\int_{B_\delta} |x - x_1|^\gamma + C(N)\delta^{\frac{N}{2}}\|U\|_{L^2(B_\delta)} \\
&\le C(N,\gamma)\delta^{1+\frac{N}{2}}|||U|||_{S_{\gamma,0}(B_\delta(x_1))}.
\end{aligned}$$

Taking $x_1 = x_0$, we see that for any $x \in B_a(x_0)$,

$$|U(x)| \;\le\; C(N,\gamma)a^{1-\frac{N}{2}}|||U|||_{S_{\gamma,0}(B_a(x_0))}.$$

Thus, for some $p > N/2$,

$$\begin{aligned}
\int_{B_\rho(x_0)} |f| &= \frac{1}{h}\int_{B_\rho(x_0)} |U| \le \frac{1}{h}\rho^{\frac{N}{p}}\left(\int_{B_\rho} |U|^{\frac{p}{p-1}}\right)^{1-\frac{1}{p}}, \quad 0 < \rho \le a \\
&\le C(N,\gamma)h^{-1}\rho^{\frac{N}{p}}a^{1-\frac{N}{2}}|||U|||_{S_{\gamma,0}(B_a(x_0))}\rho^{N(1-\frac{1}{p})} \\
&= C(N,\gamma)\rho^{\frac{N}{p}}\frac{a^{1-\frac{N}{2}}}{h}|||U|||_{S_{\gamma,0}(B_a(x_0))}\rho^{N-2+2\mu} \\
&= C(N,\gamma)\rho^{1+\frac{N}{2p}}\frac{a^{1-\frac{N}{2}}}{h}|||U|||_{S_{\gamma,0}(B_a(x_0))}\rho^{N-2+\mu}, \;\; 0 < \mu < 1 \\
&= C(N,\gamma)\rho^{2-\mu}\frac{a^{1-\frac{N}{2}}}{h}|||U|||_{S_{\gamma,0}(B_a(x_0))}\rho^{N-2+\mu} \\
&\le C(N,\gamma)a^{2-\mu}\frac{a^{1-\frac{N}{2}}}{h}|||U|||_{S_{\gamma,0}(B_a(x_0))}\rho^{N-2+\mu} \\
&= C(N,\gamma)\frac{a^2}{h}a^{1-\mu-\frac{N}{2}}|||U|||_{S_{\gamma,0}(B_a(x_0))}\rho^{N-2+\mu} \\
&=: C(N,\gamma)E(a)\rho^{N-2+\mu}. \qquad (7.33)
\end{aligned}$$

By [74, Theorem 3.1], the potential of f, denoted by V is $H^1(B_\rho)$ where $0 < \rho \le a$ and satisfies

$$\begin{aligned}\int_{B_\rho} |\nabla V|^2 &\le C(N,\gamma)E(a)^2\rho^{N-2+2\mu}, \qquad 0<\rho\le a \\ &= C(N,\gamma)\left(\frac{a^2}{h}|||U|||_{S_{\gamma,0}(B_a(x_0))}\right)^2\left(\frac{\rho}{a}\right)^{N-2+2\mu}.\end{aligned}$$

Moreover, for any $\phi \in H_0^1(B_a)$, we have $\displaystyle\int_{B_a}\phi f = -\int_{B_a}\nabla\phi\cdot\nabla V$, and so,

$$\int_{B_a}\nabla\phi\cdot\nabla(v-V)=0.$$

By [74, Theorem 3.3],

$$\int_{B_\rho}|\nabla v|^2 \le C(N,\gamma)\left(\frac{a^2}{h}|||U|||_{S_{\gamma,0}(B_a)}\right)^2\left(\frac{\rho}{a}\right)^{N-2+2\mu}, \quad 0<\rho\le a. \tag{7.34}$$

Hence, we have

$$|||v|||_{S_{\gamma,0}(B_a)} \le C(N,\gamma)\frac{a^2}{h}|||U|||_{S_{\gamma,0}(B_a)}$$

Take $a_1 > 0$ so that for any $a \le a_1$, we have $a^2 \le \frac{1}{2}hC^{-1}(N,\gamma)$. □

By Lemma 7.10, we have for sufficiently small a_1 that $\|T\| \le \frac{1}{2}$, i.e., for any $t \le a_1$, we have $|||v|||_{S_{\gamma,0}(B_t)} \le \frac{1}{2}|||U|||_{S_{\gamma,0}(B_t)}$. Since $U = v + w$, this implies

$$|||U|||_{S_{\gamma,0}(B_t)} \le |||v|||_{S_{\gamma,0}(B_t)} + |||w|||_{S_{\gamma,0}(B_t)} \le \tfrac{1}{2}|||U|||_{S_{\gamma,0}(B_t)} + |||w|||_{S_{\gamma,0}(B_t)}$$

that is, $|||U|||_{S_{\gamma,0}(B_t)} \le 2|||w|||_{S_{\gamma,0}(B_t)}$. Thus, we get

$$\begin{aligned}|||z|||_{S_\gamma(B_t)} &\le |||U|||_{S_\gamma(B_t)} + |||H|||_{S_\gamma(B_t)} \\ &\le C|||U|||_{S_{\gamma,0}(B_t)} + |||H|||_{S_\gamma(B_t)} \\ &\le C|||w|||_{S_{\gamma,0}(B_t)} + |||H|||_{S_\gamma(B_t)}.\end{aligned}$$

Meanwhile, a similar argument as in the proof of Lemma 7.10 gives

$$|||w|||_{S_{\gamma,0}(B_t)} \le \tfrac{1}{2}|||H|||_{S_{\gamma,0}(B_t)},$$

and so, we have $|||z|||_{S_\gamma(B_t)} \le C|||H|||_{S_\gamma(B_t)}$ for some constant $C > 0$.

Note that

$$\begin{aligned}\int_{B_t}|\nabla z|^2 &= \int_{B_t}\nabla(U+H)\cdot\nabla(U+H)) \\ &= \int_{B_t}\nabla U\cdot\nabla U + 2\nabla U\cdot\nabla H + \nabla H\cdot\nabla H \\ &= \int_{B_t}|\nabla U|^2 + \int_{B_t}|\nabla H|^2,\end{aligned}$$

and so, $\|\nabla H\|_{L^2(B_t)} \le \|\nabla z\|_{L^2(B_t)}$.

By [74, Theorem 2.1], we see that for $l < t < a_1$,

$$\begin{aligned}\|\nabla H\|_{L^2(B_l)} &\leq C(N)\|\nabla H\|_{L^2(B_t)}\left(\frac{l}{t}\right)^{\frac{N}{2}-1+\gamma}, \quad 0<\gamma<1.\\ &\leq C(N)\|\nabla z\|_{L^2(B_t)}\left(\frac{l}{t}\right)^{\frac{N}{2}-1+\gamma}\\ &\leq C(N)\ {}^h\|z\|_{H^1(B_t)}\left(\frac{l}{t}\right)^{\frac{N}{2}-1+\gamma} \end{aligned} \tag{7.35}$$

and so, $|||H|||_{S_\gamma(B_t)} \leq C(N)\ {}^h\|z\|_{H^1(B_t)}$. Here, we define

$${}^h\|\cdot\|_{H^1} := \frac{1}{\sqrt{h}}\|\cdot\|_{L^2} + \|\nabla(\cdot)\|_{L^2}. \tag{7.36}$$

Then, we have

$$\begin{aligned}\|\nabla z\|_{L^2(B_l)} &\leq C(N)|||H|||_{S_\gamma(B_t)}\left(\frac{l}{t}\right)^{\frac{N}{2}-1+\gamma}, \quad l<t<a_1\\ &\leq C(N)\ {}^h\|z\|_{H^1(B_t)}\left(\frac{l}{t}\right)^{\frac{N}{2}-1+\gamma},\end{aligned}$$

which proves the following lemma.

Lemma 7.11. *Suppose $z \in H^1(B_t)$ satisfies*

$$\Delta z - \frac{1}{h}z = 0, \quad \text{in } B_t.$$

Then, for $l < t < a_1$, we have

$$\|\nabla z\|_{L^2(B_l)} \leq C(N,\gamma)\ {}^h\|z\|_{H^1(B_t)}\left(\frac{l}{t}\right)^{\frac{N}{2}-1+\gamma}, \quad 0<\gamma\leq\mu<1.$$

Here, $\mu := 1 - \frac{N}{2p}$ for some $p > N/2$ and $a_1 > 0$ is the constant in Lemma 7.10.

We can in fact, extend this result to the nonhomogeneous case as follows.

Lemma 7.12. *Suppose $z \in H^1(B_t)$ satisfies*

$$\Delta z = \frac{z-g}{h}, \quad \text{in } B_t,$$

for some $h > 0$ and $g \in C^{0,1}(\overline{\Omega})$. Then, for $l < t < a_1$, we have

$$\|\nabla z\|_{L^2(B_l)} \leq C(N,\gamma)\ {}^h\|z\|_{H^1(B_t)}\left(\frac{l}{t}\right)^{\frac{N}{2}-1+\gamma}, \quad 0<\gamma\leq\mu<1.$$

Here, $\mu := 1 - \frac{N}{2p}$ for some $p > N/2$ and $a_1 > 0$ is the constant in Lemma 7.10.

Proof. This follows from a similar argument as in the proof of Lemma 7.11 employing [74, Theorem 3.1] and [74, Theorem 3.3]. Here, we write $v = U + H$ where $U \in H_0^1(B_t)$

satisfies

$$\Delta U - \frac{1}{h}U - \frac{1}{h}(H - u_{n-1}) = 0, \quad \text{in } B_t,$$

and $H \in H^1(B_t)$ is a harmonic function with $H = v$ on ∂B_t. □

In the following lemma, we establish the weak maximum principle on a Lipschitz domain with mixed boundary conditions.

Lemma 7.13. *(cf. [80, Lemma 4]) Let $\Omega \subset \mathbb{R}^N$ be a bounded, connected Lipschitz domain and let $\Gamma \subset \partial\Omega$ be a measurable set of positive Hausdorff measure in $\partial\Omega$. Let $u \in H^1(\Omega)$ satisfy the following*

1. *$\forall \phi \in \{f \in H^1(\Omega) : f \geq 0, f|_\Gamma = 0\}$, we have $\int_\Omega \nabla u \cdot \nabla \phi + \frac{u\phi}{h} \geq 0$,*
2. *$\exists u_0 \in L^2(\partial\Omega)$ such that $u|_\Gamma = u_0 \geq 0$ on Γ.*

Then, $u \geq 0$ in Ω.

Proof. Consider the function $u^- := \max(0, -u) \in H^1(\Omega)$. Note that $u^- \geq 0$ and $u^-|_\Gamma = 0$. Taking $\phi = u^-$ gives

$$\int_\Omega \nabla u \cdot \nabla u^- + \frac{uu^-}{h} \geq 0.$$

Hence, we get

$$0 \leq \int_\Omega |\nabla u^-|^2 \leq \int_\Omega |\nabla u^-|^2 + \frac{|u^-|^2}{h} \leq 0,$$

which implies that $\nabla u^- = 0$. Since Ω is connected, then u^- is constant. But $u^-|_\Gamma = 0$, and so, $u^- = 0$. Therefore, $u \geq 0$. □

We are now ready to prove Hölder continuity up to the fixed Neumann boundary.

Theorem 7.14. *(cf. [80, Lemma 2]) There exists $\gamma > 0$ such that $u_n \in C^{0,\gamma}(\overline{\Omega})$ with γ depending on N, h, and L.*

Proof. There exists $s > 0$ depending only on the Lipschitz character of Ω such that one can cover $\partial\Omega$ with balls B_s of radius s such that $B_s \cap \partial\Omega$ is a Lipschitz graph with Lipschitz constant less than or equal to L. Let $r = \frac{1}{2}\min(1, s, r_0, a_1)$ where $r_0, a_1 > 0$ are the constants in Lemma 7.8 and Lemma 7.10, respectively. Cover Ω with a finite number of balls B_r of radius r such that either $B_{2r} \subset \Omega$ or $\partial\Omega \cap B_{2r}$ is a Lipschitz graph as above. (Note that such finite covering is due to Heine-Borel Theorem.) Let x_0 be the center of one of these balls. We wish to show that $u_n \in C^{0,\gamma}(B_r(x_0) \cap \Omega)$ for some γ independent of x_0, from which we conclude the same for all of Ω.

If $B_{2r}(x_0) \subset \Omega$, then Theorem 7.4 implies that $u_n \in C^{0,\gamma}(B_r(x_0))$ for any $\gamma \in (0, 1)$. Otherwise, let $x \in B_r(x_0)$ and $t < r_x := \text{dist}(x, \partial B_{2r}(x_0))$. Denote $D_t = B_t(x) \cap \Omega$, $\Gamma_{D,t} = \partial B_t(x) \cap \Omega$, and $\Gamma_{N,t} = B_t(x) \cap \partial\Omega$.

If $\Gamma_{N,t} = \emptyset$, consider a function $v_t \in H^1(D_t)$ satisfying

$$\begin{cases} \Delta v_t = \dfrac{v_t - u_{n-1}}{h}, & \text{in } D_t \\ v_t = u_n, & \text{on } \partial\Gamma_{D,t}. \end{cases}$$

Now, extend function v_t by u_n outside D_t, and define

$$\widehat{v}_t := \begin{cases} v_t, & \text{in } D_t \\ u_n, & \text{on } \overline{\Omega \backslash D_t}. \end{cases}$$

By a similar argument as in the proof of Lemma 7.8, we get

$$\int_{D_t} \frac{|u_n - v_t|^2}{h} + |\nabla(u_n - v_t)|^2 \quad \leq \quad \lambda |\{\widehat{v}_t > 0\} \cap \{u_n = 0\} \cap D_t| \leq \lambda C(N) t^N.$$

On the other hand, if $\Gamma_{N,t} \neq \emptyset$, we consider function $v_t \in H^1(D_t)$ satisfying

$$\begin{cases} \Delta v_t = \dfrac{v_t - u_{n-1}}{h}, & \text{in } D_t, \\ v_t = u_n, & \text{on } \Gamma_{D,t}, \\ \dfrac{\partial v_t}{\partial \boldsymbol{\eta}} = 0, & \text{on } \Gamma_{N,t}. \end{cases}$$

By Theorem 7.5, we have for any $\zeta \in \{f \in H^1(\Omega) : f \geq 0,\ f|_{\Gamma_{D,t}} = 0\}$,

$$\int_{D_t} \nabla(v_t - u_n) \cdot \nabla\zeta + \frac{v_t - u_n}{h}\zeta \quad \geq \quad 0.$$

Note also that $v_t = u_n \geq 0$ on $\Gamma_{D,t}$. Hence, Lemma 7.13 gives $u_n \leq v_t$ in D_t. As above, for every $t < r_x$, we get

$$\int_{D_t} \frac{|u_n - v_t|^2}{h} + |\nabla(u_n - v_t)|^2 \leq \lambda C(N) t^N. \tag{7.37}$$

Now, since $\partial\Omega$ is a Lipschitz graph, then there exists a bilipschitz map

$$F : D_t \to B_t(0)^+$$

where $\{x_N = 0\} = F(\Gamma_{N,t})$ and $(\partial B_t(0))^+ = F(\Gamma_{D,t})$. The Lipschitz constants of F and F^{-1} are controlled solely by L. Let

$$\begin{aligned} a^{ij}(y) &= |\det \nabla F^{-1}(y)| \left((\nabla F)^T (\nabla F)\right)(F^{-1}(y)) \\ d(y) &= |\det \nabla F^{-1}(y)|, \end{aligned}$$

whenever $y_N \geq 0$. Otherwise, let

$$a^{ij}(y_1, \ldots, y_N) \quad = \quad \begin{cases} a^{ij}(y_1, \ldots, -y_N), & i \neq N \text{ and } j \neq N \\ -a^{ij}(y_1, \ldots, -y_N), & i = N \text{ or } j = N \text{ but } i \neq j \\ a^{ij}(y_1, \ldots, -y_N), & i = j = N, \end{cases}$$

and $d(y_1, \ldots, y_N) = d(y_1, \ldots, -y_N)$. Note that coefficients a^{ij} is uniformly elliptic with bounded, measurable coefficients on all of $B_t(0)$, and that the bounds of a^{ij} and d depend

only on Lipschitz constant L.

Define $\widetilde{v}_t(y) = v_t(F^{-1}y)$ on $B_t(0)$ when $y_N \geq 0$. Otherwise, set $\widetilde{v}_t(y_1,\dots,y_N) = \widetilde{v}_t(y_1,\dots,-y_N)$. Then on $B_t(0)$, we have for any $\zeta \in C_0^\infty(B_t(0))$,

$$\begin{aligned}\int_{B_t(0)}\langle a^{ij}\nabla\widetilde{v}_t,\nabla\zeta\rangle + \left\langle d\frac{\widetilde{v}_t-\widetilde{u}_{n-1}}{h},\zeta\right\rangle &= \int_{B_t^+(0)}+\int_{B_t^-(0)}\langle a^{ij}\nabla\widetilde{v}_t,\nabla\zeta\rangle + \left\langle d\frac{\widetilde{v}_t-\widetilde{u}_{n-1}}{h},\zeta\right\rangle\\ &= \int_{B_t^+(0)}\langle a^{ij}\nabla\widetilde{v}_t,\nabla\phi\rangle + \left\langle d\frac{\widetilde{v}_t-\widetilde{u}_{n-1}}{h},\phi\right\rangle\\ &\quad + \int_{B_t^+(0)}\langle a^{ij}\nabla\widetilde{v}_t,\nabla\psi\rangle + \left\langle d\frac{\widetilde{v}_t-\widetilde{u}_{n-1}}{h},\psi\right\rangle\\ &:= I + II.\end{aligned}$$

Here, ψ is defined on $B_t(0)$ by $\psi(y_1,\dots,y_N) = \phi(y_1,\dots,-y_N)$. Both test functions $\phi,\psi \in C^\infty(B_t(0)\cap\{y_N\geq 0\})$ and $\phi=\psi=0$ on $\partial B_t(0)\cap\{y_N\geq 0\}$. Define $\widetilde{\phi}=\phi\circ F$ and $\widetilde{\psi}=\psi\circ F$, which are valid test functions in $\{\zeta\in H^1(D_t):\zeta=0 \text{ on } \Gamma_{D,t}\}$. Hence, we have

$$\begin{aligned}I &= \int_{B_t^+(0)}\left\langle \nabla F(F^{-1}(y))\nabla\widetilde{v}_t(y), \nabla F(F^{-1}(y))\nabla\phi(y)\right\rangle |\det\nabla F^{-1}(y)|dy\\ &\quad + \int_{B_t^+(0)}\left\langle \frac{\widetilde{v}_t(y)-\widetilde{u}_{n-1}(y)}{h},\phi(y)\right\rangle |\det\nabla F^{-1}(y)|dy\\ &= \int_{B_t(x)\cap\overline{\Omega}}\nabla v_t\cdot\nabla\widetilde{\phi}+\frac{v_t-u_{n-1}}{h}\widetilde{\phi}=0.\end{aligned}$$

Similarly,

$$II = \int_{B_t(x)\cap\overline{\Omega}}\nabla v_t\cdot\nabla\widetilde{\psi}+\frac{v_t-u_{n-1}}{h}\widetilde{\psi}=0.$$

Thus, $\widetilde{v}_t$ satisfies (in the weak sense)

$$D_i\left(a^{ij}(y)D_j\widetilde{v}_t(y)\right) = d(y)\frac{\widetilde{v}_t(y)-\widetilde{u}_{n-1}(y)}{h} \qquad \text{in } B_t(0).$$

Set $\widetilde{w}_i := \widetilde{v}_{2^{i-1}t}-\widetilde{v}_{2^it}$. It follows that

$$\int_{B_t(0)} D_i\zeta(a^{ij}D_j\widetilde{w}_i)-\frac{1}{h}\zeta(d\widetilde{w}_i)=0,\quad \forall\zeta\in H_0^1(B_t(0)).$$

By Lemma 7.11, there exists $C>0$ and $0<\mu<1$, depending only on the coefficients a^{ij} and d (which in turn depend only on L) such that for $l<t<r$,

$$\|\nabla w_i\|_{L^2(D_l)} \leq C(N,\gamma)\,{}^h\|w_i\|_{H^1(D_t)}\left(\frac{l}{t}\right)^{\frac{N}{2}-1+\mu}.$$

Now, we return to the consideration of u_n. Choose some $t<r_x$. By (7.37), we have

$$\begin{aligned}{}^h\|w_i\|_{H^1(D_{2^{i-1}t})} &\leq {}^h\|v_{2^{i-1}t}-u_n\|_{H^1(D_{2^{i-1}t})} + {}^h\|u_n-v_{2^it}\|_{H^1(D_{2^it})}\\ &\leq \sqrt{\lambda}C(N)\left((2^{i-1}t)^{\frac{N}{2}}+(2^it)^{\frac{N}{2}}\right)\\ &= \sqrt{\lambda}C(N)(2^{i-1}t)^{\frac{N}{2}}. \qquad (7.38)\end{aligned}$$

Hence, if $\Gamma_{N,2^{i-1}t} \neq \emptyset$, we have

$$\begin{aligned} \|\nabla w_i\|_{L^2(D_t)} &\leq C(N,\gamma)\, {}^h\|w_i\|_{H^1(D_{2^{i-1}t})} \left(\frac{1}{2^{i-1}}\right)^{\frac{N}{2}-1+\mu} \\ &\leq \sqrt{\lambda} C(N,\gamma) t^{\frac{N}{2}} \left(2^{(1-\mu)i}\right). \end{aligned}$$

On the other hand, if $\Gamma_{N,2^{i-1}t} = \emptyset$, we get

$$\begin{aligned} {}^h\|v_{2t} - v_t\|_{H^1(D_t)} &\leq {}^h\|v_{2t} - u_n\|_{H^1(D_t)} + {}^h\|u_n - v_t\|_{H^1(D_t)} \\ &\leq \sqrt{\lambda} C(N) t^{\frac{N}{2}}, \end{aligned}$$

which is even better.

Finally, by triangle inequality, we see that for $t < r_x$,

$$\begin{aligned} \|\nabla u_n\|_{L^2(D_t)} &\leq \|\nabla(u_n - v_t)\|_{L^2(D_t)} + \sum_{i=1}^{\log_2(r_x/t)} \|\nabla w_i\|_{L^2(D_t)} + \|\nabla v_r\|_{L^2(D_t)} \\ &\leq \sqrt{\lambda} C(N,\gamma) t^{\frac{N}{2}} \left(1 + \sum_{i=1}^{\log_2(r_x/t)} 2^{(1-\mu)i}\right) + C(N,\gamma) t^{\frac{N}{2}-1+\mu}, \end{aligned}$$

where the last term follows from Lemma 7.12. Note that

$$\begin{aligned} 1 + \sum_{i=1}^{\log_2(r_x/t)} 2^{(1-\mu)i} &= \frac{1 - 2^{(1-\mu)(1+\log_2(r_x/t))}}{1 - 2^{(1-\mu)}} = C(N)\left(1 - C(r_x) t^{\mu-1}\right) \\ &= C(N)\left(t^{1-\mu} - C(r_x)\right) t^{\mu-1}, \quad t < r_x \\ &\leq C(N, r_x) t^{\mu-1}. \end{aligned}$$

Hence, for any $x \in B(x_0, r)$ and for any $t < r_x$,

$$\int_{B_t(x_0)\cap\Omega} |\nabla u_n|^2 \leq C(N,\gamma,r_x)(1+\sqrt{\lambda}) t^{N-2+2\mu}.$$

By [74, Theorem 2.2] ([75, Theorem 3.5.2]), we have $u_n \in C^{0,\mu}(B_r(x_0) \cap \Omega)$ where the Hölder exponent $\mu := 1 - \frac{N}{2p} < 1$ for some $p > N/2$. □

7.4.2 Lipschitz Continuity up to the Boundary

In this subsection, we establish that the minimizer is Lipschitz continuous up to the boundary employing several properties of a function satisfying an elliptic equation on a convex domain with Neumann boundary conditions, which are proven in this subsection.

First, we provide a gradient control lemma for nonnegative functions satisfying an elliptic equation near a Neumann boundary. We extend the harmonic results in [80], which employs the auxilliary function Φ first introduced in [25] and the idea in [64] of using convexity to control the Neumann boundary.

Lemma 7.15. *(cf. [80, Lemma 6]) Let $\Omega \subset \mathbb{R}^N$ be a domain with smooth convex boundary. For $0 \in \Omega$, denote $r = dist(0, \partial\Omega)$. Let $D := B_R(0) \cap \Omega$, $\Gamma = B_R(0) \cap \partial\Omega$, and*

$S = \overline{\partial B_R(0) \cap \Omega}$ where $R > 2r$. Let $u \in H^1(\Omega)$ be a nonnegative function on D bounded by A, with $\frac{\partial u}{\partial \boldsymbol{\eta}} = 0$ along Γ and satisfies

$$\Delta u - \frac{u - g}{h} = 0, \quad \text{in } D,$$

where $h > 0$ and $g \in H^1(\Omega) \cap L^\infty(\Omega) \cap C^{0,1}(\overline{\Omega})$. Here, we denote the gradient bound of g by L. Then, either one of the following is true:

i.) *$|\nabla u| \leq L$ on $B_{\frac{R}{2}}$,*

ii.) *$\exists C(N, h) > 0$ such that $|\nabla u| \leq C\frac{A}{R}$ on $B_{\frac{R}{2}}$.*

Proof. If u is constant, then we are done. Suppose not. Consider

$$\Phi(x) \quad = \quad \frac{(R^2 - |x|^2)^2 |\nabla u|^2}{(9A^2 - (u - 2A)^2)^2}.$$

Then,

1. $\Phi = 0$ on S.
2. $\Phi > 0$ inside D.
3. Φ is smooth in $D \cup \Gamma$ because u and ∇u are smooth and the denominator of Φ cannot approach 0.
4. $\max_{\Gamma} \Phi < \max_{\overline{D}} \Phi$. Indeed,

$$\begin{aligned}
\frac{\partial \Phi}{\partial \boldsymbol{\eta}} \quad &= \quad 2\left(\frac{R^2 - |x|^2}{9A^2 - (u - 2A)^2}\right)^2 \nabla u \cdot \frac{\partial}{\partial \boldsymbol{\eta}} \nabla u \\
&\quad - 4|\nabla u|^2 \left(\frac{R^2 - |x|^2}{(9A^2 - (u - 2A)^2)^2}\right) x \cdot \frac{\partial x}{\partial \boldsymbol{\eta}} \\
&\quad - 4|\nabla u|^2 \left(\frac{(R^2 - |x|^2)^2}{(9A^2 - (u - 2A)^2)^3}\right) (u - 2A) \frac{\partial u}{\partial \boldsymbol{\eta}} \\
&=: \quad I + II + III.
\end{aligned}$$

Note that $III = 0$, since $\frac{\partial u}{\partial \boldsymbol{\eta}} = 0$ on Γ. Moreover, by convexity of Ω, $x \cdot \frac{\partial x}{\partial \boldsymbol{\eta}} > 0$, and so, $II < 0$. Now, after rotation, suppose $\boldsymbol{\eta} = e_N$, so we can use $e_1, \ldots, e_{N-1}$ as local coordinates for Γ. Then,

$$\begin{aligned}
\nabla u \cdot \frac{\partial}{\partial \boldsymbol{\eta}} \nabla u \quad &= \quad \nabla u \cdot \nabla \left(\frac{\partial u}{\partial \boldsymbol{\eta}}\right) - \sum_{i,j=1}^{N-1} \frac{\partial \boldsymbol{\eta}_i}{\partial x_j} \frac{\partial u}{\partial x_i} \frac{\partial u}{\partial x_j} \\
&= \quad - \sum_{i,j=1}^{N-1} \frac{\partial \boldsymbol{\eta}_i}{\partial x_j} \frac{\partial u}{\partial x_i} \frac{\partial u}{\partial x_j}.
\end{aligned}$$

The matrix $\frac{\partial \boldsymbol{\eta}_i}{\partial x_j}$ is the second fundamental form of Γ in local coordinates, and so, by convexity, it is positive definite. Then, $\nabla u \cdot \frac{\partial}{\partial \boldsymbol{\eta}} \nabla u < 0$ along Γ. Hence, $\frac{\partial \Phi}{\partial \boldsymbol{\eta}} < 0$ along Γ, so the maximum of Φ cannot occur on Γ.

By the first and fourth properties of Φ, we see that its maximum occurs at a point $x_0 \in D$. At x_0, we have

$$\begin{aligned} 0 = \nabla\Phi &= \frac{(R^2-|x|^2)^2}{(9A^2-(u-2A)^2)^2}\nabla(|\nabla u|^2) - 2\frac{(R^2-|x|^2)|\nabla u|^2}{(9A^2-(u-2A)^2)^2}\nabla(|x|^2) \\ &\quad + 2\frac{(R^2-|x|^2)^2|\nabla u|^2}{(9A^2-(u-2A)^2)^3}\nabla((u-2A)^2) \\ &= \left(\frac{\nabla(|\nabla u|^2)}{|\nabla u|^2} - \frac{2\nabla(|x|^2)}{R^2-|x|^2} + \frac{2\nabla((u-2A)^2)}{9A^2-(u-2A)^2}\right)\Phi, \end{aligned} \tag{7.39}$$

and

$$\begin{aligned} 0 \geq \Delta\Phi &= \left(\frac{\Delta(|\nabla u|^2)}{|\nabla u|^2} - \frac{|\nabla(|\nabla u|^2)|^2}{|\nabla u|^4} - \frac{2\Delta(|x|^2)}{R^2-|x|^2} - \frac{2|\nabla(|x|^2)|^2}{(R^2-|x|^2)^2}\right. \\ &\quad \left. + \frac{2\Delta((u-2A)^2)}{9A^2-(u-2A)^2} + \frac{2|\nabla((u-2A)^2)|^2}{(9A^2-(u-2A)^2)^2}\right)\Phi. \end{aligned} \tag{7.40}$$

Note that $\nabla(|x|^2) = 2x$ and $\nabla((u-2A)^2) = 2(u-2A)\nabla u$. Then, (7.39) gives

$$0 = \frac{\nabla(|\nabla u|^2)}{|\nabla u|^2} - \frac{4x}{R^2-|x|^2} + \frac{4(u-2A)\nabla u}{9A^2-(u-2A)^2},$$

which implies that

$$\begin{aligned} \frac{|\nabla(|\nabla u|^2)|^2}{|\nabla u|^4} &= \frac{16|x|^2}{(R^2-|x|^2)^2} - \frac{32(u-2A)x\cdot\nabla u}{(R^2-|x|^2)(9A^2-(u-2A)^2)} + \frac{16(u-2A)^2|\nabla u|^2}{(9A^2-(u-2A)^2)^2} \\ &\leq \frac{16|x|^2}{(R^2-|x|^2)^2} + \frac{32|x||u-2A||\nabla u|}{(R^2-|x|^2)(9A^2-(u-2A)^2)} + \frac{16(u-2A)^2|\nabla u|^2}{(9A^2-(u-2A)^2)^2}. \end{aligned} \tag{7.41}$$

Note that $|\nabla u|^2 = \sum_{i=1}^{N}\left(\frac{\partial u}{\partial x_i}\right)^2$. Then,

$$\begin{aligned} \nabla(|\nabla u|^2) &= 2\sum_{i=1}^{N}\frac{\partial u}{\partial x_i}\left(\frac{\partial^2 u}{\partial x_i\partial x_1},\ldots,\frac{\partial^2 u}{\partial x_i\partial x_N}\right) \\ \Delta(|\nabla u|^2) &= 2\sum_{i,j=1}^{N}\left[\left(\frac{\partial^2 u}{\partial x_i\partial x_j}\right)^2 + \frac{\partial u}{\partial x_i}\frac{\partial^3 u}{\partial x_i\partial x_j^2}\right]. \end{aligned}$$

Since $\Delta u - h^{-1}(u-g) = 0$, then

$$\begin{aligned} \sum_{i,j=1}^{N}\frac{\partial u}{\partial x_i}\frac{\partial^3 u}{\partial x_i\partial x_j^2} &= \sum_{i=1}^{N}\frac{\partial u}{\partial x_i}\frac{\partial}{\partial x_i}\left(\sum_{j=1}^{N}\frac{\partial^2 u}{\partial x_j^2}\right) \\ &= \frac{1}{h}\sum_{i=1}^{N}\frac{\partial u}{\partial x_i}\frac{\partial(u-g)}{\partial x_i} = \frac{\nabla(u-g)}{h}\cdot\nabla u. \end{aligned}$$

Hence,

$$\Delta(|\nabla u|^2) = 2\sum_{i,j=1}^{N}\left(\frac{\partial^2 u}{\partial x_i\partial x_j}\right)^2 + 2\frac{\nabla(u-g)}{h}\cdot\nabla u. \tag{7.42}$$

Moreover,

$$|\nabla(|\nabla u|^2)|^2 = 4\sum_{j=1}^{N}\left(\sum_{i=1}^{N}\frac{\partial u}{\partial x_i}\frac{\partial^2 u}{\partial x_i\partial x_j}\right)^2 = 4\sum_{i,j,k}\frac{\partial u}{\partial x_i}\frac{\partial u}{\partial x_k}\frac{\partial^2 u}{\partial x_i\partial x_j}\frac{\partial^2 u}{\partial x_k\partial x_j}.$$

Thus, we have

$$2|\nabla u|^2\Delta(|\nabla u|^2) \;\geq\; |\nabla(|\nabla u|^2)|^2 + 4|\nabla u|^2\frac{\nabla(u-g)}{h}\cdot\nabla u,$$

that is,

$$\frac{\Delta(|\nabla u|^2)}{|\nabla u|^2} \;\geq\; \frac{|\nabla(|\nabla u|^2)|^2}{2|\nabla u|^4} + 2\frac{\nabla(u-g)\cdot\nabla u}{h|\nabla u|^2}. \tag{7.43}$$

Moreover, we see that $\Delta(|x|^2) = 2N$ and

$$\begin{aligned}\Delta((u-2A)^2) &= 2\left((u-2A)\Delta u + |\nabla u|^2\right)\\ &= 2(u-2A)\frac{u-g}{h} + 2|\nabla u|^2.\end{aligned}$$

Combining (7.41), (7.43), and (7.40) yields

$$\begin{aligned}0 \;\geq\; & -\frac{|\nabla(|\nabla u|^2)|^2}{2|\nabla u|^4} + 2\frac{\nabla(u-g)\cdot\nabla u}{h|\nabla u|^2} - \frac{4N}{R^2-|x|^2} - \frac{8|x|^2}{(R^2-|x|^2)^2}\\ &\quad + \frac{2h^{-1}(u-2A)(u-g)+4|\nabla u|^2}{9A^2-(u-2A)^2} + \frac{8(u-2A)^2|\nabla u|^2}{(9A^2-(u-2A)^2)^2}\\ \geq\; & -\frac{8|x|^2}{(R^2-|x|^2)^2} - \frac{16|x||u-2A||\nabla u|}{(R^2-|x|^2)(9A^2-(u-2A)^2)} - \frac{8(u-2A)^2|\nabla u|^2}{(9A^2-(u-2A)^2)^2}\\ &\quad + 2\frac{\nabla(u-g)\cdot\nabla u}{h|\nabla u|^2} - \frac{4N}{R^2-|x|^2} - \frac{8|x|^2}{(R^2-|x|^2)^2}\\ &\quad + \frac{2h^{-1}(u-2A)(u-g)+4|\nabla u|^2}{9A^2-(u-2A)^2} + \frac{8(u-2A)^2|\nabla u|^2}{(9A^2-(u-2A)^2)^2}\\ \geq\; & -\frac{16|x|^2}{(R^2-|x|^2)^2} - \frac{16|x||u-2A||\nabla u|}{(R^2-|x|^2)(9A^2-(u-2A)^2)} + 2\frac{\nabla(u-g)\cdot\nabla u}{h|\nabla u|^2} - \frac{4N}{R^2-|x|^2}\\ &\quad + \frac{2(u-2A)(u-g)}{h(9A^2-(u-2A)^2)} + \frac{4|\nabla u|^2}{9A^2-(u-2A)^2},\end{aligned}$$

that is,

$$\begin{aligned}\frac{4|\nabla u|^2}{9A^2-(u-2A)^2} \;\leq\; & \frac{16|x||u-2A||\nabla u|}{(R^2-|x|^2)(9A^2-(u-2A)^2)} + \frac{4N(R^2-|x|^2)+16|x|^2}{(R^2-|x|^2)^2}\\ & - \frac{2}{h}\left(\frac{\nabla(u-g)\cdot\nabla u}{|\nabla u|^2} + \frac{(u-2A)(u-g)}{9A^2-(u-2A)^2}\right).\end{aligned}$$

If $|\nabla g(x_0)| \leq |\nabla u(x_0)|$, then

$$-\frac{2}{h}\frac{\nabla(u-g)\cdot\nabla u}{|\nabla u|^2} \;\leq\; \frac{2}{h}\frac{|\nabla g|^2-|\nabla u|^2}{|\nabla u|^2} \leq 0.$$

Moreover, $-2(u-2A)u \le u^2+(u-2A)^2$ and $2(u-2A)g \le -2Ag \le 0$. Hence, multiplying by $(R^2-|x|^2)^2$ and dividing by $9A^2-(u-2A)^2$ yields

$$\begin{aligned} 4\Phi(x_0) &\le \frac{16|x||u-2A|\sqrt{\Phi(x_0)}}{9A^2-(u-2A)^2} + \frac{4N(R^2-|x|^2)+16|x|^2}{9A^2-(u-2A)^2} \\ &\qquad + \frac{1}{h}\left(\frac{u^2+(u-2A)^2}{9A^2-(u-2A)^2}\right)\frac{(R^2-|x|^2)^2}{9A^2-(u-2A)^2} \\ &\le \frac{48R\sqrt{\Phi(x_0)}}{5A} + \frac{(4N+16)R^2}{5A^2} + \frac{R^4}{5hA^2} := I, \end{aligned} \tag{7.44}$$

since $5A^2 \le 9A^2-(u-2A)^2 \le 8A^2$. Suppose $\Phi(x_0) \ge C_\Phi \frac{R^2}{A^2}$ for some large $C_\Phi > 0$. Then, if $C_\Phi > \frac{1}{5h}$ and $R < 1$, we get

$$\frac{R^4}{5hA^2} \le C_\Phi \frac{R^2}{A^2}.$$

Hence, the right-hand side of (7.44) gives

$$I \le \left(\frac{48}{5\sqrt{C_\Phi}} + \frac{4N+16}{5C_\Phi} + 1\right)\Phi(x_0).$$

If $|\nabla g(x_0)| \le |\nabla u(x_0)|$, then we can take C_Φ large enough so that $I < 4\Phi(x_0)$. A contradiction to (7.44). Otherwise, $|\nabla u(x_0)| \le |\nabla g(x_0)| \le L$.

Since x_0 is the maximum of Φ, we infer that on $B_R(0)\cap\Omega$, either we have

$$\Phi(x) \le C_\Phi \frac{R^2}{A^2}, \quad C_\Phi > C\max\left(\tfrac{1}{5h}, 4\sqrt{\tfrac{3}{5}}, \tfrac{(4N+16)}{5}\right),$$

or

$$\Phi(x) \le \frac{(R^2-|x|^2)^2L^2}{(9A^2-(u-2A)^2)^2} \quad \Leftrightarrow \quad |\nabla u(x)| \le L.$$

Hence, on $B_{\frac{R}{2}}(0)\cap\Omega$ where $R^2-|x|^2 \sim R^2$, we get the desired result. □

We return to the evolutionary free boundary problem setting. To show that the minimizer u_n is Lipschitz continuous up to convex Neumann boundaries, the main tool is the extension of the arguments in [4, Lemma 3.2] that gives an average growth rate of harmonic functions away from the free boundary. After which, we prove Lipschitz regularity on the Neumann boundary itself using the gradient control lemma 7.15. Using these tools, we give a complete proof of Lipschitz continuity via the maximum principle.

Lemma 7.16. *(cf. [80, Lemma 8]) If $x \in \partial\Omega$, then there exists $r_1 > 0$ and $C(h,N,L,r_1) > 0$ such that for every ball $B_r(x)$ with $r < r_1$,*

$$u_n(x) > Cr\sqrt{\lambda} \quad \textit{implies} \quad u_n > 0 \quad \textit{in } B_r\cap\Omega.$$

Proof. Without loss of generality, assume $x = 0$. Let $D_r := B_r(0)\cap\Omega$, $\Gamma_{D,r} := \partial B_r(0)\cap\Omega$ and $\Gamma_{N,r} := B_r(0)\cap\partial\Omega$. Consider a function $v \in H^1(D_r)$ satisfying

$$\Delta v - \frac{v}{h} = -\frac{u_{n-1}}{h} \le 0, \quad \text{in } D_r,$$

with $v = u_n$ in $\Gamma_{D,r}$ and Neumann boundary conditions along $\Gamma_{N,r}$. Note that v minimizes functional $\mathcal{I}_{n,D_r}$ on the set $\{f \in H^1(D_r) : f = u_n \text{ on } \Gamma_{D,r}\}$. By Lemma 7.13, we see that $v \geq 0$ in D_r, and therefore by the strong maximum principle ([49, Theorem 3.5]), v cannot achieve a nonpositive minimum in D_r, that is, we must have $v > 0$ in D_r.

Now, extend function v by u_n outside D_r, and denote this function by $\widehat{v}$. Using a similar argument (by virtue of Lemma 7.13) as in the proof of Theorem 7.14, we get (cf. (7.37))

$$\int_{D_r} \frac{|v-u_n|^2}{h} + |\nabla(v-u_n)|^2 \leq \lambda |\{\widehat{v} > 0\} \cap \{u_n = 0\} \cap D_r|,$$

that is,

$$\int_{D_r} |\nabla(v-u_n)|^2 \leq \lambda |\{u_n = 0\} \cap D_r|. \tag{7.45}$$

Next, we want to show that for some $C(N, L) > 0$,

$$\left(\frac{u_n(0)}{r}\right)^2 |\{u_n = 0\} \cap D_r| \quad \leq \quad C \int_{D_r} |\nabla(v-u_n)|^2. \tag{7.46}$$

We may assume (after rotation) that $\partial\Omega \cap B_r(0)$ is a Lipschitz graph in the x_N-direction with Lipschitz constant L. Then, there exists an $\epsilon(L)$ such that $B_{2\epsilon}(0, 0, \ldots, 0, \frac{1}{2}r) \subset D_r$. Note that $\epsilon \leq \frac{1}{4}r$.

Note that since $0 \in \partial\Omega$ and Ω is convex, then $\Gamma_{D,r}$ is simply connected and D_r is contained in $\{x \in B_r(0) : x_N > 0\}$. Let F be a bilipschitz map from D_r to $D_r' := B_r(0) \backslash \overline{D_r}$ such that F extends continuously to a map from $\overline{D_r}$ to $\overline{D_r'}$ with $F|_{\partial\Omega} = Id$ and $F(\Omega \cap \partial B_r(0)) = (\partial B_r(0)) \backslash \Omega$. The Lipschitz constants of F and F^{-1} depend only on L. Define function $\widetilde{u}_n$ on $B_r(0)$ by

$$\widetilde{u}_n = \begin{cases} u_n(x), & x \in \overline{\Omega} \cap B_r(0), \\ u_n(F^{-1}x), & x \in B_r(0) \backslash \overline{\Omega}, \end{cases}$$

and define $\widetilde{v}$ similarly. By a similar argument as in proof of Theorem 7.14 (Hölder continuity up to the fixed Neumann boundary), we see that $\widetilde{v}$ satisfies

$$D_i\left(a^{ij}(x) D_j \widetilde{v}\right) - d(x) \frac{\widetilde{v} - \widetilde{u}_{n-1}}{h} = 0, \qquad \text{in } B_r(0),$$

where

$$\begin{aligned} a^{ij}(x) &= |\det \nabla F^{-1}(x)| \left((\nabla F)^T (\nabla F)\right)(F^{-1}(x)) \\ d(x) &= |\det \nabla F^{-1}(x)|, \end{aligned}$$

when $x \in B_r(0) \backslash \overline{\Omega}$. Otherwise, $a^{ij} = d = 1$. Note that the bounds of a^{ij} and d depend only on L.

Claim 1. There exists $r_1 > 0$ and $C(N, h) > 0$ such that for any $x \in D_r$ (with $r < r_1$), we have $rv(x) \geq Cv(0)(r - |x|)$. Indeed, by Theorem 7.2, we have for any $p \geq 1$,

$$\int_{B_1(0) \cap \Omega} |u_{n-1}|^p \quad \leq \quad \int_{\Omega} |u_{n-1}|^p \leq |\Omega| \|u_0\|_\infty^p < \infty$$

and

$$\begin{aligned}\int_{B_1(0)\setminus\Omega}|\widetilde{u}_{n-1}|^p &\le \int_{B_1(0)\setminus\Omega}|u_{n-1}\circ F^{-1}|^p\\ &= \int_{F^{-1}(B_1(0)\setminus\Omega)}|u_{n-1}|^p|\det\nabla F|\\ &\le C(L)|\Omega|\|u_0\|_\infty^p<\infty\end{aligned}$$

and so, $\sup_{n\ge1}\|\widetilde{u}_{n-1}\|_{L^p(B_1(0))}<+\infty$. It follows from [49, Theorem 8.17 and 8.18] that

$$v(0) \le C_1\left(\inf_{B(0,\frac12 r)}\widetilde{v}(x)+k(r),\right) \tag{7.47}$$

where $C_1=C_1(r,h,q)>0$ with the property $\lim_{r\downarrow0}C_1(r,h,q)>0$, $q>N$, and

$$k(r)=r^{2(1-N/q)}\sup_{n\ge1}\left\|\frac{\widetilde{u}_{n-1}}{h}\right\|_{L^{q/2}(\Omega)}=o(r)\quad\text{as } r\downarrow0. \tag{7.48}$$

Hence, we can find small enough $r_1>0$ such that for any $r<r_1\ll1$, we have

$$k(r)\le r\inf_{B(0,\frac12 r)}\widetilde{v}(x)\le\inf_{B(0,\frac12 r)}\widetilde{v}(x).$$

Thus, for some constant $C_2>0$,

$$v(0) \le C_2\inf_{B(0,\frac12 r)}\widetilde{v}(x),$$

that is, for any $x\in B(0,\frac12 r)$, then

$$rv(x)\ge C_3rv(0)\ge C_4v(0)(r-|x|), \tag{7.49}$$

since $r-|x|\le r$. Here, $C_3=C_2^{-1}>0$.

For $x\in V:=D\setminus B_{\frac12 r}(0)$, we define a function

$$w(x) = C_3v(0)\left(\exp\left(\frac{-\mu|x|^2}{r^2}\right)-\exp(-\mu)\right),$$

where $\mu\ge N+\sqrt{N^2+r_1^2h^{-1}}$. By a similar argument as in Lemma 7.8, we see that

$$\Delta w-\frac{w-u_{n-1}}{h} \ge 0,\qquad\text{in } V. \tag{7.50}$$

If $x\in\partial V\cap\partial B_r(0)$, then $v(x)=u_n(x)\ge0$. Since $|x|=r$, then $w(x)=0\le v(x)$. Moreover, if $x\in\partial V\cap\partial B_{\frac12 r}(0)$, that is, $|x|=\frac12 r$, then by (7.49),

$$w(x) = C_3v(0)\left(e^{-\frac14\mu}-e^{-\mu}\right)\le C_3v(0)\le v(x). \tag{7.51}$$

Lastly, if $x\in\partial V\cap\partial\Omega$, then $\frac{\partial v}{\partial\boldsymbol{\eta}}=\frac{\partial u_n}{\partial\boldsymbol{\eta}}=0$. By convexity of D,

$$\frac{\partial w}{\partial\boldsymbol{\eta}}(x)=-\frac{2\mu C_3v(0)}{r^2}\exp\left(\frac{-\mu|x|^2}{r^2}\right)x\cdot\boldsymbol{\eta}\le0,$$

and so, $\frac{\partial(v-w)}{\partial \boldsymbol{\eta}} \geq 0$. From (7.50), we get

$$\Delta w - \frac{w}{h} \geq -\frac{u_{n-1}}{h} = \Delta v - \frac{v}{h} \quad \text{in } V.$$

Hence, for any $\phi \in \{f \in H^1(V) : f \geq 0, \text{ and } f|_{\partial V \cap \Omega} = 0\}$, we have

$$\begin{aligned} 0 &\geq -\int_V \nabla(v-w)\cdot\nabla\phi + \int_{\partial V\cap\partial\Omega} \frac{\partial(v-w)}{\partial\boldsymbol{\eta}}\phi - \frac{v-w}{h}\phi \\ &\geq -\int_V \nabla(v-w)\cdot\nabla\phi - \frac{v-w}{h}\phi. \end{aligned}$$

Moreover, from (7.51), we have $(v-w)|_{\partial V\cap\Omega} \geq 0$. By Lemma 7.13, $v - w \geq 0$ in V. Hence, for any $x \in V$, there exists $C_4 > 0$ such that

$$rv(x) \geq rw(x) \geq C_4 v(0)\,(r - |x|)\,.$$

(Indeed, if $x \in V$, then $\frac{1}{2}r \leq |x| < r$, that is, $r - |x| \leq \frac{1}{2}r$. Moreover, since the exponential function is nonincreasing, then for some $\delta > 0$,

$$rw(x) \geq \tfrac{1}{2}\delta C_3 r v(0) \geq \delta C_3 v(0)(r - |x|).$$

Take $C_4 := \delta C_3 > 0$.) Therefore for any $x \in D$, we have $rv(x) \geq Cv(0)\,(r - |x|)$ which proves the claim.

Further, we may assume $r = 1$, since we can dilate $u_n^r(y) = \frac{1}{r}u_n(ry)$ and similarly for v so that both sides of the inequality (7.46) remains unchanged. Let $z \in B_\epsilon(0, 0, \ldots, 0, \frac{1}{2})$. For every $\xi \in \partial B_1(0)$, we define

$$\begin{aligned} R_\xi &:= \sup\{r : r\xi + z \in B_1(0)\} \\ r_\xi &:= \inf\left\{r : \tfrac{1}{2}\epsilon \leq r \leq R_\xi \text{ and } \widetilde{u}_n(r\xi + z) = 0\right\}, \end{aligned}$$

if such an r exists. Otherwise, set $r_\xi = R_\xi$. Define $\tau_\xi(t) = z + t\xi$ for $r_\xi \leq t \leq R_\xi$, and denote the line segment by τ_ξ. Note that $\widetilde{v}(\tau(R_\xi)) = \widetilde{u}_n(\tau(R_\xi))$. (Indeed, if $y \in \partial(B_1(0)\backslash D)$, then $F^{-1}(y) \in \partial(B_1(0)\backslash D)$, and so, $\widetilde{v}(y) = v(F^{-1}y) = u_n(F^{-1}y) = \widetilde{u}_n(y)$). Also, we note that the path τ has unit speed at all times, and recall that $\widetilde{u}_n(\tau(r_\xi)) = 0$ (unless $r_\xi = R_\xi$, in which case $|r_\xi| = 0$). Then,

$$\begin{aligned} \widetilde{v}(r_\xi\xi + z) &= \widetilde{v}(r_\xi\xi + z) - \widetilde{u}_n(r_\xi\xi + z) = \widetilde{v}(\tau(r_\xi)) - \widetilde{u}_n(\tau(r_\xi)) \\ &= \widetilde{v}(\tau(R_\xi)) - \widetilde{u}_n(\tau(R_\xi)) - \int_{\tau_\xi} \frac{\partial}{\partial t}(\widetilde{v} - \widetilde{u}_n)(\tau_\xi(t))dt \\ &= \int_{\tau_\xi} \frac{\partial}{\partial t}(\widetilde{u}_n - \widetilde{v})(\tau_\xi(t))dt \\ &\leq \int_{\tau_\xi} |\nabla(\widetilde{v} - \widetilde{u}_n)| \leq \sqrt{R_\xi - r_\xi}\left(\int_{\tau_\xi} |\nabla(\widetilde{v} - \widetilde{u}_n)|^2\right)^{\frac{1}{2}} \end{aligned} \tag{7.52}$$

Define s_ξ to be the unique (due to convexity) $s < R_\xi$ such that $\tau(s) \in \partial\Omega$ if such an s exists. Otherwise, set $s_\xi = R_\xi$.

Claim 2. There exists $C > 0$ such that $1 - |r_\xi\xi + z| \geq C(R_\xi - r_\xi)$. Indeed, we may assume that $(1 - |r_\xi\xi + z|) < \frac{1}{4}$. (Otherwise, taking $C = \frac{1}{8}$ and noting that $R_\xi - r_\xi \leq 2$ gives the desired result.) Since $|z| \leq \frac{3}{4}$, then we can find $\tau_0 < \frac{\pi}{2}$ such that if $|r_\xi\xi + z| > \frac{3}{4}$,

the ray from 0 to point $r_\xi\xi + z$ and the ray from z to that point must meet at an angle $\tau < \tau_0$. Then,

$$R_\xi - r_\xi \quad \leq \quad \frac{1 - |r_\xi\xi + z|}{\cos(\tau)} \leq \frac{1 - |r_\xi\xi + z|}{\cos(\tau_0)} \leq C(1 - |r_\xi\xi + z|),$$

which proves the claim.

Now, Theorem 7.5 gives

$$D_i\left(a^{ij}(x)D_j(\widetilde{u}_n - \widetilde{v})\right) - d(x)\frac{\widetilde{u}_n - \widetilde{v}}{h} \quad \geq \quad 0, \qquad \text{in } B_1(0),$$

and so, [49, Theorem 8.1] gives

$$\sup_{B_1(0)}(\widetilde{u}_n - \widetilde{v}) \leq \sup_{\partial B_1(0)}(\widetilde{u}_n - \widetilde{v}) = 0.$$

This implies that $0 \leq \widetilde{u}_n(x) \leq \widetilde{v}(x)$, for any $x \in B_1(0)$. In particular, $u_n(0) \leq v(0)$.

If $r_\xi \leq s_\xi$, then by the first claim,

$$\begin{aligned} \widetilde{v}(r_\xi\xi + z) \quad &\geq \quad C(N,h)v(0)(1 - |r_\xi\xi + z|) \\ &\geq \quad C(N,h)u_n(0)(1 - |r_\xi\xi + z|). \end{aligned}$$

Otherwise,

$$\begin{aligned} \widetilde{v}(r_\xi\xi + z) \quad &= \quad v(F^{-1}(r_\xi\xi + z)) \geq C(N,h)v(0)(1 - |F^{-1}(r_\xi\xi + z)|) \\ &\geq \quad C(N,h)u_n(0)(1 - |r_\xi\xi + z|), \end{aligned}$$

since F is bilipschitz. Invoking the second claim on both cases gives

$$\widetilde{v}(r_\xi\xi + z) \quad \geq \quad C(N,h)u_n(0)(R_\xi - r_\xi).$$

By (7.52), we get

$$C(N,h)u_n(0)^2(R_\xi - r_\xi) \quad \leq \quad \int_{\tau_\xi} |\nabla(\widetilde{v} - \widetilde{u}_n)|^2. \tag{7.53}$$

Integrating the left-hand side of (7.53) with respect to ξ gives

$$\begin{aligned} \int_{\partial B_1(0)}(R_\xi - r_\xi)d\xi \quad &= \quad \int_{\partial B_1(0)}\int_{r_\xi}^{R_\xi} dr d\xi \geq \frac{1}{2^{N-1}}\int_{\partial B_1(0)}\int_{r_\xi}^{R_\xi} r^{N-1}dr d\xi \\ &\geq \quad \frac{1}{2^{N-1}}\int_{B_1(0)\setminus B_{\frac{\epsilon}{2}}(z)} \chi_{\{\widetilde{u}_n = 0\}}dx \\ &\geq \quad \frac{1}{2^{N-1}}\int_{D\setminus B_{\frac{\epsilon}{2}}(z)} \chi_{\{u_n = 0\}}dx. \end{aligned} \tag{7.54}$$

On the other hand, integrating the right-hand side of (7.53) with respect to ξ yields

$$\begin{aligned} \int_{\partial B_1(0)}\int_{r_\xi}^{R_\xi} |\nabla(\widetilde{v} - \widetilde{u}_n)|^2 dr d\xi \quad &= \quad \int_{\partial B_1(0)}\left(\int_{r_\xi}^{s_\xi} + \int_{s_\xi}^{R_\xi}\right)|\nabla(\widetilde{v} - \widetilde{u}_n)|^2 dr d\xi \\ &:= \quad I + II, \end{aligned}$$

whenever $s_\xi \geq r_\xi$. Since $r_\xi \geq \epsilon(L)/2$, then

$$\begin{aligned} I &= \int_{\partial B_1(0)} \int_{r_\xi}^{s_\xi} |\nabla(v-u_n)(r\xi+z)|^2 dr d\xi \\ &\leq \frac{2^{N-1}}{\epsilon(L)^{N-1}} \int_{\partial B_1(0)} \int_{r_\xi}^{s_\xi} |\nabla(v-u_n)(r\xi+z)|^2 r^{N-1} dr d\xi \\ &\leq C(L) \int_D |\nabla(v-u_n)|^2 dx. \end{aligned}$$

Moreover, noting that $s_\xi \geq 2\epsilon(L)$, we get

$$\begin{aligned} II &\leq \int_{\partial B_1(0)} \int_{s_\xi}^{R_\xi} |\nabla F^{-1}|^2 |\nabla(v-u_n)(F^{-1}(r\xi+z))|^2 dr d\xi \\ &\leq C(L) \int_{\partial B_1(0)} \int_{s_\xi}^{R_\xi} |\nabla(v-u_n)(F^{-1}(r\xi+z))|^2 dr d\xi \\ &\leq \frac{C(L)}{(2\epsilon(L))^{N-1}} \int_{\partial B_1(0)} \int_{s_\xi}^{R_\xi} |\nabla(v-u_n)(F^{-1}(r\xi+z))|^2 r^{N-1} dr d\xi \\ &\leq C(L) \int_{D'} |\nabla(v-u_n)(F^{-1}x)|^2 dx \\ &\leq C(L) \int_D |\nabla(v-u_n)|^2 |\det(\nabla F)| \\ &\leq C(L) \int_D |\nabla(v-u_n)|^2. \end{aligned}$$

Hence,

$$\int_{\partial B_1(0)} \int_{r_\xi}^{R_\xi} |\nabla(\widetilde{v}-\widetilde{u}_n)|^2 dr d\xi \leq C(L) \int_D |\nabla(v-u_n)|^2. \tag{7.55}$$

By a similar argument, we see that this also holds when $s_\xi < r_\xi$.

Combining (7.53), (7.54), and (7.55) gives

$$u_n(0)^2 \int_{D \setminus B_{\frac{\epsilon}{2}}(z)} \chi_{\{u_n=0\}} \leq C(h,N,L) \int_D |\nabla(v-u_n)|^2.$$

Hence, integrating with respect to $z \in B_{\epsilon(L)}(0,\ldots,0,\frac{1}{2})$ yields

$$u_n(0)^2 \int_D \chi_{\{u_n=0\}} \leq C(h,N,L) \int_D |\nabla(v-u_n)|^2,$$

which from (7.45) implies

$$u_n(0)^2 |\{u_n=0\} \cap D| \leq \lambda C(h,N,L) |\{u_n=0\} \cap D|.$$

Hence, if $\{u_n=0\} \cap D \neq \emptyset$, then we must have $u_n(0) \leq C(h,N,L)\sqrt{\lambda}$. A contradiction. □

Next, we check the Lipschitz gradient bound on the fixed Neumann boundary, near the free boundary.

Lemma 7.17. *(cf. [80, Lemma 9]) Let $\Omega \subset \mathbb{R}^N$ be an open bounded domain with convex Lipschitz boundary. There exists constants $r_2 > 0$ and $C(h, N, \mu, L, r_2) > 0$, such that if $x \in \partial\Omega$ satisfies dist$(x, \partial\{u > 0\}) < r_2$, then*

$$|\nabla u_n(x)| \le C(1 + \sqrt{\lambda}).$$

Proof. Let $x \in \partial\Omega$ and denote $r_x := \inf\{r > 0 : B(x, r) \cap \{u_n = 0\} \neq \emptyset\}$. Note that

$$\Delta u_n = \frac{u_n - u_{n-1}}{h}, \quad \text{in } D := B(x, r_x) \cap \Omega.$$

Denote $\Gamma_D = \partial B_{r_x} \cap \Omega$ and $\Gamma_N = B_{r_x} \cap \partial\Omega$. Since $\partial\Omega$ is a Lipschitz graph, then there exists a bilipschitz map $F : D_t \to B^+_{r_x}$ where $\{x_N = 0\} = F(\Gamma_N)$ and $(\partial B_{r_x})^+ = F(\Gamma_D)$. The Lipschitz constants of F and F^{-1} are controlled solely by L. As in the proof of Theorem 7.14, we can define $\widetilde{u}_n(y) = u_n(F^{-1}y)$ on B_{r_x} such that

$$D_i\left(a^{ij}(x) D_j \widetilde{u}_n\right) - d(x)\frac{\widetilde{u}_n - \widetilde{u}_{n-1}}{h} = 0, \qquad \text{in } B_{r_x},$$

where a^{ij} is uniformly elliptic with bounded, measurable coefficients on all of B_{r_x}, and that the bounds of a^{ij} and d depend only on L.

By Theorem 7.2, we have for any $p \ge 1$,

$$\begin{aligned}\int_{B_{r_x}} |\widetilde{u}_{n-1}|^p &\le \int_{B_{r_x}} |u_{n-1} \circ F^{-1}|^p \\ &= \int_{F^{-1}(B_{r_x})} |u_{n-1}|^p |\det \nabla F| \\ &\le C(L)|\Omega| \|u_0\|^p_\infty < \infty\end{aligned}$$

and so, $\sup\limits_{n\ge1} \|u_{n-1}\|_{L^p(B_{r_x})} < +\infty$. By [49, Theorem 8.17 and 8.18],

$$\sup_{B_{r_x}} \widetilde{u}_n \le C_1\left(\inf_{B_{r_x}} \widetilde{u}_n + k(r_x)\right),$$

where $C_1(r_x, h, q) > 0$ with the property $\lim_{r\downarrow0} C_1(r_x, h, q) > 0$, $q > N$, and $k(\cdot)$ is defined as in (7.48). Hence, we can find small enough $\varepsilon_1 > 0$ such that if $r_x < \varepsilon_1 \ll 1$, we have

$$k(r_x) \le r_x \inf_{B_{r_x}} \widetilde{u}_n(x) \le \inf_{B_{r_x}} \widetilde{u}_n(x),$$

that is, for some $C_2 > 0$, $\sup\limits_{B_{r_x}} \widetilde{u}_n(x) \le C_2 \widetilde{u}_n(x)$.

Now, for any $\delta > 0$, we see that $|B(x, r_x + \delta) \cap \{u_n = 0\}| > 0$. By Lemma 7.16, there exists $r_1 > 0$ small such that if $r_x + \delta < r_1$, we get

$$u_n(x) \le C(r_x + \delta)\sqrt{\lambda}.$$

Taking $\delta \downarrow 0$ gives $u_n(x) \le C r_x \sqrt{\lambda}$, provided $r_x < r_1$. Take $r_2 = \min(\varepsilon_1, r_1) > 0$. Thus, for any $y \in B(x, \frac{1}{2}r_x)$, we have

$$\widetilde{u}_n(y) \le C\sqrt{\lambda} r_x.$$

By Lemma 7.15, we see that if (**i**) holds, then we are done. Otherwise, for some $C(N,h)>0$,

$$|\nabla u_n(x)| \le C\frac{C\sqrt{\lambda}r_x}{r_x} \le C$$

□

Finally, we arrive at the Lipschitz regularity theorem.

Theorem 7.18. *If u_n minimizes $\mathcal{F}_n^h$ $(n=1,\dots,M)$ for $h,\lambda>0$, then for a.e. $x\in\Omega$,*

$$|\nabla u_n(x)| \le C_\ell(1+\sqrt{\lambda}),$$

where constant $C_\ell := C(N,L,h)>0$. Here, $\partial\Omega$ is locally a Lipschitz graph with Lipschitz constant $L>0$.

Proof by Induction. Fix n. Suppose $|\nabla u_{n-1}| \le C(N,L,h)(1+\sqrt{\lambda})$. We wish to show the same for the gradient bound of u_n.

There exists $s>0$ depending only on the Lipschitz character of Ω such that one can cover $\partial\Omega$ with balls B_s of radius s such that $B_s\cap\partial\Omega$ is a Lipschitz graph with Lipschitz constant is less than or equal to L. Let $R=\frac{1}{2}\min(1,s,r_0,r_1,r_2)$ where $r_0,r_1,r_2>0$ are the constants in Lemma 7.8, Lemma 7.16, and Lemma 7.17, respectively. Denote $U_n := \{u_n>0\}$ and $\Lambda_n := \Omega\cap\partial U_n$. Let $x\in\Omega$. Then, x belongs to one of the five regions depicted in Figure 7.1. To show the Lipschitz continuity, we consider each case separately.

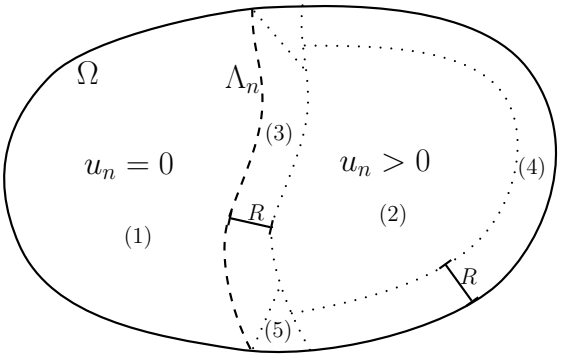

FIGURE 7.1: The subsets of domain Ω which form the five cases in consideration.

Case 1. $x\in\Omega\backslash\overline{U_n}$. Clearly, $|\nabla u_n(x)|=0$ for almost every such x.

Case 2. $x\in U_n$ and $\operatorname{dist}(x,\partial U_n)\ge R$. Note that $B_R := B(x,R)\subset U_n$. By C^2-continuity of u_n (Corollary 7.6), Hölder continuity of u_{n-1} (Theorem 7.4), and [49, Lemma 6.16], we see that $u_n\in C^{2,\gamma}(B_R)$. Hence, the elliptic Schauder estimate [49, Theorem 6.2] gives the desired result.

Case 3. $x\in U_n$ and $\operatorname{dist}(x,\Lambda_n)<\min(R,\frac{1}{4}\operatorname{dist}(x,\partial\Omega))$. By virtue of Lemma 7.8, u_n has Lipschitz continuity at the free boundary Λ_n with Lipschitz constant depending linearly on $\sqrt{\lambda}$. By Theorem 7.9, we are done.

Case 4. $x\in U_n$ and $\operatorname{dist}(x,\Lambda_n)\ge R\ge\operatorname{dist}(x,\partial\Omega)$. By Lemma 7.15, we see that if (**i**) holds, then we are done. Otherwise, Theorem 7.2 gives $|\nabla u_n|\le\frac{C}{R}\|u_0\|_\infty$ for some $C(N,h)>0$.

Case 5. $x \in U_n$ and $\frac{1}{4}\mathrm{dist}(x, \partial\Omega) \le \mathrm{dist}(x, \Lambda_n) \le R$. By slightly shrinking $U_n := \{u_n > 0\}$, we can find a set U_n' such that $x \in U_n'$, $\partial U_n' \cap \Omega$ is smooth, and

$$|\nabla u_n(x)| \le C(N, h, \gamma, \|u_0\|_\infty)(\sqrt{\lambda} + 1) \quad \text{on } \partial U_n' \cap \Omega, \tag{7.56}$$

where we employed Case 3. Since $u_n \in H^1(\Omega)$, then $\nabla u_n \in L^2(\Omega)$. By Fubini's theorem, there exists a radius r and $C(N) > 0$ such that $\frac{3}{4}R \le r \le R$ and $\nabla u_n \in L^2(\partial B_r(x))$ with

$$r^{N-1}\|\nabla u_n\|_{L^2(\partial B_r(x))} \le C\|\nabla u_n\|_{L^2(\Omega)}.$$

(Otherwise,

$$\begin{aligned}\int_\Omega |\nabla u_n|^2 &\ge \int_{B_R\cap\Omega} |\nabla u_n|^2 \ge \int_{\frac{3}{4}R}^R \int_{\partial B_r\cap\Omega} |\nabla u_n|^2 \\ &\ge C(N)\int_{\frac{3}{4}R}^R \frac{1}{r^{2(N-1)}} \int_\Omega |\nabla u_n|^2 \\ &= \frac{C(N)}{R^{2N-3}}\int_\Omega |\nabla u_n|^2,\end{aligned}$$

which gives $R^{2N-3} \ge C(N) \ge 1$.) Note that u_n satisfies

$$\Delta u_n - \frac{u_n}{h} = -\frac{u_{n-1}}{h}, \quad \text{in } D := B_r(x) \cap U_n'.$$

Moreover, ∂D has three parts: $\Gamma_1 = B_r \cap \partial\Omega \cap \partial U_n'$, $\Gamma_2 = B_r \cap \Omega \cap \partial U_n'$, and $\Gamma_3 = U_n' \cap \partial B_r$. These parts may not each be connected, but they are pairwise disjoint and $\overline{\Gamma_1} \cup \overline{\Gamma_2} \cup \overline{\Gamma_3} = \partial D$. Note that Γ_1 is a convex Lipschitz hypersurface, and so, by Lemma 7.17, we have

$$|\nabla u_n| \le C(N, L, h, R)(1 + \sqrt{\lambda}), \quad \text{on } \Gamma_1.$$

By construction, Γ_2 is a Lipschitz curve on which (7.56) holds. Moreover, Γ_3 is a smooth curve. Define function v on $B_r(x)$ by

$$\begin{cases} \Delta v = 0, & \text{in } B_r(x), \\ v = C_3^2 + (|\nabla u_n|^2)\chi_{\Gamma_3}, & \text{on } \partial B_r(x) \end{cases}$$

where $C_3 = \max(C_1(1+\sqrt{\lambda}), C_2)$. Then, on Γ_1 and Γ_2, we have $v = C_3^2 \ge |\nabla u_n|^2$. Now, if $x \in \Gamma_3$, we see that

$$v(x) = C_3^2 + |\nabla u_n(x)|^2 \ge |\nabla u_n(x)|^2.$$

Moreover, recalling (7.42) and invoking Theorem 7.5, we have

$$\begin{aligned}\Delta(|\nabla u_n|^2) &= 2\sum_{i,j=1}^N \left(\frac{\partial^2 u_n}{\partial x_i \partial x_j}\right)^2 + 2\frac{\nabla(u_n - u_{n-1})}{h} \cdot \nabla u_n \\ &\ge \frac{2|\nabla u_n|^2 - 2\nabla u_{n-1} \cdot \nabla u_n}{h} \\ &\ge \frac{|\nabla u_n|^2 - |\nabla u_{n-1}|^2}{h} \ge -\frac{|\nabla u_{n-1}|^2}{h} \quad \text{in } D\end{aligned}$$

and so, in the weak sense,

$$\Delta(|\nabla u_n|^2 - v) + \frac{|\nabla u_{n-1}|^2}{h} \geq 0, \quad \text{in } D.$$

By the induction hypothesis, we have for any $p \geq 1$,

$$\int_D |\nabla u_{n-1}|^p \leq C(N, L, h)^p (1 + \sqrt{\lambda})^p |D| < +\infty.$$

Hence, for some $q > 2N$, [49, Theorem 8.16] gives

$$\begin{aligned} \sup_D (|\nabla u_n|^2 - v) &\leq \sup_{\partial D} (|\nabla u_n|^2 - v)^+ + C(N, h, R) \left\| |\nabla u_{n-1}|^2 \right\|_{L^q(D)} \\ &=: C_4(N, L, h, R)^2 (1 + \sqrt{\lambda})^2 \end{aligned}$$

since $v \geq |\nabla u_n|^2$ in ∂D. Hence, $|\nabla u_n|^2 \leq v + C_4^2$ on $D \subset B_r$, and so,

$$|\nabla u_n(x)|^2 \leq v(x) + C_4^2 (1 + \sqrt{\lambda})^2.$$

Since v is harmonic in $B_r(x)$, we have

$$\begin{aligned} v(x) &= \fint_{\partial B_r(x)} v(y) d\sigma(y) = C_3^2 + \frac{C(N)}{\omega_N r^{N-1}} \int_{\Gamma_3} |\nabla u_n|^2 \\ &\leq C_3^2 + \frac{C(N)}{\omega_N r^{3(N-1)}} \int_\Omega |\nabla u_n|^2 \\ &\leq C_3^2 + \frac{C(N)}{\omega_N \left(\frac{3}{4}R\right)^{3(N-1)}} \|\nabla u_0\|^2_{L^2(\Omega)} \\ &\leq C(N, L, h, R)(1 + \sqrt{\lambda}). \end{aligned}$$

Hence, we have

$$|\nabla u_n(x)|^2 \leq v(x) + C_4^2 (1 + \sqrt{\lambda})^2 \leq C(1 + \sqrt{\lambda}).$$

Thus, for almost every $x \in \Omega$, $|\nabla u_n| \leq (1 + \sqrt{\lambda}) C_\ell(N, L, h)$.

□

7.5 Behavior of the minimizer for large λ

This section investigates the behavior of minimizer u_n for sufficiently large penalty $\lambda > 0$. In particular, we show that the solution to the original problem (7.1) is attained without having to take λ to infinity.

Note that Theorem 7.7 implies that our penalization does not affect those functions whose $|\{u > 0\}|$ is less than the prescribed measure. This allows us to avoid smooth outward perturbations of $\{u > 0\}$. Inward perturbations, on the other hand, can be done in a natural way (cf. [93]) by replacing u in the set $u > 0$ by $w_\delta := (u - \delta)_+$. When λ is large enough, we rule out the case $|\{u_n > \delta\}| > \alpha$ by showing that, in this case, $\mathcal{F}_n^h(u_n) \leq \mathcal{F}_n^h(w_\delta)$ for small δ, contrary to the minimality of u_n. The crucial point here is the gradient bound for u_n (Theorem 7.18).

Theorem 7.19. *Suppose*

$$\lambda > \max\left(\frac{2\|\nabla u_0\|^2_{L^2(\Omega)}}{|\Omega| - \alpha}, \ \frac{\left[(C_* + \sqrt{h})\|u_0\|_\infty + h \right]^2}{h^2} \right),$$

where

$$C_* := \frac{2C_S C_\ell |\Omega|^{2+1/N}}{\alpha(|\Omega| - \alpha)}.$$

If u_n minimizes $\mathcal{F}^h_n$ $(n = 1, \dots, M)$, then $|\{u_n > 0\}| = \alpha$. As a consequence, u_n solves (7.3) *if and only if it solves* (7.1).

Here, C_S is the Sobolev-Poincaré constant relative to Ω, that is, the smallest number such that

$$\int_\Omega \left| v - \fint_\Omega v \right| \le C_S |\Omega|^{1/N} \|Dv\|(\Omega), \quad \forall v \in BV(\Omega) \tag{7.57}$$

where $\|Dv\|(\Omega)$ is the total variation of the distributional derivative of v.

Proof. By Theorem 7.7, it suffices only to show that $|\{u_n > 0\}| \le \alpha$. Suppose not. Then, we can find a sufficiently small $\delta \in (0, 1)$ such that

$$|\{u_n > \delta\}| \ge \alpha. \tag{7.58}$$

For such δ, consider the comparison function $w_\delta := (u_n - \delta)_+ \in H^1(\Omega)$. Note that $\{w_\delta > 0\} = \{u_n > \delta\}$. Then, $\mathcal{F}^h_n(u_n) \le \mathcal{F}^h_n(w_\delta)$ implies

$$\begin{aligned} \int_\Omega \frac{|u_n - u_{n-1}|^2}{h} - \frac{|w_\delta - u_{n-1}|^2}{h} + \int_\Omega |\nabla u_n|^2 - |\nabla w_\delta|^2 &\le \lambda(|\{w_\delta > 0\}| - |\{u_n > 0\}|) \\ &\le -\lambda |\{0 < u_n < \delta\}|. \end{aligned} \tag{7.59}$$

By the definition of w_δ, we have

$$\begin{aligned} \int_\Omega |\nabla w_\delta|^2 - |\nabla u_n|^2 &= \int_{\{u_n > \delta\}} |\nabla u_n|^2 - \int_\Omega |\nabla u_n|^2 \\ &= -\int_{\{0 < u_n < \delta\}} |\nabla u_n|^2 \le 0, \end{aligned}$$

and

$$\begin{aligned} \int_\Omega \frac{|w_\delta - u_{n-1}|^2}{h} &- \frac{|u_n - u_{n-1}|^2}{h} \\ &= \int_{\{0 < u_n < \delta\}} \frac{u^2_{n-1}}{h} + \int_{\{u_n \ge \delta\}} \frac{|u_n - \delta - u_{n-1}|^2}{h} - \int_\Omega \frac{|u_n - u_{n-1}|^2}{h} \\ &= \int_{\{0 < u_n < \delta\}} \left(\frac{u^2_{n-1}}{h} - \frac{|u_n - u_{n-1}|^2}{h} \right) + \frac{\delta}{h} \int_{\{u_n \ge \delta\}} (\delta - 2(u_n - u_{n-1})) \\ &\le \int_{\{0 < u_n < \delta\}} \frac{u^2_{n-1}}{h} + \frac{\delta}{h} \int_{\{u_n \ge \delta\}} (2u_{n-1} - \delta) \\ &\le \frac{\|u_0\|^2_\infty}{h} |\{0 < u_n < \delta\}| + \delta |\Omega| \frac{2\|u_0\|_\infty}{h}. \end{aligned}$$

Thus, (7.59) becomes

$$\lambda \leq \frac{\|u_0\|_\infty^2}{h} + \frac{2\delta|\Omega|\|u_0\|_\infty}{h|\{0 < u_n < \delta\}|}. \tag{7.60}$$

We will estimate the second term on the right-hand side of (7.60) by a quantity independent of δ, which will lead to a contradiction. To this end, consider set $A_t := \{u_n < t\}$ for $t \in (0, \delta)$. Then, $\{u_n > \delta\} \subset \Omega \backslash A_t \subset \{u_n > 0\}$. By (7.58) and Theorem 7.7, we get

$$\alpha \leq |\Omega| - |A_t| \leq \alpha + \lambda^{-1}\|\nabla u_0\|_{L^2(\Omega)}^2,$$

which implies that

$$\begin{aligned}
\int_\Omega \left|\chi_{A_t} - \fint_\Omega \chi_{A_t}\right| &= \int_{A_t} \left|1 - \frac{|A_t|}{|\Omega|}\right| + \int_{\Omega\backslash A_t} \frac{|A_t|}{|\Omega|} \\
&= 2(|\Omega| - |A_t|)\frac{|A_t|}{|\Omega|} \\
&\geq 2\alpha \frac{|\Omega| - \alpha - \lambda^{-1}\|\nabla u_0\|_{L^2(\Omega)}^2}{|\Omega|} \\
&\geq \frac{\alpha(|\Omega| - \alpha)}{|\Omega|},
\end{aligned} \tag{7.61}$$

since $\lambda^{-1}\|\nabla u_0\|_{L^2(\Omega)}^2 < (|\Omega| - \alpha)/2$. Note that the total variation of $u_n \in H^1(\Omega)$ is

$$\int_\Omega |\nabla u_n| \leq |\Omega|^{1/2}\|\nabla u_n\|_{L^2(\Omega)} \leq |\Omega|^{1/2}\|\nabla u_0\|_{L^2(\Omega)} < \infty,$$

which follows from Hölder's inequality and Lemma 7.3. Then, by [38, Section 5.5, Theorem 1], A_t has finite perimeter, that is, $\mathcal{H}^{N-1}(\partial A_t) < \infty$ for $\mathcal{L}^1$ a.e. $t \in (0, \delta)$. This implies that $\chi_{A_t} \in BV(\Omega)$, and so, by the isoperimetric inequality (7.57) and (7.61), we have

$$\frac{\alpha(|\Omega| - \alpha)}{|\Omega|} \leq \int_\Omega \left|\chi_{A_t} - \fint_\Omega \chi_{A_t}\right| \leq C_S|\Omega|^{\frac{1}{N}}\mathcal{H}^{N-1}(\partial A_t). \tag{7.62}$$

By the Coarea formula and Theorem 7.18, we have for some $C_\ell(N, L, h) > 0$,

$$\int_0^\delta \mathcal{H}^{N-1}(\partial A_t)dt = \int_{\{0<u_n<\delta\}} |\nabla u_n| \leq (1 + \sqrt{\lambda})C_\ell|\{0 < u_n < \delta\}|.$$

Integrating (7.62) with respect to t over $(0, \delta)$ and multiplying $|\Omega|$ yields

$$\delta\alpha(|\Omega| - \alpha) \leq C_S C_\ell(1 + \sqrt{\lambda})|\Omega|^{1+1/N}|\{0 < u_n < \delta\}|$$

Thus, (7.60) becomes

$$\lambda \leq \frac{\|u_0\|_\infty^2}{h} + C_*(1 + \sqrt{\lambda})\frac{\|u_0\|_\infty}{h}.$$

By the quadratic formula, we get $\sqrt{\lambda} \leq C_* \frac{\|u_0\|_\infty}{h} + \frac{\|u_0\|_\infty}{\sqrt{h}} + 1$. A contradiction. □

7.6 Construction of Minimizing Movement

This section presents the minimizing movement for our evolutionary free boundary problem and some of its properties.

For $h, \lambda > 0$, let u_n be the minimizer of functional $\mathcal{F}_n^h (n = 1, \ldots, M)$. Define *h-step function* $\widetilde{u}^h : [0, T] \times \Omega \to \mathbb{R}$ by

$$\widetilde{u}^h(t, x) := u_{\lfloor t/h \rfloor + 1}(x) = \begin{cases} u_0(x), & t = 0 \\ u_n(x), & t \in ((n-1)h, nh],\ n = 1, \ldots, M \end{cases} \tag{7.63}$$

and *h-piecewise linear function* $u^h : [0, T] \times \Omega \to \mathbb{R}$ by

$$u^h(t, x) := (1 - \tau) u_{\lfloor t/h \rfloor}(x) + \tau u_{\lfloor t/h \rfloor + 1}(x), \tag{7.64}$$

where $\tau = t/h - \lfloor t/h \rfloor \in [0, 1]$. Here, $\lfloor \cdot \rfloor$ denotes the floor function. Hence, for any $t \in [(n-1)h, nh]$ where $n = 1, \ldots, M$,

$$u^h(t, x) = \frac{nh - t}{h} u_{n-1}(x) + \frac{t - (n-1)h}{h} u_n(x).$$

Remark. By Theorem 7.2, we have

$$0 \le \widetilde{u}^h(t, x), u^h(t, x) \le \|u_0\|_\infty, \tag{7.65}$$

for any $t \in [0, T]$ and for almost every $x \in \Omega$. Moreover, for any $t \in (0, T)$,

$$\lim_{h \downarrow 0} \|\widetilde{u}^h(t, \cdot) - u^h(t, \cdot)\|_{L^2(\Omega)} = 0. \tag{7.66}$$

Indeed,

$$\begin{aligned} \int_\Omega \left| \widetilde{u}^h(t, x) - u^h(t, x) \right|^2 dx &= (1 - \tau)^2 \int_\Omega \left| u_{\lfloor t/h \rfloor}(x) - u_{\lfloor t/h \rfloor + 1}(x) \right|^2 dx \\ &\le h \|\nabla u_0\|^2_{L^2(\Omega)}, \end{aligned}$$

which follows from Lemma 7.3.

First, we state the definition of the generalized minimizing movement.

Definition 7.20 (Generalized Minimizing Movement)**.** Consider a separable Hilbert space X, a functional

$$\mathcal{F} : (0, 1) \times X \times X \longrightarrow \mathbb{R} \cup \{-\infty, +\infty\},$$

and an initial datum $u_0 \in X$. We say that $u : [0, +\infty) \to X$ is a *generalized minimizing movement* in X associated to $\mathcal{F}$ and u_0, written as

$$u \in GMM(\mathcal{F}, u_0; X)$$

if there exists a family of sequences $\left\{u_n^h\right\}_{n=1}^\infty$ depending on $h \in (0, 1)$ such that

$$\begin{cases} u_0^h = u_0 \\ \mathcal{F}(h, u_n^h, u_{n-1}^h) = \min\limits_{v \in X} \mathcal{F}(h, v, u_{n-1}^h), \quad \forall n \in \mathbb{N},\ h \in (0, 1) \end{cases} \tag{7.67}$$

and u is the pointwise limit in X, as h goes to 0, of the h-step functions $\widetilde{u}^h$ (defined in (7.63)), that is,

$$\lim_{h\downarrow 0} \widetilde{u}^h(t) = u(t) \text{ in } X \quad \forall t \in [0, +\infty). \tag{7.68}$$

Theorem 7.21. *There exists $u \in GMM(\mathcal{F}, u_0, L^2(\Omega))$.*

Proof. Consider a sequence $\{h\} \subset (0,1)$ such that $h \to 0$. For each $h > 0$, there exists a sequence $\{u_n^h\}_{n=0}^{\infty}$ such that (7.67) holds (Theorem 7.1).

Note that for any $t \in (0,T)$,

$$\begin{aligned}
\int_\Omega |\nabla u^h(t)|^2 &= \int_\Omega \left|(1-\tau)\nabla u_{\lfloor t/h\rfloor} + \tau \nabla u_{\lfloor t/h\rfloor+1}\right|^2 \\
&= \int_\Omega (1-\tau)^2 \left|\nabla u_{\lfloor t/h\rfloor}\right|^2 + 2\tau(1-\tau)\nabla u_{\lfloor t/h\rfloor}\cdot\nabla u_{\lfloor t/h\rfloor+1} + \tau^2\left|\nabla u_{\lfloor t/h\rfloor+1}\right|^2 \\
&\le \int_\Omega \left|\nabla u_{\lfloor t/h\rfloor}\right|^2 + 2\left|\nabla u_{\lfloor t/h\rfloor}\right|\left|\nabla u_{\lfloor t/h\rfloor+1}\right| + \left|\nabla u_{\lfloor t/h\rfloor+1}\right|^2 \\
&\le 2\int_\Omega \left|\nabla u_{\lfloor t/h\rfloor}\right|^2 + 2\int_\Omega \left|\nabla u_{\lfloor t/h\rfloor+1}\right|^2 \le 4\|\nabla u_0\|^2_{L^2(\Omega)},
\end{aligned} \tag{7.69}$$

which follows from Lemma 7.3. Moreover, by Poincaré-Wirtinger inequality and Lemma 7.3, there exists $C_P > 0$ such that

$$\|u^h(t) - u^h_\Omega(t)\|^2_{L^2(\Omega)} \le C_P \|\nabla u^h(t)\|^2_{L^2(\Omega)} \le C\|\nabla u_0\|^2_{L^2(\Omega)},$$

where $u^h_\Omega(t) = \fint_\Omega u^h \le \|u_0\|_\infty$. Hence,

$$\int_\Omega \left|u^h_\Omega(t)\right|^2 \le |\Omega|\|u_0\|^2_\infty.$$

By triangle inequality, we have

$$\|u^h(t)\|_{L^2(\Omega)} \le \|u^h(t) - u^h_\Omega(t)\|_{L^2(\Omega)} + \|u^h_\Omega(t)\|_{L^2(\Omega)} < +\infty.$$

It follows that $\{u^h(t)\}_{h>0}$ is uniformly bounded in $H^1(\Omega)$ for any $t \in (0,T)$. Hence, Rellich-Kondrachov theorem implies that for a fixed $t_0 \in (0,T)$, there exists a subsequence $\{\widetilde{u}^{h_j}(t_0)\}_{j=1}^{\infty}$ such that for some $u(t_0) \in L^2(\Omega)$, we have

$$\widetilde{u}^{h_j}(t_0) \longrightarrow u(t_0) \text{ strongly in } L^2(\Omega).$$

By a diagonal argument, we can find a subsequence $\{\widetilde{u}^{h_j}\}_{j=1}^{\infty}$ such that

$$\widetilde{u}^{h_j}(q) \longrightarrow u(q) \text{ strongly in } L^2(\Omega) \text{ for } q \in \mathbb{Q}^+ \cap (0,T). \tag{7.70}$$

We wish to extend this result from $q \in \mathbb{Q}^+ \cap (0,T)$ to $t \in (0,T)$. To do so, we utilize the idea of [7] and derive an estimate for $\|\widetilde{u}^h(s) - \widetilde{u}^h(t)\|_{L^2(\Omega)}$ for any $s,t \in (0,T)$. From the proof of Lemma 7.3, recall that

$$\int_\Omega \frac{|u_n - u_{n-1}|^2}{h} \le \mathcal{J}(u_{n-1}) - \mathcal{J}(u_n).$$

Then, for $t > s$,

$$\begin{aligned}
\|\widetilde{u}^{h_j}(t) - \widetilde{u}^{h_j}(s)\|_{L^2(\Omega)} &\le \sum_{n=\lfloor s/h_j\rfloor+1}^{\lfloor t/h_j\rfloor} \|u_n - u_{n-1}\|_{L^2(\Omega)} \\
&\le \left(\sum_{n=\lfloor s/h_j\rfloor+1}^{\lfloor t/h_j\rfloor} 1^2\right)^{1/2} \left(\sum_{n=\lfloor s/h_j\rfloor+1}^{\lfloor t/h_j\rfloor} \|u_n - u_{n-1}\|^2_{L^2(\Omega)}\right)^{1/2} \\
&\le \sqrt{\lfloor t/h_j\rfloor - \lfloor s/h_j\rfloor}\left(h_j \sum_{n=\lfloor s/h_j\rfloor+1}^{\lfloor t/h_j\rfloor} (\mathcal{J}(u_{n-1}) - \mathcal{J}(u_n))\right)^{1/2} \\
&= \sqrt{\lfloor t/h_j\rfloor - \lfloor s/h_j\rfloor}\sqrt{h_j\left(\mathcal{J}(u_{\lfloor s/h_j\rfloor}) - \mathcal{J}(u_{\lfloor t/h_j\rfloor})\right)} \\
&\le \sqrt{\mathcal{J}(u_0)}\sqrt{h_j\left(\lfloor t/h_j\rfloor - \lfloor s/h_j\rfloor\right)} \\
&\le \|\nabla u_0\|_{L^2(\Omega)}\sqrt{t - s + h_j}. \qquad (7.71)
\end{aligned}$$

This shows that step functions $\widetilde{u}^{h_j}$ are (almost) equicontinuous and equibounded in $C([0,+\infty); L^2(\Omega))$. Hence, they converge uniformly.

Now, given $\varepsilon > 0$ and an arbitrary $t \in (0,T)$, we select $q \in \mathbb{Q}^+$ so that

$$2\|\nabla u_0\|_{L^2(\Omega)}\sqrt{|t-q|} < \tfrac{1}{3}\varepsilon.$$

By (7.70), we can find $\delta_1 > 0$ such that for all $h^i, h^j < \delta_1$, we have

$$\|\widetilde{u}^{h_i}(q) - \widetilde{u}^{h_j}(q)\|_{L^2(\Omega)} < \tfrac{1}{3}\varepsilon.$$

Take $\delta = \min(\delta_1, \delta_2^2)$, where $\delta_2 = \varepsilon/(6\|\nabla u_0\|_{L^2(\Omega)}) > 0$. Then, for all $h^i, h^j < \delta$, we get

$$\begin{aligned}
&\|\widetilde{u}^{h_i}(t) - \widetilde{u}^{h_j}(t)\|_{L^2(\Omega)} \\
&\quad\le \|\widetilde{u}^{h_i}(t) - \widetilde{u}^{h_i}(q)\|_{L^2(\Omega)} + \|\widetilde{u}^{h_i}(q) - \widetilde{u}^{h_j}(q)\|_{L^2(\Omega)} + \|\widetilde{u}^{h_j}(q) - \widetilde{u}^{h_j}(t)\|_{L^2(\Omega)} \\
&\quad\le \|\nabla u_0\|_{L^2(\Omega)}\sqrt{t - q + h_i} + \tfrac{1}{3}\varepsilon + \|\nabla u_0\|_{L^2(\Omega)}\sqrt{t - q + h_j} \\
&\quad\le \tfrac{2}{3}\varepsilon + \|\nabla u_0\|_{L^2(\Omega)}\left(\sqrt{h_i} + \sqrt{h_j}\right) \\
&\quad\le \tfrac{2}{3}\varepsilon + 2\|\nabla u_0\|_{L^2(\Omega)}\sqrt{\delta} < \varepsilon.
\end{aligned}$$

By the completeness of $L^2(\Omega)$, we conclude that

$$\widetilde{u}^{h_j}(t) \longrightarrow u(t) \ \text{ in } L^2(\Omega) \quad \text{for } t \in (0,T).$$

Moreover, thanks to (7.66), the same holds for the sequence $u^{h_j}(t)$. □

To end, we present some properties of the minimizing movement in the following theorem.

Theorem 7.22. *$u \in GMM(\mathcal{F}, u_0, L^2(\Omega))$ belongs to $L^2((0,T); H^1(\Omega)) \cap L^\infty((0,T)\times\Omega)) \cap C^{0,1/2}([0,T]; L^2(\Omega))$ and satisfies (in the weak sense) $u_t \le \Delta u$ in $(0,T)\times\Omega$.*

Proof. Passing to the limit as $h_j \to 0$ in (7.65) gives

$$0 \le u(t) \le \|u_0\|_\infty, \quad \forall t \in (0,T). \qquad (7.72)$$

Using (7.71) for $t > s$, we find (by dropping the index j from h_j),

$$\begin{aligned}\|u(t)-u(s)\|_{L^2(\Omega)} &\le \|u(t)-\widetilde{u}^h(t)\|_{L^2(\Omega)} + \|\widetilde{u}^h(t)-\widetilde{u}^h(s)\|_{L^2(\Omega)} + \|\widetilde{u}^h(s)-u(s)\|_{L^2(\Omega)}\\ &\le \|u(t)-\widetilde{u}^h(t)\|_{L^2(\Omega)} + \|\nabla u_0\|_{L^2(\Omega)}\sqrt{t-s+h} + \|\widetilde{u}^h(s)-u(s)\|_{L^2(\Omega)}\\ &\to \|\nabla u_0\|_{L^2(\Omega)}\sqrt{t-s}, \quad h\to 0,\end{aligned}$$

and thus, $u \in C^{0,1/2}([0,+\infty); L^2(\Omega))$.

Moreover, adding the inequalities $\mathcal{F}_n^h(u_n) \le \mathcal{F}_n^h(u_{n-1})$ up to an arbitrary $n = \lfloor t/h \rfloor$ gives that for any $t \in (0,T)$,

$$\int_0^t \|u_t^h\|^2_{L^2(\Omega)}dt + \|\nabla \widetilde{u}_t^h(t)\|^2_{L^2(\Omega)} \quad \le \quad \|\nabla u_0\|^2_{L^2(\Omega)}.$$

Hence, we can find a subsequence $\{u^{h_j}\}$ such that

$$\begin{aligned} u_t^{h_j} &\rightharpoonup u_t \qquad \text{weakly in } L^2((0,T)\times\Omega)\\ \nabla u^{h_j} &\rightharpoonup \nabla u, \qquad \text{weakly in } L^2((0,T)\times\Omega).\end{aligned}$$

Finally, we show the subsolution property. For any $h > 0$ and $n = 1, 2, \ldots, M$, and an arbitrary nonnegative $\phi \in C_0^\infty((0,T)\times\Omega)$, define

$$\phi_n^h(x) \quad := \quad \frac{1}{h}\int_{(n-1)h}^{nh} \phi(t,x)dt$$

and set for all $t > 0$, $\phi^h(t,x) := \phi^h_{[t/h]+1}(x)$. Note that as $h \to 0$,

$$\begin{aligned}\phi^h &\longrightarrow \phi \quad \text{strongly in } L^2((0,T)\times\Omega),\\ \nabla\phi^h &\longrightarrow \nabla\phi \quad \text{strongly in } L^2((0,T)\times\Omega;\mathbb{R}^N).\end{aligned}$$

By Theorem 7.5, we have for any $t \in (0,T)$,

$$\int_\Omega \frac{u_n - u_{n-1}}{h_j}\phi_n^{h_j} + \nabla u_n \cdot \nabla \phi_n^{h_j} \le 0,$$

where $n = \lfloor t/h_j \rfloor + 1$. Adding up to $\lfloor T/h_j \rfloor$ and multiplying by h_j gives

$$\begin{aligned} 0 \quad &\ge \quad \sum_{n=1}^{\lfloor T/h_j\rfloor} h_j \int_\Omega \frac{\partial u^{h_j}}{\partial t}\phi^{h_j} + \nabla\widetilde{u}^{h_j}\cdot\nabla\phi^{h_j}\\ &= \quad \int_0^T\int_\Omega \frac{\partial u^{h_j}}{\partial t}\phi^{h_j} + \nabla\widetilde{u}^{h_j}\cdot\nabla\phi^{h_j}.\\ &= \quad \int_0^T\int_\Omega \frac{\partial u^{h_j}}{\partial t}\left(\phi^{h_j}-\phi\right) + \frac{\partial u^{h_j}}{\partial t}\phi + \int_0^T\int_\Omega \nabla\widetilde{u}^{h_j}\cdot\left(\nabla\phi^{h_j}-\nabla\phi\right) + \nabla\widetilde{u}^{h_j}\cdot\nabla\phi.\end{aligned}$$

Taking $h_j \to 0$ yields the desired result. □

7.7 Concluding Remarks

For any given time step size $h > 0$, we have shown that one can choose penalty parameter λ (independent of n) large enough that the measure of set $\{u_n > 0\}$ automaticaly adjusts to its prescribed value. This means that one can achieve the solution to the original problem (7.1) without having to take λ to infinity in (7.3) – a clear advantage in numerical computations.

There is still a number of questions on this problem which we plan to address in the future. First, we wish to investigate the behavior of the sequence of minimizers for sufficiently large penalty λ independent of h and n. Since the techniques introduced in this chapter are not applicable, we instead, opt to use a smoothing technique on our penalization term and employ the Bernstein method to first establish uniform regularity of the minimizer (cf. [96]). Second, we would like to extend these results to the two-phase case where the initial datum u_0 is not required to be nonnegative. Our goal is to prove the convergence of the volume-preserving MBO algorithm, which requires investigation of the regularity of free boundary. Is the free boundary (in some sense) a "nice" hypersurface? What is its shape as it comes into the fixed boundary? Does it hit the fixed boundary smoothly? Finally, we wish to generalize the results in Section 7.4 (regularity up to the fixed Neumann boundary) to other elliptic operators. What is the most general type of operator to which it should apply? Does it also work with other boundary conditions, aside from the Neumann boundary condition?

Appendix A

Reference Vectors: Its Construction and Properties

In this appendix, we construct reference unit vectors, denoted by $\mathbf{p}_i$ corresponding to each phase region P_i as vectors of dimension $k-1$ pointing from the centroid of a standard k-simplex to its vertices as in [94]. Based on this construction, we list down some of its useful properties.

Consider the standard $(k-1)$-simplex in $\mathbb{R}^k$ given by

$$S_{k-1} = \left\{ (x_1, x_2, \ldots, x_k) \in \mathbb{R}^k : \sum_{i=1}^{k} x_i = 1 \,\text{and}\, x_i \geq 0, \,\text{for}\, i = 1, 2, \ldots, k \right\}.$$

Then, its vertices form the natural basis $\{\mathbf{e}_i : 1 \leq i \leq k\}$ for the Euclidean space $\mathbb{R}^k$.

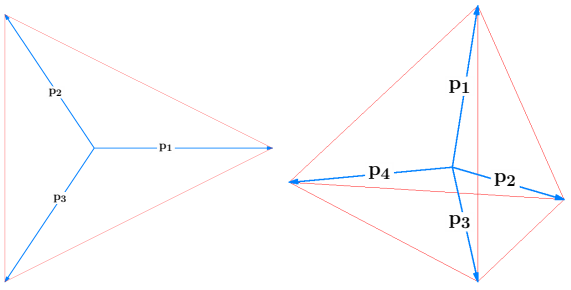

FIGURE A.1: A 3-phase regular simplex (left) and a 4-phase regular simplex (right).

Translate the simplex so that its centroid lies in the origin. Hence, the translated vertices are now of the form

$$\mathbf{v}_i = \frac{1}{k}\left(k\mathbf{e}_i - \sum_{i=1}^{k} \mathbf{e}_i \right).$$

Fix an orthonormal basis for the $(k-1)$-dimensional hyperplane containing the simplex. Take, for example, the first translated vertex $\mathbf{v}_1$ as the first basis vertex (after

normalization), and construct the remaining vectors as follows:

$$\begin{aligned}
\mathbf{q}_1^k &= \frac{1}{\sqrt{(k-1)k}}\,(k-1,-1,-1,-1\ldots,-1)\\
\mathbf{q}_2^k &= \frac{1}{\sqrt{(k-2)(k-1)}}\,(0,k-2,-1,-1,\ldots,-1)\\
\mathbf{q}_3^k &= \frac{1}{\sqrt{(k-3)(k-2)}}\,(0,0,k-3,-1,\ldots,-1)\\
&\vdots\\
\mathbf{q}_{k-1}^k &= \frac{1}{\sqrt{2}}\,(0,\ldots,0,1,-1)
\end{aligned}$$

Let Q_k be the matrix having$\mathbf{q}_1^k, \mathbf{q}_2^k, \ldots, \mathbf{q}_{k-1}^k$ as its rows. Then, the reference vectors $\mathbf{p}_i$ are obtained by normalized projection of $\mathbf{v}_i (i = 1, \ldots, k)$ into this orthonormal system, that is,

$$\mathbf{p}_i^T = \frac{1}{|Q_k \mathbf{v}_i^T|} Q_k \mathbf{v}_i^T.$$

Note that for any pair $i, j = 1, 2, \ldots, k$, we have

1. $\mathbf{p}_i \cdot \mathbf{p}_j = \begin{cases} 1, & i = j \\ \dfrac{1}{1-k}, & i \neq j \end{cases}$
2. $(\mathbf{p}_i + \mathbf{p}_j) \cdot (\mathbf{p}_i - \mathbf{p}_j) = 0,$
3. $|\mathbf{p}_i + \mathbf{p}_j| = \sqrt{\dfrac{2(k-2)}{k-1}}$, when $i \neq j$,
4. $|\mathbf{p}_i - \mathbf{p}_j| = \sqrt{\dfrac{2k}{k-1}}$, when $i \neq j$.

Moreover, if θ denotes the angle between any pair of reference vectors, say $\mathbf{p}_i$ and $\mathbf{p}_j$, then, the following is true:

1. $\cos\theta = \dfrac{\mathbf{p}_i \cdot \mathbf{p}_j}{|\mathbf{p}_i||\mathbf{p}_j|} = -\dfrac{1}{k-1},$
2. $\cos(\frac{\theta}{2}) = \frac{1}{2}|\mathbf{p}_i + \mathbf{p}_j|,$
3. $\sin(\frac{\theta}{2}) = \frac{1}{2}|\mathbf{p}_i - \mathbf{p}_j|.$

The above properties of the reference vectors are used in the calculation of the velocity of the interface.

Appendix B

Expansion of Scalar Signed Distance Function

Consider the scalar signed distance function $\hat{d}_S : \mathbb{R}^2 \to \mathbb{R}$ with respect to set $S \subset \mathbb{R}^2$, defined by

$$\hat{d}_S = \begin{cases} \text{dist}(x, S^c), & x \in S, \\ -\text{dist}(x, S), & x \in S^c. \end{cases}$$

In this appendix, we write out its Taylor expansion around a point x on the smooth boundary ∂S where the expansion coefficients are expressed in terms of the geometry (curvature and derivatives of curvature) of ∂S as in [36].

Let us rotate and translate the coordinate system so that $x = 0$ in the new coordinate system and the outer unit normal $\boldsymbol{\eta}$ at the origin lies in the negative x_2 direction (Figure B.1).

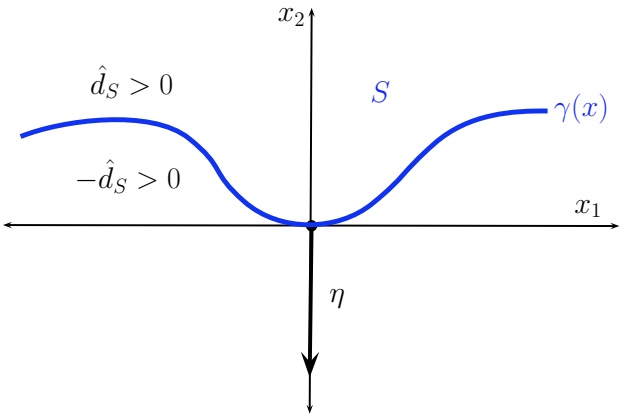

FIGURE B.1: Setting up ∂S in the new coordinate system.

Let $\gamma(x)$ be the smooth function whose graph $(x_1, \gamma(x_2))$ describes the smooth boundary ∂S in the neighborhood of the origin. Then, if κ defines the curvature of the interface γ_{ij} at point $x = (0, 0)$, then $\gamma(0) = 0$, $\gamma'(0) = 0$, and $\gamma''(0) = -\kappa$. Note that $\hat{d}_S(x_1, x_2) > 0$ if $x_2 > \gamma(x_1)$ (which implies that $\hat{d}_S(x_1, x_2) < 0$ if $x_2 < \gamma(x_1)$).

Proposition B.1. *(cf. [36, Proposition 2]) The scalar signed distance function $\hat{d}_S(x_1, \gamma(x_1))$ has the following Taylor expansion at $x = 0$:*

$$\hat{d}_S(x) = x_2 + \tfrac{1}{2}\kappa x_1^2 + \tfrac{1}{6}\kappa_{x_1} x_1^3 - \tfrac{1}{2}\kappa^2 x_1^2 x_2 + O(|x|^4).$$

Proof. For convenience, denote $d := \hat{d}_S$. Take $r > 0$ small enough so that $\hat{d}_S \in C^{k,m}$ where $k \geq 2$ and $m \geq 0$ in a neighborhood $B := B(0, r)$ of $x = 0 \in \partial S$. Then, for all $x \in B$, we have

$$\hat{d}_S(x) = (x - P(x)) \cdot \eta(P(x)),$$

where $P : \mathbb{R}^2 \to \partial S$ denotes the closest point projection. Hence, for sufficiently small x_2, we have $d(0, x_2) = x_2$ and so, $d_{x_2}(0) = 1$ and

$$\frac{\partial^k}{\partial x_2^k} d(0) = 0, \quad k \geq 2.$$

Moreover, the scalar signed distance function satisfies the Eikonal equation

$$|\nabla d(x)|^2 = d_{x_1}^2(x) + d_{x_2}^2(x) = 1, \tag{B.1}$$

which implies that $d_{x_1}(0) = 0$. Now, differentiating B.1 with respect to x_1, we have

$$d_{x_1}(x) d_{x_1 x_1}(x) + d_{x_2}(x) d_{x_1 x_2}(x) \equiv 0. \tag{B.2}$$

It follows that $d_{x_1 x_2}(0) = 0$ and

$$\frac{\partial^k}{\partial x_2^k} d_{x_1}(0) = 0, \quad k \geq 1.$$

Meanwhile, recall that the Laplacian of the signed distance function $\hat{d}$ at a point gives the mean curvature H of the isosurface of $\hat{d}$ passing through the point, that is,

$$\Delta d(x_1, \gamma(x_1)) = d_{x_1 x_1}(x_1, \gamma(x_1)) + d_{x_2 x_2}(x_1, \gamma(x_1)) = H(x_1, \gamma(x_1)), \tag{B.3}$$

which implies that $d_{x_1 x_1}(0) = H(0, 0) = \kappa$.

Now, differentiating (B.2) with respect to x_1, we get

$$d_{x_1 x_1}^2(x) + d_{x_1}(x) d_{x_1 x_1 x_1}(x) + d_{x_1 x_2}^2(x) + d_{x_2}(x) d_{x_1 x_1 x_2}(x) \equiv 0. \tag{B.4}$$

Thus, we have $d_{x_1 x_1 x_2}(0) = -\kappa^2$. On the other hand, differentiating (B.3) with respect to x_1 yields

$$\begin{aligned} H_{x_1}(x_1, \gamma(x_1)) \;=\; & d_{x_1 x_1 x_1}(x_1, \gamma(x_1)) + d_{x_1 x_1 x_2}(x_1, \gamma(x_1)) \gamma'(x_1) \\ & + d_{x_2 x_2 x_1}(x_1, \gamma(x_1)) + d_{x_2 x_2 x_2}(x_1, \gamma(x_1)) \gamma'(x_1), \end{aligned}$$

which implies that $d_{x_1 x_1 x_1}(0) = H_{x_1}(0, 0) =: \kappa_{x_1}$. Finally, collecting the expansion coefficient terms yields the desired Taylor expansion. □

Appendix C

A Junction-based Signed Distance Vector Approach

This appendix presents an alternative construction of the signed distance vector function [70],which when set as an initial condition in Algorithm 3.1 evolves the interface with a normal velocity of minus mean curvature.

§ Construction of Signed Distance Vector

Consider a partition of $\mathbb{R}^N = P_1 \cup P_2 \cup \cdots \cup P_k$ into $k > 2$ mutually exclusive phase regions $P_i \subset \mathbb{R}^N (i = 1, 2, \ldots, k)$. Fix a point $x \in \mathbb{R}^N$. Without loss of generality, say $x \in P_i$ with P_j as the nearest phase to x. Denote the interface between phase P_i and P_j by $\gamma_{ij} = \gamma_{ji}$. As in Appendix A, set up the reference vectors $\mathbf{p}_i$ corresponding to each phase P_i as vectors of dimension $k-1$ pointing from the centroid of a standard k-simplex to its vertices. Denote θ as the angle between any pair of reference vectors (depends only on the number of phases).

Let $d_1 : \mathbb{R}^N \to \mathbb{R}^+ \cup \{0\}$ be the distance of point x to the nearest interface, defined by:

$$d_1(x) := \min_{i \neq n} \operatorname{dist}(x, \gamma_{in}) = \operatorname{dist}(x, \gamma_{ij}),$$

and $s : \mathbb{R}^N \to \mathbb{R}^+ \cup \{0\}$, be the distance to the nearest junction point

$$s(x) := \min \{\operatorname{dist}(x, z) : z \in T_{ij}\},$$

where T_{ij} is the set of all junction points on interface γ_{ij}.

Definition C.1. We define the **signed distance vector** $\boldsymbol{\delta} : \mathbb{R}^N \to \mathbb{R}^{k-1}$, as follows:

$$\boldsymbol{\delta}(x) := s(x)\mathbf{rot}_{ji}\left(\frac{\mathbf{p}_i + \mathbf{p}_j}{|\mathbf{p}_i + \mathbf{p}_j|}, \frac{d_1(x)}{s(x)}\frac{\theta}{2}\right),$$

where $\mathbf{rot}_{ji}(\mathbf{v}, \alpha)$ means rotating vector $\mathbf{v}$ by angle α in the direction of rotation from reference vector $\mathbf{p}_j$ to reference vector $\mathbf{p}_i$.

From this construction, we see that $\boldsymbol{\delta}(x) = \mathbf{0}$ when x is a junction point; and

$$\boldsymbol{\delta}(x) = s(x)\frac{\mathbf{p}_i + \mathbf{p}_j}{|\mathbf{p}_i + \mathbf{p}_j|}$$

when point x lies on interface γ_{ij}. An example of this signed distance vector is shown in Figure C.1.

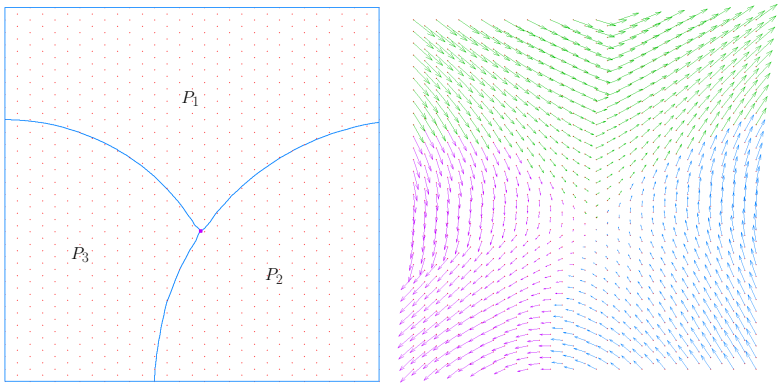

FIGURE C.1: Three-phase initial condition (left) and its corresponding signed distance vector field (right).

Proposition C.2. *If $x \in P_i$ with γ_{ij} as its nearest interface, then,*

$$\boldsymbol{\delta}(x) = s(x)\left[\cos\alpha(x)\frac{\mathbf{p}_i + \mathbf{p}_j}{|\mathbf{p}_i + \mathbf{p}_j|} + \sin\alpha(x)\frac{\mathbf{p}_i - \mathbf{p}_j}{|\mathbf{p}_i - \mathbf{p}_j|}\right],$$

where $\alpha(x) := \dfrac{d_1(x)}{s(x)}\dfrac{\theta}{2}$.

Proof. Let $\boldsymbol{\delta}(x) = s(x)\mathbf{r}$, where $\mathbf{r} := \mathbf{rot}_{ji}(\mathbf{v}, \alpha)$.

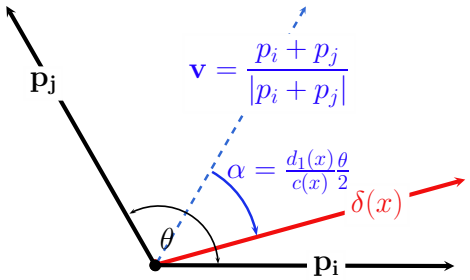

FIGURE C.2: Construction of the junction-based signed distance vector.

Write $\mathbf{r} = a\mathbf{v} + b\mathbf{p}_i$ for some $a, b \in \mathbb{R}$. Since $\mathbf{p}_i \cdot \mathbf{p}_j = \cos\theta$, then taking the dot product $\mathbf{r} \cdot \mathbf{v}$ gives $\cos\alpha = a + b\cos\frac{\theta}{2}$. Hence, $a = \cos\alpha - b\cos\frac{\theta}{2}$. On the other hand, taking the dot product $\mathbf{r} \cdot \mathbf{p}_i$ gives

$$\cos\left(\tfrac{\theta}{2} - \alpha\right) = a\cos\tfrac{\theta}{2} + b = \left(\cos\alpha - b\cos\tfrac{\theta}{2}\right)\cos\tfrac{\theta}{2} + b,$$

which gives $b = \dfrac{\sin\alpha}{\sin\frac{\theta}{2}}$.

Thus, we have

$$\begin{aligned}\mathbf{r} &= \left(\cos\alpha - b\cos\tfrac{\theta}{2}\right)\frac{\mathbf{p}_i+\mathbf{p}_j}{|\mathbf{p}_i+\mathbf{p}_j|} + b\mathbf{p}_i \\ &= \left(\frac{\cos\alpha}{|\mathbf{p}_i+\mathbf{p}_j|}+\frac{b}{2}\right)\mathbf{p}_i + \left(\frac{\cos\alpha}{|\mathbf{p}_i+\mathbf{p}_j|}-\frac{b}{2}\right)\mathbf{p}_j \\ &= \cos\alpha\frac{\mathbf{p}_i+\mathbf{p}_j}{|\mathbf{p}_i+\mathbf{p}_j|} + \sin\alpha\frac{\mathbf{p}_i-\mathbf{p}_j}{|\mathbf{p}_i-\mathbf{p}_j|}.\end{aligned}$$

□

We remark that for any point $x \in \mathbb{R}^N$ having $\gamma_{ij}(i,j \in \{1,2,\ldots,k\})$ as its nearest interface, we have,

$$\boldsymbol{\delta}(x)\cdot(\mathbf{p}_i-\mathbf{p}_j) = \begin{cases} \sqrt{\frac{2(k-2)}{k-1}}s(x)\sin\alpha(x), & x\in P_i \\ -\sqrt{\frac{2(k-2)}{k-1}}s(x)\sin\alpha(x), & x\in P_j. \end{cases} \tag{C.1}$$

Meanwhile, if $x \in P_m \subset \mathbb{R}^N$ with $\gamma_{mn}(m,n \in \{1,2,\ldots,k\}\backslash\{i,j\})$ as its nearest interface, then we can find a constant $C>0$ such that

$$|\boldsymbol{\delta}(x)\cdot(\mathbf{p}_i-\mathbf{p}_j)| \le \sqrt{\frac{2k}{k-1}}|s(x)|. \tag{C.2}$$

§ Velocity of the Interface

Next, we estimate the "normal velocity" of the interface evolving according to the junction-based SDV scheme.

Theorem C.3. *The velocity of the interface γ at any point $x \in \gamma \subset \mathbb{R}^N$ is*

$$v = -\kappa + O(\sqrt{\Delta t}), \quad \Delta t \to 0,$$

where κ denotes the $(N-1)$-times mean curvature of γ at x with respect to the outer normal $\boldsymbol{\eta}$.

Proof. For simplicity, take $N=2$ and write $t=\Delta t$. We proceed in the same manner as in the proof of Theorem 3.3. The normal velocity v of interface γ_{ij} can be found from the relation

$$0 = \int_Q + \int_{\mathbb{R}^2\backslash Q} \boldsymbol{\delta}(x)\cdot(\mathbf{p}_i-\mathbf{p}_j)\Phi_t(x-z)dx := I + II$$

where $z=(0,vt)$. Using equation (C.2) and the fact that $|s(x)| \le |x| + M$ for some $M>0$, we get

$$\begin{aligned}|II| &\le C\int_{\mathbb{R}}\int_{\mathbb{R}\backslash(-\tau,\tau)} + \int_{\mathbb{R}\backslash(-\tau,\tau)}\int_{\mathbb{R}} \left(|x_1|+|x_2|+M\right)\varphi_t(x_1)\varphi_t(x_2-vt)dx_2dx_1 \\ &\le C\int_0^\infty\left(\int_{\tau+vt}^\infty + \int_{\tau-vt}^\infty\right) + \int_\tau^\infty\int_{\mathbb{R}}(x_1+|x_2|+|v|t+M)\varphi_t(x_1)\varphi_t(x_2)dx_2dx_1 \\ &\le C\left(\sqrt{t}+t+1\right)e^{-\frac{\tau^2}{4t}} \end{aligned} \tag{C.3}$$

On the other hand, it follows from equation (C.1) that for some $C > 0$,

$$\begin{aligned} I &:= \sqrt{\frac{2(k-2)}{k-1}} \int_{Q\cap P_i} - \int_{Q\cap P_j} s(x) \sin\left(\frac{\operatorname{dist}(x,\gamma_{ij})}{s(x)}\frac{\theta}{2}\right) \Phi_t(x)dx \\ &= \sqrt{\frac{2(k-2)}{k-1}} \int_{Q} s(x) \sin\left(\frac{d(x)}{s(x)}\frac{\theta}{2}\right) \Phi_t(x-z)dx \end{aligned}$$

where $d : \mathbb{R}^2 \to \mathbb{R}$ is the scalar signed distance to $Q_\epsilon \cap P_i$. Using the Taylor expansion of sine up to the third order, we have

$$\begin{aligned} I &= \frac{\theta\sqrt{k-2}}{\sqrt{2(k-1)}} \int_Q s(x) \left[\frac{d(x)}{s(x)} + O\left(\frac{d^3(x)}{s^3(x)}\right)\right] \Phi_t(x-z)dx \\ &=: \frac{\theta\sqrt{k-2}}{\sqrt{2(k-1)}} (I_1 + I_2) \end{aligned}$$

Moreover, using the Taylor expansion of the scalar signed distance (Proposition B.1), we get

$$I_1 = \int_Q \left[\left(x_2 + \tfrac{1}{2}\kappa x_1^2\right) + O\left(|x|^3\right)\right] \varphi_t(x_1)\varphi_t(x_2 - vt)dx_2dx_1 =: I_{11} + I_{12}.$$

We estimate these integrals in the following claims.

Claim 1: $I_{11} = (v+\kappa)\, t + O(e^{-\frac{\tau^2}{4t}})$, as $t \to 0$.
Indeed,

$$\begin{aligned} \int_{\mathbb{R}^2} \left(x_2 + \tfrac{1}{2}\kappa x_1^2\right) \Phi_t(x-z)dx &= \int_{\mathbb{R}} (x_2 + vt)\varphi_t(x_2)dx_2 + \kappa \int_0^\infty x_1^2 \varphi_t(x_1)dx_1 \\ &= \frac{1}{2\sqrt{\pi t}} \int_{\mathbb{R}} (x_2 + vt)\, e^{-\frac{x_2^2}{4t}} dx + \kappa t = vt + \kappa t \end{aligned}$$

Moreover, we have

$$\begin{aligned} \left|\int_{\mathbb{R}^2\setminus Q} x_2 \Phi_t(x-z)dx\right| &\le \int_{\mathbb{R}} \int_{\mathbb{R}\setminus(-\tau,\tau)} + \int_{\mathbb{R}\setminus(-\tau,\tau)} \int_{\mathbb{R}} |x_2|\varphi_t(x_1)\varphi_t(x_2-vt)dx_2dx_1 \\ &\le \int_{\tau+vt}^\infty + \int_{\tau-vt}^\infty + e^{-\frac{\tau^2}{4t}} \int_{\mathbb{R}} (|x_2| + |v|t)\varphi_t(x_2)dx_2 \\ &\le C\left(1 + \sqrt{t} + t\right) e^{-\frac{\tau^2}{4t}}, \end{aligned}$$

and

$$\begin{aligned} \left|\int_{\mathbb{R}^2\setminus Q} \tfrac{1}{2}\kappa x_1^2 \Phi_t(x-z)dx\right| &\le C \int_{\mathbb{R}} \int_{\mathbb{R}\setminus(-\tau,\tau)} + \int_{\mathbb{R}\setminus(-\tau,\tau)} \int_{\mathbb{R}} x_1^2 \varphi_t(x_1)\varphi_t(x_2-vt)dx_2dx_1 \\ &\le C\left(\int_{\tau+vt}^\infty + \int_{\tau-vt}^\infty t\varphi_t(x_2)dx_2 + 2\int_\tau^\infty x_1^2\varphi_t(x_1)dx_1\right) \\ &\le C\left(t + \sqrt{t}(\tau + \sqrt{t})\right) e^{-\frac{\tau^2}{4t}}, \end{aligned}$$

which proves the claim.

Claim 2: $I_{12} = O\left(t\sqrt{t}\right)$, as $t \to 0$.
Indeed,

$$\begin{aligned} |I_{12}| &\leq C \int_Q \left(|x_1| + |x_2|\right)^3 \varphi_t(x_1)\varphi_t(x_2 - vt) dx_2 dx_1 \\ &\leq C \left(\int_0^\infty x_1^3 \varphi_t(x_1) \int_{\mathbb{R}} \varphi_t(x_2) + \int_{\mathbb{R}} \varphi_t(x_1) \int_0^\infty (x_2 + |v|t)^3 \varphi_t(x_2) \right) dx_2 dx_1 \\ &\leq Ct\sqrt{t} \left(1 + (1 + |v|\sqrt{t})^3\right), \end{aligned}$$

which proves the claim.

For the second term I_2, it is enough to consider the first two terms of the Taylor expansion (Proposition B.1) of the scalar signed distance. Moreover, we can take $\tau > 0$, small enough so that $\min_{x \in Q} s(x) > 0$. Thus,

$$\begin{aligned} |I_2| &\leq C \max_Q \frac{1}{s^2(x)} \int_Q \left| d^3(x) \right| \Phi_t(x - z) dx \\ &\leq C \int_Q \left(|x_2| + |x_1|\right)^3 \varphi_t(x_1)\varphi_t(x_2 - vt) dx_2 dx_1 \\ &\leq C \int_0^\infty \int_{\mathbb{R}} \left(|x_2| + |v|t + x_1\right)^3 \varphi_t(x_1)\varphi_t(x_2) dx_2 dx_1 \\ &\leq Ct\sqrt{t} \left(1 + (1 + |v|\sqrt{t})^3\right), \end{aligned} \tag{C.4}$$

Finally, it follows from claims 1 and 2, and equations (C.3) and (C.4) that

$$0 = I + II = (v + \kappa)\, t + O\left(t\sqrt{t} + e^{-\frac{\tau^2}{4t}}\right), \text{ as } t \to 0,$$

which gives the desired result. □

§ Numerical Example

We present examples of mean curvature evolution of a three-phase smooth interface and a four-phase triple bubble using a junction-based signed distance vector approach in figures C.3 and C.4, respectively. Here, the domain $\Omega := [0, 1] \times [0, 1]$ is triangulated into 5000 elements with 2576 nodes and the evolution time step $\Delta t = 0.0005$ is discretized into 30 DMF iterations.

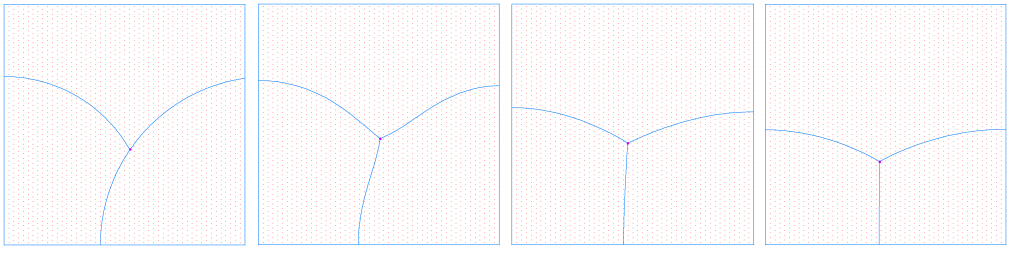

FIGURE C.3: Evolution of a 3-phase smooth interface via junction-based SDV scheme at $t = 0, 10\Delta t, 80\Delta t, 300\Delta t$.

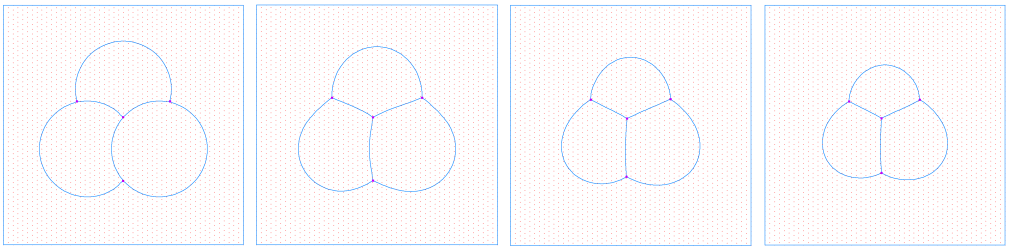

FIGURE C.4: An example of a shrinking triple bubble via junction-based SDV scheme at $t = 0, 20\Delta t, 50\Delta t, 70\Delta t$.

Note that under these configurations, the original MBO algorithm gets "stuck", while, our multiphase signed distance vector approach naturally alleviates the time and grid restriction (cf. [36]), without having to retriangulate elements based on the interfacial geometry.

Appendix D

Gaussian Function: Some Useful Integrals and Estimates

Consider the Gaussian function $\Phi_t : \mathbb{R}^N \to \mathbb{R}$ defined by:

$$\Phi_t(x_1, x_2, \ldots, x_N) := \varphi_t(x_1)\varphi_t(x_2)\cdots\varphi_t(x_N)$$

where $\varphi_t(\xi) = \frac{1}{\sqrt{4\pi t}} e^{-\frac{\xi^2}{4t}}$. We list down some integrals involving the Gaussian function which were utilized in our calculations and proofs, as follows:

1. $\displaystyle\int_{\mathbb{R}} \varphi_t(\xi)d\xi = 1$
2. $\displaystyle\int_{\mathbb{R}} \xi^k \varphi_t(\xi)d\xi = 0$, where k is odd
3. $\displaystyle\int_{\mathbb{R}} \xi^{2k} \varphi_t(\xi)d\xi = O(t^k)$, as $t \to 0$ where $k \in \mathbb{N}$
4. $\displaystyle\int_{\mathbb{R}} \varphi_t(\xi)d\xi = \int_{\mathbb{R}} \varphi_t(v-\xi)d\xi$
5. $\displaystyle\int_0^\infty \xi\varphi_t(\xi)d\xi = \frac{\sqrt{t}}{\sqrt{\pi}}$
6. $\displaystyle\int_0^\infty \xi^2\varphi_t(\xi)d\xi = t$
7. $\displaystyle\int_\alpha^\infty \xi\varphi_t(\xi)d\xi = \frac{\sqrt{t}}{\sqrt{\pi}} e^{-\frac{\alpha^2}{4t}}$

§ Some Useful Estimates involving the Gaussian Functions

In this section, we prove some estimates of Gaussian integrals.

Lemma D.1. *For any $\alpha \geq 0$,* $\displaystyle\int_\alpha^\infty e^{-\xi^2} d\xi \leq \frac{1}{2}\sqrt{\pi} e^{-\alpha^2}$.

Proof. Note that $\xi \geq \alpha \geq 0$. Then,

$$\xi^2 = (\xi-\alpha)^2 + 2\alpha\xi - \alpha^2 \geq (\xi-\alpha)^2 + \alpha^2.$$

Hence,

$$\int_\alpha^\infty e^{-\xi^2} dx \;\; \leq \;\; e^{-\alpha^2} \int_\alpha^\infty e^{-(\xi-\alpha)^2} d\xi = \tfrac{1}{2}\sqrt{\pi} e^{-\alpha^2}.$$

□

Lemma D.2. *For any $\alpha > 0$, $\displaystyle\int_{\mathbb{R}\setminus(-\alpha,\alpha)} \varphi_t(\xi - vt) d\xi = O\left(e^{-\frac{\alpha^2}{4t}}\right)$ as $t \to 0$.*

Proof. Applying Lemma D.1 yields

$$\begin{aligned}\left| \frac{1}{\sqrt{4\pi t}} \int_{\mathbb{R}\setminus(-\alpha,\alpha)} e^{-\frac{(\xi-vt)^2}{4t}} d\xi \right| &= \frac{1}{\sqrt{\pi}} \int_{\frac{\alpha-vt}{\sqrt{4t}}}^\infty + \int_{\frac{\alpha+vt}{\sqrt{4t}}}^\infty e^{-\xi^2} d\xi \\ &\leq \frac{1}{2}\left[e^{-\frac{(\alpha-vt)^2}{4t}} + e^{-\frac{(\alpha+vt)^2}{4t}} \right] \leq C e^{-\frac{\alpha^2}{4t}}.\end{aligned}$$

□

Lemma D.3. *For any $\alpha > 0$ and $n \in \mathbb{N}$, we have*

1. $\displaystyle\int_{\mathbb{R}\setminus(-\alpha,\alpha)} \xi^n \varphi_t(\xi) d\xi = O\left(\sqrt{t}(\alpha+\sqrt{t})^{n-1} e^{-\frac{\alpha^2}{4t}}\right)$, $t \to 0$.
2. $\displaystyle\int_{\mathbb{R}\setminus(-\alpha,\alpha)} \xi^n e^{-\frac{(\xi-vt)^2}{4t}} d\xi = O\left(t^{\frac{n+1}{2}}(\alpha+\sqrt{t})^{n-1} e^{-\frac{\alpha^2}{4t}}\right)$, $t \to 0$.

Proof. Note that

$$I := \left| \frac{1}{\sqrt{4\pi t}} \int_{\mathbb{R}\setminus(-\alpha,\alpha)} \xi^n e^{-\frac{\xi^2}{4t}} d\xi \right| \;\; \leq \;\; C(\sqrt{t})^n \int_{\frac{\alpha}{\sqrt{4t}}}^\infty |\xi|^n \, e^{-\xi^2} d\xi \tag{D.1}$$

Applying integration by parts and Lemma D.1, we have for $\tau = \frac{\alpha}{\sqrt{4t}}$,

$$\begin{aligned}\int_\tau^\infty \xi^n e^{-\xi^2} d\xi \;&=\; \tfrac{1}{2}\tau^{n-1} e^{-\tau^2} \left[1 + \sum_{i=1}^k \frac{(n-1)(n-3)\cdots(n-2i+1)}{2^i \tau^{2i}} \right] + \begin{cases} \displaystyle\int_\tau^\infty e^{-x^2} dx, & n, \text{ even}, \\ e^{-\tau^2}, & n, \text{ odd}. \end{cases} \\ &\leq C\left[\tau^{n-1} + \tau^{n-3} + \cdots + \tau^{n-2k-1} + 1 \right] e^{-\tau^2}\end{aligned}$$

where $k = \frac{n-2}{2}$ when n is even and $\frac{n-3}{2}$, otherwise. Thus,

$$\begin{aligned} I \;&\leq\; C\left[\alpha^{n-1}\sqrt{t} + \alpha^{n-3}(\sqrt{t})^3 + \cdots + \alpha^{n-2k-1}(\sqrt{t})^{2k-1} + (\sqrt{t})^n \right] e^{-\alpha^2} \\ &\leq\; C\sqrt{t}(\alpha+\sqrt{t})^{n-1} e^{-\frac{\alpha^2}{4t}}, \; t \to 0. \end{aligned} \tag{D.2}$$

On the other hand, using (D.2), we get

$$\begin{aligned}
\left|\int_{\mathbb{R}\setminus(-\alpha,\alpha)} \xi^n e^{-\frac{(\xi-vt)^2}{4t}} d\xi\right| &= \frac{(2\sqrt{t})^n}{\sqrt{\pi}} \int_{-\infty}^{-\frac{\alpha+vt}{\sqrt{4t}}} + \int_{\frac{\alpha-vt}{\sqrt{4t}}}^{\infty} \left|\xi + \frac{v}{2}\sqrt{t}\right|^n e^{-\xi^2} d\xi \\
&\leq C(\sqrt{t})^n \int_{\frac{\alpha-vt}{\sqrt{4t}}}^{\infty} + \int_{\frac{\alpha+vt}{\sqrt{4t}}}^{\infty} \left(|\xi| + \sqrt{t}\right)^n e^{-\xi^2} d\xi \\
&\leq Ct^n \sum_{m=0}^{n} \binom{n}{m} \frac{1}{(\sqrt{t})^m} \int_{\frac{\alpha}{\sqrt{4t}}}^{\infty} \xi^m e^{-\xi^2} d\xi \\
&\leq Ct^n e^{-\frac{\alpha^2}{4t}} \left[1 + \sum_{m=0}^{n-1} \binom{n}{m} \left(\frac{\alpha+\sqrt{t}}{\sqrt{t}}\right)^m\right] \\
&= Ct^n e^{-\frac{\alpha^2}{4t}} \left[1 + \left(2 + \frac{\alpha}{\sqrt{t}}\right)^{n-1}\right] \\
&\leq Ct^{\frac{n+1}{2}} (\alpha + \sqrt{t})^{n-1} e^{-\frac{\alpha^2}{4t}}, \quad t \to 0.
\end{aligned}$$

□

§ Gaussian Integrals over a Region

We list down some integrals used in the proof of Lemma 3.4, as follows:

Lemma D.4. *Let* $R_1 := \left\{x \in \mathbb{R}^2 : -x_1 \cot\theta \leq x_2 \leq x_1 \tan\theta\right\}$ *where* $\theta \in (0, \frac{\pi}{2})$. *Then, the following is true:*

1. $\displaystyle\int_{R_1} x_1 \Phi_t(x) dx = \frac{\sqrt{t}}{2\sqrt{\pi}}(\sin\theta + \cos\theta)$
2. $\displaystyle\int_{R_1} x_2 \Phi_t(x) dx = \frac{\sqrt{t}}{2\sqrt{\pi}}(\sin\theta - \cos\theta)$
3. $\displaystyle\int_{R_1} x_1 x_2 \Phi_t(x) dx = -\frac{t}{\pi}\cos 2\theta$
4. $\displaystyle\int_{R_1} x_2^2 \Phi_t(x) dx = t\left(\frac{1}{2} - \frac{1}{\pi}\sin 2\theta\right)$
5. $\displaystyle\int_{R_1} x_1^3 \Phi_t(x) dx = \frac{t\sqrt{t}}{\sqrt{\pi}}(\sin\theta + \cos\theta)(2 + \sin\theta\cos\theta)$
6. $\displaystyle\int_{R_1} x_2^3 \Phi_t(x) dx = \frac{t\sqrt{t}}{\sqrt{\pi}}(\sin\theta - \cos\theta)(2 - \sin\theta\cos\theta)$
7. $\displaystyle\int_{R_1} x_1^2 x_2 \Phi_t(x) dx = \frac{t\sqrt{t}}{\sqrt{\pi}}(\sin\theta - \cos\theta)(1 + \sin\theta\cos\theta)$
8. $\displaystyle\int_{R_1} x_1 x_2^2 \Phi_t(x) dx = \frac{t\sqrt{t}}{\sqrt{\pi}}(\sin\theta + \cos\theta)(1 - \sin\theta\cos\theta)$

Proof. Indeed, we have

$$
\begin{aligned}
1.\int_{R_1} x_1\Phi_t(x)dx &= \frac{1}{4\pi t}\int_0^\infty\int_{\frac{x_2}{\tan\theta}}^\infty + \int_{-\infty}^0\int_{-\frac{x_2}{\cot\theta}}^\infty x_1 e^{-\frac{x_1^2}{4t}}e^{-\frac{x_2^2}{4t}}dx_1dx_2\\
&= \frac{1}{\sqrt{4\pi t}}\left[\int_0^\infty \frac{\sqrt{t}}{\sqrt{\pi}}e^{-\frac{x_2^2}{4t}\left(\frac{1}{\tan^2\theta}+1\right)}dx_2 + \int_{-\infty}^0 \frac{\sqrt{t}}{\sqrt{\pi}}e^{-\frac{x_2^2}{4t}\left(\frac{1}{\cot^2\theta}+1\right)}dx_2\right]\\
&= \frac{\sqrt{t}}{2\sqrt{\pi}}\left[\frac{\tan\theta}{\sqrt{1+\tan^2\theta}}+\frac{\cot\theta}{\sqrt{1+\cot^2\theta}}\right]\\
&= \frac{\sqrt{t}}{2\sqrt{\pi}}\left(\sin\theta+\cos\theta\right).
\end{aligned}
$$

$$
\begin{aligned}
2.\int_{R_1} x_2\Phi_t(x)dx &= \frac{1}{4\pi t}\int_0^\infty\int_{-x_1\cot\theta}^{x_1\tan\theta} x_2 e^{-\frac{x_2^2}{4t}}e^{-\frac{x_1^2}{4t}}dx_2dx_1\\
&= \frac{1}{\sqrt{4\pi t}}\frac{\sqrt{t}}{\sqrt{\pi}}\int_0^\infty\left[e^{-\frac{x_1^2}{4t}(\cot^2\theta+1)}-e^{-\frac{x_1^2}{4t}(\tan^2\theta+1)}\right]dx_1\\
&= \frac{\sqrt{t}}{2\sqrt{\pi}}\left[\frac{1}{\sqrt{1+\cot^2\theta}}-\frac{1}{\sqrt{1+\tan^2\theta}}\right]\\
&= \frac{\sqrt{t}}{2\sqrt{\pi}}\left(\sin\theta-\cos\theta\right).
\end{aligned}
$$

$$
\begin{aligned}
3.\int_{R_1} x_1x_2\Phi_t(x)dx &= \frac{1}{4\pi t}\int_0^\infty x_1\int_{-x_1\cot\theta}^{x_1\tan\theta} x_2 e^{-\frac{x_2^2}{4t}}e^{-\frac{x_1^2}{4t}}dx_2dx_1\\
&= \frac{1}{\sqrt{4\pi t}}\frac{\sqrt{t}}{\sqrt{\pi}}\int_0^\infty x_1\left[e^{-\frac{x_1^2}{4t}(\cot^2\theta+1)}-e^{-\frac{x_1^2}{4t}(\tan^2\theta+1)}\right]dx_1\\
&= \frac{\sqrt{t}}{\sqrt{\pi}}\left(\sin^2\theta-\cos^2\theta\right)\cdot\frac{1}{\sqrt{4\pi t}}\int_0^\infty x_1e^{-\frac{x_1^2}{4t}}dx_1 = -\frac{t}{\pi}\cos 2\theta,
\end{aligned}
$$

$$
\begin{aligned}
4.\int_{R_1} x_2^2\Phi_t(x)dx &= \frac{1}{4\pi t}\int_{\theta-\frac{\pi}{2}}^\theta\int_0^\infty r^2\sin^2\rho e^{-\frac{r^2}{4t}}rdrd\rho\\
&= \int_{\theta-\frac{\pi}{2}}^\theta \sin^2\rho d\rho\cdot\frac{1}{4\pi t}\int_0^\infty r^3e^{-\frac{r^2}{4t}}rdr\\
&= \int_{\theta-\frac{\pi}{2}}^\theta \frac{1-\cos 2\rho}{2}d\rho\cdot\frac{4t}{\pi}\int_0^\infty r^3e^{-r^2}dr = \frac{t}{2\pi}\left(\pi-2\sin 2\theta\right).
\end{aligned}
$$

$$
\begin{aligned}
5.\int_{R_1} x_1^3\Phi_t(x)dx &= \frac{1}{4\pi t}\int_{\theta-\pi/2}^\theta\int_0^\infty r^4\cos^3\rho e^{-\frac{r^2}{4t}}drd\rho\\
&= \frac{1}{\pi}(2\sqrt{t})^3\int_{\theta-\pi/2}^\theta\left(1-\sin^2\rho\right)\cos\rho d\rho\cdot\int_0^\infty r^4e^{-r^2}dr\\
&= \frac{1}{\pi}(2\sqrt{t})^3\left(\sin\theta+\cos\theta-\tfrac{1}{3}\sin^3\theta-\tfrac{1}{3}\cos^3\theta\right)\cdot\frac{3\sqrt{\pi}}{8}\\
&= \frac{t\sqrt{t}}{\sqrt{\pi}}\left(\sin\theta+\cos\theta\right)\left(2+\sin\theta\cos\theta\right),
\end{aligned}
$$

$$
\begin{aligned}
6.\int_{R_1} x_2^3\Phi_t(x)dx &= \frac{1}{4\pi t}\int_{\theta-\pi/2}^{\theta}\int_0^{\infty} r^4\sin^3\rho e^{-\frac{r^2}{4t}}\,dr d\rho \\
&= \frac{1}{\pi}(2\sqrt{t})^3\int_{\theta-\pi/2}^{\theta}\left(1-\cos^2\rho\right)\sin\rho d\rho\cdot\int_0^{\infty} r^4e^{-r^2}dr \\
&= \frac{1}{\pi}(2\sqrt{t})^3\left(\sin\theta-\cos\theta+\tfrac{1}{3}\cos^3\theta-\tfrac{1}{3}\sin^3\theta\right)\cdot\frac{3\sqrt{\pi}}{8} \\
&= \frac{t\sqrt{t}}{\sqrt{\pi}}\left(\sin\theta-\cos\theta\right)\left(2-\sin\theta\cos\theta\right).
\end{aligned}
$$

$$
\begin{aligned}
7.\int_{R_1} x_1^2x_2\Phi_t(x)dx &= \frac{1}{4\pi t}\int_0^{\infty} x_1^2e^{-\frac{x_1^2}{4t}}\int_{-x_1\cot\theta}^{x_1\tan\theta} x_2e^{-\frac{x_2^2}{4t}}\,dx_2dx_1 \\
&= \frac{1}{\sqrt{4\pi t}}\frac{\sqrt{t}}{\sqrt{\pi}}\int_0^{\infty} x_1^2\left[e^{-\frac{x_1^2}{4t}(\cot^2\theta+1)}-e^{-\frac{x_1^2}{4t}(\tan^2\theta+1)}\right]dx_1 \\
&= \frac{\sqrt{t}}{\sqrt{\pi}}\left(\sin^3\theta-\cos^3\theta\right)\cdot\frac{1}{\sqrt{4\pi t}}\int_0^{\infty} x_1^2e^{-\frac{x_1^2}{4t}}dx_1 \\
&= \frac{t\sqrt{t}}{\sqrt{\pi}}\left(\sin\theta-\cos\theta\right)\left(1+\sin\theta\cos\theta\right),
\end{aligned}
$$

$$
\begin{aligned}
8.\int_{R_1} x_1x_2^2\Phi_t(x)dx &= \frac{1}{4\pi t}\int_0^{\infty}\int_{\frac{x_2}{\tan\theta}}^{\infty}+\int_{-\infty}^{0}\int_{-\frac{x_2}{\cot\theta}}^{\infty} x_1x_2^2e^{-\frac{x_1^2}{4t}}e^{-\frac{x_2^2}{4t}}dx_1dx_2 \\
&= \frac{\sqrt{t}}{\sqrt{\pi}}\frac{1}{\sqrt{4\pi t}}\left[\int_0^{\infty} x_2^2e^{-\frac{x_2^2}{4t}\left(\frac{1}{\tan^2\theta}+1\right)}dx_2+\int_{-\infty}^{0} x_2^2e^{-\frac{x_2^2}{4t}\left(\frac{1}{\cot^2\theta}+1\right)}dx_2\right] \\
&= \frac{\sqrt{t}}{\sqrt{\pi}}\left(\sin^3\theta+\cos^3\theta\right)\cdot\frac{1}{\sqrt{4\pi t}}\int_0^{\infty} x_2^2e^{-\frac{x_2^2}{4t}}dx_2 \\
&= \frac{t\sqrt{t}}{\sqrt{\pi}}\left(\sin\theta+\cos\theta\right)\left(1-\sin\theta\cos\theta\right).
\end{aligned}
$$

□

Appendix E

Calculations involving the Interface Normal

In this appendix, we expound on the proof of Theorem 3.7. We evaluate the normal N^{ij} to interface $\gamma_{ij}(i,j=1,2,3)$ and its partial derivatives with respect to θ_1 and θ_2 at the triple junction point $z := z(\frac{\pi}{3}, \frac{\pi}{3})$ at time t. We define the normal as follows:

$$\begin{aligned} N^{ij}(z) &:= \nabla\left(\mathbf{u}(t,z)\cdot(\mathbf{p}_i-\mathbf{p}_j)\right) \\ &= \frac{k}{\varepsilon(k-1)}\left(\zeta^j_{z_1}(z)-\zeta^i_{z_1}(z),\ \zeta^j_{z_2}(z)-\zeta^i_{z_2}(z)\right)+O(e^{-\frac{\tau^2}{4t}}),\quad t\to 0, \end{aligned}$$

where partial derivatives of the convolution are evaluated from its Taylor expansion (3.10), as follows:

$$\begin{aligned} \zeta^1_{z_1}(z) &= \tfrac{2}{\sqrt{t}}D(\theta_1)z_1+\psi(t)(1+\tfrac{1}{\sqrt{t}}z_2)+O\left(t^{-1}z_1|z|\right) =: \beta_1(\theta_1,z) \\ \zeta^1_{z_2}(z) &= B(\theta_1)+\tfrac{2}{\sqrt{t}}E(\theta_1)z_2+\psi(t)(1+\tfrac{1}{\sqrt{t}}z_1)+O\left(t^{-1}z_2|z|\right) =: \beta_2(\theta_1,z) \\ \zeta^2_{z_1}(z) &= -\beta_1(\theta_2,u)\cos\theta_3+\beta_2(\theta_2,u)\sin\theta_3 \\ \zeta^2_{z_2}(z) &= -\beta_1(\theta_2,u)\sin\theta_3-\beta_2(\theta_2,u)\cos\theta_3 \\ \zeta^3_{z_1}(z) &= \beta_1(\theta_3,v)\cos\theta_2-\beta_2(\theta_3,v)\sin\theta_2 \\ \zeta^3_{z_2}(z) &= -\beta_1(\theta_3,v)\sin\theta_2-\beta_2(\theta_3,v)\cos\theta_2 \end{aligned}$$

where $\theta_3=\pi-\theta_1-\theta_2$ and

$$\begin{aligned} u &= (-\cos\theta_3 z_1-\sin\theta_3 z_2,\ \sin\theta_3 z_1-\cos\theta_3 z_2) \\ v &= (\cos\theta_2 z_1-\sin\theta_2 z_2,\ -\sin\theta_2 z_1-\cos\theta_2 z_2). \end{aligned}$$

Thus, if $\theta_1=\theta_2=\frac{\pi}{3}$, we have by Lemma 3.6 that $z=O(t)$, and so, $u=v=O(t)$, as $t\to 0$. This implies that

$$\begin{aligned} &\beta_1(\tfrac{\pi}{3},u)=\beta_1(\tfrac{\pi}{3},v)=O(\sqrt{t}),\quad t\to 0, \\ &\beta_2(\tfrac{\pi}{3},u)=\beta_2(\tfrac{\pi}{3},v)=B(\tfrac{\pi}{3})+O(\sqrt{t}),\quad t\to 0. \end{aligned}$$

Then, we get

$$\begin{array}{lll} \zeta^1_{z_1}(z)=O(\sqrt{t}), & \zeta^2_{z_1}(z)=\frac{\sqrt{3}}{2}B(\frac{\pi}{3})+O(\sqrt{t}), & \zeta^3_{z_1}(z)=-\frac{\sqrt{3}}{2}B(\frac{\pi}{3})+O(\sqrt{t}), \\ \zeta^1_{z_2}(z)=B(\frac{\pi}{3})+O(\sqrt{t}), & \zeta^2_{z_2}(z)=-\frac{1}{2}B(\frac{\pi}{3})+O(\sqrt{t}), & \zeta^3_{z_2}(z)=-\frac{1}{2}B(\frac{\pi}{3})+O(\sqrt{t}), \end{array}$$

as $t \to 0$. Hence,

$$\begin{aligned} N^{12}(z) &= \tfrac{k}{\varepsilon(k-1)} B(\tfrac{\pi}{3}) \left(\tfrac{\sqrt{3}}{2}, -\tfrac{3}{2}\right) + O(\sqrt{t} + e^{-\frac{\tau^2}{4t}}), \quad t \to 0 \\ N^{23}(z) &= \tfrac{k}{\varepsilon(k-1)} B(\tfrac{\pi}{3}) \left(-\sqrt{3}, 0\right) + O(\sqrt{t} + e^{-\frac{\tau^2}{4t}}), \quad t \to 0 \\ N^{31}(z) &= \tfrac{k}{\varepsilon(k-1)} B(\tfrac{\pi}{3}) \left(\tfrac{\sqrt{3}}{2}, \tfrac{3}{2}\right) + O(\sqrt{t} + e^{-\frac{\tau^2}{4t}}), \quad t \to 0, \end{aligned}$$

which implies that

$$\|N^{12}\| = \|N^{23}\| = \|N^{31}\| = \tfrac{k\sqrt{3}}{\varepsilon(k-1)} B(\tfrac{\pi}{3}) + O(\sqrt{t})), \quad t \to 0,$$

and

$$N^{31} \cdot N^{12} = N^{12} \cdot N^{23} = -\tfrac{1}{2} \left(\tfrac{k\sqrt{3}}{\varepsilon(k-1)} B(\tfrac{\pi}{3})\right)^2 + O(\sqrt{t}), \quad t \to 0.$$

Let us now take the partial derivatives of $\zeta^1_{z_i} \circ z$ (for $i = 1, 2$) with respect to θ_1 and θ_2. First, we note by Lemma 3.6 that

$$\begin{aligned} &\frac{\partial z_1}{\partial \theta_1} = \frac{\sqrt{t}}{\sqrt{3\pi} B(\frac{\pi}{3})} + O(t) =: C_1\sqrt{t} + O(t), && \frac{\partial z_2}{\partial \theta_1} = C_1\sqrt{3t} + O(t), \\ &\frac{\partial z_1}{\partial \theta_2} = 2C_1\sqrt{t} + O(t), && \frac{\partial z_2}{\partial \theta_2} = O(t), \end{aligned}$$

as $t \to 0$. Thus, we get

$$\begin{aligned} \frac{\partial}{\partial \theta_1} \zeta^1_{z_1} \circ z(\tfrac{\pi}{3}, \tfrac{\pi}{3}) &= 2C_1 D(\tfrac{\pi}{3}) + O(\sqrt{t}), \quad t \to 0, \\ \frac{\partial}{\partial \theta_2} \zeta^1_{z_1} \circ z(\tfrac{\pi}{3}, \tfrac{\pi}{3}) &= 4C_1 D(\tfrac{\pi}{3}) + O(\sqrt{t}), \quad t \to 0, \\ \frac{\partial}{\partial \theta_1} \zeta^1_{z_2} \circ z(\tfrac{\pi}{3}, \tfrac{\pi}{3}) &= B'(\tfrac{\pi}{3}) + 2\sqrt{3} C_1 E(\tfrac{\pi}{3}) + O(\sqrt{t}), \quad t \to 0, \\ \frac{\partial}{\partial \theta_2} \zeta^1_{z_2} \circ z(\tfrac{\pi}{3}, \tfrac{\pi}{3}) &= O(\sqrt{t}), \quad t \to 0. \end{aligned}$$

Morever, we note that

$$\begin{aligned} &\frac{\partial u_1}{\partial \theta_1} = -2C_1\sqrt{t} + O(t), && \frac{\partial v_1}{\partial \theta_1} = -C_1\sqrt{t} + O(t), \\ &\frac{\partial u_1}{\partial \theta_2} = -C_1\sqrt{t} + O(t), && \frac{\partial v_1}{\partial \theta_2} = C_1\sqrt{t} + O(t), \\ &\frac{\partial u_2}{\partial \theta_1} = O(t), && \frac{\partial v_2}{\partial \theta_1} = -C_1\sqrt{3t} + O(t), \\ &\frac{\partial u_2}{\partial \theta_2} = C_1\sqrt{3t} + O(t), && \frac{\partial v_2}{\partial \theta_2} = -C_1\sqrt{3t} + O(t), \quad t \to 0, \end{aligned}$$

Hence, if $\theta_1 = \theta_2 = \frac{\pi}{3}$, we have

$$\begin{aligned} &\frac{\partial}{\partial \theta_1} \beta_1(\theta_2, u) = -4C_1 D(\tfrac{\pi}{3}) + O(\sqrt{t}), && \frac{\partial}{\partial \theta_1} \beta_2(\theta_2, u) = O(\sqrt{t}), \\ &\frac{\partial}{\partial \theta_2} \beta_1(\theta_2, u) = -2C_1 D(\tfrac{\pi}{3}) + O(\sqrt{t}), && \frac{\partial}{\partial \theta_2} \beta_2(\theta_2, u) = B'(\tfrac{\pi}{3}) + 2\sqrt{3} C_1 E(\tfrac{\pi}{3}) + O(\sqrt{t}), \end{aligned}$$

and

$$\frac{\partial}{\partial\theta_1}\beta_1(\theta_3,v) = -2C_1D(\tfrac{\pi}{3}) + O(\sqrt{t}), \quad \frac{\partial}{\partial\theta_1}\beta_2(\theta_3,v) = -B'(\tfrac{\pi}{3}) - 2\sqrt{3}C_1E(\tfrac{\pi}{3}) + O(\sqrt{t}),$$
$$\frac{\partial}{\partial\theta_2}\beta_1(\theta_3,v) = 2C_1D(\tfrac{\pi}{3}) + O(\sqrt{t}), \quad \frac{\partial}{\partial\theta_2}\beta_2(\theta_3,v) = -B'(\tfrac{\pi}{3}) - 2\sqrt{3}C_1E(\tfrac{\pi}{3}) + O(\sqrt{t}),$$

as $t \to 0$. Thus, we get the following partial derivatives

$$\begin{aligned}
\frac{\partial}{\partial\theta_1}\zeta^2_{z_1}\circ z(\tfrac{\pi}{3},\tfrac{\pi}{3}) &= -\tfrac{1}{2}B(\tfrac{\pi}{3}) + 2C_1D(\tfrac{\pi}{3}) + O(\sqrt{t}),\\
\frac{\partial}{\partial\theta_2}\zeta^2_{z_1}\circ z(\tfrac{\pi}{3},\tfrac{\pi}{3}) &= -\tfrac{1}{2}B(\tfrac{\pi}{3}) + \tfrac{\sqrt{3}}{2}B'(\tfrac{\pi}{3}) + C_1(D(\tfrac{\pi}{3}) + 3E(\tfrac{\pi}{3})) + O(\sqrt{t}),\\
\frac{\partial}{\partial\theta_1}\zeta^2_{z_2}\circ z(\tfrac{\pi}{3},\tfrac{\pi}{3}) &= -\tfrac{\sqrt{3}}{2}B(\tfrac{\pi}{3}) + 2\sqrt{3}C_1D(\tfrac{\pi}{3}) + O(\sqrt{t}),\\
\frac{\partial}{\partial\theta_2}\zeta^2_{z_2}\circ z(\tfrac{\pi}{3},\tfrac{\pi}{3}) &= -\tfrac{\sqrt{3}}{2}B(\tfrac{\pi}{3}) - \tfrac{1}{2}B'(\tfrac{\pi}{3}) + \sqrt{3}C_1(D(\tfrac{\pi}{3}) - E(\tfrac{\pi}{3})) + O(\sqrt{t}),\\
\frac{\partial}{\partial\theta_1}\zeta^3_{z_1}\circ z(\tfrac{\pi}{3},\tfrac{\pi}{3}) &= \tfrac{\sqrt{3}}{2}B'(\tfrac{\pi}{3}) - C_1(D(\tfrac{\pi}{3}) - 3E(\tfrac{\pi}{3})) + O(\sqrt{t}),\\
\frac{\partial}{\partial\theta_2}\zeta^3_{z_1}\circ z(\tfrac{\pi}{3},\tfrac{\pi}{3}) &= -\tfrac{1}{2}B(\tfrac{\pi}{3}) + \tfrac{\sqrt{3}}{2}B'(\tfrac{\pi}{3}) + C_1(D(\tfrac{\pi}{3}) + 3E(\tfrac{\pi}{3})) + O(\sqrt{t}),\\
\frac{\partial}{\partial\theta_1}\zeta^3_{z_2}\circ z(\tfrac{\pi}{3},\tfrac{\pi}{3}) &= \tfrac{1}{2}B'(\tfrac{\pi}{3}) + \sqrt{3}C_1(D(\tfrac{\pi}{3}) + E(\tfrac{\pi}{3})) + O(\sqrt{t}),\\
\frac{\partial}{\partial\theta_2}\zeta^3_{z_2}\circ z(\tfrac{\pi}{3},\tfrac{\pi}{3}) &= \tfrac{\sqrt{3}}{2}B(\tfrac{\pi}{3}) + \tfrac{1}{2}B'(\tfrac{\pi}{3}) - \sqrt{3}C_1(D(\tfrac{\pi}{3}) - E(\tfrac{\pi}{3})) + O(\sqrt{t}),
\end{aligned}$$

as $t \to 0$. For $u, v, w \in \mathbb{R}^2$, define the mapping $\zeta : \mathbb{R}^2 \times \mathbb{R}^2 \times \mathbb{R}^2 \longrightarrow \mathbb{R}^2$ by

$$\zeta(u,v,w) = uB(\tfrac{\pi}{3}) + vB'(\tfrac{\pi}{3}) + wC_1(D(\tfrac{\pi}{3}) - E(\tfrac{\pi}{3})).$$

Then for any $p \in \mathbb{R}^2$, we have $p \cdot \zeta(u,v,w) = \zeta(p\cdot u, p\cdot v, p\cdot w)$. Hence,

$$\begin{aligned}
\frac{\partial}{\partial\theta_1}N^{12}(\tfrac{\pi}{3},\tfrac{\pi}{3}) &= \tfrac{k}{\varepsilon(k-1)}\,\zeta\Big((-\tfrac{1}{2},-\tfrac{\sqrt{3}}{2}),\ (0,-1),\ (0,2\sqrt{3})\Big) + O(\sqrt{t}+e^{-\frac{\tau^2}{4t}})\\
\frac{\partial}{\partial\theta_2}N^{12}(\tfrac{\pi}{3},\tfrac{\pi}{3}) &= \tfrac{k}{\varepsilon(k-1)}\,\zeta\Big((-\tfrac{1}{2},-\tfrac{\sqrt{3}}{2}),\ (\tfrac{\sqrt{3}}{2},-\tfrac{1}{2}),\ (-3,\sqrt{3})\Big) + O(\sqrt{t}+e^{-\frac{\tau^2}{4t}})\\
\frac{\partial}{\partial\theta_1}N^{23}(\tfrac{\pi}{3},\tfrac{\pi}{3}) &= \tfrac{k}{\varepsilon(k-1)}\,\zeta\Big((\tfrac{1}{2},\tfrac{\sqrt{3}}{2}),\ (\tfrac{\sqrt{3}}{2},\tfrac{1}{2}),\ (-3,-\sqrt{3})\Big) + O(\sqrt{t}+e^{-\frac{\tau^2}{4t}})\\
\frac{\partial}{\partial\theta_2}N^{23}(\tfrac{\pi}{3},\tfrac{\pi}{3}) &= \tfrac{k}{\varepsilon(k-1)}\,\zeta\big((0,\sqrt{3}),\ (0,1),\ (0,-2\sqrt{3})\big) + O(\sqrt{t}+e^{-\frac{\tau^2}{4t}})\\
\frac{\partial}{\partial\theta_1}N^{31}(\tfrac{\pi}{3},\tfrac{\pi}{3}) &= \tfrac{k}{\varepsilon(k-1)}\,\zeta\Big((0,0),\ (-\tfrac{\sqrt{3}}{2},\tfrac{1}{2}),\ (3,-\sqrt{3})\Big) + O(\sqrt{t}+e^{-\frac{\tau^2}{4t}})\\
\frac{\partial}{\partial\theta_2}N^{31}(\tfrac{\pi}{3},\tfrac{\pi}{3}) &= \tfrac{k}{\varepsilon(k-1)}\,\zeta\Big((\tfrac{1}{2},-\tfrac{\sqrt{3}}{2}),\ (-\tfrac{\sqrt{3}}{2},-\tfrac{1}{2}),\ (3,\sqrt{3})\Big) + O(\sqrt{t}+e^{-\frac{\tau^2}{4t}})
\end{aligned}$$

Finally, we evaluate the partial derivatives of

$$(\Psi^1,\Psi^2) = \left(\frac{N^{31}\cdot N_{12}}{\|N^{31}\|\|N^{12}\|}, \frac{N^{12}\cdot N^{23}}{\|N^{12}\|\|N^{23}\|}\right),$$

with respect to θ_1 and θ_2.

Note that if $\theta_1 = \theta_2 = \frac{\pi}{3}$, we have $\Psi^1 = \Psi^2 = -\frac{1}{2}$. Hence,

$$\begin{aligned}
\frac{\partial}{\partial\theta_1}\Psi^1(\tfrac{\pi}{3},\tfrac{\pi}{3}) = &\ \frac{\big(N^{31}-\Psi^1 N^{12}\big)\cdot\frac{\partial}{\partial\theta_1}N^{12}(\frac{\pi}{3},\frac{\pi}{3})}{\|N^{31}\|\|N^{12}\|} + \frac{\big(N^{12}-\Psi^1 N^{31}\big)\cdot\frac{\partial}{\partial\theta_1}N^{31}(\frac{\pi}{3},\frac{\pi}{3})}{\|N^{31}\|\|N^{12}\|} \\
= &\ \frac{-\sqrt{3}}{12B(\frac{\pi}{3})}\Big\{(-3,-\sqrt{3})\cdot\zeta\Big((-\tfrac{1}{2},-\tfrac{\sqrt{3}}{2}),\ (0,-1),\ (0,2\sqrt{3})\Big) \\
&\qquad + (-3,\sqrt{3})\cdot\zeta\Big((0,0),\ (-\tfrac{\sqrt{3}}{2},\tfrac{1}{2}),\ (3,-\sqrt{3})\Big)\Big\} + O(\sqrt{t}) \\
= &\ \frac{-\sqrt{3}}{12B(\frac{\pi}{3})}\big\{3B(\tfrac{\pi}{3}) + 3\sqrt{3}B'(\tfrac{\pi}{3}) - 18C_1(D(\tfrac{\pi}{3}) - E(\tfrac{\pi}{3}))\big\} \\
= &-\frac{\sqrt{3}}{4}\left[1 + \sqrt{3}\frac{B'(\frac{\pi}{3})}{B(\frac{\pi}{3})} + \frac{2\sqrt{3}}{\sqrt{\pi}}\frac{E(\frac{\pi}{3})-D(\frac{\pi}{3})}{B(\frac{\pi}{3})^2}\right] + O(\sqrt{t}),\ \ t\to 0.
\end{aligned}$$

In a similar fashion, we get

$$\begin{aligned}
\frac{\partial}{\partial\theta_2}\Psi^1(\tfrac{\pi}{3},\tfrac{\pi}{3}) = &\ \frac{\big(N^{31}-\Psi^1 N^{12}\big)\cdot\frac{\partial}{\partial\theta_2}N^{12}(\frac{\pi}{3},\frac{\pi}{3})}{\|N^{31}\|\|N^{12}\|} + \frac{\big(N^{12}-\Psi^1 N^{31}\big)\cdot\frac{\partial}{\partial\theta_2}N^{31}(\frac{\pi}{3},\frac{\pi}{3})}{\|N^{31}\|\|N^{12}\|} \\
= &\ \frac{-\sqrt{3}}{12B(\frac{\pi}{3})}\Big\{(-3,-\sqrt{3})\cdot\zeta\Big((-\tfrac{1}{2},-\tfrac{\sqrt{3}}{2}),\ (\tfrac{\sqrt{3}}{2},-\tfrac{1}{2}),\ (-3,\sqrt{3})\Big) \\
&\qquad + (-3,\sqrt{3})\cdot\zeta\Big((\tfrac{1}{2},-\tfrac{\sqrt{3}}{2}),\ (-\tfrac{\sqrt{3}}{2},-\tfrac{1}{2}),\ (3,\sqrt{3})\Big)\Big\} + O(\sqrt{t}) \\
= &\ O(\sqrt{t}),\ \ t\to 0.
\end{aligned}$$

Moreover,

$$\begin{aligned}
\frac{\partial}{\partial\theta_1}\Psi^2(\tfrac{\pi}{3},\tfrac{\pi}{3}) = &\ \frac{\big(N^{12}-\Psi^2 N^{23}\big)\cdot\frac{\partial}{\partial\theta_1}N^{23}(\frac{\pi}{3},\frac{\pi}{3})}{\|N^{12}\|\|N^{23}\|} + \frac{\big(N^{23}-\Psi^2 N^{12}\big)\cdot\frac{\partial}{\partial\theta_1}N^{12}(\frac{\pi}{3},\frac{\pi}{3})}{\|N^{12}\|\|N^{23}\|} \\
= &\ \frac{-\sqrt{3}}{12B(\frac{\pi}{3})}\Big\{(0,2\sqrt{3})\cdot\zeta\Big((\tfrac{1}{2},\tfrac{\sqrt{3}}{2}),\ (\tfrac{\sqrt{3}}{2},\tfrac{1}{2}),\ (-3,-\sqrt{3})\Big) \\
&\qquad + (3,\sqrt{3})\cdot\zeta\Big((-\tfrac{1}{2},-\tfrac{\sqrt{3}}{2}),\ (0,-1),\ (0,2\sqrt{3})\Big)\Big\} + O(\sqrt{t}) \\
= &\ O(\sqrt{t}),\ \ t\to 0.
\end{aligned}$$

and

$$\begin{aligned}
\frac{\partial}{\partial\theta_2}\Psi^2(\tfrac{\pi}{3},\tfrac{\pi}{3}) = &\ \frac{\big(N^{12}-\Psi^2 N^{23}\big)\cdot\frac{\partial}{\partial\theta_2}N^{23}(\frac{\pi}{3},\frac{\pi}{3})}{\|N^{12}\|\|N^{23}\|} + \frac{\big(N^{23}-\Psi^2 N^{12}\big)\cdot\frac{\partial}{\partial\theta_2}N^{12}(\frac{\pi}{3},\frac{\pi}{3})}{\|N^{12}\|\|N^{23}\|} \\
= &\ \frac{-\sqrt{3}}{12B(\frac{\pi}{3})}\Big\{(0,2\sqrt{3})\cdot\zeta\Big((0,\sqrt{3}),\ (0,1),\ (0,-2\sqrt{3})\Big) \\
&\qquad + (3,\sqrt{3})\cdot\zeta\Big((-\tfrac{1}{2},-\tfrac{\sqrt{3}}{2}),\ (\tfrac{\sqrt{3}}{2},-\tfrac{1}{2}),\ (-3,\sqrt{3})\Big)\Big\} + O(\sqrt{t}) \\
= &\ \frac{-\sqrt{3}}{12B(\frac{\pi}{3})}\big\{3B(\tfrac{\pi}{3}) + 3\sqrt{3}B'(\tfrac{\pi}{3}) - 18C_1(D(\tfrac{\pi}{3}) - E(\tfrac{\pi}{3}))\big\} \\
= &-\frac{\sqrt{3}}{4}\left[1 + \sqrt{3}\frac{B'(\frac{\pi}{3})}{B(\frac{\pi}{3})} + \frac{2\sqrt{3}}{\sqrt{\pi}}\frac{E(\frac{\pi}{3})-D(\frac{\pi}{3})}{B(\frac{\pi}{3})^2}\right] + O(\sqrt{t}),\ \ t\to 0.
\end{aligned}$$

Appendix F

Discrete Morse Flow Method

This appendix introduces a variational method known as the *discrete Morse flow* [61, 78], that solves time-dependent problems by discretizing time and defining a sequence of minimization problems approximating the original problem. The corresponding minimizers are then interpolated with respect to time and the discretization parameter taken to zero.

We shall explain this idea on the heat equation. Consider the following problem:

$$\begin{cases} u_t(t,x) = \Delta u(t,x), & \text{in } Q_T = (0,T)\times\Omega \\ u(t,x) \ = 0, & \text{on } (0,T)\times\partial\Omega \\ u(0,x) = \Delta u_0(x), & \text{in } \Omega. \end{cases}$$

Fix a natural number $N > 0$ and determine time step size $h = T/K$. We approximate solution u_n at time $t = nh$ by minimizer of the following functional in $H_0^1(\Omega)$

$$\mathcal{J}_n(u) \ = \ \int_\Omega \frac{|u-u_{n-1}|^2}{2h}dx + \int_\Omega \frac{|\nabla u|^2}{2}dx.$$

Note that the second term of the functional is lower-semicontinuous with respect to sequentially weak convergence in $H^1(\Omega)$ while the first term is continuous in $L^2(\Omega)$. The existence of the minimizers then follows immediately from the fact that the functionals are bounded from below.

We define the approximate solutions $\overline{u}^h(t,x)$ and $u^h(t,x)$ by interpolations of the minimizers $\{u_n\}_{n=0}^K$ in time as follows:

$$\overline{u}^h(t,x) \ = \ \begin{cases} u_0(x), & t = 0 \\ u_n(x), & t \in ((n-1)h, nh],\ n = 1,\dots,K, \end{cases}$$

and

$$u^h(t,x) = \begin{cases} u_0(x), & t = 0 \\ \dfrac{nh-t}{h}u_{n-1}(x) + \dfrac{t-(n-1)h}{h}u_n(x), & t \in ((n-1)h, nh],\ n = 1,...,K. \end{cases}$$

Since u_n minimizes $\mathcal{J}_n$, then the first variation of $\mathcal{J}_n$ vanishes at u_n. Hence, for any $\phi \in L^2(0,T;H_0^1(\Omega))$,

$$\int_0^T \int_\Omega \left(u_t^h \phi + \nabla \overline{u}^h \cdot \nabla \phi \right) dx = 0.$$

Next, we want to take time step h to zero. To do so, we first establish the following estimate

$$\int_0^t \|u_t^h\|_{L^2(\Omega)} dt + \|\nabla \overline{u}^h(t)\|_{L^2(\Omega)} \quad \leq \quad C_E \quad \text{for a.e. } t \in (0,T),$$

where constant C_E depends on H^1-norm of the initial data, but is independent of h. Thanks to this estimate, we can extract a subsequence of the approximate solutions such that for some $u \in H^1(Q_T)$, we have

$$\begin{aligned} \nabla \overline{u}^h &\rightharpoonup \nabla u, \quad \text{in } \left(L^2(Q_t)\right)^N \\ u_t^h &\rightharpoonup u_t, \quad \text{in } L^2(Q_T). \end{aligned}$$

Finally, passing the limit in h yields

$$\int_0^T \int_\Omega \left(u_t \phi + \nabla u \cdot \nabla \phi \right) dx = 0,$$

for any $\phi \in L^2(0,T;H_0^1(\Omega))$. Moreover, it can be shown that u satisfies the initial and boundary conditions in the sense of traces. Thus, we have shown by discrete Morse flow method that there exists a weak solution $u \in H^1(Q_T)$ to the heat equation.

Appendix G

Multiphase MBO Method considering Bulk Energies

This appendix presents our earlier work on the multiphase extension of MBO method to approximate mean curvature motions considering space-dependent bulk energies e_i. In particular, we extend the results in [50, 94] to the multiphase case.

Consider the vector analogue of the scalar nonhomogenous heat equation considered in [50, 94], as follows:

$$\mathbf{u}_t(t,x) \quad = \quad \Delta \mathbf{u}(t,x) + \frac{\mathbf{w}(x)}{\sqrt{4\pi t}} \tag{G.1}$$

where $\mathbf{w}$ is a term related to the prescribed phase energies. Following a similar argument as in Chapter 5, we apply the vector threshold dynamics [94] to the above partial differential equation (see Algorithm G.1) and construct $\mathbf{w}$ so that a normal velocity $v = -\kappa - e_i + e_j$ is achieved at each interface γ_{ij}.

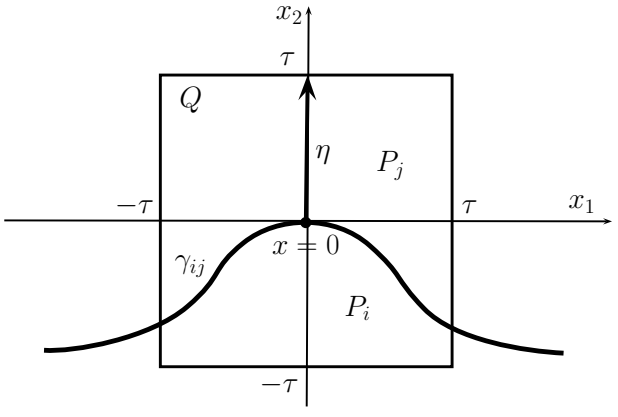

FIGURE G.1: Setting up interface γ_{ij} in the new coordinate system.

For simplicity, consider $N = 2$. Fix $x \in \mathbb{R}^2$ on interface γ_{ij}. Now, rotate and translate the coordinate system so that $x = 0$ in the new coordinate system and the normal $\boldsymbol{\eta}$ to γ_{ij} pointing into P_j lies in the positive x_2 direction (see Figure G.1). Choose $\tau > 0$, small enough so that $Q := [-\tau, \tau] \times [-\tau, \tau]$ contains only phases P_i and P_k. Assume

Algorithm G.1 MBO Method for Multiphase MCF considering Bulk Energies

Given time step size $\Delta t > 0$ and initial interface network $\Gamma_0 := \bigcup \{\gamma_{ij} : i, j = 1, 2, \ldots, k\}$ where each phase region P_i have prescribed energy density e_i, we obtain an approximation of its *multiphase mean curvature flow* by generating a sequence of time discrete interface networks $\{\Gamma_m\}_{m=1}^{M}$ at times $t = m\Delta t$ $(m = 1, \ldots M)$, as follows:

1. Initialization. Given phase regions $P_i (i = 1, 2, 3)$ defined by the interface network Γ_{m-1}, initialize
$$\mathbf{u}_0(x) = \mathbf{p}_i \quad \text{for } x \in P_i.$$
2. Diffusion Step. With $\mathbf{u}_0$ as the initial condition, solve (G.1) until time Δt.
3. Projection Step. For each x, identify the reference vector $\mathbf{p}_i$ closest to the solution $\mathbf{u}(\Delta t, x)$, that is,
$$\mathbf{p}_i \cdot \mathbf{u}(\Delta t, x) = \max_{j=1,2,\ldots,k} \mathbf{p}_j \cdot \mathbf{u}(\Delta t, x). \tag{G.2}$$
This redistribution of reference vectors determines the approximate new phase regions after time Δt, which in turn, defines the new interface network Γ_m.

that there exists a smooth function $\gamma : \mathbb{R} \to \mathbb{R}$ whose graph $(x_1, \gamma(x_1))$ describes the interface γ_{ij} inside the cube Q. Hence, if κ defines the curvature of the interface γ_{ij} at point $x = (0, 0)$, then $\gamma(0) = 0$, $\gamma'(0) = 0$, and $\gamma''(0) = -\kappa$.

Let $\mathbf{u}$ be the solution of the vector-type heat equation (G.1). For convenience, we will write t instead of Δt. Then, the normal velocity v of interface γ_{ij} at point $x = 0$ obtained from Algorithm G.1 can be found from the relation

$$\begin{aligned}
0 &= \mathbf{u}(t, 0, vt) \cdot (\mathbf{p}_i - \mathbf{p}_j) \\
&= \int_Q + \int_{\mathbb{R}^2 \setminus Q} \mathbf{u}_0(x) \cdot (\mathbf{p}_i - \mathbf{p}_j) \Phi_t(x - z) dx \\
&\qquad + \int_0^t \left(\int_Q + \int_{\mathbb{R}^2 \setminus Q} \right) \frac{\mathbf{w}(x) \cdot (\mathbf{p}_i - \mathbf{p}_j)}{\sqrt{4\pi s}} \Phi_{t-s}(x - z) dx ds \\
&=: I_A + I\!I_A + I_B + I\!I_B,
\end{aligned}$$

where $z := (0, vt)$. We estimate the above integrals in the following claims.

Claim 1. $I\!I_A = O(e^{-\frac{\tau^2}{4t}})$, as $t \to 0$.
Indeed,

$$\begin{aligned}
|I\!I_A| &\leq C \int_{\mathbb{R}} \int_{\mathbb{R} \setminus (-\tau, \tau)} + \int_{\mathbb{R} \setminus (-\tau, \tau)} \int_{\mathbb{R}} \varphi_t(x_1) \varphi_t(x_2 - vt) dx_2 dx_1 \\
&\leq C \left[\int_{\frac{\tau - vt}{2\sqrt{t}}}^{\infty} + \int_{\frac{\tau + vt}{2\sqrt{t}}}^{\infty} e^{-x_2^2} dx_2 + 2 \int_{\frac{\tau}{2\sqrt{t}}}^{\infty} e^{-x_1^2} dx_1 \right] \\
&\leq C e^{-\frac{\tau^2}{4t}},
\end{aligned}$$

which proves the claim.

Claim 2. $I_A = -(1-\mathbf{p}_i\cdot\mathbf{p}_j)\,(v+\kappa)\,\frac{\sqrt{t}}{\sqrt{\pi}} + O(t\sqrt{t})$, as $t\to 0$.
Indeed,

$$\begin{aligned} I_A &= M\int_{-\tau}^{\tau}\varphi_t(x_1)\left(\int_{-\tau}^{\gamma(x_1)} - \int_{\gamma(x_1)}^{\tau}\right)\varphi_t(x_2-vt)dx_2dx_1 \\ &= M\int_{-\infty}^{\infty}\varphi_t(x_1)\left(\int_{-\infty}^{\gamma(x_1)} - \int_{\gamma(x_1)}^{\infty}\right)\varphi_t(x_2-vt)dx_2dx_1 + O(e^{-\frac{\tau^2}{4t}}) \\ &= 2M\int_{-\infty}^{\infty}\varphi_t(x_1)\int_{0}^{\gamma(x_1)}\varphi_t(x_2-vt)dx_2dx_1 + O(e^{-\frac{\tau^2}{4t}}) \\ &= \frac{2M}{\sqrt{\pi}}\int_{-\infty}^{\infty}\varphi_t(x_1)\int_{0}^{\frac{\gamma(x_1)-vt}{2\sqrt{t}}} e^{-x_2^2}dx_2dx_1 + O(e^{-\frac{\tau^2}{4t}}), \end{aligned} \tag{G.3}$$

where $M := 1-\mathbf{p}_i\cdot\mathbf{p}_j > 0$. We write out the Taylor expansion of γ around $x_1 = 0$ to obtain

$$\begin{aligned} \frac{\gamma(x_1)-vt}{2\sqrt{t}} &= \frac{1}{2\sqrt{t}}\left[\gamma(0)+\gamma'(0)x_1+\tfrac{1}{2}\gamma''(0)x_1^2 - vt + O(x_1^3)\right] \\ &= -\tfrac{1}{4}t^{-1/2}\kappa x_1^2 - \tfrac{1}{2}v\sqrt{t} + O(t^{-1/2}x_1^3). \end{aligned}$$

Recall that

$$\int_0^s e^{-\xi^2}d\xi = s + O(s^3).$$

Also, note that

$$\int_{-\infty}^{\infty}\varphi_t(\xi)d\xi = 1, \qquad \int_{-\infty}^{\infty}\xi^2\varphi_t(\xi)d\xi = 2t,$$
$$\int_{-\infty}^{\infty}\xi^3\varphi_t(\xi)d\xi = 0, \qquad \int_{-\infty}^{\infty}\xi^4\varphi_t(\xi)d\xi = O(t^2).$$

Then, (G.3) becomes

$$I_A = -\frac{M\sqrt{t}}{\sqrt{\pi}}\,(\kappa+v) + O(t\sqrt{t}+e^{-\frac{\tau^2}{4t}}), \tag{G.4}$$

which proves the claim.

Claim 3. $II_B = O(t\sqrt{t}e^{-\frac{\tau^2}{4t}})$, as $t\to 0$.
Indeed, if $\mathbf{w}(x)\cdot(\mathbf{p}_i-\mathbf{p}_j)$ is bounded in $\mathbb{R}^2$, we have

$$\begin{aligned} |II_B| &\le \max_{\mathbb{R}^2}|\mathbf{w}(x)\cdot(\mathbf{p}_i-\mathbf{p}_j)|\int_0^t\frac{1}{\sqrt{4\pi s}}\int_{\mathbb{R}^2\setminus Q}\Phi_{t-s}(x-z)dxds \\ &\le C\int_0^t\frac{1}{\sqrt{s}}e^{-\frac{\tau^2}{4(t-s)}}ds \\ &\le \frac{C}{\sqrt{t}}\int_{\frac{\tau^2}{4t}}^{\infty}\frac{1}{s^2}e^{-s}ds \\ &\le Ct\sqrt{t}\int_{\frac{\tau^2}{4t}}^{\infty}e^{-s}ds = O(t\sqrt{t}e^{-\frac{\tau^2}{4t}}), \end{aligned}$$

which proves the claim.

Claim 4. $I_B = \mathbf{w}(0)\cdot(\mathbf{p}_i-\mathbf{p}_j)\frac{\sqrt{t}}{\sqrt{\pi}} + O(t)$, as $t\to 0$.
Indeed,

$$\begin{aligned} I_B &= \int_0^t \frac{1}{\sqrt{4\pi s}} \int_{-\tau}^{\tau}\int_{-\tau}^{\tau} \mathbf{w}(x)\cdot(\mathbf{p}_i-\mathbf{p}_j)\Phi_{t-s}(x-z)dxds \\ &= \int_0^t \frac{1}{\sqrt{4\pi s}} \int_{-\infty}^{\infty}\int_{-\infty}^{\infty} (\mathbf{w}(0)+O(x))\cdot(\mathbf{p}_i-\mathbf{p}_j)\Phi_{t-s}(x-z)dxds + O(t\sqrt{t}e^{-\frac{\tau^2}{4t}}) \\ &=: I_1 + I_2 + O(t\sqrt{t}e^{-\frac{\tau^2}{4t}}). \end{aligned}$$

Note that

$$\begin{aligned} I_1 &= \mathbf{w}(0)\cdot(\mathbf{p}_i-\mathbf{p}_j)\int_0^t \frac{1}{\sqrt{4\pi s}}\int_{-\infty}^{\infty}\varphi_{t-s}(x_1)\int_{-\infty}^{\infty}\varphi_{t-s}(x_2)dx_2dx_1ds \\ &= \mathbf{w}(0)\cdot(\mathbf{p}_i-\mathbf{p}_j)\frac{\sqrt{t}}{\sqrt{\pi}}. \end{aligned}$$

and

$$\begin{aligned} |I_2| &\le C\int_0^t \frac{1}{\sqrt{4\pi s}}\int_{-\infty}^{\infty}\int_{-\infty}^{\infty}|x\cdot(\mathbf{p}_i-\mathbf{p}_j)|\Phi_{t-s}(x-z)dxds \\ &\le C\int_0^t \frac{1}{\sqrt{4\pi s}}\int_{-\infty}^{\infty}\int_{-\infty}^{\infty}|x_1+x_2|\varphi_{t-s}(x_1)\varphi_{t-s}(x_2-vt)dx_2dx_1ds \\ &\le C\int_0^t \frac{1}{\sqrt{4\pi s}}\left(\int_0^{\infty} x_1\varphi_{t-s}(x_1)\int_{-\infty}^{\infty}\varphi_{t-s}(x_2)\right. \\ &\qquad\left. + \int_{-\infty}^{\infty}\varphi_{t-s}(x_1)\int_{-\infty}^{\infty}|x_2|\varphi_{t-s}(x_2-vt)\right)dx_1dx_2ds \\ &\le C\int_0^t \frac{1}{\sqrt{4\pi s}}\left(\frac{\sqrt{t}}{\sqrt{\pi}} + \int_0^{\infty}(x_2+|v|t)\varphi_{t-s}(x_2)dx_2\right)ds \\ &\le C\int_0^t \frac{1}{\sqrt{4\pi s}}\left(\frac{2\sqrt{t}}{\sqrt{\pi}} + |v|t\right)ds \\ &\le C\left(\sqrt{t}+t\right)\int_0^t\frac{ds}{\sqrt{s}} = O(t), \end{aligned}$$

which proves the claim.

Finally, combining all four claims yields

$$0 = -(1-\mathbf{p}_i\cdot\mathbf{p}_j)(v+\kappa)\frac{\sqrt{t}}{\sqrt{\pi}} + \mathbf{w}(0)\cdot(\mathbf{p}_i-\mathbf{p}_j)\frac{\sqrt{t}}{\sqrt{\pi}} + O(t).$$

Hence, Algorithm G.1 evolves interface γ_{ij} with a normal velocity

$$v = -\kappa - e_i + e_j + O(\sqrt{t}),$$

if we choose

$$\mathbf{w}(x) = \begin{cases} \dfrac{(e_i-e_j)(\mathbf{p}_i\cdot\mathbf{p}_j-1)}{|\mathbf{p}_i-\mathbf{p}_j|^2}(\mathbf{p}_i-\mathbf{p}_j), & x\in D_{\omega_1,\omega_2} \\ 0, & \text{otherwise,} \end{cases}$$

where

$$D_{\omega_1,\omega_2} := \{x \in \Omega : \operatorname{dist}(x, \gamma_{ij}) < \omega_1,\ \operatorname{dist}(x, P_r) > \omega_2\,(\forall r \neq i, j)\},$$

for some $\omega_1, \omega_1 > 0$.

§ Numerical Example

In [89], we rewrote Algorithm G.1 in a variational scheme and added a volume penalization term (analogous to Algorithm 5.1) to simulate a three-phase volume-preserving mean curvature evolution of interfaces with prescribed contact angles and considering bulk energies.

We consider a three-phase initial condition where P_1 is the region below the horizontal line at $x = 0.15$, phase region P_2 is the interior of a partial ellipse (representing a gas bubble), and the remaining region as external phase P_3. Here, we set $e_1 = e_2 = 0$ and $e_3 = \beta y$, where y denotes the coordinate direction of gravity and $\beta = 150$ is a constant expressing buoyancy. The junction angle condition $\theta_1 - \theta_2 - \theta_3$ is prescribed using nonsymmetric reference vectors, as follows:

$$\mathbf{p}_1 = \left(-\frac{\theta_1^2\theta_3^2 - 4A}{\theta_1\theta_3}, \frac{2\sqrt{A}}{\theta_1\theta_3}\right), \quad \mathbf{p}_2 = \left(-\frac{\theta_2^2\theta_3^2 - 4A}{\theta_2\theta_3}, \frac{2\sqrt{A}}{\theta_2\theta_3}\right), \quad \mathbf{p}_3 = (1, 0)\,,$$

where $\theta_1 + \theta_2 + \theta_3 = 2\pi$ and $A = \pi(\pi - \theta_1)(\pi - \theta_2)(\pi - \theta_3)$. Here, $\theta_i\,(i = 1, 2, 3)$ denotes interior angle measure of phase region P_i at the triple junction.

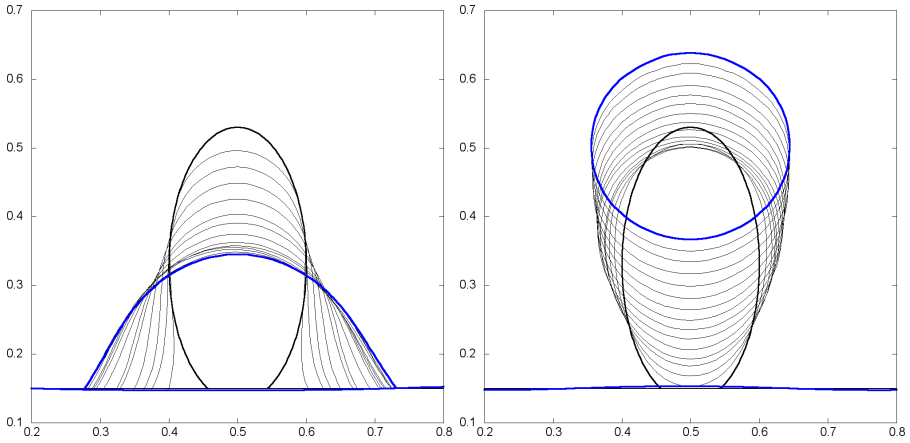

FIGURE G.2: Initial three-phase configuration (black in bold) and its volume-preserving mean curvature evolution considering bulk energies $e_1 = e_2 = 0$ and $e_3 = 150y$ with prescribed contact angles: 180°–60°–120° (left) and 180°–120°–60° (right) at different times.

The domain $\Omega = [0, 1] \times [0, 1]$ is triangulated into 12,800 elements (with mesh size $\Delta x = 0.0125$) and time step $\Delta t = 0.0050$ is discretized into $K = 30$ DMF partitions. Under the penalty parameter $\varrho = 10^{-5}$ and $\omega_1 = \omega_2 = \Delta x$, we run our algorithm for two prescribed junction angle conditions $180° - 60° - 120°$ and $180° - 120° - 60°$. The evolution of the interface network at time intervals of $2\Delta t$ are shown in Figure G.2. The resulting motion is a contest between the buoyant force $f = 150y$ pushing the bubble upwards and the surface tension force pressing the bubble towards the bottom phase (as set by the contact angle conditions).

Appendix H

Notations and Preliminaries

The present appendix fixes notations and states some preliminary results utilized in Chapter 7. For theories on elliptic partial differential equations of second order, we mainly refer to Gilbarg and Trudinger's book [49]. For results on measure theory, we refer to Evans' and Gariepy expository notes [38]. Other preliminaries not found in these two reference texts are laid out in this appendix.

Let us start with familiar notations as follows.

$\mathbb{N}$	set of natural numbers
$\mathbb{Q}$	set of rational numbers
$\mathbb{R}^N$	N-dimensional real Euclidean space, $\mathbb{R} = \mathbb{R}^1$
∂S	boundary of set S
$\overline{S}$	closure of set S, i.e. $\overline{S} = S \cup \partial S$
$\lvert S\rvert$	N-dimensional Lebesgue measure of $S \subset \mathbb{R}^N$
$B(x,r)$	open ball in $\mathbb{R}^N$ with center x and radius $r > 0$, i.e. $\{y \in \mathbb{R}^N : \lvert x-y\rvert < r\}$
$vol(N)$	volume of unit ball $B(0,1)$ in $\mathbb{R}^N$, $\dfrac{\pi^{N/2}}{\Gamma(\frac{N}{2}+1)}$
$\fint_S f$	mean value of function f over S, defined by $\dfrac{1}{\lvert S\rvert}\displaystyle\int_S f(x)dx$

Function Spaces.

$C(S)$	class of continuous functions $f : S \to \mathbb{R}$. If $f \in C(S)$ is bounded, we write $\lVert f\rVert_{C(S)} := \sup_{x\in S} \lvert f(x)\rvert$.
$C^k(S)$	class of k-times continuously differentiable functions $f : S \to \mathbb{R}$ $(0 \le k < \infty)$. Here, $C^0(S) = C(S)$.
$C^\infty(S)$	class of infinitely differentiable functions $f : S \to \mathbb{R}$
$C^{0,1}(S)$	class of Lipschitz continuous functions $f : S \to \mathbb{R}$, which by definition satisfy $\lvert f(x) - f(y)\rvert \le C\lvert x-y\rvert, \quad x, y \in S,$ for some constant $C > 0$.
$C^{0,\gamma}(S)$	class of Hölder continuous functions $f : S \to \mathbb{R}$ with exponent $\gamma \in (0,1)$, that is, for some constant $C > 0$, we have $\lvert f(x) - f(y)\rvert \le C\lvert x-y\rvert^\gamma, \quad x, y \in S.$

$C^{k,\gamma}(S)$ Hölder space consisting of all functions $f \in C^k(S)$ for which the norm

$$\|f\|_{C^{k,\gamma}(S)} := \sum_{|\alpha|\le k} \|D^\alpha f\|_{C(S)} + \sum_{|\alpha|=k} [D^\alpha f]_{C^{0,\gamma}(S)} < \infty.$$

$L^p(S)$ class of Lebesgue measure functions $f : S \to \mathbb{R}$ such that $\|f\|_{L^p(S)} < \infty$ where $1 \le p < \infty$. Here, the L^p-norm is given by

$$\|f\|_{L^p(S)} := \left(\int_S |f|^p\right)^{\frac{1}{p}}.$$

$L^\infty(S)$ class of Lebesgue measure functions $f : S \to \mathbb{R}$ such that $\|f\|_{L^\infty(S)} := \operatorname{ess\,sup}_S |f| < \infty$

$H^k(S)$ Sobolev space $W^{k,2}(S)$ consisting of all locally summable functions $f : S \to \mathbb{R}$ such that for each multiindex α with $|\alpha| \le k$, $D^\alpha f$ exists in the weak sense and belongs to $L^2(S)$. Here, the norm is defined by

$$\|f\|_{H^k(S)} := \left(\sum_{|\alpha|\le k} \int_S |D^\alpha f|^2\right)^{1/2}.$$

$C^k_{loc}(S)$, $L^p_{loc}(S)$, etc. denotes those functions $f : S \to \mathbb{R}$ such that for every compact subset D of S, we have $f \in C^k(D)$, $L^p(D)$, etc. Equivalently, if $x \in S$, then we can find a neighborhood $B_r := B(x, r)$ such that $f \in C^k(B_r)$, $L^p(B_r)$, etc.

$C^k_0(S)$, $H^k_0(S)$, etc. denote those functions $f : S \to \mathbb{R}$ in $C^k(S)$, $H^k(S)$, etc. with compact support in S, written $\operatorname{supp} f \subset S$.

Young's inequality. For $a, b \in \mathbb{R}$,

$$ab \le \epsilon a^2 + \frac{b^2}{4\epsilon}, \quad (\epsilon > 0).$$

Hölder inequality. For $f, g \in L^2(S)$,

$$\int_S |fg| \le \|f\|_{L^2(S)} \|g\|_{L^2(S)}.$$

Definition H.1. Let X and Y be Banach spaces, $X \subset Y$. We say that X is compactly embedded in Y, written

$$X \subset\subset Y,$$

provided

1. $\|u\|_Y \le C\|u\|_X$ $(u \in X)$ for some constant C
2. each bounded sequence in X is precompact in Y. More precisely, if $\{u_k\}$ is a sequence in X with $\sup_k \|u_k\|_X < \infty$, then some subsequence $\{u_{k_j}\} \subseteq \{u_k\}$ converges in Y to some limit u:

$$\lim_{j\to\infty} \|u_{k_j} - u\|_Y = 0.$$

Theorem H.2 (Rellich-Kondrachov Compactness Theorem). *Let $N \ge 2$. Assume a bounded open domain $S \subset \mathbb{R}^N$ with Lipschitz continuous boundary. Suppose $1 \le p < N$. Then,*

$$W^{1,p}(S) \subset\subset L^q(S)$$

for each $1 \leq q < p^* := \frac{pN}{N-p}$.

Theorem H.3 (**Poincaré-Wirtinger inequality**). *Let* $N \geq 2$. *Assume a connected bounded open domain* $S \subset \mathbb{R}^N$ *with Lipschitz continuous boundary. Then, there exists a constant* $C_P > 0$ *such that for every* $f \in H^1(S)$,

$$\left\| f - \fint_S f \right\|_{L^2(S)} \leq C_P \|f\|_{H^1(S)}.$$

Theorem H.4. *Let* $N \geq 2$. *Assume a connected bounded open domain* $S \subset \mathbb{R}^N$ *with Lipschitz continuous boundary. If* $\{f_n\}$ *is a sequence in* $H^1(S)$ *such that*

$$f_n \rightharpoonup f \text{ weakly in } H^1(S),$$

then

$$f_n \to f \text{ strongly in } L^2(S).$$

Definition H.5 (**Di Giorgi Class**). We denote by $\mathcal{B}_2(\Omega, M, \gamma, \delta, \frac{1}{q})$, the class of functions $f \in H^1(\Omega)$ with essential $\max_{\Omega} |f| \leq M$ such that for f and $-f$, the following inequalities are valid in an arbitrary ball $B_r \subset \Omega$ for arbitrary $\sigma \in (0,1)$:

$$\int_{A_{k,r-\sigma r}} |\nabla f|^2 dx \leq \gamma \left(\frac{1}{\sigma^2 r^{2(1-\frac{N}{q})}} \max_{A_{k,r}} |f(x) - k|^2 + 1 \right) |A_{k,r}|^{1-\frac{2}{q}},$$

for $k \geq \max_{B_r} f(x) - \delta$. Here, $A_{k,r} := \{f > k\} \cap B_r$ and $B_{r-\sigma r}$ is concentric with B_r.

Lemma H.6. *There exists a positive number* s *such that, for an arbitrary ball* B_r *belonging to* Ω *together with the ball* B_{4r} *concentric with it and for an arbitrary* $f \in \mathcal{B}_2(\Omega, M, \gamma, \delta, \frac{1}{q})$, *at least one of the following two inequalities holds:*

$$\begin{aligned} osc\{f, B_r\} &\leq 2^s R^{1-\frac{N}{q}} \\ osc\{f, B_r\} &\leq \left(1 - \frac{1}{2^{s-1}}\right) osc\{f, B_{4r}\}. \end{aligned}$$

Theorem H.7. *([62, Chapter 2, Theorem 6.1]) Let* f *be an arbitrary function in the class* $\mathcal{B}_2(\Omega, M, \gamma, \delta, \frac{1}{q})$ *and let* $B_R \subset \Omega$ *be a ball of radius* $r \leq 1$. *Then, for any ball* B_r *where* $r \leq R$ *that is concentric with* B_R, *the oscillation of* f *in* B_r *satisfies the inequality*

$$osc\{f, B_r\} \leq c \left(\frac{r}{R}\right)^{\alpha},$$

where

$$\begin{aligned} \alpha &= \min\left\{ -\log_4 \left(1 - \frac{1}{2^{s-1}}\right), 1 - \frac{N}{q} \right\}, \\ c &= 4^{\alpha} \max\left\{ 2M, 2^s R^{1-\frac{N}{q}} \right\}, \end{aligned}$$

and the number s *is taken from Lemma H.6*

Bibliography

[1] H. Abels, H. Garcke, and L. Müller, *Local well-posedness for volume-preserving mean curvature and willmore flows with line tension*, preprint (2014).

[2] N. Aguilera, H.W. Alt, and L.A. Caffarelli, *An optimization problem with volume constraint*, SIAM Journal of Control and Optimization **24** (1986), no. 2, 191–198.

[3] F. Almgren, J.E. Taylor, and L. Wang, *Curvature-driven flows: a variational approach*, SIAM Journal of Control and Optimization **31** (1993), no. 2, 387–438.

[4] H.W. Alt and L.A. Caffarelli, *Existence and regularity for a minimimum problem with free boundary*, Journal für die reine und angewandte Mathematik **325** (1981), 105–144.

[5] H.W. Alt, L.A. Caffarelli, and A. Friedman, *Variational prrblems with two phases and their free boundaries*, Transactions of the American Mathematical Society **282** (1984), 431–461.

[6] L. Alvarez, P.-L. Lions, and J.-M. Morel, *Image selective smoothing and edge detection by nonlinear diffusion ii*, SIAM Journal on Numerical Analysis **29** (1992), 845–866.

[7] L. Ambrosio, *Movimenti minimizzanti*, Rend. Accad. Naz. Sci. dei XL, Mem. Mat. **113** (1995), 191–246.

[8] L. Ambrosio and H.M. Soner, *Level set approach to mean curvature flow in arbitrary codimension*, Journal of Differential Geometry **43** (1996), no. 4, 693–737.

[9] B. Andrews, *Volume-preserving anisotropic mean curvature flow*, Indiana University Mathematics Journal **50** (2001), 783–827.

[10] S. Angenent and M. Gurtin, *Multiphase thermodynamics with interfacial structure ii: Evolution of an isothermal surface*, Archive for Rational Mechanics and Analysis **108** (1989), 323–391.

[11] M. Athanassenas, *Volume-preserving mean curvature flow of rotationally symmetric surfaces*, Commentarii Mathematici Helvetici **72** (1998), 52–66.

[12] G. Barles and C. Georgelin, *A simple proof of convergence of an approximation scheme for computing motions by mean curvature*, SIAM Journal on Numerical Analysis **32** (1995), no. 2, 484–500.

[13] J.W. Barrett, H. Garcke, and R. Nürnberg, *Parametric approximation of willmore flow and related geometric evolution equations*, SIAM Journal on Scientific Computing **31** (2008), no. 1, 225–253.

[14] K.A. Brakke, *The motion of a surface by its mean curvature*, Mathematical Notes, Princeton University Press, Princeton, New Jersey, 1978.

[15] L. Bronsard and F. Reitich, *On three-phase boundary motion and the singular limit of a vector-valued ginzburg-landau equation*, Archive for Rational Mechanics and Analysis **124** (1993), 355–379.

[16] L. Bronsard and B. Stoth, *Volume-preserving mean curvature flow as a limist of a nonlocal ginzburg-landau equation*, SIAM Journal on Mathematical Analysis **28** (1997), no. 4, 769–807.

[17] L. Bronsard and B.T.R. Wetton, *A numerical method for tracking curve networks moving with curvature motion*, Journal of Computational Physics **120** (1995), no. 1, 66–87.

[18] J.W. Cahn, C.A. Handwerker, and J.E. Taylor, *Geometric models of crystal growth*, Acta Metallurgy **40** (1992), 1443–1474.

[19] F. Cao, *Geometric curve evolution and image processing*, Lecture notes in mathematics, Springer-Verlag, Berlin Heidelberg, 2003.

[20] F. Catte, P.-L. Lions, and J.-M. Morel, *Image selective smoothing and edge detection by nonlinear diffusion*, SIAM Journal on Numerical Analysis **29** (1992), 182–193.

[21] A. Chambolle and M. Novaga, *Convergence of an algorithm for the anisotropic and crytalline mean curvature flow*, SIAM Journal on Mathematical Analysis **37** (2006), no. 6, 1978–1987.

[22] ———, *Approximation of the anisotropic mean curvature flow*, Mathematical Models and Methods in Applied Sciences **17** (2007), no. 6, 833–844.

[23] T.F. Chan and J. Shen, *Image processing and analysis: Variational, pde, wavelets, and stochastic methods*, Society for Industrial and Applied Mathematics, 2005.

[24] V.G. Chen, V. Giga, and S. Goto, *Uniqueness and existence of viscosity solutions of generalized mean curvature flow equations*, Journal of Differential Geometry **33** (1991), 749–786.

[25] S.-Y. Cheng, *Liouville theorem for harmonic maps*, Proceedings of Symposia in Pure Mathematics **36** (1980), 147–151.

[26] K. Deckelnick and G. Dziuk, *Discrete anisotropic curvature flow of graphs*, Mathematical Modelling and Numerical Analysis **33** (1999), 1203–1222.

[27] ———, *A fulls discrete numerical scheme for weighted mean curvature flow*, Numerische Mathematik **91** (2002), 423–452.

[28] K. Deckelnick, G. Dziuk, and C.M. Elliot, *Computation of geometric partial differential equations and mean curvature flow*, Acta Numerica **14** (2005), 1–94.

[29] I.C. Dolcetta, S.F. Vita, and R. March, *Area preserving curve shortening flows: from phase separation to image processing*, Interfaces and Free Boundaries **4** (2002), 325–343.

[30] G. Dziuk, *Discrete anisotropic curve shortening flow*, SIAM Journal on Numerical Analysis **36** (1999), 1808–1830.

[31] K. Ecker and G. Huisken, *Mean curvature evolution of entire graphs*, Annals of Mathematics **130** (1989), 453–471.

[32] ———, *Interior estimates for hypersurfaces moving by mean curvature*, Inventiones mathematicae **105** (1991), 547–569.

[33] C. Eilks and C.M. Elliott, *Numerical simulation of dealloying by surface dissolution via evolving surface finite element method*, Journal of Computational Physics **227** (2008), no. 23, 9727–9741.

[34] M. Elsey, S. Esedoglu, and P. Smereka, *Diffusion generated motion for grain growth in two and three dimensions*, Journal of Computational Physics **228** (2010), 8015–8033.

[35] J. Escher and G. Simonett, *The volume preserving mean curvature flow near spheres*, Proceedings of the American Mathematical Society **126** (1998), 2789–2796.

[36] S. Esedoglu, S. Ruuth, and R. Tsai, *Diffusion-generated motion using signed distance functions*, Journal of Computational Physics **229** (2010), 1017–1042.

[37] L.C. Evans, *Convergence of an algorithm for mean curvature motion*, Indiana University Mathematics Journal **42** (1993), 533–557.

[38] L.C. Evans and R.F. Gariepy, *Measure theory and fine properties of functions*, CRC Press, Inc., 1992.

[39] L.C. Evans, M. Soner, and P. Souganidis, *Phase transitions and generalised motion by mean curvature*, Communications on Pure and Applied Mathematics **45** (1992), 1097–1123.

[40] L.C. Evans and J. Spruck, *Motion of level sets by mean curvature i*, Journal of Differential Geometry **33** (1991), 635–681.

[41] ———, *Motion of level sets by mean curvature ii*, Transactions of the American Mathematical Society **330** (1992), no. 1, 321–332.

[42] ———, *Motion of level sets by mean curvature iii*, Journal of Geometric Analysis **2** (1992), 121–150.

[43] ———, *Motion of level sets by mean curvature iv*, Journal of Geometric Analysis **5** (1995), 77–114.

[44] M. Gage, *Curve shortening makes convex curves circular*, Inventiones mathematicae **76** (1984), 357–364.

[45] ———, *On an area-preserving evolution equation for plane curves*, Contemporary Mathematics **51** (1986), 51–62.

[46] H. Garcke, B. Nestler, and B. Stoth, *A multi phase field concept: numerical simulations of moving phase boundaries and multiple junctions*, SIAM Journal on Applied Mathematics **60** (1999), 295–315.

[47] M.-H. Giga and Y. Giga, *Evolving graphs by singular weighted curvature*, Archive for Rational Mechanics and Analysis **141** (1998), 117–198.

[48] Y. Giga, *Surface evolution equations*, Birkhäuser, Basel, 2006.

[49] D. Gilbarg and N.S. Trudinger, *Elliptic partial differential equations of second order*, Springer, 2001.

[50] E. Ginder, S. Omata, and K. Švadlenka, *A variational method for diffusion-generated area-preserving interface motion*, Theoretical and Applied Mechanics Japan **60** (2011), 265–270.

[51] M.E. Gurtin, *Towards a nonequilibrium thermodynamics of two-phase materials*, Archive for Rational Mechanics and Analysis **104** (1988), 195–221.

[52] M.E. Gurtin, H.M. Soner, and P.E. Souganidis, *Anisotropic motion of an interface relaxed by the formation of infinitesimal wrinkles*, Journal of Differential Equations **119** (1995), 54–108.

[53] J. Hass, M. Hutchings, and R. Schlafly, *The double bubble conjecture*, Electronic Research Announcements of the American Mathematical Society **1** (1995), 98–102.

[54] C. Herring, *Surface tension as a motivation for sintering*, The Physics of Powder Metallurgy (W. Kingston, ed.), McGraw-Hill, 1951, pp. 143–179.

[55] G. Huisken, *Flow by mean curvature of convex surfaces into spheres*, Journal of Differential Geometry **20** (1984), no. 1, 237–266.

[56] ———, *The volume preserving mean curvature flow*, Journal für die reine und angewandte Mathematik **382** (1987), 237–266.

[57] ———, *Asymptotic behaviour for singularities of the mean curvature flow*, Journal of Differential Geometry **31** (1990), 285–299.

[58] ———, *Local and global behaviour of hypersurfaces moving by mean curvature*, Proceedings of Symposia in Pure Mathematics **54** (1993), 175–191.

[59] G. Huisken and C. Sinestrari, *Mean curvature flow singularities for mean convex surfaces*, Calculus of Variations and Partial Differential Equations **8** (1999), 1–14.

[60] K. Ishii, *Mathematical analysis to an approximation scheme for mean curvature flow*, International Symposium on Computational Science 2011, Mathematical Sciences and Applications (S. Omata and K. Švadlenka, eds.), GAKUTO International Series, vol. 34, 2011, pp. 67–85.

[61] N. Kikuchi, *An approach to the construction of morse flows for variational functionals*, Nematics-Math. and Phys. Aspects (J-M. Coron, J-M. Ghidaglia, and F. Helein, eds.), NATO Advanced Science Institutes Series C: Mathematical and Physical Sciences, vol. 332, Kluwer Acad. Publ., Dordrecht, Boston, London, 1991, pp. 195–198.

[62] O. Ladyzhenskaya and N. Ural'tseva, *Linear and quasilinear elliptic equations*, Academic Press, 1968.

[63] M.-C. Lai, C.-W. Hsu, and H. Huang, *A front tracking method for motion by mean curvature with surfactant*, Advances in Applied Mathematics and Mechanics **1** (2009), no. 2, 288–300.

[64] P. Li and S.T. Yau, *On the parabolic kernel of the schrödinger operator"*, Acta Mathematica **156** (1986), 153–201.

[65] C. Mantegazza, *Lecture notes on mean curvature flow*, Progress in Mathematics, vol. 290, Springer Basel AG, 2011.

[66] C. Mantegazza, M. Novaga, and V.M. Tortorelli, *Motion by curvature of planar networks*, Annali della Scuola Normale Superiore di Pisa – Classe di Scienze **3** (2004), 235–324.

[67] U.F. Mayer, *Numerical solutions for the surface diffusion flow in three space dimensions*, Computational and Applied Mathematics **20** (2001), 361–379.

[68] B. Merriman, J. Bence, and S. Osher, *Motion of multiple junctions: a level set approach*, Journal of Computational Physics **112** (1994), 334–363.

[69] K. Mikula and D. Sevcovic, *Computational and qualitative aspects of evolution of curves driven by curvature and external force*, Computing and Visualization in Science **6** (2004), no. 4, 211–225.

[70] R.Z. Mohammad, *Multiphase mean curvature flow: signed distance vector approach*, Recent Development in Computational Science: Selected Papers from the International Symposium on Computational Science (V. Suendo, K. Švadlenka, R. Simanjuntak, and S. Miura, eds.), vol. 4, 2013, pp. 115–123.

[71] R.Z. Mohammad and K. Švadlenka, *Multiphase volume-preserving interface motions via localized signed distance vector scheme*, to appear in Discrete and Continuous Dynamical Systems – Series S, American Institute of Mathematical Sciences.

[72] ———, *On a penalization method for an evolutionary free boundary problem with volume constraint*, to appear in Advances in Mathematical Sciences and Applications, Gakkotosho Tokyo, Japan.

[73] ———, *Diffusion-generated volume preserving motions: a comparison of mbo-variant algorithms*, Proceedings of Computational Engineering and Science Conference **17** (2012).

[74] C.B. Morrey, *Second order elliptic equations in several variables and hölder continuity*, Mathematische Zeitschrift **72** (1959), 146–164.

[75] ———, *Multiple integrals in the calculus of variations*, Springer-Verlag, New York, 1966.

[76] W.W. Mullins, *Two-dimensional motion of idealized grain boundaries*, Journal of Applied Physics **27** (1956), 900–904.

[77] T. Nagasawa and S. Omata, *Discrete morse semiflows of a functional with free boundary*, Advances in Mathematical Sciences and Applications **2** (1993), no. 1, 147–187.

[78] S. Omata, M. Kazama, and K. Švadlenka, *Discrete morse flow for nonlocal problems*, RIMS Kokyuroku **1628** (2009), 42–47.

[79] J. Prüss and G. Simonett, *On the two-phase navier-stokes equations with surface tension*, Interfaces and Free Boundaries **12** (2010), no. 3, 311–345.

[80] S. Raynor, *Neumann fixed boundary regularity for an elliptic free boundary problem*, Communications in Partial Differential Equations **33** (2008), no. 11, 1975–1995.

[81] F. Reitich and H.M. Soner, *Three-phase boundary motions under constant velocities i: the vanishing surface tension limit*, Proceedings of the Royal Society **126A** (1996), 837–865.

[82] E. Rothe, *Zweidimensionale parabolische randwertaufgaben als grenzfall eindimensionaler randwertaufgaben*, Mathematische Annalen **102** (1930), 650–670.

[83] J. Rubinstein and P. Sternberg, *Nonlocal reaction diffusion equations and nucleation*, IMA Journal of Applied Mathematics **48** (1992), 249–264.

[84] S. Ruuth, *Efficient algorithms for diffusion-generated motion by mean curvature*, Journal of Computational Physics **144** (1998), 603–625.

[85] S. Ruuth and B. Wetton, *A simple scheme for volume-preserving motion by mean curvature*, Journal of Scientific Computing **19** (2003), 373–384.

[86] G. Sapiro, *Geometric partial differential equations and image analysis*, Cambridge University Press, 2001.

[87] G. Sapiro and A. Tannenbaum, *Area and length preserving geometric invariant scale-spaces*, IEEE Transactions on Pattern Analysis and Machine Intelligence **17** (1993), 67–72.

[88] N. Shofianah, R.Z. Mohammad, and K. Švadlenka, *Simulation of triple junction motion with arbitrary surface tensions*, to appear in International Journal of Applied Mathematics.

[89] ———, *On a numerical method for the simulation of contact angle dynamics*, Proceedings of Computational Engineering and Science Conference **19** (2014).

[90] J.E. Taylor, *Motion of curves by crystalline cruvature, including triple junctions and boundary points*, Proceedings of Symposia in Pure Mathematics **51** (1993), 417–438.

[91] ———, *Anisotropic interface motion*, Mathematics of Microstructure Evolution (L.-Q. Chen, B. Fultz, J.W. Cahn, J.R. Manning, J.E. Morral, and J. Simmons, eds.), SIAM, vol. 4, 1996, pp. 135–148.

[92] N. Thürey, C. Wojtan, M. Gross, and G. Turk, *A multiscale approach to mesh-based surface tension flows*, ACM Transactions on Graphics **29** (2010), no. 4, 48:1–48:10.

[93] P. Tilli, *On a constrained variational problem with an arbitrary number of free boundaries*, Interfaces and Free Boundaries **2** (2000), 201–212.

[94] K. Švadlenka, E. Ginder, and S. Omata, *A variational method for multiphase area-preserving interface motions*, Journal of Computational and Applied Mathematics **257** (2014), 157–179.

[95] B. White, *Partial regularity of mean-convex hypersurfaces flowing by mean curvature*, International Mathematics Research Notices **4** (1994), 186.

[96] Y. Yamaura, *Uniform lipschitz continuity of solutions to discrete morse flows*, International Journal of Pure and Applied Mathematics **67** (2011), no. 2, 193–223.

[97] K. Yokoi and F. Xiao, *Mechanism of structure formation in circular hydraulic jumps: numerical studies of strongly deformed free-surface shallow flows*, Physica D: Nonlinear Phenomena **161** (2002), 202–219.

[98] H.-K. Zhao, B. Merriman, S. Osher, and L. Wang, *Capturing the behavior of bubbles and drops using the variational level set approach*, Journal of Computational Physics **143** (1998), 495–518.